BIOACTIVE NANO-LIPOSHELLS MATRICIZED WITHIN A POLYMERIC SCAFFOLD FOR PROLONGED SITE-SPECIFIC NEUROTHERAPY OF SCHIZOPHRENIA

THIRESEN GOVENDER

A dissertation submitted to the Faculty of Health Sciences, University of the Witwatersrand, in fulfillment of the requirements for the degree of

Master of Pharmacy

Supervisor:

Professor Viness Pillay
University of the Witwatersrand, Department of Pharmacy and Pharmacology, South Africa

Co-Supervisors:

Professor Yahya E. Choonara
University of the Witwatersrand, Department of Pharmacy and Pharmacology, South Africa
Professor Girish Modi
University of the Witwatersrand, Department of Neurology, Division of Neurosciences, South Africa
Doctor Dinesh Naidoo
University of the Witwatersrand, Department of Neurosurgery, Division of Neurosciences, South Africa
Miss Lisa Claire du Toit
University of the Witwatersrand, Department of Pharmacy and Pharmacology, South Africa

Johannesburg, 2012

DECLARATION

I, Thiresen Govender, declare that this dissertation is my own work. It has been submitted for the degree of Master of Pharmacy in the Faculty of Health Sciences at the University of Witwatersrand, Parktown, Johannesburg, South Africa. It has not been submitted before for any degree or examination at this or any other University.

.....

This.....day of November 2012

RESEARCH OUTPUTS

PUBLICATIONS

Book Chapter

Polymeric intracorporeal devices for the management of neurological disorders

Viness Pillay, Thiresen Govender, Yahya E. Choonara, Valence M.K. Ndesendo, Lisa C. du Toit, Girish Modi and Dinesh Naidoo, Polymers Research Journal, 4 (2-3), Nova Science Publishers Inc., Hauppauge, NY, USA, 2011 (Abstract in Appendix A1).

Papers

A polyamide-based membranous device for specialized drug delivery

Thiresen Govender, Viness Pillay, Yahya E. Choonara, Lisa C. du Toit, Girish Modi and Dinesh Naidoo, Journal of Pharmacy and Pharmacology, 62 (10), 1243-1244, 2010 (Abstract in Appendix A2).

Novel approaches to antipsychotic drug delivery: Design, development and optimization of chlorpromazine containing polycaprolactone nanoparticles by a novel melt-dispersion technique

Thiresen Govender, Viness Pillay, Yahya E. Choonara, Lisa C. du Toit, Girish Modi and Dinesh Naidoo, (To be submitted)(Abstract in Appendix A3).

An Intracranial Nano-Enabled Polymeric Membranous Device for the Site-Specific Delivery of Chlorpromazine Hydrochloride

Thiresen Govender, Yahya E. Choonara, Lisa C. du Toit, Girish Modi, Dinesh Naidoo and Viness Pillay, (To be submitted)(Abstract in Appendix A4).

POSTERS

Evaluation of chlorpromazine release from a polyamide-ethylcellulose implantable mini disc

Thiresen Govender, Viness Pillay, Girish Modi, Dinesh Naidoo, Yahya E. Choonara and Lisa C. du Toit

5th International Conference on Pharmaceutical and Pharmacological Sciences, Potchefstroom, South Africa, 23-26th September 2009 (Abstract in Appendix B1).

A polyamide-based membranous device for specialized drug delivery

Thiresen Govender, Viness Pillay, Girish Modi, Dinesh Naidoo, Yahya E. Choonara and Lisa C. du Toit

Presented at the APS UKPHARMSCI Conference, Nottingham, United Kingdom, September 2010 (Abstract in Appendix B2).

Design, development and optimisation of a novel neurotherapeutic intracranial implantable composite device

Thiresen Govender, Viness Pillay, Girish Modi, Dinesh Naidoo, Yahya E. Choonara and Lisa C. du Toit

Presented at the British and Irish Group for the Study of Personality Disorders (BIGSPD) Conference, Manchester, United Kingdom, March 2012 (Abstract in Appendix B3).

Novel approaches to personality disorder treatment: Design of dual-acting nanoparticles for the enhanced neurotherapy of Borderline Personality Disorder

Thiresen Govender, Nabeela Bhabha, Viness Pillay, Girish Modi, Dinesh Naidoo, Yahya E. Choonara and Lisa C. du Toit

Presented at the British and Irish Group for the Study of Personality Disorders (BIGSPD) Conference, Manchester, United Kingdom, March 2012 (Abstract in Appendix B4).

Advances in neurotherapeutics: Intracranial implantation of a novel optimised polymeric composite in the New Zealand White Rabbit cadaver

Thiresen Govender, Viness Pillay, Girish Modi, Dinesh Naidoo, Yahya E. Choonara, Lisa C. du Toit and Leith Meyer

Presented at the British and Irish Group for the Study of Personality Disorders (BIGSPD) Conference, Manchester, United Kingdom, March 2012 (Abstract in Appendix B5).

PODIUM PRESENTATIONS

A membrane-fixated nano-liposhell device for specialized central nervous system drug delivery.

Thiresen Govender, Viness Pillay, Girish Modi, Dinesh Naidoo, Yahya E. Choonara and Lisa C. du Toit

3rd Postgraduate Cross Faculty Symposium, University of the Witwatersrand, Johannesburg, South Africa, 29th October 2010 (Abstract in Appendix C1).

Development of chlorpromazine-loaded, polycaprolactone based nanoparticles utilizing a novel melt-dispersion technique

Thiresen Govender, Viness Pillay, Girish Modi, Dinesh Naidoo, Yahya E. Choonara and Lisa C. du Toit

School of Therapeutic Sciences Research Day, University of the Witwatersrand, 24th August 2011 (Abstract in Appendix C2).

ADDITIONAL OUTPUTS FOR COLLABORATIVE RESEARCH

Intonation of diphenhydramine release from a multifaceted tablet configuration

Kovanya Moodley, Thiresen Govender, Viness Pillay, Yahya E. Choonara and Lisa C. du Toit

Presented at the Academy of Pharmaceutical Sciences of South Africa (APSSA) conference, Magaliesburg, September 2008.

PATENTS

A drug delivery device

Thiresen Govender, Viness Pillay, Yahya E. Choonara, Lisa C. du Toit, Girish Modi, Dinesh Naidoo and Maluta Steven Mufamadi

International Application Number: PCT/IB2011/055345, Publication Number: WO/2012/070034, 31st October 2012 (Abstract in Appendix D).

SUMMARY

An impediment in the long-term treatment and positive therapeutic outcome of psychoses is patient non-compliance to treatment regimens. The cognitive impairment associated with psychoses together with the inability to manage the intolerable side-effects of antipsychotic drug, inevitably predisposes the psychotic patient to non-compliance. Furthermore, the highly restricting Blood-Brain Barrier (BBB) has proved to be a significant limitation for the systemic delivery of antipsychotic drugs to the brain.

The benefits of site-specific drug delivery combined with nanobiotechnology serves to enhance drug therapy by evading the BBB, increasing the bioavailability of the drug, enabling effective drug penetration into the brain, avoiding the need to administer potentially toxic doses of antipsychotic drugs and reducing systemic toxicity. In addition, controlled drug release over a prolonged period will ensure improved patient compliance and reduced rates of relapse. Therefore, the aim of this study was to develop of a drug-loaded Nano-enabled Polymeric Membranous Device (NPMD) for intraparenchymal implantation into the sub-arachnoid space in the region of the frontal lobe of the brain that circumvents the limitations of current antipsychotic modes of treatment.

Chlorpromazine hydrochloride (CPZ)-loaded, polycaprolactone (PCL)-based nanoparticles were synthesized by a novel melt-dispersion technique.CPZ was selected as a model drug owing to the fact that it is a highly hydrophilic, cost-effective antipsychotic drug and its use has declined due to its significantly low bioavailability. The employment of a Face-Centered Central Composite Design resulted in an optimized formulation with a desirable size (140.30±3.39nm), stability in terms of its zeta potential (-26.40±2.11mV) and CPZ entrapment (8170.23±173.39µg) (~16%). Drug release was biphasic with an initial burst release followed by controlled release over 30 days. Furthermore, no thermo-degradation of the drug and constituent polymers were observed with the novel melt-dispersion technique.

Novel implantable polyamide-ethylcellulose (PA 6,10-EC) composite membranes were prepared by a modified wet-phase inversion reaction employing a dialysis apparatus. Composites were optimized by experimental design, which resulted in highly resilient devices with an unhydrated and hydrated matrix resilience of 74.24±0.88 and 84.35±1.22% respectively. Furthermore, minimal erosion was observed over a period of 30 days (3.64±0.08%). The optimized CPZ-loaded, PCL-based nanoparticle formulation was combined with the optimized PA 6,10-EC composite membrane formulation to form the intracranial implantable NPMD to be further evaluated in vivo.

A further preliminary study investigated the synthesis of encapsulated or adsorbed essential fatty acids in the form of cod-liver oil (CLO) (Gadus Morrhua) within the CPZ-loaded, PCL nanoparticles to form dual-acting nano-liposhells that combine the benefits of conventional with complementary medicine. The rationale for incorporating CLO was due to its high levels of omega-3 fatty acids, Docosahexaenoic acid (DHA) and Eicosapentaenoic acid (EPA), which have been proven to be neuroprotective with proven benefits in conditions such as schizophrenia. Transmission electron microscopy (TEM) revealed that the nano-liposhells were small and denser when compared to nanoparticles devoid of CLO (16.50±6.79nm in size). A highest absolute zeta potential of -30.25±0.06mV confirmed the stability of the nano-liposhells and a highest CLO and CPZ entrapment of 98.26±0.13% and 6690.55±207.30µgrespectively was determined.

Ex vivo cytotoxicity studies using mammalian Pheochromocytoma (PC12) neuronal cells were carried out on the NPMD and the CLO and CPZ-loaded nano-liposhells as well as both their componential elements. A lactate dehydrogenase (LDH) release assay was undertaken and proved that the NPMD and its componential elements were biocompatible and displayed no significant cytotoxicity ($p>0.05$). The nano-liposhells and the CLO itself did display significant ($p<0.05$) cytotoxicity and reduced cell viability by 23.27±2.40% and 45.68±6.12% respectively and was attributed to free radical formation by auto-oxidation.

An in vivo pilot study explored the surgical intraparenchymal implantation of the NPMD into the brain of the New Zealand White Rabbit model. The study was performed over 30 days and Cerebrospinal Fluid (CSF) as well as blood plasma samples were withdrawn at predetermined intervals to evaluate the release of CPZ from the NPMD using Ultra Performance Liquid Chromatography. Results were compared to a group of rabbits given commercially available CPZ in the form of intramuscular (I.M.) Fresenius Chlorpromazine hydrochloride® 25mg/mL. Results revealed higher levels of CPZ in the CSF (2.08-2.92ng/mL) from the NPMD when compared to the I.M. dose (0.85-2.32ng/mL). Furthermore, miniscule quantities of CPZ from the NPMD were detected in the blood (≤0.95ng/mL) The CPZ release from the NPMD was far superior to the commercially available form of the drug. Implantation at the site of action allowed for a drastic increase in the CPZ bioavailability. Furthermore, the drug was released in a pseudo-steady state with CSF levels being maintained between 2.00-3.00ng/mL with no fluctuations observed. Ultrasonic imaging was utilized to view the NPMD post-implantation. Rabbits displayed no evidence of motor dysfunction or general brain damage post-implantation for the duration of the study. Histomorphological analysis revealed that the NPMD was biocompatible as no evidences of bleeding, ischemia or major chronic inflammation was observed. Light microscopy was used to characterize the bioerosion of the NPMD midway through as well as at the end of the study and revealed minimal erosion at the termination of the study (14.87%).

ACKNOWLEDGEMENTS

In completion of this work, the author would like to convey his sincerest gratitude and appreciation to various individuals that have assisted and guided him towards this goal.

My sincerest and everlasting gratitude and appreciation goes to God, without whom, nothing is possible. Thank you for watching over me in my darkest hours and being there for me in my greatest times of need.

To my parents, Krish and Mallie Govender, I could write an entire dissertation on the sacrifices you have made to fuel my quest for excellence. No words could ever describe how much I appreciate everything you have done for me and how much you mean to me.

Thank you to my sisters, Anusha and Naressa, my grandparents, Bob and Logie Naicker and every single member of my family for all the support you have given me over the years. Although you are far away, you are close at heart. Thank you for everything.

To my late grandparents, Venketsamy and Ammoyi Govender, even though I did not get the chance to spend the time I desired with you, I know you are always looking down on me, guiding me through every walk of my life, including this. Thank you.

My further gratitude goes towards my Supervisor, Professor Viness Pillay, for without you; the knowledge I have gained and the opportunities I have experienced would not be possible. Your intelligence, dedication, hunger for knowledge and strive for perfection goes beyond anything. My extended thanks go to my Co-Supervisors, Professor Yahya E. Choonara, Professor Girish Modi, Doctor Dinesh Naidoo and Miss Lisa Claire du Toit for your help and passion in this work.

Thank you to all my colleagues and members of WADDP, past and present. It is impossible to name each and every single one of you without inadvertently missing one of you. You have all made such an important impact and invaluable contribution to my research. Thank you for sharing in my joys and sorrows and for the remarkable experience over the past few years.

A special Thank You to Nabeela Bhabha, Pradeep Kumar, Lisa du Toit, Steven Mufamadi, Felix Mashingaidze, Raeesa Moosa, Valence Ndesendo and Dinesh Naidoo. You possess a wealth of knowledge in the field, and your willingness to help cannot go unnoticed. You have contributed immensely and have allowed me to elevate my research to another level.

Thank you to the staff of the Department of Pharmacy and Pharmacology for molding me into the health professional that I am and for your constant help with any request of mine.

To my extended family, Siandran, Nolan, Fharzana, Yusuf, Yashodan, Dipesh, Keshia, Sheena, Zia, Sam and Dereshen. No words could ever describe how grateful I am for having you in my life. Thank you for making the days go by faster and for your continuous support and motivation.

My sincerest appreciation goes to Kleinbooi, Bafana, Busi, Tebogo and the technical staff of the Department for all your help. You bent over backwards in assisting me with my research.

To Sister Mary-Ann Costello and the staff of the CAS, I extend my deepest gratitude to you for assisting me greatly with my animal studies. I sincerely appreciate your dedication, professionalism and the overall manner in which you run the Department. Keep up the good work.

Thank you to the late Abe Seema for all your help with the electron microscopy analysis of my samples. You will never be forgotten. Rest In Peace.

Finally, to every person who has had an influence and has been part of my life, I am who I am because of you. Thank you.

DEDICATION

This dissertation is dedicated to my parents, Krish and Mallie Govender.

If I reach the pinnacle of my life being half the person that you have molded me to be, I would be extremely proud of myself.

I Kiss the Ground You Walk On

This work is also dedicated to my niece, Diya Kimeya Chetty.

A bundle of joy whose introduction to our lives has brought unmatched happiness, laughter and love

"The only way of finding the limits of the possible is by going

beyond them into the impossible"

Arthur C. Clarke

ANIMAL ETHICS DECLARATION

I hereby confirm that the following study entitled *"IN VIVO EVALUATION OF AN IMPLANTABLE NANO-ENABLED POLYMERIC MEMBRANOUS DEVICE CONTAINING CHLORPROMAZINE HYDROCHLORIDE IN THE RABBIT MODEL"* has received the approval from the Animal Ethics Screening Committee of the University of the Witwatersrand with ethics clearance number 2011/51/04 (Appendix E).

TABLE OF CONTENTS

Chapter 3

Chapter 4

Chapter 5

Chapter 6

Chapter 7

Chapter 8

LIST OF FIGURES

Page

LIST OF TABLES

Page

CHAPTER 1
INTRODUCTION

1.1 Background to this Study

Central Nervous System (CNS) disorders remain one of the world's leading causes of disability despite the extensive research and advances in the field. CNS disorders are responsible for more hospitalizations and long-term care than almost all other diseases combined (Misra et al., 2003). The poor quality of life associated with psychoses such as schizophrenia is primarily due to patients experiencing symptoms such as hallucinations, delusions, uncoordinated speech, avolition, poor memory, marked decline in intellectual capacity, changes in appearance, social withdrawal, increased risk of suicide and violent behavior. Despite the fact that pharmacological and non-pharmacological treatment may notably suppress symptoms, the overall positive effects achieved by treatment are generally modest when compared to the transformation achieved with treatment of other mental illnesses (Frith et al., 1996; Kane, 1996; Lincoln et al., 2007).

An impediment in the long term treatment and positive therapeutic outcome in psychoses such as schizophrenia is non-compliance to treatment regimens; which is the primary cause for a poor quality of life (Kane et al., 1998; Gharabawi et al., 2007; Rabin et al., 2008). Non-compliance as well as minimal flexibility in the proposed treatment plan increases the chance of a psychotic patient being hospitalized (Pfeiffer et al., 2008). Apart from frequent hospitalizations, other consequences of non-compliance include an increased deterioration of mental capacity, loss of employment and relationships, as well as increased relapse. A major challenge with continuous relapse is that remission after the next episode is extremely difficult to achieve, ultimately producing a negative feedback loop which negatively affects the patient's quality of life (Rabin et al., 2008).

Non-compliance with antipsychotic medication may be as a result of numerous factors. One of the most significant is the intolerable side-effects associated with anti-psychotic medication (Lieberman et al., 2005). Atypical antipsychotic drugs are the popular choice in the treatment due to their lack of associated extrapyramidal side-effects as well as their superior safety profile regarding prolactin (Arulmozhi et al., 2006). Examples of atypical antipsychotics include olanzapine, which has been linked to weight gain and an increased lipid and glucose metabolism. Clozapine, another atypical antipsychotic causes agranulocytosis and has been implicated in cases of fatal constipation (Claas, 1989; Ellis, 1989; Lieberman et al., 2005). It has been documented that the use of antipsychotics in

general increases the risk of metabolic syndrome. However, due to the severity and complexity of psychoses such as schizophrenia, physicians continue to use antipsychotic drugs despite the life-threatening ramifications (Lieberman, 2004). The challenges represented by the systemic side-effects of oral antipsychotics warrants the use of targeted drug delivery to the brain (Mak et al., 1995; Bodor and Buchwald, 2003). Non-compliance to treatment regimens is also related to the dosing frequency of certain antipsychotic medication (Pfeiffer et al., 2008). Oral treatment for conditions such as schizophrenia may be dosed from two to four times a day (Cheng et al., 2000).

Currently, the convenient and preferred drug delivery system for antipsychotic drugs includes conventional tablet or capsule formulations. As with most conventional oral drug delivery systems, they exhibit first-order drug release kinetics where drug levels are higher after ingestion but decrease exponentially, not allowing optimum prolonged plasma levels for therapeutic efficacy resulting in dose-dependent side-effects (Shahiwala et al., 2004; Landgraf et al., 2005). The success of maintenance therapy in psychosis depends on a number of variables, including the constant release of neurotherapeutics, a reduction in the dosing frequency, a greater antipsychotic drug bioavailability and ultimately improved patient compliance, many of which is not achievable by conventional oral formulation schizophrenia therapy (Pranzatelli, 1999; Cheng et al., 2000).

Achieving a positive therapeutic outcome and a reduction in hospitalizations generally relies on the use of depot formulations of antipsychotic drugs (Kane et al., 1998; Gutwinski et al., 2007). Several clinical studies have proved the safety and efficacy of long-acting injectable atypical antipsychotic drugs and have warranted their use as maintenance therapy. Gharabawi and co-workers (2007) showed that a single depot injection of long-acting risperidone administered once monthly is generally well tolerated, with evident improvement in both the positive and negative symptoms of schizophrenia. However, there are limitations of depot formulations that may affect compliance or efficacy.

Disadvantages of depot formulations include patients unwillingness to receive injections, the inability to rapidly cease the medication if serious side-effects occur, difficulties in dose adjustments, complex and intricate pharmacokinetics, abscess formation, pruritis and extended periods of pain at the injection site. Furthermore, depot formulations containing the decanoate functional group are restricted by their chemistry (Kane, et al., 1998; McCauley and Connolly, 2004; Rabin, et al., 2008).

Therefore this study proposes a novel and definite means of addressing the above mentioned challenges through the development of a drug-loaded Nano-enabled Polymeric Membranous Device (NPMD) for implantation into the sub-arachnoid space in the region of the frontal lobe of the brain for the site-specific delivery of the antipsychotic drug chlorpromazine hydrochloride (CPZ).

1.2 Rationale and motivation for this study

The vast prevalence of schizophrenia, its chronic and debilitating nature as well as the risk of relapse and suicide makes effective treatment of psychoses mandatory. The highly restricting Blood-Brain Barrier (BBB) has proved to be a significant limitation for the systemic delivery of antipsychotic drugs to the brain rendering sub-therapeutic and ineffective treatment of neurological diseases (Mak et al., 1995; Pardridge, 1997 and 2005;Bodor and Buchwald, 2003; Unger et al., 2004; Abbott, 2005; Gelperina, 2006; Koo et al., 2006; Koziara et al., 2006; Krauze et al., 2006; Kwan P and Brodie, 2006; Tiwari et al., 2006; Nelson et al., 2010). Therapeutic failure of the majority of neurotherapeutic drugs relies on the fact that these drugs are only transported minimally across the BBB. Apart from the BBB, another obstacle is the Blood-Cerebrospinal fluid Barrier (BCB). The intimate contact between cerebrospinal fluid (CSF) and the brain parenchyma allows the CSF to exchange molecules with the interstitial fluid of the brain parenchyma and due to this, any blood-borne agents into the CSF is regulated by the BCB (Misra et al., 2003). Apart from these physical barriers, the lack of innovation in product development to counteract these challenges is also a major contributing factor to a poor therapeutic outcome (Pardridge, 2005).

Site-specific drug delivery coupled with nanotechnology, as described in this study by the NPMD, circumvents the difficulties posed by the BBB and BCB. In addition, it avoids the need to administer potentially toxic doses of antipsychotic drugs for the sake of achieving therapeutic doses in the CNS. Furthermore, the diffusivity of the nanoparticles is not lengthy as are other systemically injected nano-enabled formulations. Systemically administered nano-enabled formulations have a greater chance of degrading or being metabolized by the body. Lastly, active drug can be released from the nanoparticles by simple diffusion from the NPMD, erosion of the nanoparticle itself or evaporation of the core as opposed to other nano-enabled formulations like polymeric micro or nanobubbles where ultrasound energy is required (Hynynen, 2009).

Much emphasis is placed on the sufferers and far less on the caregivers and loved ones faced with the responsibility of caring for these ill patients. The chronic nature of the disorder

may be physically, emotionally, psychologically and economically challenging to the caregiver. The “burden of care” is a phrase applied to the caregiver that describes the hardship and consequences faced by them in their quest to assist those living with schizophrenia. “Burden of care” also encompasses distressing thoughts and perceptions such as self-blame, embarrassment, shame and guilt, all of which may be debilitating to the caregiver (Awad and Voruganti, 2008). The advent of developing an implantable, biodegradable polymeric device that releases antipsychotic drug in a controlled manner over a prolonged period of time virtually eliminates the issue of non-compliance and decreases the need for having a constant caregiver for schizophrenic patients who are on chronic maintenance therapy.

The proposed NPMD will be synthesized using a cost-effective rate controlling polymer or blends thereof and will provide advantages that include a decrease in systemic side-effects, a decrease in serum protein binding of the drug CPZ, reduced hepatic metabolism and peripheral drug inactivation and polymeric protection of active drug by the membranous device thereby reducing degradation. Furthermore, larger doses of drug can be localized in the areas of the brain where it is required the most. The fact that the NPMD will be biodegradable ensures that no additional surgery will be required to remove the device (Mak et al., 1995). In addition to this, CPZ will be released with zero-order kinetics over a prolonged period (minimum of 365 days), maintaining optimum levels in the CNS compartment and preventing relapse.

Figure 1.1 represents the proposed mechanism of action of the NPMD post-implantation. CPZ was selected as a model drug owing to the fact that it is a cost-effective antipsychotic drug. However, its use has declined due to its significantly low bioavailability (approximately 20% plasma bioavailability, of which, only a fraction reaches the site of action which is the brain). This, in turn, results in a higher dosing frequency in order to achieve therapeutic quantities of drug at the site of action subsequently leading to dose-dependent side-effects. Furthermore, the notable systemic side-effects of CPZ have also resulted in CPZ being an unpopular first choice antipsychotic drug. The NPMD will therefore dramatically improve the bioavailability of the CPZ as a result of site-specific drug delivery. In addition, site-specific CPZ delivery will reduce the systemic side-effects experience by conventional oral and injectable CPZ formulations. These traits coupled with the controlled zero-order release of CPZ from the NPMD will virtually eliminate the aforementioned challenges associated with conventional commercially available CPZ formulations.

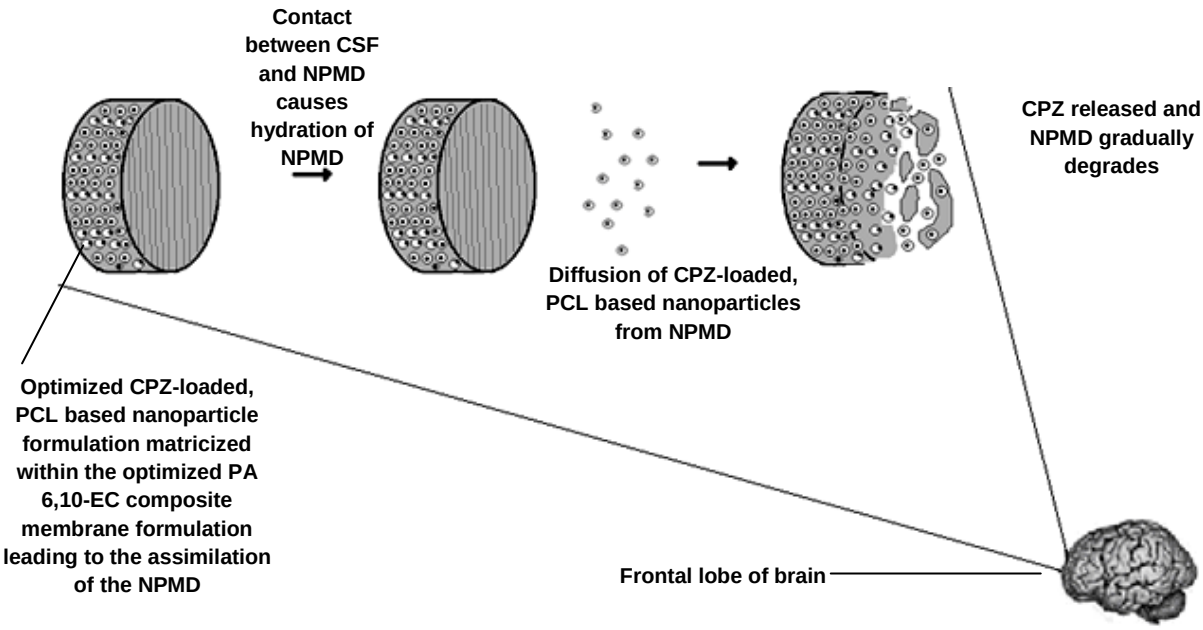

Figure 1.1: Proposed mechanism of action of the NPMD post-implantation into the frontal lobe of the brain.

1.3 Aims and objectives of this study

The aim of this study was to develop an implantable novel NPMD for the chronic treatment of psychoses such as schizophrenia. To supplement the benefits of nanotechnology and nanoneuropharmaceutics in particular, a novel polymeric composite membrane was used as a rate-controlling device with the aim of achieving controlled release of CPZ from the nanoparticles in the CNS compartment in particular, the frontal lobe of the brain.

In order to achieve this aim, the following objectives were outlined:

1. Selection of suitable and appropriate polymers that offer controlled and prolonged release of drug
2. Standardization of CPZ-loaded, PCL-based nanoparticle synthesis
3. Design, development and optimization of the polymeric membranous device and matricization of the CPZ-loaded PCL-based nanoparticles within the implantable polymeric membranous device
4. To perform *in vitro* release studies to assess drug release over time in order to determine if the NPMD can provide controlled release of CPZ over extended periods of time
5. Extensive investigation of the physicochemical and physicomechanical properties of the optimized membranous device such as swelling, erosion, textural attributes, morphological analysis and porosity analysis

6. To perform *in vivo* animal studies to assess the pharmacokinetic parameters as well the degradation of the NPMD in the New Zealand White Rabbit model and to further assess its histopathological effects on the brain of the rabbit

1.4 Potential benefits of this study

1. Development of a novel biodegradable, biocompatible, neurodurable implantable polymeric drug-carrier device capable of modulated release of an antipsychotic drug over a prolonged period (minimum of 365 days)
2. Increase in patient compliance by decreasing the number of doses to be taken daily
3. Increase in patient compliance by reducing systemic side-effects of antipsychotic drugs
4. Eliminate the “burden of care” phenomenon experienced by care-givers of patients suffering from psychosis
5. Emphasize the benefits of nanobiotechnology and polymeric implantable systems for prolonged targeted CNS drug delivery
6. Creating a platform and expanding polymer-based brain disease therapy to other compounds and neurodegenerative disorders
7. Patenting the developed technology and presentation of results of this study at conferences and publication in high impact factor journals

1.5 Overview of this dissertation

Chapter One provides an introduction and background to this study and outlines the challenges faced with psychoses and CNS drug delivery. This chapter highlights the rationale, aim, objectives and potential benefits of this study.

Chapter Two reviews the polymer-based implantable and transdermal devices previously used the management of major CNS related disorders. In addition, this chapter also focuses on drug delivery approaches employed to traverse the BBB to achieve therapeutic levels of drug within the CNS compartment.

Chapter Three describes the design, development and optimization of the CPZ-loaded, PCL-based nanoparticles utilizing a novel melt-dispersion technique. Preliminary studies investigated the size and stability of the nanoparticles. Furthermore, the ability of the PCL nanoparticles to efficiently entrap the drug of choice, CPZ, was investigated. Preliminary studies led to the establishment of formulation parameters which allowed for the construction of a Face-Centered Central Composite Design (FCCCD) for optimizing the nanoparticle

formulation and attaining a candidate formulation to be incorporated within the implantable membrane. The *in vitro* CPZ release as well as extensive physicochemical and physicomechanical properties of the formulations of the experimental design was studied.

Chapter Four describes the synthesis of a dual-acting nanoparticle formulation that combines the benefits of conventional medicine with complementary and alternative medicines. The fundamentals of this chapter are based on that of Chapter Three in terms of the synthesis method and the materials used. Nanoparticles were synthesized according to a 'One Variable at a Time' (OVAT) approach and comprised cod-liver oil (CLO) from the *Gadus Morrhua* fish. The rationale for the inclusion of CLO into the nanoparticle formulation was based on the well-established neuroprotective and cognitive benefits of omega-3 fatty acids on the brain as well as its ability to aid synaptogenesis and enhance transmission through synapses. The effects of CLO on nanoparticle size, stability, CPZ entrapment and release were investigated.

Chapter Five elucidates the design, development and optimization of a novel polyamide 6,10 (PA 6,10)-ethylcellulose (EC) implantable composite membrane by a novel, modified wet-phase inversion reaction. Preliminary studies investigated the need for an increased unhydrated and hydrated matrix resilience and a decrease in swelling behavior of the composite membranes. Formulation parameters were established to construct a FCCCD to optimized the PA 6,10-EC composite membrane and attain a candidate formulation with a desirable unhydrated and hydrated matrix resiliences and a low swelling potential. Extensive physicochemical as well as physicomechanical testing was conducted on the formulations of the experimental design and the candidate optimized formulation. In addition, the chapter also described the incorporation and assimilation of the optimized CPZ-loaded PCL-based nanoparticle formulation of Chapter Three into the optimized PA 6,10-EC composite membrane to assemble the implantable NPMD. CPZ release from the NPMD was evaluated and compared to that of a commercially available CPZ formulation (Largactil®).

Chapter Six is an *ex vivo* cytotoxicity evaluation of the componential elements of the NPMD, the NPMD itself as well as the CLO and CPZ-loaded nanoparticles and its componential elements synthesized in Chapter Four. Studies were performed on the mammalian PC12-neuronal cell line and details of the assay are highlighted within the chapter.

Chapter Seven describes the *in vivo* evaluation of the NPMD in the New Zealand White Rabbit model. The pilot study describes the implantation of the NPMD in the parenchyma of the rabbit brain in the region of the frontal lobe and assesses parameters such as CPZ

release into the CNS and systemic circulation, degradation behavior of the NPMD as well as its matrix resiliences pre and post-implantation. Histopathophysiological studies were conducted on the brain tissue to assess the biocompatibility of the NPMD. Furthermore, a bioavailability comparison was made between the NPMD and an intramuscular dose of commercially available CPZ (Fresenius Chlorpromazine Hydrochloride®25mg/mL).

Chapter Eight provides the conclusion of this dissertation and discusses limitations, recommendations and future investigations to be performed.

CHAPTER 2

POLYMER-BASED IMPLANTABLE AND TRANSDERMAL DEVICES EMPLOYED FOR THE MANAGEMENT OF MAJOR CENTRAL NERVOUS SYSTEM RELATED DISORDERS

2.1 Introduction

The brain is essential for managing a variety of vital bodily functions and maintaining normality within the healthy body. Higher order neural activity is the consequence of a combination of essential conditions in the brain namely; the efficient liberation of nutrients to the brain, effective waste elimination, neuroprotection from toxic and neuroactive substances circulating within the body, maintenance and repair processes and ultimately homeostasis of the neural micro-environment (Abbott, 2005; Cole and Vassar, 2007; Hsu et al., 2008; Ewing, 2009; Cunnane et al., 2010; Schlegelmilch et al., 2010). Any imbalances in the above-mentioned processes may result in neuropathological, cerebrovascular, inflammatory, carcinogenic or neurodegenerative disorders (Abbot, 2005).

Various innovative strategies including, but not limited to, Deep Brain Stimulation (DBS), cell grafts and gene delivery, have shown potential in treating some of the above mentioned disorders, however drug delivery remains the most popular. Apart from common neuropathological and neurodegenerative diseases, another prime example includes the ever-growing AIDS pandemic. During the course of the disease the HI-Virus may infect the brain. The density of the viral load in the peripheral compartments is effectively reduced by Highly Active Anti-Retroviral Therapy (HAART) however this is not the case in the brain. Owing to the fact that drugs such as azidothymidine, 3TC, or protease inhibitors have minimal penetration into the brain parenchyma, the virus seeks refuge here and continues to multiply, shortening even further the lifespan of the infected individual (Antinori et al., 2003; Kandanearatchi et al., 2003; Pardridge, 2005). Such an occurrence exemplifies the delicate nature of the brain and the vast array of disorders which may affect it. Furthermore, it emphasizes the great need for prolonged drug delivery for CNS disorder in patients on maintenance therapy.

The advent of utilizing polymer-based implantable devices offers many advantages including the ability to accurately control the release of specific quantities of active drugs, macromolecules and proteins over prolonged periods of time as well as the protection of active molecules from degradation prior to release. The issues of non-compliance and the consequences of missing doses, the daily use of oral psychotropic medication and some of the intolerable peripheral side-effects of most psychotropic medication are virtually

eliminated. In addition, polymeric implantable devices decrease the need for having a constant caregiver for CNS patients who are on chronic maintenance therapy. This article reviews the polymer-based implantable and transdermal devices utilized in the treatment of major CNS disorders.

2.2. Drug delivery approaches employed to traverse the blood brain barrier

In order for a small drug molecule to cross the Blood-Brain Barrier (BBB), it must fulfill two general criteria namely: (a) a molecular mass below 400-500 Da and (b) high lipid solubility. It is evident that most drugs do not possess these criteria (Pardridge, 2005). Consequently, the most debilitating and life-threatening diseases are ineffectively and sub-therapeutically treated. The BBB is a pharmacological and physiological barrier situated at the capillaries of the brain where a large variety of cells are present (Figure 2.1).

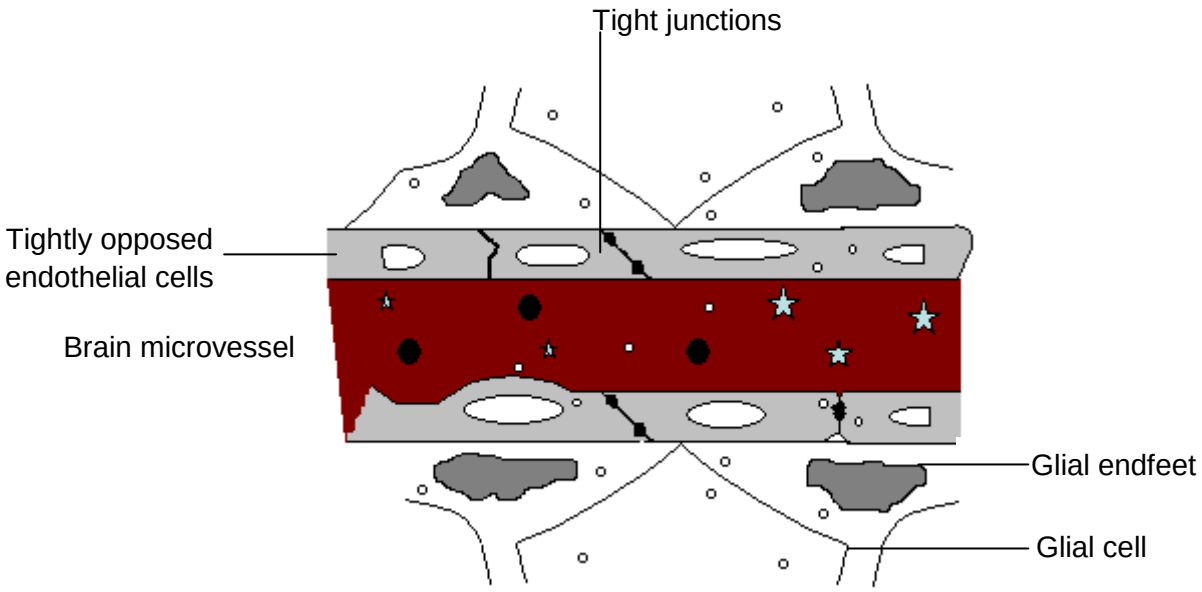

Figure 2.1: A schematic depicting the morphology of the BBB, [Adapted from Patel, 2007].

Tight junctions form an integral morphological trait characteristic of the brain micro-vessel endothelial cells that form the BBB. This coupled with a weakened pinocytic activity and the absence of fenestrations; effectively limits the passage of certain compounds from the blood into the extra-cellular cerebral environment. While nutrients and essential gases are readily exchanged through the barrier, larger molecules such as immune cells, certain microbes and a large variety of drugs are denied entry through the barrier (Soppimath et al., 2001; Wang et al., 2002; Jaypraker et al., 2009). Figure 2.2 is a schematic of the BBB illustrating the various routes of molecular transport across brain capillary endothelial cells.

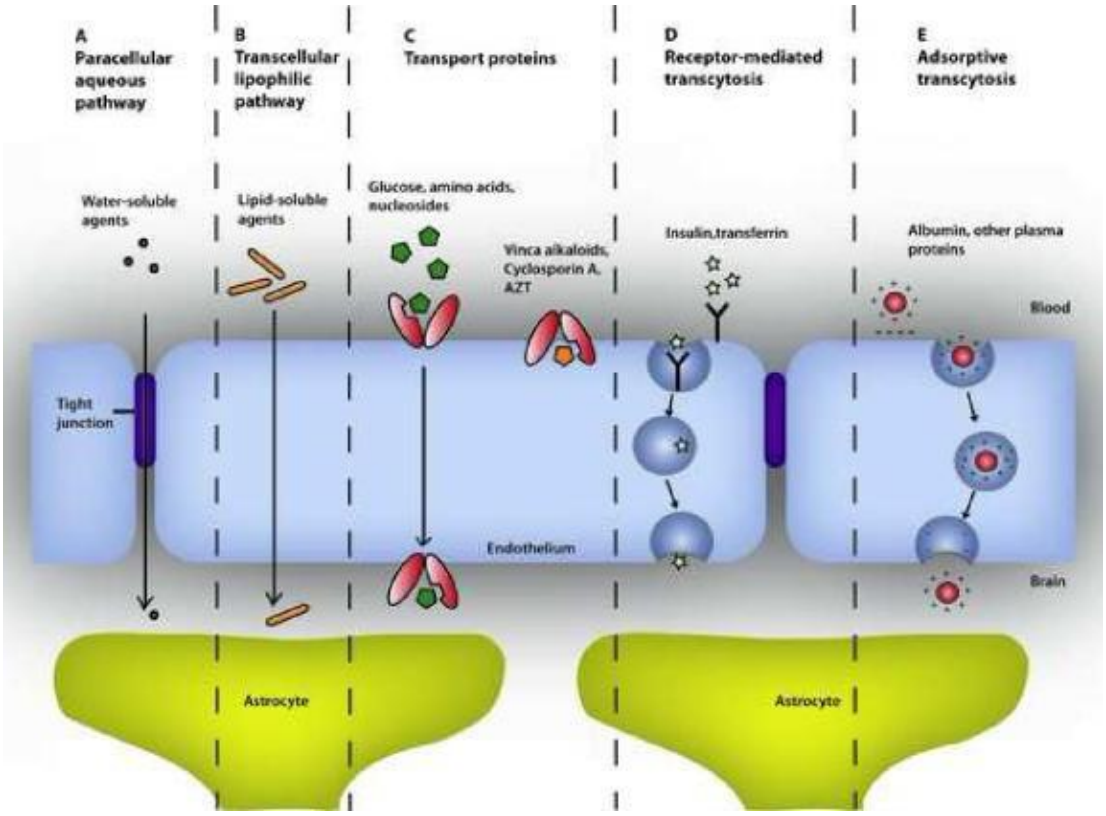

Figure 2.2: Schematic of the BBB illustrating the various routes of molecular transport across brain capillary endothelial cells: A) Water-soluble agents can travel between the endothelial cells via tight junctions, but passage is highly restricted; B) In contrast, lipid-soluble agents easily penetrate the BBB by diffusing across the endothelial cell membranes; C) Carrier proteins present in the membrane facilitate crossing of substances such as monosaccharides, amino acids, peptides, nucleosides, choline, and organic cations and AZT; D) Receptors specific for transferrin, insulin, insulin-like growth factor, lipoproteins, and leptin are also exposed on the surface of the endothelium to aid in penetration via transcytosis; and E) Positively charged molecules can traverse the BBB through adsorptive transcytosis, [Adapted from Bennewitz and Saltzman W.M., 2009].

A difference between the uptake and efflux processes in the BBB determines the net uptake of a given drug by the brain through the BBB (Figure 2.3) (Scherrmann, 2002).
Specific properties of the endothelial cells and the systemic disposition of the drug are integral factors that regulate the uptake of the drug. Drug binding to blood cells or plasma proteins elucidates the unbound drug fraction that may influence uptake. Protein binding may however limit drug uptake by the brain (Park S. and Sinko, 2005; Banks, 2009). The efflux of drug from the Brain Extra-Cellular Fluid (BECF) into the blood through the BBB is modulated by similar properties however protein binding in the BECF does not exist due to the absence of proteins. Consequently, the quantities of drug crossing the BBB in both

directions are actively controlled by the permeability of the endothelial cells and their ability to metabolize the drug.

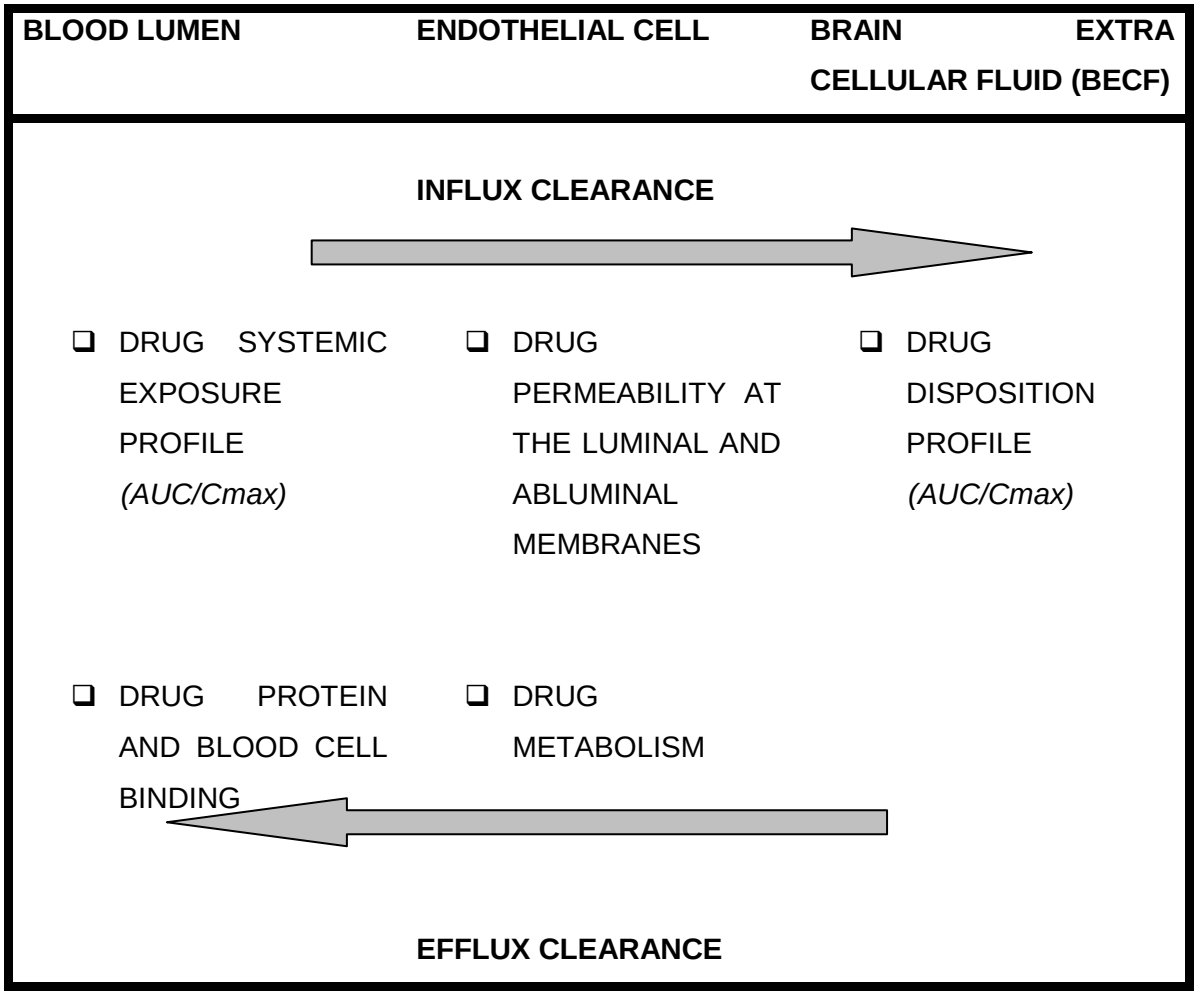

Figure 2.3: Representation of the net uptake of a drug by the brain through the endothelial cell of the BBB determined by the difference of the overall uptake and efflux processes, [Adapted from Scherrmann, 2002].

A variety of techniques have been adopted in an attempt to obtain therapeutic drug levels across the BBB without having to administer potentially toxic oral or intravenous doses of a specific drug. Included in this is injecting the patient at the carotid artery with a hypertonic solution such as mannitol, essentially shocking the tight junctions of the BBB and subsequently opening them momentarily. During this window period, the drug is administered via the carotid artery (Rapoport and Thompson, 1973; Yamaguchi et al., 1990; Guo-yu et al., 2000; Cudmore, 2002; Bryan, 2004). The major shortcoming of this method is that it is non-selective and during the time of junction opening, substances that are potentially toxic to the brain, may enter (Bryan, 2004).

Another method is direct injection into the CNS (Cudmore, 2002). Convection-enhanced delivery deals with the continuous injection of therapeutics under positive pressure through the interstitial space of the parenchyma. This technique, used for optimizing brain disease treatment, allows the passage of larger therapeutic substances across the BBB (Raghavan et al., 2006). Other strategies make use of endothelial cell proteins that would conventionally transport hormones and nutrients to the brain. It is evident that this method could transport a host of molecules, including genes, enzymes and monoclonal antibody drugs, previously too large and incapable of crossing the BBB (Ferber, 2007). Some scientists have used nasal inhalation as a delivery route with direct access to the brain through olfactory and trigeminal nerves, which relay sensory signals from the nose and mouth (Ferber, 2007). Studies have shown that this depends on the molecular weight and lipophilicity of the drug (Perras et al., 1999; Fehm et al., 2000; Illum, 2000; Quay, 2001). Insulin-like growth factor has been shown to bypass the BBB via the intranasal route (Frey, 2001).

Another pivotal area of research involves the use of nanobiotechnology to effectively cross the BBB. Modern therapeutic agents generally have a low permeability across biological membranes, are unstable in the physiological environment, have poor solubilities and essentially exhibit a very low bioavailability. Nanobiotechnology is believed to counteract these negative traits and confer upon the drug an enhanced therapeutic efficacy (Sahoo et al., 2008). Despite the previous methods of drug delivery across the BBB, much focus is on developing novel delivery systems employing nano-particles and nano-liposomes (Bryan, 2004). Using a variety of chemically synthesized polymeric nanoparticles, researchers are exploring the possibilities of delivering oligonucleotides, genes, antineoplastic agents and MRI contrast agents (Silva, 2007).

Site-specific drug delivery utilizing polymeric implantable devices circumvents the difficulties posed by the BBB, limits systemic side-effects, decreases serum protein binding and reduces hepatic metabolism and peripheral drug inactivation. In addition, it avoids the need to administer potentially toxic doses of drugs to achieve therapeutic doses in the CNS (Domb, 1995; Begley, 2004). Varieties of biocompatible synthetic and non- synthetic polymers may be explored for local drug delivery to the brain and include the non-biodegradable ethylene-vinyl acetate copolymer (EVAc), certain polyurethanes and acrylate-based hydrogels as well as the biodegradable poly (lactic-co-glycolic acid) (PLGA), poly (lactic acid) (PLA), poly (hydroxybutyrate), poly (caprolactone), polyanhydrides, cellulose and gelatin (Zhong and Bellamkonda, 2008). Examples of non- synthetic polymers employed for local drug delivery to the brain for the treatment of epilepsy are silk-based polymers.

2.3 Polymer-based implantable devices for major CNS disorders

2.3.1 Intracranial implants

2.3.1.1 Early intracranial implantation

One of the very first attempts to use a controlled release polymeric system implanted in the brain was intended to improve labeling of perivascular meningeal projections in the trigeminal ganglia of the cat model. Elucidating the neuronal connections within the central and peripheral nervous system was made possible through the use of the marker enzyme, Horseradish Peroxidase (HRP). When using HRP in the CNS, the enzyme was often in aqueous solution and administered either by microiontophoresis or stereotaxic injections. A major shortfall of using HRP in an aqueous solution was the fact that the enzyme diffused away from the target site once injected ultimately resulting in false positive results. This was a problem when using the enzyme to map out specific pathways in the brain. This study therefore established an efficient means of overcoming the problem which proved to be effective. Incorporating the HRP within a poly (vinyl alcohol) (PVA) casting solution and simply applying this to the cerebral blood vessels, localizes the HRP delivery to a greater extent. Diffusion of HRP was further curbed by modification of PVA using pure polymer (Mayberg et al., 1981). The ease of implantation led to many researchers exploring the possibility of polymer-based neurotherapy and site-specific drug delivery to the brain for the treatment of various CNS disorders.

2.3.1.2 Application of polymer-based implantable devices in Parkinson's disease

2.3.1.2.1 Biocompatible dopamine-loaded polymeric matrix device

The proposal of using monolithic polymeric brain implants for the treatment of various CNS disorders long exists. The development of a biocompatible dopamine-loaded polymeric matrix device for intracerebral implantation bears testament to this. The device was developed to optimize CNS disorder therapy and to overcome the difficulties presented with drug delivery to the brain. The device comprised dopamine as the active drug dispersed within a variety of EVAc matrix configurations. Initially, it was noted that the *in vitro* cumulative dopamine release from the conventional configurations was found to depend on the original concentration of dopamine matricized within the EVAc network. Modification of the initial systems by coating them with an impermeable layer of EVAc and then forming a void or aperture in the coating resulted in constant, linear and desirable dopamine release characteristics. This optimized formulation was then subjected to *in vivo* analysis in the rat model. Stable dopamine levels in the brain extra-cellular fluid were reached twenty days post implantation and it remained stable for the duration of the experiment which lasted sixty five days. All rats survived the study and histopathological analysis revealed that the striatal

morphology was normal (During et al., 1989; Freese et al., 1989). Despite the promising results of the study, a major concern regarding such a formulation is the fact that EVAc is a non-biodegradable polymer. Apart from implanting the device, additional surgery will be required to remove the device. Furthermore, the sterility of an EVAc device may be questioned if left non-degraded and bathing in the Cerebrospinal Fluid (CSF) as it may pose as an environment for thriving of pathogens.

2.3.1.2.2 Glial cell line Derived Neurotrophic Factor

The symptoms experienced by the patients suffering from Parkinson's Disease (PD) are primarily due to the loss of axons in the striatum which is a result of degeneration and deterioration of nerve cells in the substantia nigra. Early attempts to repair striatal dopaminergic neurons by grafting fetal cells were limited, primarily due to ethical concerns, mortality of the grafted cells and the disposability of donor tissues. Glial cell line Derived Neurotrophic Factor (GDNF) represents the relatively recent identification of neurotrophic factors capable of regenerating and protecting the affected dopaminergic neurons. Despite the benefits of GDNF, its use clinically is limited due to the complexity involved with delivering proteins to brain tissue and the fact that its receptor is located in several areas of the brain causing neurological side-effects. Pre-clinical trials have been conducted and include; the use of non-biodegradable polymeric devices, intraparenchymatous injection, fibrin glue preparation, the grafting of genetically-engineered cells, *in vivo* gene transfer and intracerebro-ventricular infusion. These studies led to a trial using the intracerebro-ventricular infusion method however results depicted a lack of niagrostriatal neuron regeneration and the occurrence of neurological side-effects thus necessitating an alternate means of delivery (Unsicker, 1994; Tomac et al., 1995; Cheng et al., Choi-Lundberg et al., 1997; Rosenblad et al., 1998; Hoane et al., 1999; Kordower et al., 1999; Aoi et al., 2000; Nakao et al., 2000; Tornqvis et al., 2000).

2.3.1.2.3 Biodegradable PLGA microspheres containing GDNF

In a study by Jollivet and co-workers (2004), biodegradable PLGA microspheres containing GDNF were implanted in the rat brain striatum. The Sprague-Dawley rats utilized represented a partial and progressive model of PD. Microspheres were prepared by specialized water in oil in water (W/O/W) emulsion-solvent evaporation technique. Resultant PLGA microspheres produced were smooth, regular and contained a GDNF entrapment of 84%. Prior to stereotaxic implantation into the striatum, microspheres were dispersed in a suspending agent comprising distilled water, Tween 80 and mannitol. Each rat was implanted twice with 1.5mg microspheres in 10µl suspending agent. *In vivo* release kinetics confirmed that GDNF can be released for up to 2 months. In addition, implantable

microspheres were well tolerated and most importantly demonstrated the ability to stimulate sprouting of the preserved dopaminergic fibers with synaptogenesis. This was accompanied by a significant improvement in behavior and function. This study provided a unique and promising advance in the treatment of PD. A major shortfall to the study was the fact that the microspheres were not optimized allowing for a smaller volume for implantation. In addition, there is a need for complementary studies with retrograde labeling (Jollivet et al., 2004). *In vivo* GDNF release could have been improved through incorporation of the microspheres within a polymeric matrix however; the relative ease of microsphere implantation may have been compromised and could have resulted in the need for sophisticated neurosurgery. Furthermore, incorporating the microspheres in a suspending agent could cause premature release of GDNF by diffusion.

2.3.1.2.4 Polymeric scaffold for site-specific delivery of dopamine

A novel comprehensive *in vitro* and *in vivo* study by Pillay and co-workers (2009) illustrated he combined benefits of polymeric nanotechnology and polymer scaffold science to augment the site-specific delivery of dopamine for the possible treatment of PD. The study encompassed the design, biometric simulation and optimization of dopamine-loaded cellulose acetate phthalate nanoparticles matricized within a structured intracranial binary crosslinked alginate scaffold. Nanoparticles were prepared by an adapted oil in water emulsification-diffusion process and displayed a drug entrapment efficiency of approximately 63% after optimization using a Box-Benhken experimental design. The alginate scaffolds, also optimized by a Box-Benhken experimental design, were prepared by crosslinking an alginate in water solution with a primary crosslinking solution, molding the resultant gel-like mass, lyophilizing and suspending the lyophilized structures in a secondary crosslinking solution. Integration of the nanoparticles within the scaffold was completed through a lyo-fusion process. Upon completion of extensive and successful *in vitro* testing, the device was stereotactically implanted into the frontal lobe parenchyma of the Sprague-Dawley Rat Model (Figure 2.4). Blood and CSF samples were taken at predetermined intervals and subjected to Ultra Performance Liquid Chromatography analysis. Results from this study illustrated that the device can provide prolonged, controlled, desirable release of dopamine in the CSF of the Sprague-Dawley rat thus establishing its potential as a candidate for the long-term management of PD (Pillay et al., 2009). Digital images depicting the surgical procedure employed for stereotactically implanting the polymeric scaffold device into the frontal lobe parenchyma of the Sprague-Dawley rat model are presented in Figure 2.4.

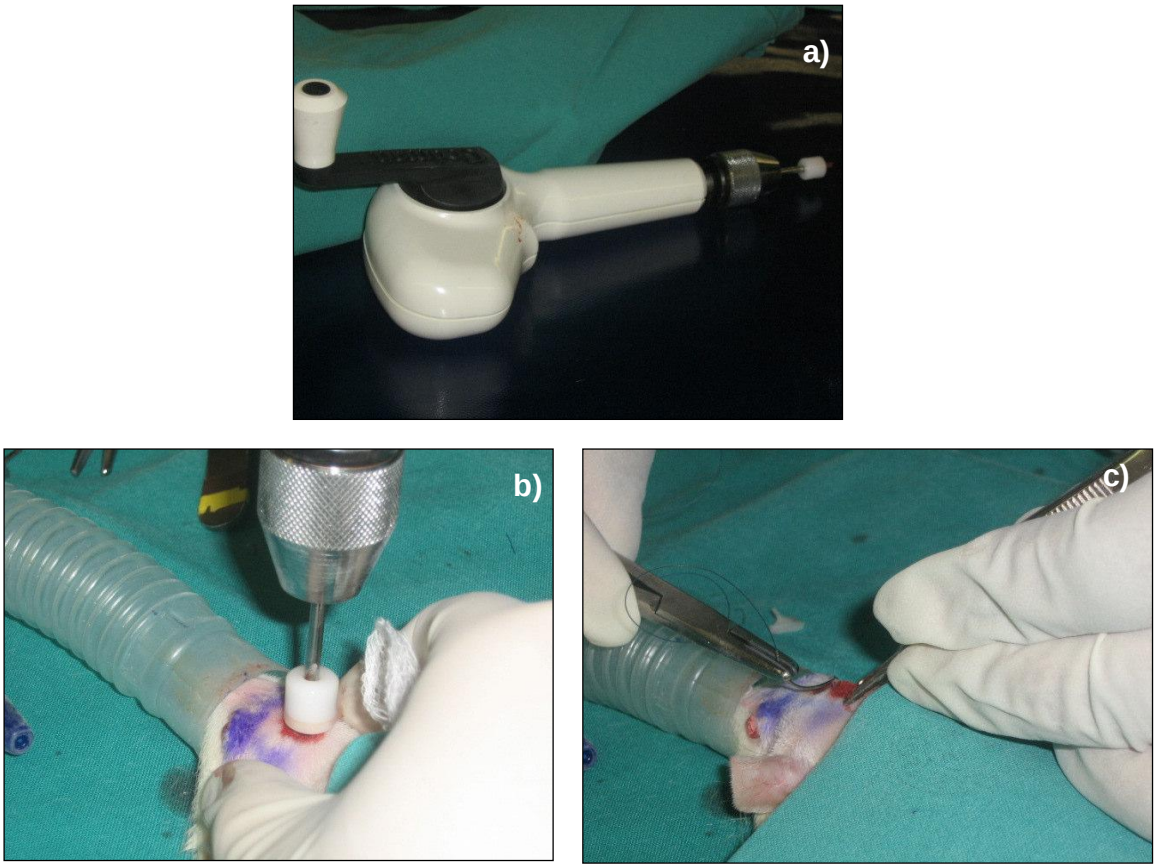

Figure 2.4: Digital images depicting the surgical procedure employed for stereotactically implanting the polymeric scaffold device into the frontal lobe parenchyma of the Sprague-Dawley rat model: a) manual drill used for incision; b) actual perforation of the skull; and c) suturing of the incision [Source: Pillay et al., 2009].

2.3.1.3 Application of polymer-based implantable devices in Alzheimer's disease

2.3.1.3.1 Bethanechol-loaded microspheres for implantation into denervated hippocampal region of the brain

The impairment in learning and memory associated with Alzheimer's disease (AD) is hypothesized to be as a result of a deficiency of acetylcholine in the cortex of the brain. The treatment outcomes of conventional therapy for AD have generally been poor. This, together with the severe recurrent side-effects associated with conventional therapies could be due to a lack of local specificity within the brain as conventional dosage forms are unable to deliver therapeutic agents to specific sub-regions of the brain persistently. To counteract this challenge, bethanechol-loaded microspheres were synthesized. These biodegradable microspheres comprised a 50: 50 copolymer blend of poly-bis-p-(carboxyphenoxy)propane anhydride and sebacic acid (PCPP-SA) and were implanted in the denervated hippocampal region of the rat brain to assess local administration effects. The effectiveness of the technology was determined by a performance score achieved by rats when completing a

maze exercise. Results revealed that hippocampal implants were well-tolerated by all rats. Furthermore, the rats implanted with the bethanechol-loaded microspheres generally exhibited significant and desirable improvement post-implantation, although individual performances did vary within this improved treatment group. Desirable treatment outcomes occurred throughout the duration of the experiment and the study thus established a novel method of localizing neurotransmitter delivery which proved effective in reversing lesion-induced spatial memory deficits in the rat brain (Howard et al., 1989). Figure 2.5 is a schematic depicting the microsphere implantation technique employed.

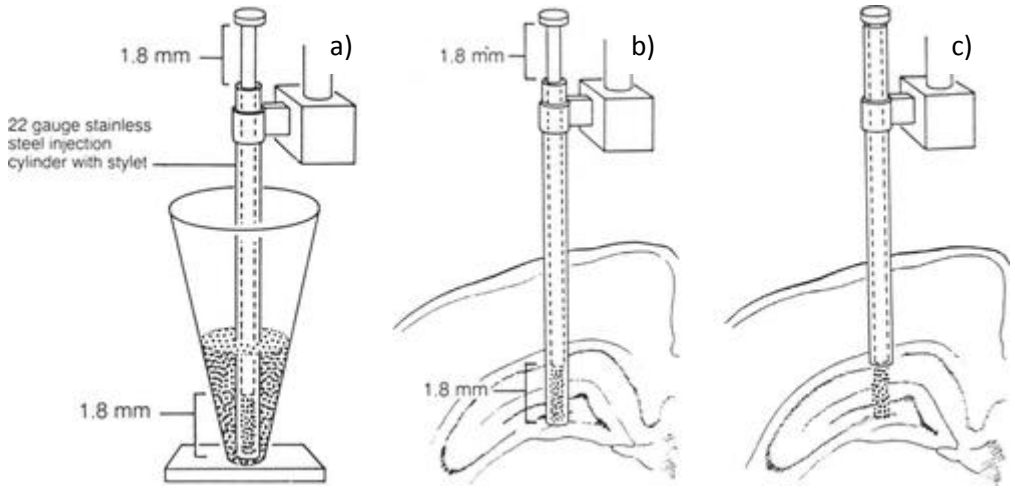

Figure 2.5: A schematic depicting the microsphere implantation technique: a) microspheres are impacted into a No. 22 stainless steel cylinder to a depth of 1.8 mm; b) The implantation assembly is stereotactically placed into the hippocampal formation; and c) the implantation stylette is held stationary as the stainless steel cylinder is slowly raised, leaving a polymer implant column within the hippocampus [Adapted from Howard et al., 1989].

2.3.1.3.2 A biocompatible EVAc matrix incorporating nerve growth factor (NGF) for the potential site-specific treatment of AD

Powell and co-workers (1989) synthesized a biocompatible EVAc matrix incorporating nerve growth factor (NGF) for the potential site-specific treatment of AD. The first stage in the process of synthesizing these matrices involved the production of solid particles containing NGF and ficoll. Briefly, the NGF was reconstituted with phosphate-buffered saline (PBS) and bovine serum albumin (BSA). The solution underwent quick-freezing and lyophilization thereby resulting in a homogenous powder which was then crushed to obtain a uniform particle size. Purified EVAc was dissolved in methylene chloride and the NGF/ficoll powder was added to this solution to obtain a 30-50% loading. The resultant solution was vortexed, producing a homogenous suspension which was cast into a cooled level glass mould. This resulted in the formation of solidified slabs that were subjected to methylene removal.

Resulted slabs were cut into uniform disks and were placed in 10ml PBS at 40°C. BSA was added to the PBS to stabilize the NGF following its release from the polymeric matrix. The study demonstrated a controlled release of NGF over a period of one month and the stimulation of neurite sprouting in NGF sensitized PC-12 cells thus confirming its potential for the treatment of AD (Powell et al., 1989).

2.3.1.4 Application of polymer-based implantable devices in Huntington's disease

Huntington's disease (HD) is a hereditary neurodegenerative disease that is more often than not fatal. The fact that genetic screening may be used to predict persons destined to acquire the disease, makes treatment strategies and formulation approaches for HD very interesting. It has been demonstrated that several neurotrophic factors such as NGF can prevent the neurodegeneration and the behavioral characteristics associated quinolinic acid (QA)-induced HD however; various limitations with the delivery of these proteins do occur including the ability to attain controlled and sustained delivery of these proteins. Menei and co-workers (1999) successfully synthesized NGF-loaded PLGA microspheres to evaluate its release kinetics and its effects against QA-induced excitotoxic damage. Smooth, regular, porous PLGA microspheres were produced by a W/O/W emulsion-solvent evaporation technique. *In vitro* release kinetics was evaluated utilizing radio-labeled NGF, PC-12 cell bioassay and immunozymatic bioassay. This was followed by *in vivo* evaluation following sterotaxic implantation in the rat striatum. Microspheres were implanted a week prior to infusion with QA. *In vitro* results showed that approximately half of the encapsulated NGF was released in a sustained manner over a period of five weeks. Implanted microspheres appeared to contain NGF after two and a half months, degraded after three months and were effective in reducing QA-induced lesions by 40% when compared to control models. The study confirmed that biodegradable NGF-loaded polymeric microspheres implanted locally are neuroprotective against excitotoxic lesions and thus may be effective in the treatment of HD (Menei et al., 2000).

2.3.1.5 Application of polymer-based implantable devices in epilepsy

2.3.1.5.1 Gamma-aminobutyric acid (GABA)-loaded and non-loaded polymeric matrices

Intracerebral implantable devices have been used for the delivery of anti-epileptic drugs (AEDs) and agents known to be beneficial in the treatment of epilepsy. Gamma-aminobutyric acid (GABA)-loaded and unloaded polymeric matrices were successfully implanted in the substantia nigra of the rat brain to evaluate its anti-epileptic potential following electrical stimulation. On the second day following implantation, rats implanted with GABA-loaded matrices only experienced focal limbic seizures and were devoid of major generalized

seizures of whereas rats implanted with unloaded matrices experienced generalized seizures. However, GABA levels did drop a week after implantation and thus the anti-epileptic effects of the implant diminished (Kokaia et al., 1994).

Kubek and co-workers (1998) successfully developed a polyanhydride-based micro-disk implant containing thyrotropin-releasing hormone (TRH) intended for the treatment of epilepsy. TRH is not a traditional AED but is an endogenous hormone known to have anticonvulsant effects in animal seizure models and intractable epileptic patients. Its use however, is limited by its minimal site-specific bioavailability and short duration of action. The micro-disk was sterotactically implanted in the amygdala of the rat kindling model of temporal lobe epilepsy. The implant was successful in extensively suppressing the kindling expression. In addition, anticonvulsive effects were still observed fifty days after implantation thus verifying that the device is a potential long-term epilepsy treatment modality (Kubek et al., 1998).

2.3.1.5.2 EVAc as a prototype biocompatible polymer employed for local drug delivery to the brain

EVAc polymers have found a wide application for use as an intracerebral delivery vehicle for a variety of neurological conditions (During et al., 1989; Freese et al., 1989; Hoffman et al., 1990; Saltzman et al., 1999; Sanberg et al., 1993). The first polymer-based Adenosine Augmentation Therapy (AAT) approach was performed by Boison and co-workers (1999) using EVAc polymers engineered to release adenosine. Individual polymers were implanted into the lateral brain ventricles of rats that had been kindled in the hippocampus. It was observed that, in these rats stimulus-induced epileptic seizures were drastically reduced after polymer implantation. This was demonstrated by a strong reduction of stage 5 seizures for at least 7 days and by suppression or reduction of epileptiform electrical after discharges up to 3 days as recorded bilaterally in the hippocampus. Upon diminishing the supply of adenosine, the anti-seizure effects gradually decreased and had expired after 14 days. Control implants that were loaded with BSA failed to display any antiepileptic activity or changes in stimulus-evoked EEGs. It was further confirmed that the local release of 20 to 50ng adenosine per day is sufficient to exert a significant antiepileptic effect. This study demonstrated that the focal controlled release of adenosine within the brain could suppress epileptic seizures.

2.3.1.5.3 EVAc implants containing phenytoin

Phenytoin is a commonly used AED that has been investigated for use intracerebrally. EVAc implants containing phenytoin have been implanted in the cortex of the rat model. Seizures,

induced by the delivery of cobalt chloride to the cortex, were significantly reduced in rats receiving phenytoin from the implant when compared to a control group (Tamargo et al., 2002). In another study, phenytoin was loaded in a titanium dioxide (TiO_2) reservoir and implanted in the temporal lobe of Wistar rats. The device was deemed biocompatible and safe as no histological damage was observed. The study, however, did not assess the extent of anticonvulsive effects produced by the device (Lopez et al., 2007). In a related study, a nanostructured sol-gel TiO_2 reservoir was implanted into the amygdala of kindled rats. The reservoir contained valproic acid and twelve months after implantation, it remained undamaged and showed no evidence of injury to surrounding neuronal tissue (Lopez et al., 2007). The use of intracerebral AED delivery in general is highly beneficial considering the spontaneous onset of seizures and the intolerable systemic side-effects of AEDs. Prolonged therapy is ideal as issues of AED non-compliance are abolished and epileptic patients are kept in maintenance and safeguarded from the consequences of seizures in general.

2.3.1.5.4 Stem cells as direct transplantation tools for epilepsy therapy

Recently, stem cells, stem cell-derived neural precursors, neuronal cell lines and fetal hippocampal neurons have received much attention as direct transplantation tools for epilepsy therapy (Boison, 2007; Raedt et al., 2007; Shetty and Hattiangady, 2007; Loscher et al., 2008; Suter and Krause, 2008; Boison, 2009). It has been shown that with the use of stem cells, therapeutic strategies are possible and may synergistically augment each other. Noteworthy is that, fetal hippocampal cell grafts exhibited robust long-term survival (> six months) and integration in animal models of epilepsy (Rao et al., 2006). While functional integration of graft-derived cells is needed for these restorative approaches, stem cell- or neural progenitor-derived brain-implants can be engineered to release therapeutically active molecules with the aim to provide therapeutic benefit by paracrine mechanisms. Thus, a combination of functional integration and paracrine drug delivery may provide synergistic benefits.

2.3.1.5.5 Silk-based polymers as an alternative to synthetic drug delivery systems for the treatment of epilepsy

A novel generation of silk-based drug-delivery systems has recently been developed as an alternative to synthetic drug delivery-systems for the treatment of epilepsy (Boison, 2009). Among the several advantages that they offer is the fact that silk fibroin is biocompatible (Altman et al., 2003) and capable of steady biodegradation (Horan et al., 2005). The degradation lifetimes of silk can be regulated by the extent of physical crosslinking for beta sheet formation, thus allowing control of degradation timeframes from weeks to years (Horan et al., 2005). Silk can also be processed under aqueous conditions, thus allowing for the

incorporation of labile biomolecules without loss of biological activity (Jin and Kaplan, 2003; Li et al., 2006). Furthermore, the frequent use of silk sutures in brain and nerve tissue confirms the feasibility of implantation of silk biomaterials in the brain (Boison, 2009). In a study that was conducted by Wilz and co-workers (2008), silk-based polymers were engineered to release target release rates of 0, 40, 200, and 1000ng adenosine per day. These polymers were implanted into the intrahippocampal fissure of rats prior to the onset of kindling. It was demonstrated that by using this approach the focal adenosine release from silk-based polymers was effective in retarding kindling epileptogenesis in a dose-dependent manner (Boison, 2009).

2.3.1.6 Application of polymer-based implantable devices in AIDS Dementia Complex

AIDS Dementia Complex (ADC) is a debilitating complication of HIV/AIDS that affects the brain and CNS and culminates in cognitive impairment as well as motor and behavioral dysfunction. Zidovudine (AZT) is generally used as the drug of choice due to its desirable brain and CNS penetration (Portegies et al., 1989; Frumkin, 1992; Kim et al., 1996; Cysique et al., 2006). A novel study by Harilall (2011) investigated the design development and optimization of a multipolymeric nanoparticulate scaffold for implantation into the frontal lobe of the Sprague Dawley Rat brain for the treatment of ADC (Harilall, 2011). AZT-loaded, alginate nanoparticles were prepared by a controlled gelification approach and optimized utilizing an experimental design. A multipolymeric implantable scaffold containing the biodegradable polymers; polycaprolactone (PCL), epsilon caprolactone (ECL) and cellulose acetate phthalate (CAP) were prepared by crosslinking and optimized using an experimental design. The optimized nanoparticle formulation was then dispersed with the optimized multipolymeric scaffold to form novel implantable device and the device was sterotactically implanted into the frontal lobe of the Sprague Dawley Rat as depicted in Figure 2.6. Results revealed that the implantation procedure was successful with a considerable distribution of AZT in the CSF.

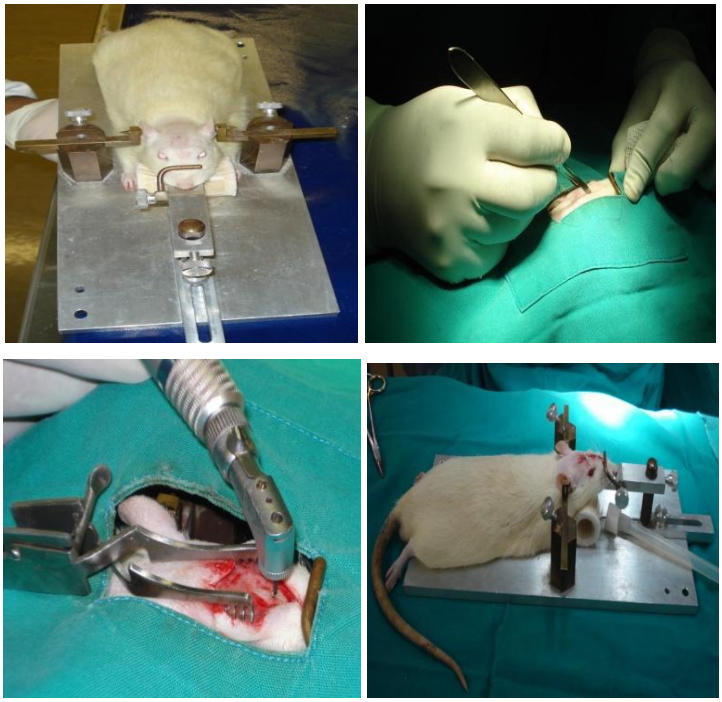

Figure 2.6: Intracranial implantation of the multipolymeric nanoparticulate scaffold in the Sprague Dawley Rat for the potential treatment of ADC, [Adapted from Harilall, 2011].

2.3.1.7 Application of polymer-based implantable devices in brain tumors and carcinogenesis

2.3.1.7.1 Gliadel® technology for the localized treatment of glioblastoma multiforme

Gliadel® is an innovative technology, approved by the United States Food and Drug Authority (FDA) and other regulatory agencies worldwide, for the localized treatment of glioblastoma multiforme. Despite aggressive therapy with surgery, chemotherapy and radiation, the prognosis for primary malignant gliomas is poor, as the average survival time is below a year. Furthermore, recurrence of tumors is a common problem. The Gliadel® polymeric device is a PCPP-SA copolymer blend and houses the drug carmustine (BCNU) (Figure 2.7). Up to eight Gliadel® wafers may be utilized following removal of the tumor and results appear to be promising. Pre-clinical testing demonstrated a localized inflammatory reaction which was not linked to any neurological deficits or pathological changes in the relevant animal model. The localized inflammation was transient and resolved within a period of five weeks.

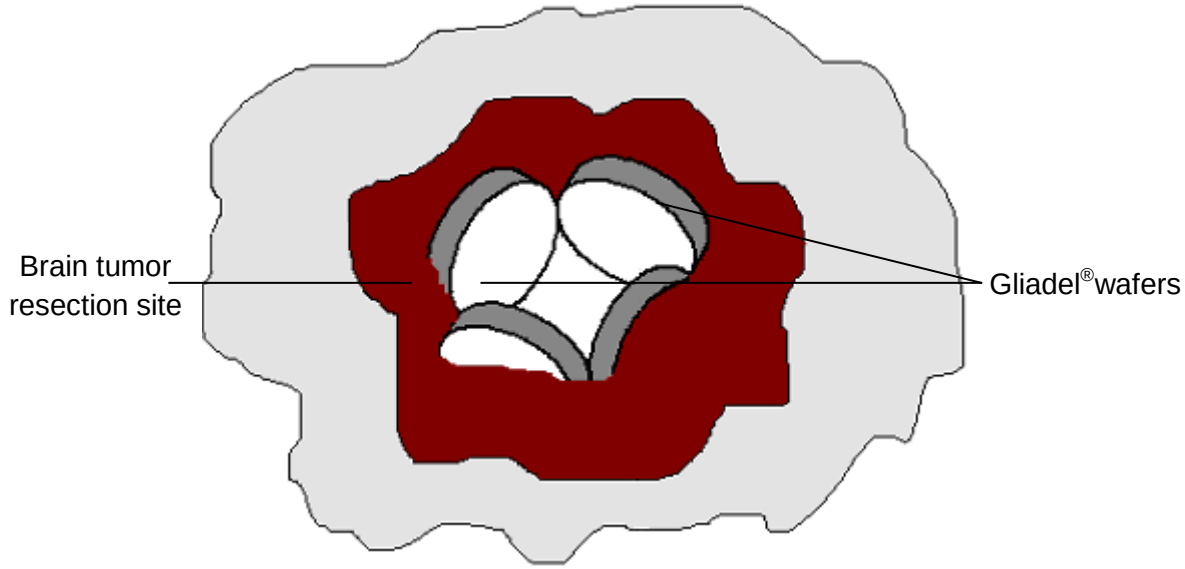

Figure 2.7: Implantation of Gliadel® at tumor resection site, [Modified from Jain et al., 2005].

Biodistribution studies indicated that the device exhibited desirable drug concentrations at the site of action for prolonged periods. Metabolic distribution and elimination studies were also performed on the device and results confirmed the biodegradable nature of the copolymer blend and its potential to be used for the specific delivery of drug to certain target organs. Furthermore, the device is excreted from the body principally through the kidneys whereby the water-soluble BCNU and sebacic acid are rapidly removed and the carboxyphenoxypropane is gradually excreted due to its insoluble nature. Toxicity studies established that the device was non-toxic and biocompatible. Lastly, efficacy testing revealed a 5.4-7.3-fold increase in median survival as compared to a 2.4-fold attained by conventional systemic therapy. Clinical trials confirmed its safety and efficacy and hence it was granted FDA approval in 1996 (Domb et al., 1994 and 1995; Brem et al., 1995; Guerin et al., 2004; Jain et al., 2005).

2.3.1.7.2 Amsacrine-loaded polymeric device for interstitial malignant glioma chemotherapy

An amsacrine-loaded polymeric rod is an additional matrix type implantable delivery system investigated for use in interstitial malignant glioma chemotherapy. This is an EVAc rod synthesized by an extrusion method. *In vitro* release studies displayed a burst release of amsacrine followed by a stable sustained linear release for a minimum of six months. Further *in vitro* studies utilizing rat glioma (RG2) in cell culture depicted that the device was effective in killing these cells in a dose-dependent manner. *In vivo* studies employing a tumor-implanted rat model demonstrated potent anti-tumor activity as well as an increased

survival when compared to control models. In addition, the device proved to be biocompatible as no evidence of toxicity was observed (Wahlberg et al., 1996).

2.3.1.7.3 A polyanhydride-based implantable matrix for intracranial glioma therapy

Combination therapy with a biomodulator drug, radiosensitizer and External Beam Radiotherapy (EBR) has been investigated for the treatment of intracranial glioma in the rat model. Tumors, induced by sterotaxic implantation of cultured C6 cells into the rat brain, were treated with a polyanhydride-based, bis(*p*-carboxyphenoxy)propane-sebacic acid (CPP-SA), implantable polymeric rod. The C6 cell line is a clonal line derived from a rat glioblastoma induced by administration of *N*-nitrosomethylurea in Winstar rats. Once implanted, the C6 cells produce intracerebral tumors that closely resemble the traits of spontaneous gliomas. Bromodeoxyuridine (BrdUrd), a radiosensitizing agent and *N*-(phosphonacetyl)-L-aspartic acid (PALA), a biomodulator drug were incorporated into the polyanhydride-based implantable rod. Implantation of the BrdUrd-PALA-loaded polymeric rod was at the site of C6 cell implantation twelve days following tumor implantation. EBR treatment was given as 10-MeV X-rays following anesthesia. The efficacy of the combination therapy was evaluated on the basis of survival of the rats and the "triple therapy" was shown to be highly effective with clinical potential (Li et al., 2004). Regardless of the promising results of the study, treatment involves two procedures namely; implantation of the polymeric rod followed by anesthesia and EBR. This can be highly technical and may prove to be impractical.

2.3.1.7.4 Drug-loaded PLGA microspheres as an effective anti-cancer agent against malignant glioma

The use of carboplatin as an effective anti-cancer agent against malignant glioma is limited due to the significantly high systemic dose required to achieve therapeutic levels at the tumor. This is primarily due to the inability of the drug to traverse the BBB. Chen and co-workers (1997) successfully synthesized carboplatin-loaded PLGA microspheres that were delivered intracerebrally in the rat model. There were no signs of neurotoxicity or systemic toxicity associated with the microspheres although implantation did cause a transient, localized inflammatory reaction that was well tolerated. *In vivo* release studies demonstrated apparent zero-order kinetics over a period of one month thus confirming a novel method of prolonged effective carboplatin delivery for the treatment of malignant glioma (Chen et al., 1997). In another study, Gavin and co-workers (2005) ascertained that Poly(D,L-Lactide) microspheres carboplatin can be easily prepared by the emulsification-spray drying technique. The microspheres obtained (Figure 2.8) displayed a well controlled delivery of carboplatin *in vitro*. Both drug-free and carboplatin-containing microspheres displayed skin

biocompatibility. Furthermore, they didn't induce any local toxic reaction (Gavin et al., 2005). These results indicate that biodegradable microspheres may have a potential application as an efficient system for the local delivery of carboplatin in supporting surgical resection of tumors.

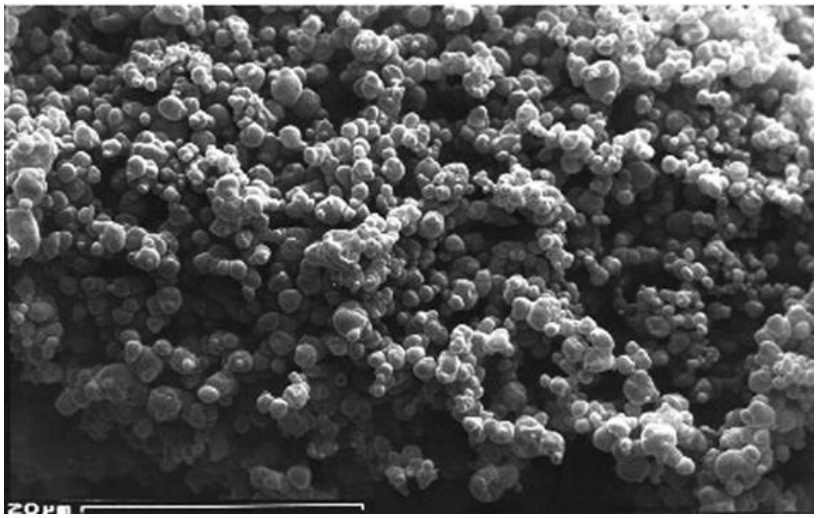

Figure 2.8: SEM depicting spray-dried Poly (D,L-Lactide) microspheres containing carboplatin for post surgical chemotherapy against malignant glioma (magnification 575x362), [Adapted from Gavin et al., 2005].

A pilot study by Menei and co-workers (1999) demonstrated the use of biodegradable lactic and glycolic acid copolymer microspheres for the local and sustained delivery of 5-Fluorouracil (5-FU) for the radiosensitization of glioblastoma following surgical resection. The study included eight patients with newly diagnosed glioblastoma. Following resection, patients were implanted with 5-FU microspheres in the wall of the surgical bed. EBR was given to patients approximately seven days post implantation. Results depicted sustained concentrations of 5-FU in the CSF and relatively low concentrations in the blood. Furthermore, limited systemic toxicities were observed and the advent of using implantable microspheres for the treatment of glioblastoma was very promising (Menei et al., 1999).

A Phase 1 clinical study by Menei and co-workers (2004) involved implantation of the microspheres by sterotaxy, into deeply situated and inoperable tumors. The microspheres were generally well tolerated except in four of ten patients, who experienced worsening of pre-existing symptoms. There were no signs of edema or hematological complications and the system was therefore deemed efficient for the treatment of certain inoperable and deep brain tumors (Menei et al., 2004). Roullin and co-workers (2004) determined the effectiveness radiosensitizing 5-FU-loaded PLGA microspheres implanted sterotactically in

Sprague-Dawley rats bearing C6 tumors. The study proved that the controlled release of 5-FU from these PLGA microspheres is a highly effective approach for radiosensitizing gliomas (Roullin et al., 2004). A related study utilizing NGF-loaded PLGA microspheres focused on the intraseptal implantation of the microspheres in the region of axotomized septal cholinergic neurons. To evaluate the microspheres *in vivo* activity, both NGF-loaded and unloaded PLGA microspheres were sterotactically implanted in the rat brain. A third group of non-treated axotomized rats were also evaluated. Both NGF-loaded and unloaded microspheres displayed an identical non-specific glial cell reaction post implantation. Furthermore, the microspheres were biocompatible as there was no evidence of neuronal toxicity. The survival of axotomized cholinergic neurons was significantly enhanced following NGF-loaded microsphere implantation whereas unloaded microspheres offered no neuroprotection. Non-treated rats displayed a noticeable loss of cholinergic neurons on the lesion side when compared to the contra-lateral side. The study thus confirmed the neuroprotective capabilities of NGF and an effective implantable polymeric carrier of the neurotrophic factor in PLGA (Pèan et al., 2000).

The use of implantable microspheres in general can be enhanced and optimized in the formulation process. Administration of microspheres which are not matricized, leads to the delivery of a finite quantity of active delivered all at once. Incorporating the microspheres in a biocompatible matrix further controls the release of active and release rates ranging from months to years can be achieved. This is beneficial for patients suffering from neurodegenerative diseases and psychiatric conditions where prolonged therapy is required. Furthermore, microspheres are protected from degradation and it is theoretically easier to achieve delivery at a desired region of the brain and at the very site of implantation as microspheres are not allowed to disperse to multiple regions of the brain.

2.3.1.7.5 Paclitaxel-loaded PLGA discs for the treatment of malignant glioma

Biodegradable microfiber discs and sheets are additional technologies investigated for the treatment of malignant glioma *in vitro* and *in vivo*. The PLGA discs and sheets containing paclitaxel were produced by a specialized electrospinning process. The fibrous nature of the discs and sheets are advantageous to drug release in that it displays a greater surface area to volume ratio. *In vitro* release studies depicted a sustained release of paclitaxel for over eighty days after an initial minor burst release. *In vitro* cell apoptosis testing revealed that the PLGA discs/sheets were superior to conventional paclitaxel delivery in terms of cytotoxic effects and drug sustainability. *In vivo* studies involved the implantation of C6 glioma cells subcutaneously in the BALB/c nude male mice model followed by implantation of the polymeric matrices after twelve days. Mice treated with the PLGA discs/sheets displayed

significant tumor inhibition when compared to controls and mice treated with conventional paclitaxel therapy (Ranganath and Wang, 2008).

Earlier related studies by Lee and co-workers (2005) involved the synthesis of a BCNU-loaded PLGA wafer for 9L gliosarcoma chemotherapy. Wafers were produce by vortex-mixing the BCNU and PLGA and then compressing using a Carver Hydraulic Press. The anti-tumor effects of the wafers were investigated *in vitro* against 9L gliosarcoma cells and *in vivo* against a subcutaneous solid tumor model of 9L gliosarcoma. The wafers inhibited the growth of the tumors significantly when compared to BCNU powder and increasing the dose of BCNU within the PLGA wafer resulted in an increased release rate of BCNU as well as significant regression of tumor (Lee et al., 2005). The major shortfall with these studies is that the *in vivo* models used possessed subcutaneous-induced tumors. Whilst desirable tumor inhibition was observed, this does not indicate directly, the effects on surrounding brain tissue or brain function as the environments differ. Furthermore, it is difficult to make the assumption that the same behavior will be observed intracranially.

2.3.1.7.6 Therapeutic efficacy study in an intracranial humanglioblastoma xenograft model using paclitaxel-loaded PLGA nanofiber discs

In one of the most recently conducted studies, Ranganath and co-workers (2010) evaluated and demonstrated the therapeutic efficacy of local chemotherapy of malignant glioblastoma using 9.1% ($^{w}/_{w}$) paclitaxel-loaded polylactide-co-glycolide (PLGA) nanofiber discs and 16.7% ($^{w}/_{w}$) paclitaxel-loaded PLGA microspheres entrapped in hydrogel matrix, through bioluminescence luciferase imaging. The study concluded that submicron/nanoscale implants were able to demonstrate optimal paclitaxel pharmacokinetics in the brain/tumor with significant tumor inhibition in a glioblastoma xenograft model in mice and hence may be potentially useful in the treatment of highly recurrent malignant glioblastoma (Ranganath et al., 2010).

2.3.1.8 Application of polymer-based implantable devices in cerebral edema

The use of a dexamethasone-loaded EVAc matrix system as an intracranial or intraperitoneal implant for the reduction of cerebral edema associated with brain tumors has been well studied (Reinhard et al., 1991; Park et al., 2003; Tamilvanan et al., 2008; Saraon et al., 2010). Steroids have been shown to be effective in the treatment of cerebral edema however; their use is limited due to their systemic side-effects. Reinhard and co-workers (1991) investigated an alternate method of steroid delivery to the brain which involved the local or site-specific delivery of dexamethasone using a polymeric carrier. The Fisher 344 rat model was used and tissue concentration post implantation was quantified by high

performance liquid chromatography and selective extraction. Dexamethasone was present in the brain in significant concentrations for up to twenty one days post intracranial implantation. Further research suggested that it was possible to attain drug release for up to several months. The study confirmed that intracranial implantation of dexamethasone-loaded polymeric implants are just as effective as high-dose systemic dexamethasone when treating peritumoral edema and has significant benefits over conventional dosage forms (Reinhard et al., 1991).

2.3.2 Subcutaneous and subdermal implants

Subcutaneous implants have the potential to be an effective means of treating certain psychoses such as schizophrenia (Siegel et al., 2002; Rabin et al., 2008). Surgically implantable haloperidol-loaded, biodegradable PLGA pellets have demonstrated stable drug release patterns over a period of five months *in vitro* thereby superseding conventional depot formulations as a more effective means of treating psychotic episodes over prolonged periods of time. Furthermore, *in vivo* results in the rat model depicted an increase in striatal dopamine (D_2) receptor expression thus validating the effectiveness of the drug delivery system (Siegel et al., 2002).

A similar study by Rabin and co-workers (2008) utilizing risperidone-loaded PLGA implantable pellets and rods, describes drug release patterns for a minimum of two months confirming the value of such a system for the long-term treatment of schizophrenia (Rabin et al., 2008). Should a patient experience intolerable side-effects, the implants can be immediately removed thereby conferring upon the systems, a degree of reversibility not offered by conventional dosage forms. Furthermore, the biodegradability of the system ensures that no additional surgery will be required to remove the device.

Other applications of subcutaneous implants relate to the use of non-biodegradable but biocompatible polymer matrices for the treatment of cancer pain and opioid dependence (US Patent 6126956). Included in this, is the incorporation of hydromorphone within a polyethylene-vinyl acetate matrix which was subsequently coated with methyl methacrylate. The device offers the controlled release of hydromorphone with pseudo-zero order kinetics for prolonged periods thereby providing adequate analgesia for cancer pain and significantly controlling opiate addiction. Hydromorphone levels are kept within therapeutic range, preventing the potentially lethal consequences of fluctuating drug levels. In addition, the device does not cause an immune response and cannot be abused.

Gold and co-workers (1993) demonstrated the use of implantable morphine pellets in the rat model to effectively determine the time course for the progression of tolerance, dependence and abstinence (Gold et al., 1993). Related studies display the use of buprenorphine (Probuphine®) (Figure 2.9) and naltrexone implantable devices for opioid dependence (Iyer et al., 2007; Montoya and Vocci, 2008; Reece, 2009; White et al., 2009).

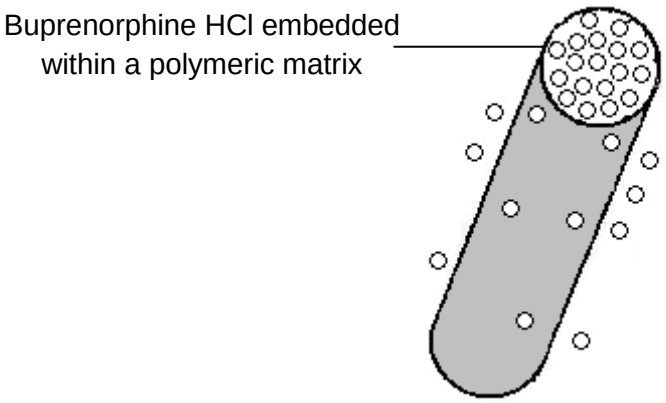

Figure 2.9: Probuphine® comprising buprenorphine HCl embedded within an EVAc matrix for the potential prolonged treatment of opioid addiction modified from http://www.titanpharm.com/products-candidates-probuphine.php [Accessed November 21, 2010].

Naltrexone, an opioid receptor antagonist, proved to be a desirable option when formulating the subcutaneous implant owing to the fact that non-compliance is a major impediment to treatment and furthermore, the drug is marketed as an oral formulation. Probuphine®, intended for the treatment of heroin addiction, comprises the opioid receptor partial agonist buprenorphine within an EVAc matrix in the form of match-stick sized formulations implanted in the subdermal region with the potential to release drug over a period of six months. This sustained release formulation elicits therapeutic dominance over the conventional daily or every-other day sublingual formulations (White et al., 2009). The non-biodegradable nature of the EVAc may prove disadvantageous however the use of biodegradable polymers may yield toxic metabolites upon degradation thereby rendering the product hazardous. The use of subcutaneous and subdermal implantable devices in general offers a host of benefits when compared to conventional dosage forms. Among these include, a reduced hepatic metabolism and peripheral drug inactivation resulting in a greater bioavailability of the drug when compared to oral dosage forms. Furthermore, drug release over an extensive period provides remission and stability to the patient for prolonged periods when compared to depot formulations. Despite the advantages, systemic toxicities are not evaded as seen with the majority of intracerebral implants.

2.3.3 Intrathecal implants

The foundations of Intrathecal Drug Delivery (ITDD) are based on the fact that therapeutic efficacy of strong analgesics can be achieved by the action of the drugs at the dorsal horn of the spinal cord, without the need to administer potentially toxic doses of the drug systemically. Conventional types of ITDD devices include: the percutaneous catheter (tunneled or not tunneled) used with an external pump; the totally implanted catheter with a subcutaneous injection port connected to an external pump; fully implanted fixed rate intrathecal drug delivery systems and fully implanted programmable intrathecal drug delivery systems. Due to cost issues, external pumps are preferred to implantable systems for the management of cancer pain (The British Pain Society, 2008).

A novel approach by Jeon and co-workers (2006) investigated the possibility of intrathecally implanting micro-encapsulated xenogenic Adrenal Medullary Chromaffin Cells (AMCCs) for the purpose of chronic neuropathic pain relief. Neuropathic pain can be a result of injury or dysfunction of the CNS and is generally unresponsive to conventional analgesic or to interventional therapies. Furthermore, it is a major medical and social burden with considerable cost implications. Owing to the fact that the AMCCs produce endogenous opioids and catecholamines which act as effective analgesics in the CNS, their antiallodynic effects on chronic neuropathic pain induced by Chronic Constriction Injury (CCI) of the sciatic nerve in the rat model were investigated. AMCCs, obtained from bovine adrenal glands, were encapsulated with alginate and poly-L-lysine, rendering them undetectable by the immune system of the body. The major advantage of micro-encapsulation is the fact that high dosage immunosuppressant drugs are not required for AMCCs implantation. High dose immunosuppressants are associated with severe systemic side-effects and susceptibility to opportunistic infections. AMCCs-loaded microcapsules were produced by first suspending the cells in a sodium alginate and sodium chloride mixture and dropping this suspension into a calcium chloride solution thereby forming AMCCs-loaded microcapsules. The microcapsules were coated in poly-L-lysine and finally re-suspended in a sodium alginate solution to form the outer layer of the capsule membrane. Implantation of approximately five hundred AMCCs-loaded and unloaded microcapsules occurred a week after CCI in two randomly allocated rat groups. Briefly, implantation involved a L5 posterior laminectomy and an incision in the dura mater. The outcomes of the study suggest that CSF levels of endogenous opioids and catecholamines were significantly higher than controls and the intrathecal implantation of encapsulated AMCCs resulted in a decreased mechanical and cold allodynia in a neuropathic pain model (Jeon et al., 2006).

The use of microcapsules can also be further optimized to achieve prolonged desired release rates. Considering the financial burden associated with treatment of chronic neuropathic pain, this approach would be particularly valuable.

2.4 Transdermal patches

Transdermal Drug Delivery Systems (TDDS) are of great benefit when a patient experiences intolerable gastro-intestinal side-effects as well as dysphagia when using conventional oral dosage forms. Furthermore, it may be of particular importance to patients who should not self-medicate with their analgesia and those with cognitive impairment. The skin presents a large surface area for absorption of drug and it is a non-invasive procedure. In addition, first-pass metabolism is avoided and predictable extended duration of activities may be achieved (Sugibayashi and Morimoto, 1994; Naik et al., 2000).

Theoretically, TDDS operate via a simplistic mechanism whereby relatively high concentrations of a particular drug are loaded within a patch which is applied to the skin. The high concentration of drug in the patch relative to the lower blood concentration facilitates diffusion of the drug into the blood through the skin maintaining a constant drug concentration in the blood (Chopda, 2006) (Figure 2.10). TDDS systems bearing nicotinic agonists, nicotine in particular have been vastly used as an adjunct to smoking cessation and in the treatment of nicotine withdrawal (Balfour and Fagerström, 1996). Furthermore, these agents have been found to treat and alleviate the symptoms of cognitive impairment associated with neurodegenerative diseases, psychoses such as schizophrenia and attention disorders (Decina et al., 1990; Sahakian and Jones., 1991; Jones et al., 1992; Levin, 1992; Adler et al., 1993; Wilson et al., 1995; Conners et al., 1996; Levin and Simon, 1998; Gorell et al., 1999; White and Levin, 1999; Rusted et al., 2000; Rezvani and Levin, 2001; Quik, 2004; Singh et al., 2007).

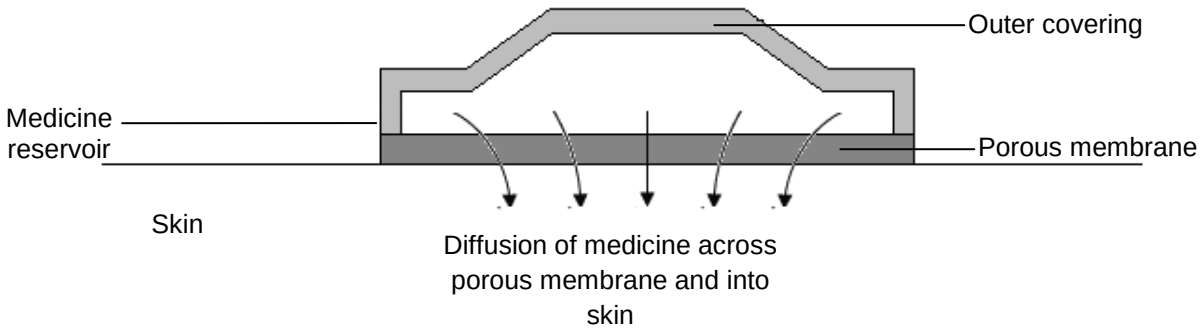

Figure 2.10: Simplistic representation of the mechanism of action of a typical TDDS, [Adapted from Shah, 2008].

It is believed that the neuroprotective properties of nicotine are a result of stimulation of the α7 nicotinic receptors. Stimulation of these receptors allow for an increased release of dopamine from the striatum thereby conferring protection upon the neurons of the nigrostriatal pathway (Rezvani and Levin, 2001; Singh et al., 2007). This proves to be beneficial when considering the neurodegenerative diseases namely PD and AD.

Through unknown mechanisms, transdermal nicotine can improve the symptoms of ADHD. Drugs such as methylphenidate and amphetamine are conventional therapeutics used for ADHD and work by increasing dopamine stimulation. Considering the fact that nicotine causes increased dopamine release, the two are closely related which may be the reason for nicotine's beneficial traits when treating ADHD (Rezvani and Levin, 2001).

A similar study by Arnold and co-workers (2007) establishes the use of a novel methylphenidate patch as an effective means of treating ADHD over a prolonged period of time. In this system, the matrix serves as the skin adhesive as well as the reservoir. By manipulating patch size and duration of patch adhesion to the body, it is possible to calculate the optimum dose required for the individual patient (Arnold et al., 2007).

A study conducted by Sittl and co-workers (2002) described the use of a buprenorphine transdermal system as an effective means of treating severe chronic pain associated with cancer and other disorders, without needing to use oral analgesic preparations. In addition, transdermal buprenorphine was associated with an improved duration of sleep. Central and gastro-intestinal side-effects experienced were mild to moderate in nature and were probably associated with the initiation of opioid therapy (Sittl et al., 2002).

A novel transdermal system containing the antidepressant drug selegiline, has revealed significant inhibition of central monoamine oxidase A (MAO-A) and B (MAO-B) enzymes. Although the overall antidepressant effects of the system are relatively modest, this system possesses the advantage of bypassing liver and intestinal monoamine oxidase enzymes (Amsterdam, 2003).

Commercially available TDDS affecting the CNS include; NeuproR®, a rotigotine-loaded TDDS used to alleviate the symptoms of early-stage idiopathic PD, Nicotinell®, Nicodern® and Prostep® containing nicotine for smoking cessation, Matrifen® and Duragesic® containing the opioid fentanyl for the treatment of moderate to severe pain and Transderm-Scop® housing the drug scopolamine for the treatment of motion sickness. Patented TDDS include

a transdermal buprenorphine device for the treatment of pain associated with sickle cell disease (Shah, 2008).

Despite the advantages of TDDS, a major shortcoming of the technology is the fact that systemic side-effects are not completely prevented and may still affect patient compliance and disease prognosis especially with disorders of the CNS (Henningfield et al., 2005). Furthermore, the device may not be suitable when using drugs which require rapid titration. A minor disadvantage of the system could possibly be that the patient has complete control and access with regards to removal of the device at any time due to occurrences such as local irritation at the site. Although trivial, such spontaneous actions may negatively affect disease prognosis especially when addressing certain CNS disorders.

2.5 Concluding Remarks

CNS disorders are extremely common and are generally sub-therapeutically treated. There is thus a great need for prolonged, controlled psychotropic drug release which allows for an extended duration of action, increased patient compliance and a decrease in rates of relapse and care-giver burden. This is, more often than not, unachievable by conventional therapies. Implantable polymeric and transdermal drug delivery systems have been shown to be capable of curbing the difficulties associated with conventional therapy. Despite some of the disadvantages of these systems, the insurmountable benefits outweigh the risks and there is thus potential for polymer-based implantable and transdermal devices being used as first-line therapy when managing CNS disorders.

CHAPTER 3

DESIGN, DEVELOPMENT AND OPTIMIZATION OF CHLORPROMAZINE-LOADED, POLCAPROLACTONE-BASED NANOPARTICLES UTILIZING A SPECIALIZED MELT-DISPERSION TECHNIQUE

3.1 Introduction

Nanotechnology provides many promising solutions to impediments arising from conventional neurotherapy. One of the major advantages of using nano-carriers is the fact that modification of the drug, intended for CNS delivery, is not required. Furthermore, surface modification of these diminutive particles may allow for brain entry of the drug molecules after an intravenous dose. This is achieved by receptor-mediated transport (Wohlfart et al. 2011). A number of studies have established the successful nano-encapsulation of antipsychotic drugs in order to optimize neurotherapy of psychotropic disorders (Manjunath and Venkateswarlu, 2005; Muthu et al., 2009; Benvegnu et al., 2011; Seju et al., 2011; Silva et al., 2011).

Benvengu and co-workers (2011) successfully incorporated the antipsychotic drug, haloperidol into polysorbate nanocapsules. Extensive *in vivo* testing on the Wistar rat model proved that the method was feasible in terms of improving the efficacy of haloperidol with antipsychotic effects of the drug being maintained for longer periods of time when compared to free haloperidol. In addition, the acute and sub-acute extra-pyramidal motor disorders were also significantly reduced when compared to the administration of free haloperidol (Benvengu et al., 2011).

Muthu and co-workers 2009 synthesized risperidone-loaded, poly(D,L-lactide-co-glycolide) (PLGA) nanoparticles that were matricized in a thermo-responsive *in situ* gel and administered subcutaneously in the Swiss albino mouse model. The antipsychotic effects of risperidone as well the marked lack of extra-pyramidal side effects were demonstrated by the system, thus confirming its success (Muthu et al., 2009). A similar study by Silver and co-workers 2011, investigated the potential of entrapping risperidone in solid lipid nanoparticles (SLN), intended for oral administration. Results revealed highly stable risperidone-loaded SLN's with negligible toxicity when tested with Caco-2 cells using the (4,5-dimethylthiazol-2-yl)2,5-diphenyl-tetrazolium bromide MTT assay (Silva et al., 2011).

With regard to the design of nanoparticles in optimizing therapeutic efficacy and success, various parameters need to be considered. Factors such as lipophilicity, polarity, particle

size, drug entrapment and drug release kinetics are all relevant. Popular methods for the design and development of nanoparticles include, 1) the solvent evaporation method, 2) spontaneous emulsification/solvent diffusion method, 3) salting-out/emulsification-diffusion method, 4) supercritical fluid technology, 5) ionic gelation and 6) polymerization of monomers techniques (Soppimath et al., 2001; Hans and Lowman, 2002; Reis et al., 2006). Most of these methods prove unsatisfactory and are related to many shortcomings such as; the inability to scale-up for large-scale pilot production, limited solubility of polymers in supercritical fluids and most of all, toxicity of using organic solvents. Apart from being environmentally hazardous, organic solvent impurities may remain in the nanoparticle post-synthesis and become physiologically dangerous and may even cause degradation of the active within the polymer matrix (Soppimath et al., 2001).

Therefore, this study uses the principle of adaptation and implements a melt-dispersion technique for the preparation of chlorpromazine hydrochloride (CPZ)-loaded nanoparticles taking into consideration the chemical and molecular properties of the polymer to be used, poly-ε-caprolactone (PCL) and the active drug CPZ. PCL is a hydrophobic, semi-crystalline, thermoplastic polymer with five non-polar methylene groups in its repeating unit and a relatively polar ester group. Under physiological conditions, PCL undergoes very slow biodegradation by hydrolysis of its ester linkages and is biocompatible with surrounding tissues. This has sparked widespread interest in the polymer for use in long-term drug delivery systems lasting greater than a year (Sinha et al., 2004; Wei et al., 2009; Kumari et al., 2010). The use of PCL nanoparticles to successfully entrap a variety of pharmacological actives to improve their therapeutic efficacy has been well documented and some of these actives include but are not limited to; anti-cancer drugs, anti-inflammatories, beta-blockers, anti-infective agents, insulin, immune modulators, proteins and psychotropic agents (Sinha et al., 2004; Kumari et al., 2010). The majority of PCL nano-carriers are synthesized by nanoprecipitation, solvent displacement and solvent evaporation (Kumari et al., 2010). As previously discussed, these methods utilize hazardous and potentially physiologically dangerous organic solvents.

The aim of this study was to design, synthesize and optimize CPZ-loaded, PCL-based nanoparticles using a melt-dispersion technique that is non-arduous, inexpensive and devoid of any hazardous organic solvents, thereby eliminating the limitations of conventional nanoparticle synthesis, in particular, PCL-based nanoparticle synthesis. The study also takes advantage of the thermoplastic nature of PCL which allows it to become soft and pliable once heated passed its melting point and then subjected to extreme shear whilst cooling to room temperature, thereby reforming the PCL and maintaining its integrity.

3.2 Materials and Methods

3.2.1 Materials

Poly-ε-caprolactone (PCL), chlorpromazine hydrochloride (CPZ) (*M*w 355.33 g/mol), glycerol B.P. and polysorbate 80 were purchased from Sigma Aldrich (St. Louise, MO, USA). De-ionized water was obtained from a Milli-Q water purification system (Milli-Q, Millipore, Billerica, MA, USA). All other reagents were of analytical grade and used as purchased.

3.2.2 Construction of a Face-Centered Central Composite Design

The processing variables required for the synthesis of the novel CPZ-loaded, PCL-based nanoparticle formulations and a summary of the effects reflected in advanced preformulation studies are shown in Table 3.1. Subsequent to this, the most influential variables were used to construct a Face-Centered Central Composite Design (FCCCD) comprising 13 statistically derived formulations (Table 3.2). The design was used to determine the direct additive effects of the study variables on the physicochemical and physicomechanical properties and interactive effects on the novel CPZ-loaded, PCL based nanoparticle formulation. Experimental trials were performed on formulations of various combinations of polymers and stabilizers. PCL (1000-3000mg) and polysorbate 80 (2-5%$^{v}/_{v}$) were selected as the independent formulation variables. Particle size, zeta potential and drug entrapment efficiency were selected as the formulation responses. The stirring speed was kept constant at 1500rpm despite preformulation studies indicating that variations in stirring speed affected both the size of the nanoparticles as well as the CPZ entrapment. The rationale for this was simply because the accurate and precise measurement of speeds from 500-1000rpm, 1000-1500rpm and 1500-2000rpm was impossible due to the graduating limitations of the equipment. The speed of 1500rpm did prove to have a desirable effect on the responses achieved during advanced preformulation studies. Similarly, a temperature of 90°C was also used constantly as temperatures below 90°C and up to the melting point presented with difficulties as the molten PCL could not be appropriately sheared by the top stirrer resulting in large agglomerates and the inability to form nanoparticles. In addition, a modest increase in temperature > 90°C resulted in the CPZ entrapment being decreased and drastic increases > 90°C resulted in minor changes to the chemical backbones of both PCL and CPZ. A statistical model incorporating interactive and polynomial terms was utilized to evaluate the responses. Response surface plots were constructed to visually represent the influence of the stabilizer and polymeric concentrations on the nanoparticle size, zeta potential as well as CPZ encapsulation efficiency.

Table 3.1: Processing variables required for the synthesis of the novel CPZ-loaded, PCL based nanoparticles and their effects on the nanoparticle formulation based on advanced preformulation studies.

Processing variable	Effect on nanoparticle formulation
PCL levels	
< 1000mg	Very poor CPZ entrapment (≤875.32µg) Good sizes achieved (≤232.70nm) No change to zeta potential
> 3000mg	CPZ entrapment more desirable then when PCL<1000mg but only modestly better when compared to CPZ entrapment when 1000mg≤PCL≤3000mg. Size of particles dramatically increase over and above the range for optimal nanoneuropharmaceutics (≥672.30nm) No change to zeta potential
Polysorbate 80 levels	
< 2%$^{w}/_{v}$	Incipient loss of stability of emulsion (clumping)
> 5%$^{w}/_{v}$	Decrease in CPZ entrapment (≤4172.31µg) Moderate increase in zeta potential (-29.30 to -30.30mV) Moderate increase in particle size (253.40-267.50nm) Incipient phase inversion
Top stirrer speed	
General ↓ < 1500rpm	Particle size increase above the range for optimal nanoneuropharmaceutical application Inability to achieve high sheering, PCL agglomerates rapidly upon cooling to room temperature Moderate increase in CPZ entrapment (8955.78-9325.85µg) No change to zeta potential
General ↑ >1500rpm	Modest decrease in particle size (113.30-130.70nm) Decrease in CPZ entrapment (≤1632.56µg) No change to zeta potential
Temperature	
General ↓ < 90°C up to melting point of PCL	Inability to form particles by shearing force of top stirrer, rapid agglomeration.
General ↑ > 90°C	Decrease in particle size (≤95.30nm) Drastic decrease in CPZ entrapment (≤535µg) No change to zeta potential

Table 3.2: FCCCD template with statistically generated formulations.

Std Order	Run Order	Pt Type	Blocks	Polycaprolactone (mg)	Polysorbate 80 (%v/v)	Glycerol (mL)	Stirring Speed (rpm)	CPZ (%w/v)
10	1	0	1	2000	3.5	65	1500	5
4	2	1	1	3000	5	65	1500	5
2	3	1	1	3000	2	65	1500	5
11	4	0	1	2000	3.5	65	1500	5
5	5	-1	1	1000	3.5	65	1500	5
6	6	-1	1	3000	3.5	65	1500	5
9	7	0	1	2000	3.5	65	1500	5
1	8	1	1	1000	2	65	1500	5
7	9	-1	1	2000	2	65	1500	5
8	10	-1	1	2000	5	65	1500	5
12	11	0	1	2000	3.5	65	1500	5
3	12	1	1	1000	5	65	1500	5
13	13	0	1	2000	3.5	65	1500	5

3.2.3 Preparation of nanoparticles

Nanoparticles were prepared by a novel melt-dispersion technique according to the FCCCD template shown in Table 3.2 and the process is outlined in Figure 3.1. PCL (1000-3000mg) was firstly dispersed in 65mL of glycerol and this was subjected to heating to 90°C and magnetic stirring at 200rpm while on a heat modulated magnetic stirrer. A 5%$^{w}/_{v}$ aqueous CPZ solution containing polysorbate 80 (2-5%$^{w}/_{v}$) was also heated to 90°C. Following adequate melting of PCL in the glycerol melting base, the molten solution was transferred to a high-speed, high-shear top stirrer rotated at 1500rpm. This was followed by the drop-wise addition of the heated CPZ and polysorbate 80 solution to the molten solution. The solution was allowed to stir at 1500rpm on the top stirrer for 45 minutes until cooled to room temperature. Nanoparticles were allowed to cure for 15 minutes and were processed by centrifuging at 3000rpm, removing the supernatant, re-dispersing in de-ionized water three times followed by collection of the nanoparticle sediment, freezing at -75°C for 48 hours and lyophilization to form a free-flowing powder. Due to the high viscosity of glycerol, de-ionized water was added to the nanoparticle solution just prior to centrifuging. Glycerol was chosen as the appropriate melting base due to the fact that it degrades at a temperature >280°C (Glycerol MSDS, Santa Cruz Biotechnology, Inc.).

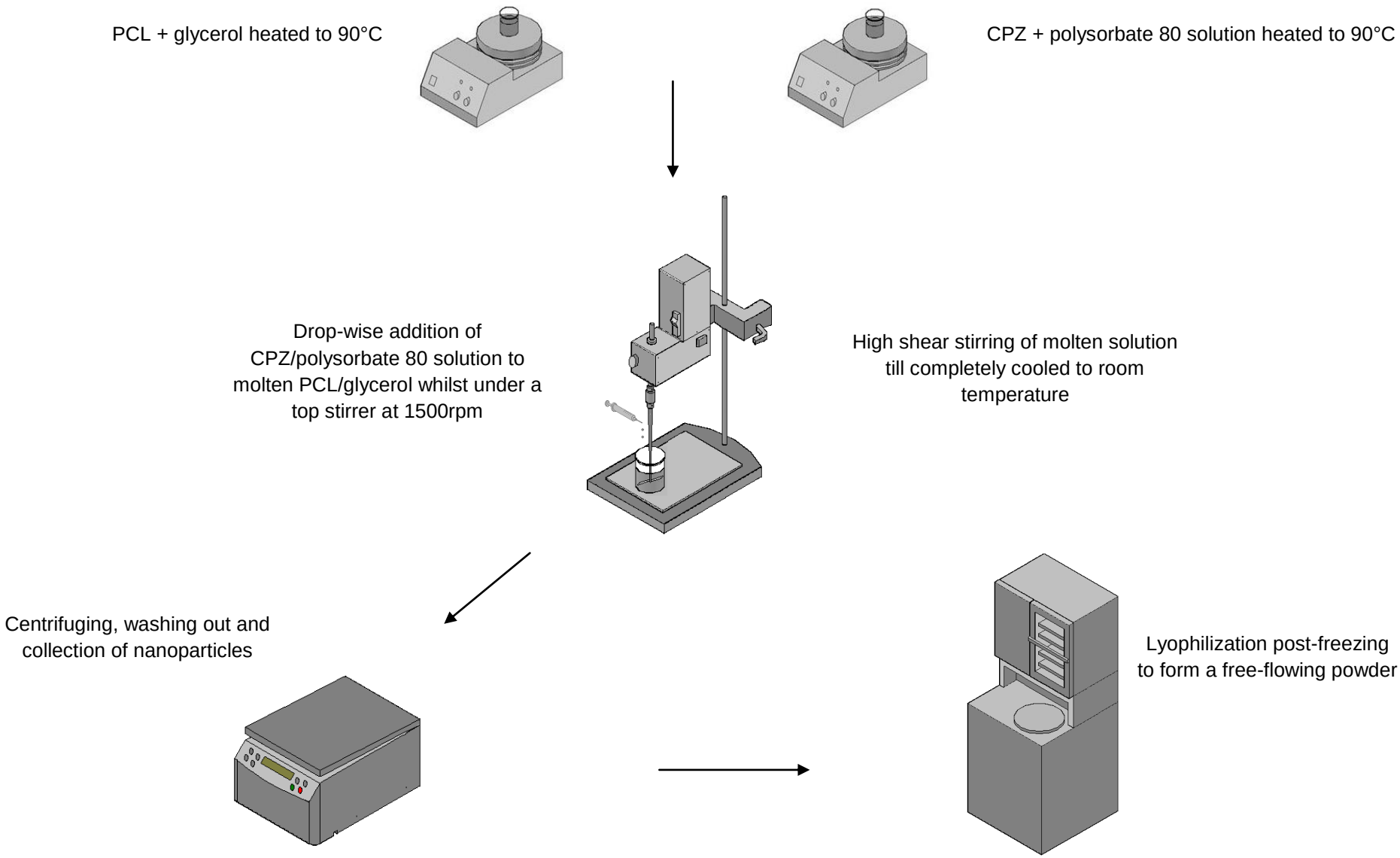

Figure 3.1: Schematic depicting the synthesis process of the CPZ-loaded, PCL-based nanoparticles by the novel melt-dispersion technique.

3.2.4 Polymeric structural variation analysis and thermal transition behavior to determine the possibility of thermo-degradation of constituents used for nanoparticle synthesis

Owing to the fact that the melt-dispersion technique is a process that uses relatively high temperatures, Fourier Transform Infrared (FTIR) spectroscopy, Differential Scanning Calorimetry (DSC) and Temperature-Modulated Differential Scanning Calorimetry (TMDSC) were performed to assess the possible presence of thermo-degradation.

3.2.4.1. Fourier transform infrared spectroscopy

Fourier Transform Infrared Spectroscopy (FTIR) utilizing a Spectrum 100 FTIR Spectrometer (PerkinElmerLife And Analytical Sciences Inc., Shelton, CT USA) was used to detect the vibration characteristics of chemical functional groups in a sample, in response to infrared light interactions. The structures of PCL, CPZ and polysorbate 80 were firstly assessed at room temperature. This was followed by heating of PCL, CPZ and polysorbate 80 to 100°C, allowing it to cool and then assessing the structural backbones of these agents once again. Any obvious discrepancies between both sets of results would confirm possible changes to the chemical compounds and possible degradation. FTIR was also performed on CPZ-loaded PCL nanoparticle formulations to assess the potential for any variation in vibrational frequency caused as a result of nanoparticle formulation.

3.2.4.2. Differential scanning calorimetry and temperature-modulated differential scanning calorimetry

Differential Scanning Calorimetry (DSC) and Temperature-Modulated Differential Scanning Calorimetry (TMDSC) (DSC 1 STAR^{e} Mettler Toledo system, Uster, Zürich, Switzerland) were performed on native CPZ, PCL and the CPZ-loaded, PCL-based nanoparticles to further assess the thermal behavior of the constituents and thus pinpoint any thermo-degradation at the temperatures used in the melt-dispersion technique. DSC and TMDSC were also performed to determine the possibility of any interactions that may have occurred during the melt-dispersion technique. Calibration of temperature and enthalpy on the instrument were done using indium and zinc. The heating rate was set at 10°Cmin^{-1} under a dry nitrogen atmosphere (Afrox, Germiston, Gauteng, South Africa) with a flow rate of 200mLmin^{-1} acting as the purge gas in order to reduce oxidation. Samples sizes of 5-10mg were accurately weighed into standard 40µL aluminium open pans and sealed hermetically. This was followed by pinholes being punched on the lids of the aluminium pans. Samples were then heated from 0-300°C and held at 300°C for 3 minutes. This was done to evaporate any moisture in the sample and to eliminate any thermal history. The samples were then quenched from 300-0°C at a rate of 20°Cmin^{-1}. The midpoint melting point (T_m)

obtained from the melting point depression was determined according to the peaks generated on the experimental DSC curves on heating the samples from 0-300 °C.

3.2.5. Construction of calibration curves for the ultraviolet spectrophotometric determination of CPZ entrapment and release

An ultraviolet spectrophotometric scan was run to determine the maximum wavelength for CPZ absorption in Phosphate Buffered Saline (PBS). It was found that CPZ exhibits two maximum wavelengths at λ_{254} and λ_{319}. This is consistent with the literature published on CPZ (Abadi et al., 1999). Using a known series of concentrations of CPZ in PBS, two calibration curves at both the aforementioned wavelengths were constructed. The linear curve was plotted with the observed absorbance of CPZ as the dependent variable and the concentration of CPZ as the independent variable. A statistical representation of the degree at which the function fits the set of values (R^2 value) was computed for both curves.

3.2.6 Drug entrapment and yield of nanoparticles

The dry weight of the PCL nanoparticles was measured and compared to the dry weight of the initial formulation components. CPZ entrapment was determined by dissolving 100mg nanoparticles in 100mL of PBS, pH 7.4, 37°C. CPZ content (µg) was assessed in triplicate and determined by ultraviolet spectroscopy (Cecil CE 3021, Cecil Instruments Ltd., Milton, Cambridge, UK) at 319nm against standard constructed curves.

3.2.7 Size and Zeta-Potential determination of nanoparticles by Dynamic Light Scattering

A Zetasizer NanoZS (Malvern Instruments Ltd, Malvern, Worcestershire, UK) incorporating dynamic light scattering techniques at 37°C at varying angles was used to determine the average sizes and size distribution of the nanoparticles produced, as well as their zeta potentials. A $1\%^{w}/_{v}$ was appropriately diluted with de-ionized water, filtered using a 0.22µm filter (Millipore Co., Massachusetts, USA) and placed into disposal cuvettes (size) or capillary cells (zeta potential) (Malvern Instruments Ltd., Malvern, Worcestershire, UK). The viscosity and refractive index of the continuous phase were set to those specific to de-ionized water. Measurements were taken in triplicate to validate the reproducibility of the experiment.

3.2.8 Morphological characterization of nanoparticles using Transmission Electron Microscopy

Nanoparticle size and shape was explored in great detail utilizing cryo-Transmission Electron Microscopy (TEM) (JEOL 1200 EX, Tokyo, Japan, 120keV). Samples were

prepared by placing a dispersion of nanoparticles in ethanol on a copper grid with a perforated carbon film followed by evaporation and viewing at room temperature.

3.2.9 *In vitro* CPZ release studies from PCL nanoparticles

In vitro release studies were performed on the CPZ-loaded PCL nanoparticle formulations utilizing an orbital shaker bath (Labex, Stuart SBS40®, Gauteng, South Africa) set at 25rpm. Due to the diminutive size of the nanoparticles and concerns of particle loss when sampling, particles were placed in dialysis tubing membranes and then immersed in 100mL PBS (pH 7.4, 37°C) contained in 150mL glass jars. At predetermine time intervals 3mL samples of the release media were removed, filtered through a 0.22µm Cameo Acetate membrane filter (Millipore Co., Bedford, MA, USA) and analyzed by UV spectroscopy at a maximum wavelength of 319nm for CPZ content analysis. CPZ release was quantified using a linear standard curve (R^2=0.99). To maintain sink conditions an equal volume of CPZ-free PBS was replaced into the release media. A model independent analysis, the time point approach, was used to analyze dissolution data to provide a more accurate analysis of CPZ release kinetics whereby mean dissolution time after 30 days (MDT_{30}) was calculated using Equation 3.1.

$$\mathrm{MDT} = \sum_{i=1}^{n} \mathrm{t}i \frac{\mathrm{Mt}}{\mathrm{M}\infty} \qquad \textit{Equation 3.1}$$

Where Mt is the fraction of dose released in time ti = (ti + ti-1)/2 and M∞ corresponds to the loading dose (Pillay and Fassihi, 1999).

3.2.10 Constraint optimization of formulation responses

A model-independent approach (Minitab® V15, Minitab Inc., PA, USA) was used to optimize the nanoparticles. Statistical optimization was therefore employed to ascertain the ideal polymeric and stabilizer combination with the desired physicochemical properties capable of attaining desirable particle sizes, zeta potentials and CPZ entrapment efficiencies.

3.3 Results and Discussion

3.3.1 Preparation of nanoparticles

The melt-dispersion technique is a non-arduous technique that does not require the use of organic solvents as do most conventional methods for conventional nanoparticle synthesis. This is highly beneficial considering the toxicity associated with organic solvents and the cost implications thereof. The thermoplastic nature of PCL has proved to be of great benefit in that PCL can easily be manipulated once passed its melting point and exposed to high

shearing force. Nanoparticle collection post-curing is one of the major difficulties associated with the melt-dispersion technique. The high viscosity of glycerol makes separation and centrifuging of the particles complex as particles tend to be dispersed in the supernatant as opposed to sedimenting. This was overcome by the addition of de-ionized water to the nanoparticle solution post-curing. The miscibility of water with glycerol allowed for a decrease in viscosity of the solution which made it more favorable to centrifuging and the nanoparticle sedimenting thereby allowing for collection, freezing and lyophilizing, forming a free-flowing powder (Figure 3.2). The addition of water could however impact parameters such as drug-loading and diffusion of the highly water-soluble CPZ out of the nanoparticles.

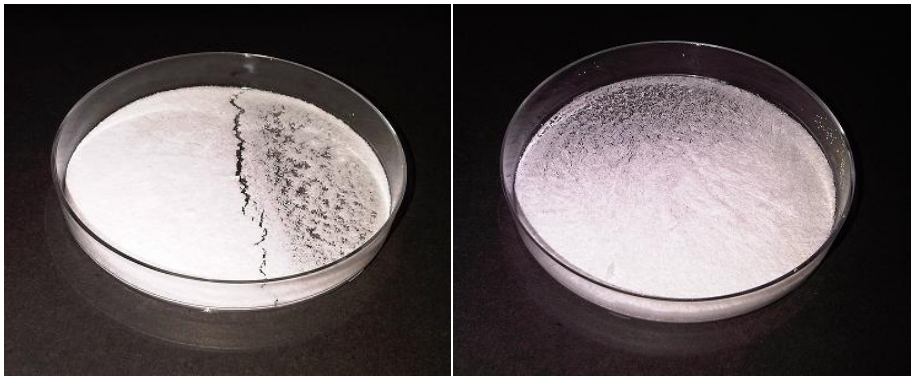

Figure 3.2: Digital images of nanoparticle formulations post lyophilization.

3.3.2Polymeric structural variation analysis and thermal transition behavior to determine the possibility of thermo-degradation of constituents used for nanoparticle synthesis

FTIR was performed on PCL, CPZ and polysorbate 80 at room temperature as well as samples of PCL, CPZ and polysorbate 80 which were heated to 100°C and then allowed cool (Figure 3.3). Spectra obtained for room temperature samples as well as samples that were heated too 100°C and cooled were super-imposable. This thereby confirmed that the temperatures used for the melt-dispersion technique did not degrade each of the components utilized in the melt-dispersion technique. The characteristic peaks of PCL (2944.96cm^{-1}, 2866.68cm^{-1}, 1720.81cm^{-1}, 850-1480cm^{-1}) all appear in both PCL at room temperature and PCL heated to 100°C then cooled to room temperature. 2944.96cm^{-1} is indicative of asymmetric CH_2 stretching whereas the peak at 2866.68 cm^{-1} is indicative of symmetrical CH_2 stretching. The strong band at 1720.81 cm^{-1} is a result of the carbonyl stretching vibration (Elzein et al., 2004; Wu et al., 2004). The characteristic peaks of CPZ (2934.21cm^{-1}, 2394.92cm^{-1}, 1563.67cm^{-1}, 1458.12cm^{-1}, 730-850cm^{-1}) all appear in both CPZ at room temperature and CPZ heated to 100°C then cooled to room temperature and are indicative of aliphatic C-H stretching (2934.21cm^{-1}), H_3C-$^{+}$NH stretching and combination

modes (2394.92cm^{-1}), Phenyl ring vibrational modes (1563.67cm^{-1}), C-H deformational modes (1458.12cm^{-1}) and aromatic C-H bending modes (730-850cm^{-1}) (Abadi et al., 1999).

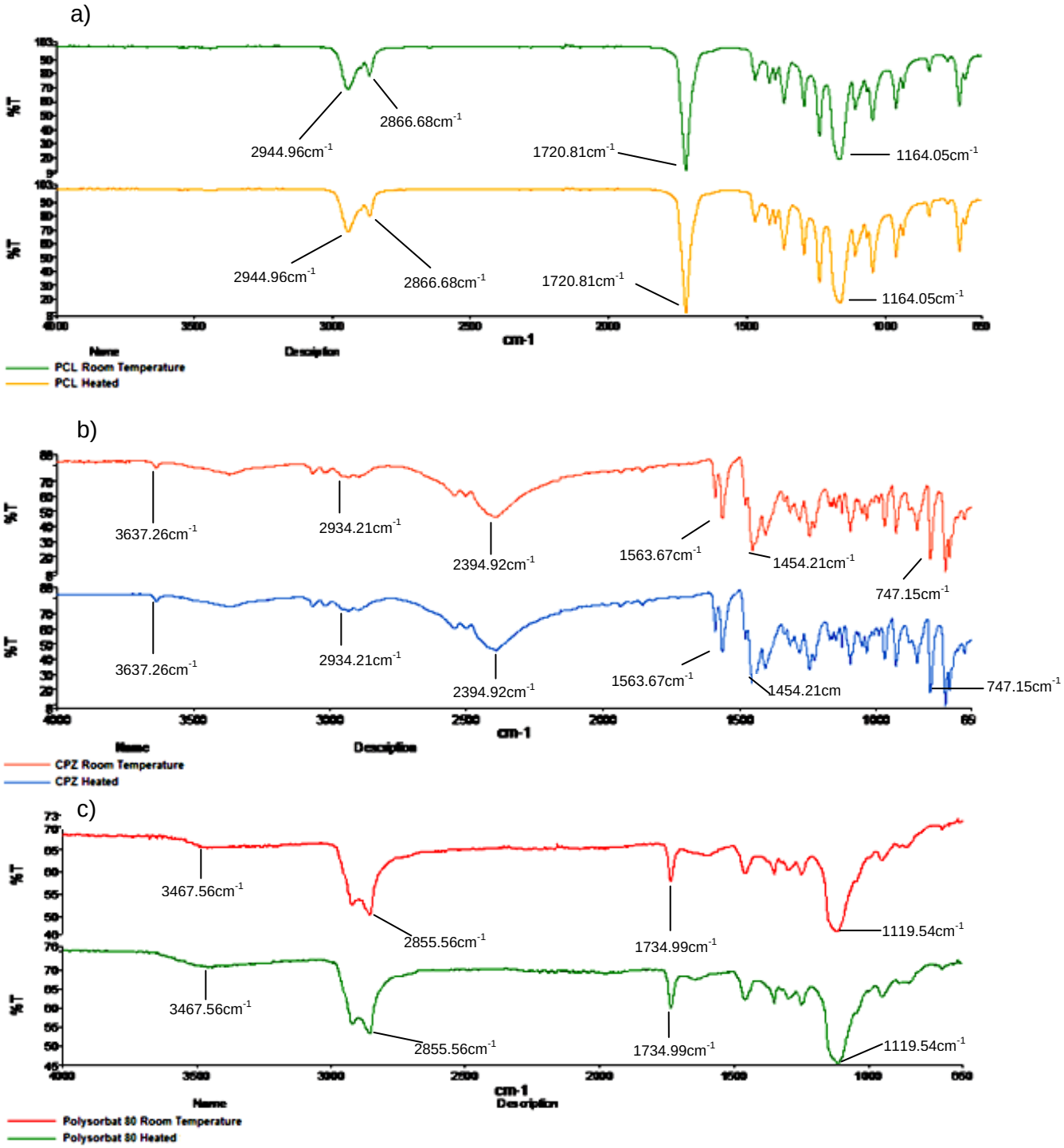

Figure 3.3: FTIR spectra of a) PCL (room temperature and heated) b) CPZ (room temperature and heated and c) polysorbate 80 (room temperature and heated).

The characteristic peaks of polysorbate 80 (3467.56cm^{-1}, 2855.56cm^{-1}, 1734.99cm^{-1} and 1119.54cm^{-1}) appear on both polysorbate 80 at room temperature as well as heated polysorbate 80 and correspond to the stretching vibrations of O-H, C=O, C-O-C bonds

respectively (Khan et al., 2010). The mere fact that all major peaks of each of PCL, CPZ and polysorbate 80 remained intact and were reproducible post-heating to 100°C and cooling confirms that the chemical backbones of each compound exhibited no thermodegradation and that the melt-dispersion technique was a viable nanoparticle synthesis technique.

DSC thermograms of CPZ, PCL and the CPZ-loaded PCL nanoparticles revealed strong endothermic peaks at 198.20°C, 66.19°C and 61.99°C respectively and corresponds to the melting transition (T_m) of these compounds (Figure 3.4). The continuous baseline on either side of the melting points of CPZ and PCL indicate that these compounds melt without degradation. With regards to CPZ, a decline in the baseline is noted from 230°C onwards. This could be a result of degradation. Despite this, the baseline covers and goes beyond temperatures used in the melt-dispersion technique thus confirming that there is no thermodegradation when utilizing the melt-dispersion technique. The T_m of the CPZ-loaded PCL nanoparticles exhibited a decrease from 66.19-61.99°C when compared to pure PCL. Furthermore, a pronounced endotherm at 39.54°C was observed and overlaps with the melting endotherm of the nanoparticles. TMDSC [Figure 3.4 d)] revealed that the peak at 39.54°C does not occur and is an unexpected transition in the DSC thermogram. In addition, transitions pertaining to the non-reversible heat flow curve and the Total heat flow curve occur at 58.29°C. Transitions on these curves are indicative of crystallization or melting. The fact that the transition is endothermic confirms melting is occurring. The moderate decrease in melting point of the drug-loaded PCL could possibly be as a result of the incorporation of CPZ which may in fact restrict the periodic arrangement of PCL chains into its lattice thereby causing the crystalline structure of PCL to be less perfect in the nanoparticle form as opposed to pure PCL (Zhao et al., 2008).

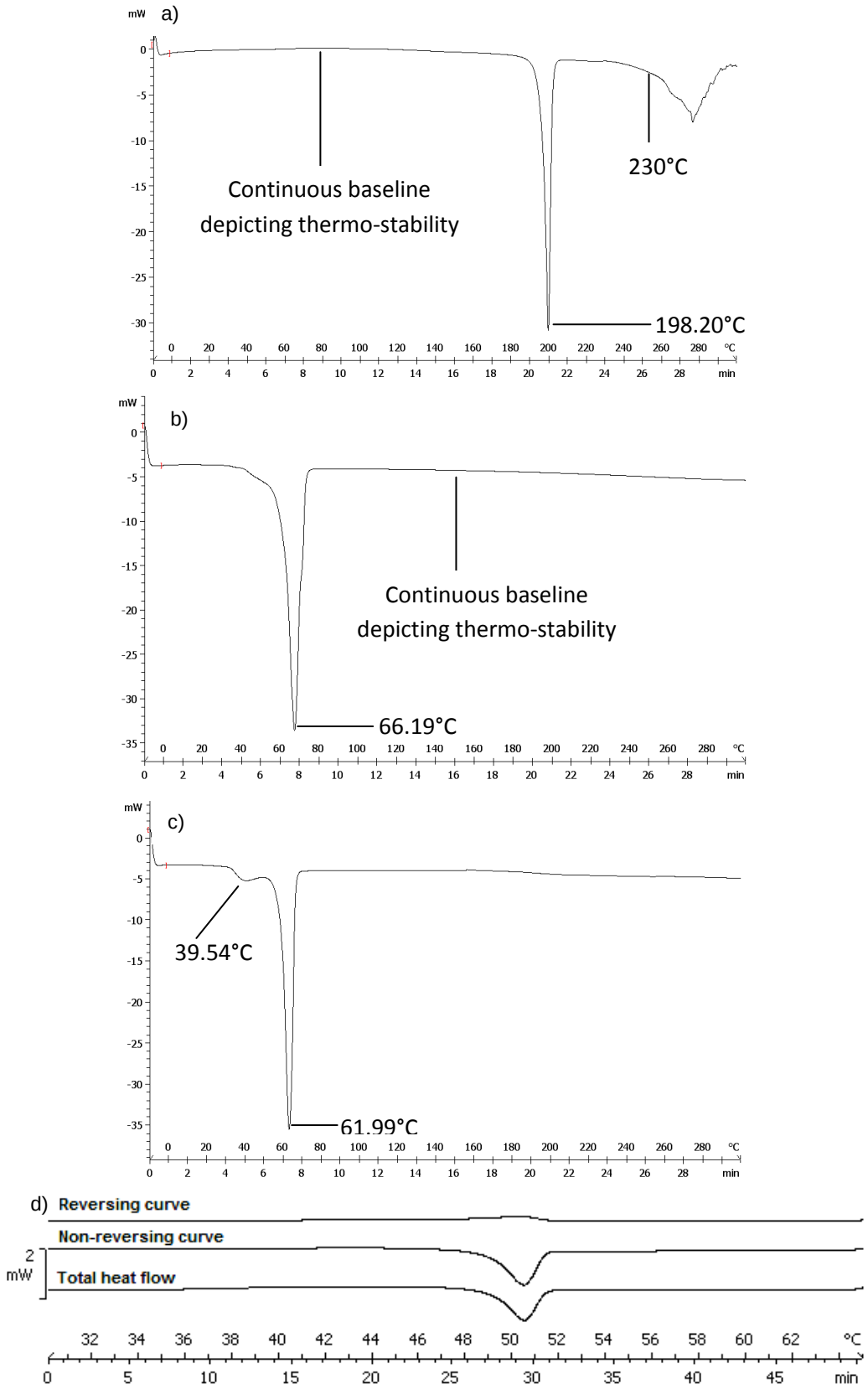

Figure 3.4: DSC of a) CPZ b) PCL and c) CPZ-loaded PCL based nanoparticle formulation and TMDSC profile of d) CPZ-loaded PCL based nanoparticle formulation between 30 and 80°C.

3.3.3 Construction of calibration curves for the ultraviolet spectrophotometric determination of CPZ entrapment and release

Figure 3.5 portrays the calibration curves obtained for CPZ in PBS (pH 7.4, 37°C) at a) λ_{254} and b) λ_{319}. Concentrations for CPZ at λ_{254} ranged from 0-0.0125mg/mL and concentrations for CPZ at λ_{319} ranged from 0-0.0508mg/mL. Due to the extremely high ultraviolet intensity energy of CPZ at λ_{254}, *in vitro* assays were conducted at the other maximum, λ_{319}.

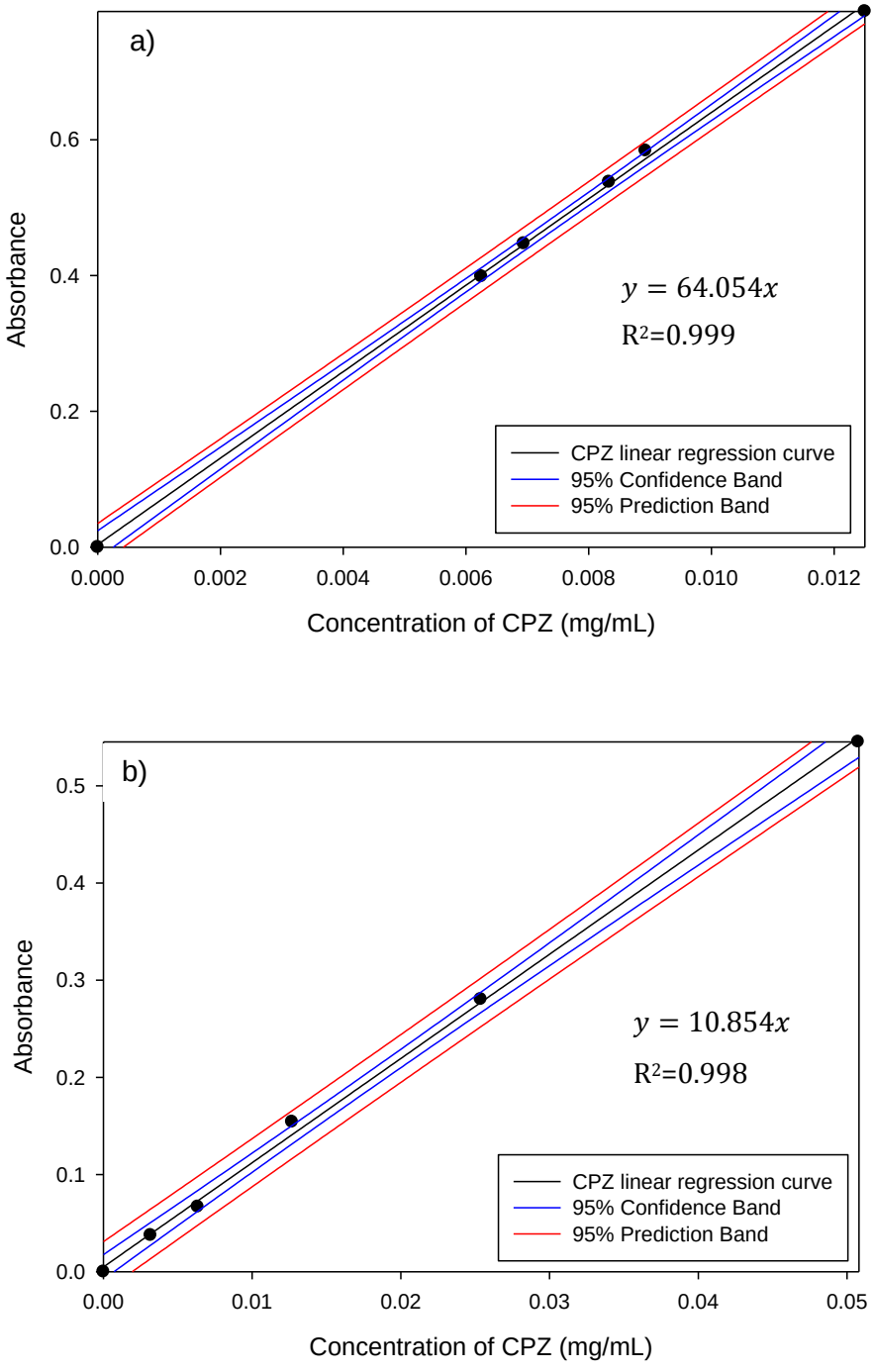

Figure 3.5: Calibration curves of CPZ in PBS at a) 254nm and b) 319nm.

3.3.4 Drug entrapment and yield of nanoparticles

Nanoparticle yield from the 13 formulations ranged from 89.58-99.54% with an average of 94.74% and is illustrated in Figure 3.6. High yield values are due to the relatively high levels of PCL used in each formulation. The amount of CPZ entrapped within the PCL nanoparticles ranged from 1933.51-8230µg (SD≤60.34, N=3). Figure 3.7 provides the amount of CPZ entrapped within the PCL nanoparticles for each formulation of the FCCCD template. The relatively low CPZ entrapment values bear testament to the fact that CPZ is highly hydrophilic and PCL itself is highly hydrophobic hence both entities are less chemotactic towards each other. Furthermore, low CPZ entrapment values could also be due to the addition of water to the formed nanoparticle solution post-curing to aid in decreasing the viscosity of the solution, centrifuging and collection of nanoparticles. Further leaching of CPZ out of the nanoparticles could also be a result of washing out the particles during the collection process of the nanoparticle synthesis. The highly hydrophilic CPZ has a great affinity towards the aqueous phase invariably resulting in massive amount of drug loss. Nanoparticles in general, due to their diminutive sizes and large surface areas allow for very limited amounts of drug to be entrapped (Mohanraj and Chen, 2006).

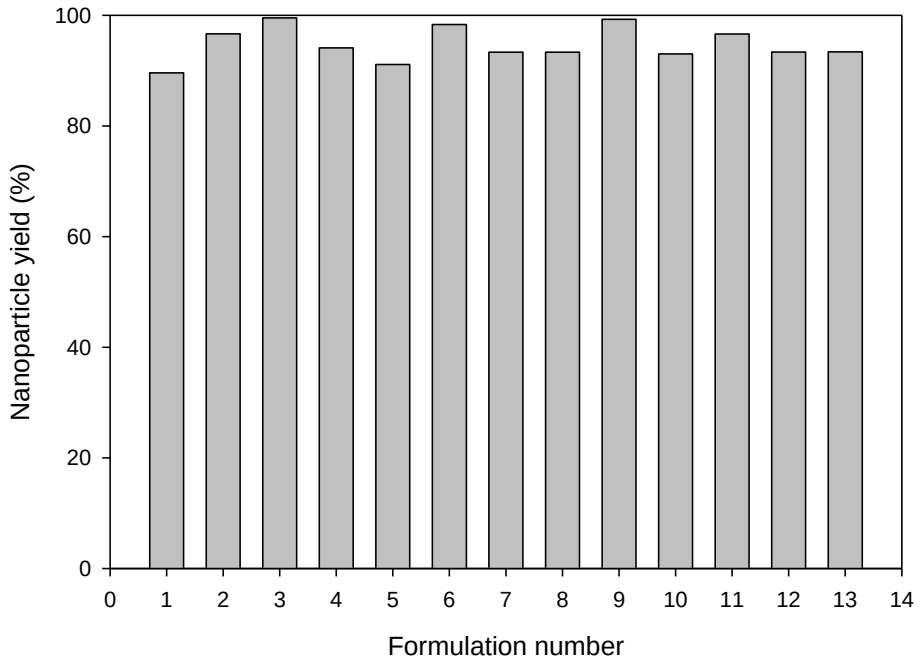

Figure 3.6: Nanoparticle yield of each formulation as per statistically generated design template (SD≤2.52 in all cases, N=3).

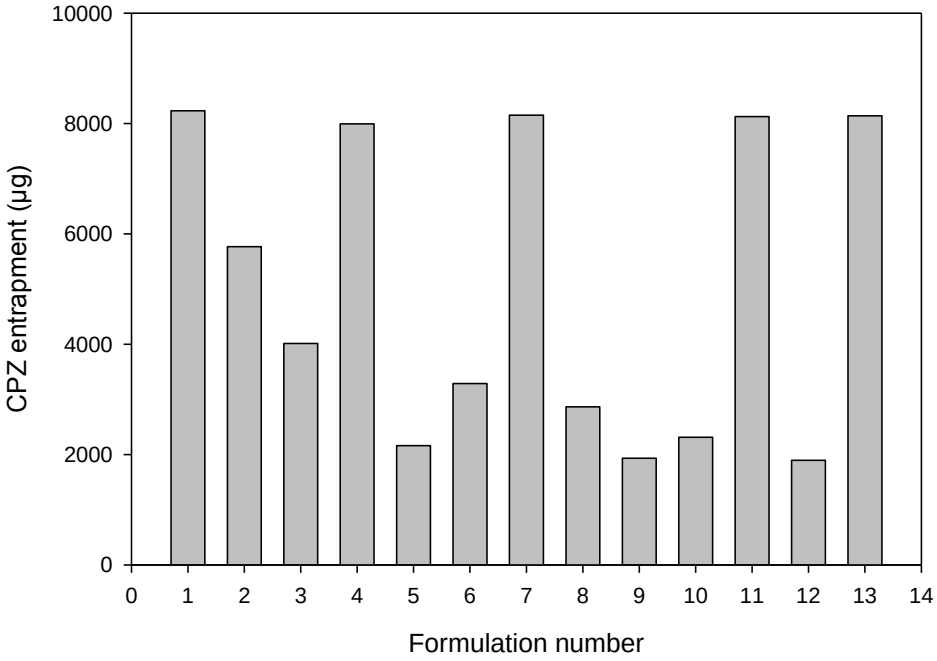

Figure 3.7: Amount of CPZ entrapped with the PCL nanoparticles as per the statistical experimental design template generated (SD≤60.34 in all cases, N=3).

3.3.5 Size and Zeta-Potential determination of nanoparticles by Dynamic Light Scattering

The z-average size of CPZ-loaded, PCL-based nanoparticles ranged from 132.70-566.60nm as per experimental design template and is depicted in Figure 3.8 a). In general, increasing levels of PCL above 3000mg and concentration of polysorbate 80 above 5% resulted in larger particles which are typical findings. The particle sizes achieved were desirable and in the range for nano-pharmaceutical applications. Zeta potential values ranged from -15.10 to -28.80mV and are depicted in Figure 3.8 b). These results represent nanoparticles that are incipiently to moderately stable. Increased concentrations of polysorbate 80 resulted in particles with high absolute zeta potential values whereas a decrease in polysorbate 80 concentration below 2% resulted in lower absolute zeta potentials and unstable particles that tend to aggregate. The stability of the nanoparticles was maintained by the steric interactions and weak electrostatic repulsive forces of adsorbed polysorbate 80 on the surface of the nanoparticles (Kato et al., 2009; Ruckmani and Sanket, 2010). In addition, the stability of the form nanoparticles in suspension was due to the high viscosity of the suspension mainly as a result of the glycerol used in the formulations. This increased viscosity resulted in a decreased terminal settling velocity and thus the nanoparticles were dispersed for longer periods of time and took longer to settle hence high stability was conferred upon them (Aulton, 2002). The distribution profiles for size and zeta potential of Formulation 8 of the experimental design are represented in Figure 3.9 a)-b). A single peak is desirable as it describes a formulation with limited distribution in size or zeta potential. The distribution

profiles of a non-drug loaded Formulation 8 are also depicted in Figure 3.9 c)-d). It can be seen that the sizes of the particles are significantly smaller i.e. 63.46nm for non-drug loaded particles as compared to 132.70nm of the drug-loaded nanoparticles. This is a typical result as the addition of drug to the particle would generally result in an increase in particle size. Furthermore, the absolute zeta potential of non-drug loaded particles (-10.80mV) was lower than that of drug-loaded nanoparticles (-28.80mV) and were less stable.

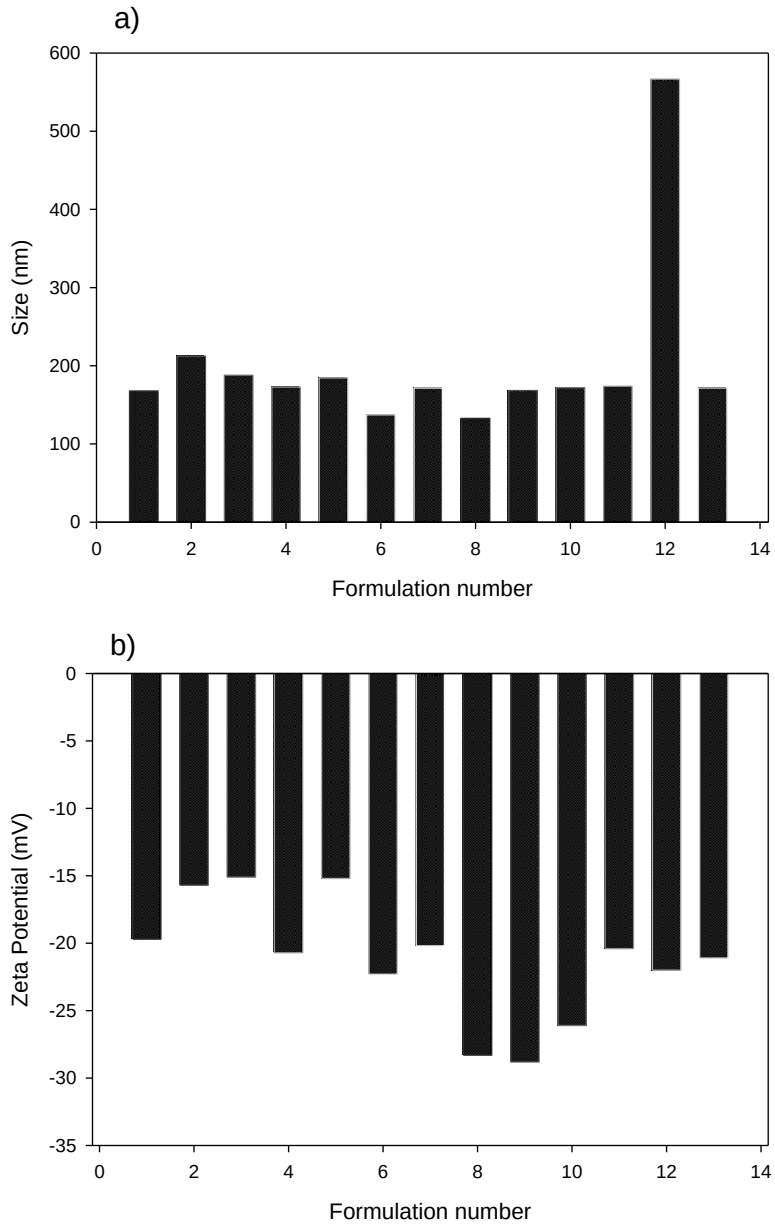

Figure 3.8: Graphical representation of a) sizes achieved (SD≤1.08 in all cases, N=3) and b) zeta potentials achieved (SD≤1.20 in all cases, N=3) for CPZ-loaded PCL-based nanoparticles as per statistical design.

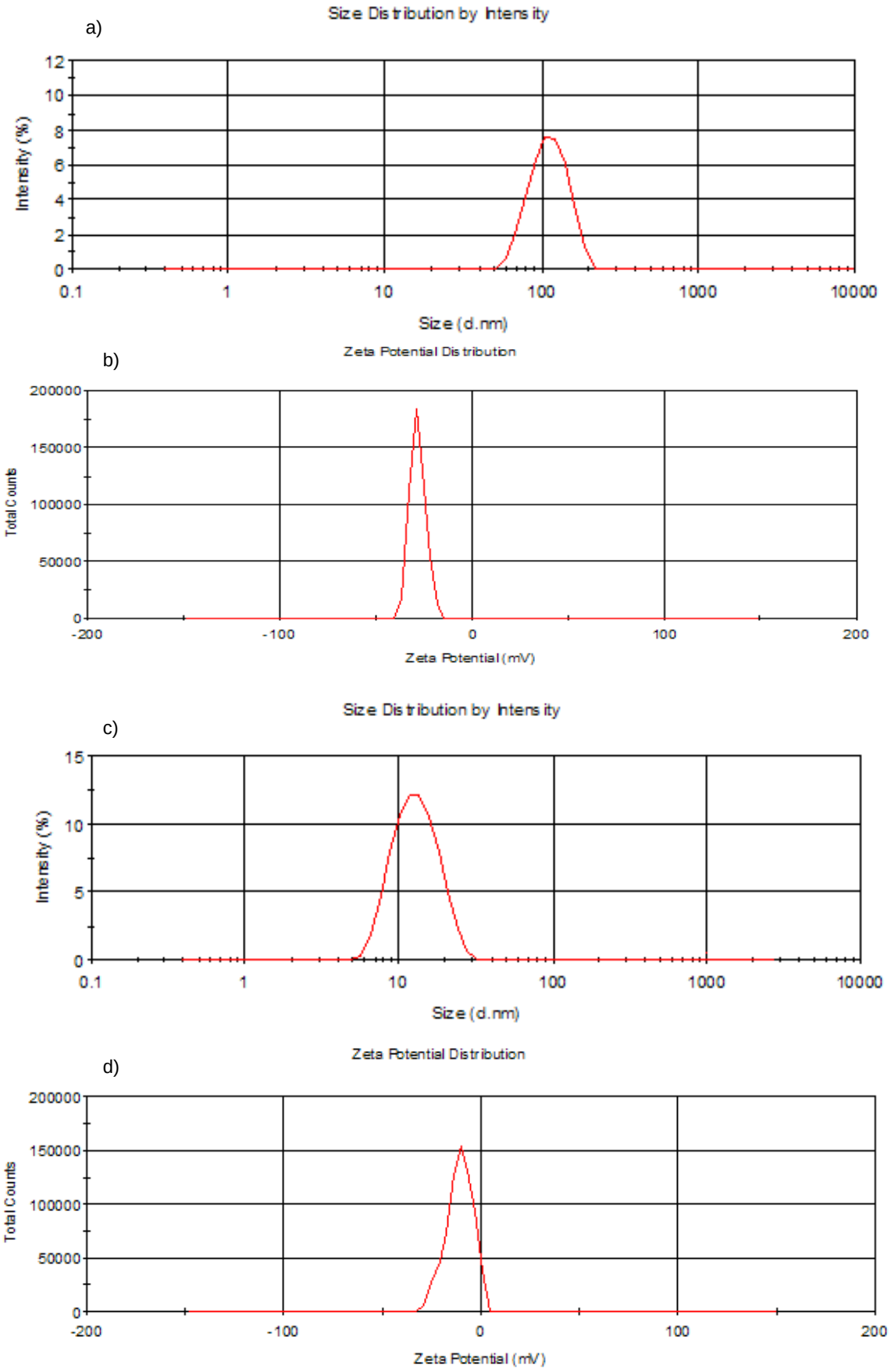

Figure 3.9: Distribution profiles of a) size and b) zeta potential of drug-loaded nanoparticles of Formulation 8 of the experimental design. Distribution profiles of c) size and d) zeta potential of non-drug loaded nanoparticles of Formulation 8 are also depicted.

3.3.6 Morphological characterization of nanoparticles using Transmission Electron Microscopy

TEM revealed spherical particles which were of consistent size. CPZ-free particles [Figure 3.10 a)-b)] appeared denser in structure whereas CPZ-loaded particles [Figure 3.10 c)-e)] appeared to be opaque. Both drug-loaded and non-drug-loaded particles exhibited a high degree of flocculation which is consistent with zeta potential results, thereby displaying moderate and incipient stability from weak steric forces instead of a highly stable, de-flocculated suspension. Despite this, particles were well individualized.

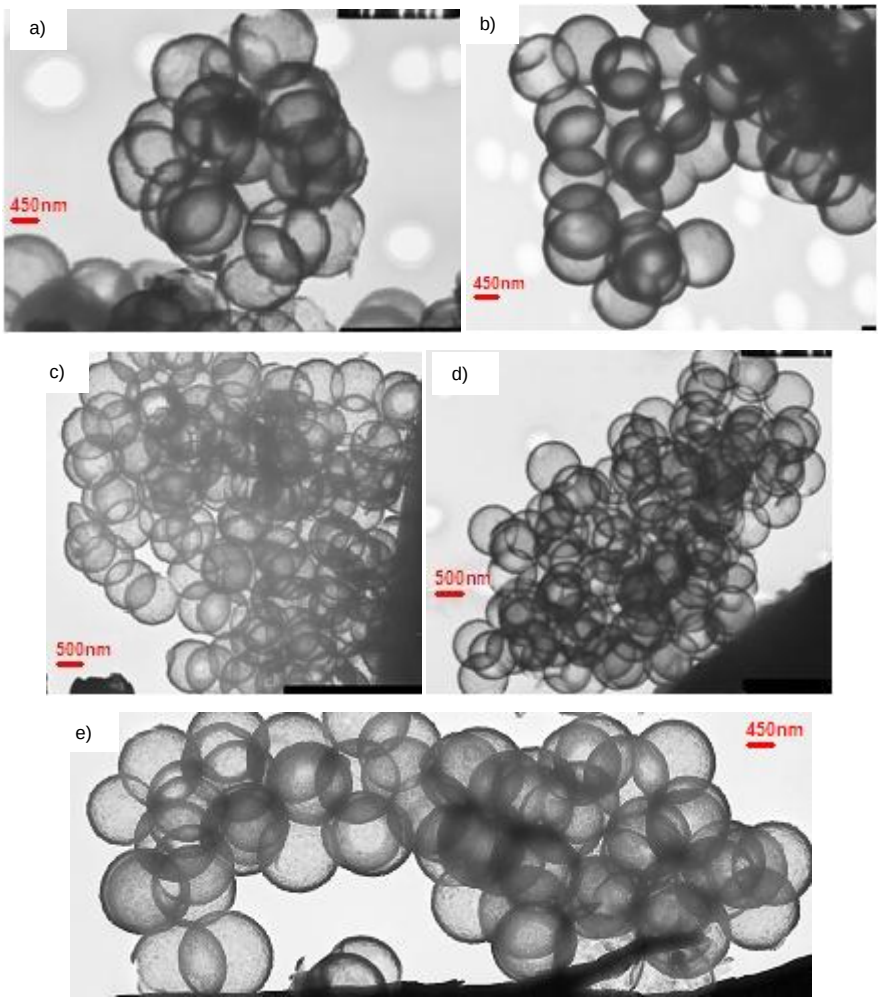

Figure 3.10: TEM of a)-b) non-drug loaded, PCL-based nanoparticles and c)-e) CPZ-loaded PCL based nanoparticles [Magnification 50000x (a, b, e); 40000x (c, d)].

3.3.7 *In vitro* drug release studies

All formulations of the experimental design exhibited biphasic CPZ release characteristics with an initial burst release followed by controlled pseudo-steady release over a period of 30 days and is depicted in Figure 3.11. The initial burst release is characteristic of PCL nano and microparticles and is mainly due to weakly bound or adsorbed CPZ on the surface of the PCL particle compounded by the highly hydrophilic nature of CPZ which generally tends to dissolute in aqueous media (PBS) rapidly. The burst release could also be as a result of CPZ diffusion through the superficial layers of the PCL particle whereas the controlled, steady release kinetics could be a result of CPZ diffusing from the inner PCL matrix as a result of polymer degradation (Midhun et al., 2012). Other possible reasons for the initial burst release includes; particle sizes, drug-loading, low molecular weight of the drug and drying conditions (Hans and Lowman, 2002; Chawla and Amiji, 2002). Larger particles generally have a smaller initial burst release and a longer sustained release than smaller particles. This is confirmed by comparing the release kinetics of Formulation 6 to the release kinetics of Formulation 12 in the experimental design. Formulation 6 had a z-average particle size of 137.20nm and exhibited an initial burst release of 58.3% of the entrapped CPZ. Formulation 12 had a z-average particle size of 566.60nm and displayed a burst release of 19% of entrapped CPZ. Furthermore at day 30, Formulation 6 had release 69.50% of entrapped CPZ whereas Formulation 12 had released 22.40%. In addition, greater nanoparticle drug-loading results in greater burst release effects (Hans and Lowman, 2002). This again is confirmed by comparing Formulations 6 and Formulation 12 with a CPZ entrapment of 3286.56 and 1896.04µg respectively. CPZ-loading of PCL nanoparticles in general was extremely low (as discussed in Section 3.2 of this chapter) hence the burst release effects of the majority of the formulations in the experimental design were relatively low. Furthermore, all formulations of the experimental design displayed controlled release of CPZ after the initial phase with drug release ranging from 22.40% to 69.50% after 30 days. This highlights the potential of the synthesized formulations for controlling release of CPZ over prolonged periods of time which is highly beneficial. MDT_{30} ranged from 48.94-100.81 hours thereby confirming the extended CPZ release potential of all formulations of the experimental design (Table 3.3). Greater MDT_{30} values corresponded with nanoparticle formulations that exhibited a faster CPZ release and is once again confirmed by Formulations 6 and 12. Lower MDT_{30} values corresponded to formulations with a more controlled, steadier release profile. Possible strategies for controlling CPZ release further and counter-acting the burst release characteristics of the PCL-based nanoparticles revolve around incorporating the particles with a polymeric matrix. In this case CPZ release would be separated into two phases; 1) diffusion of CPZ-loaded nanoparticles from the polymeric matrix upon hydration and 2) dissolution of the nanoparticles causing CPZ release.

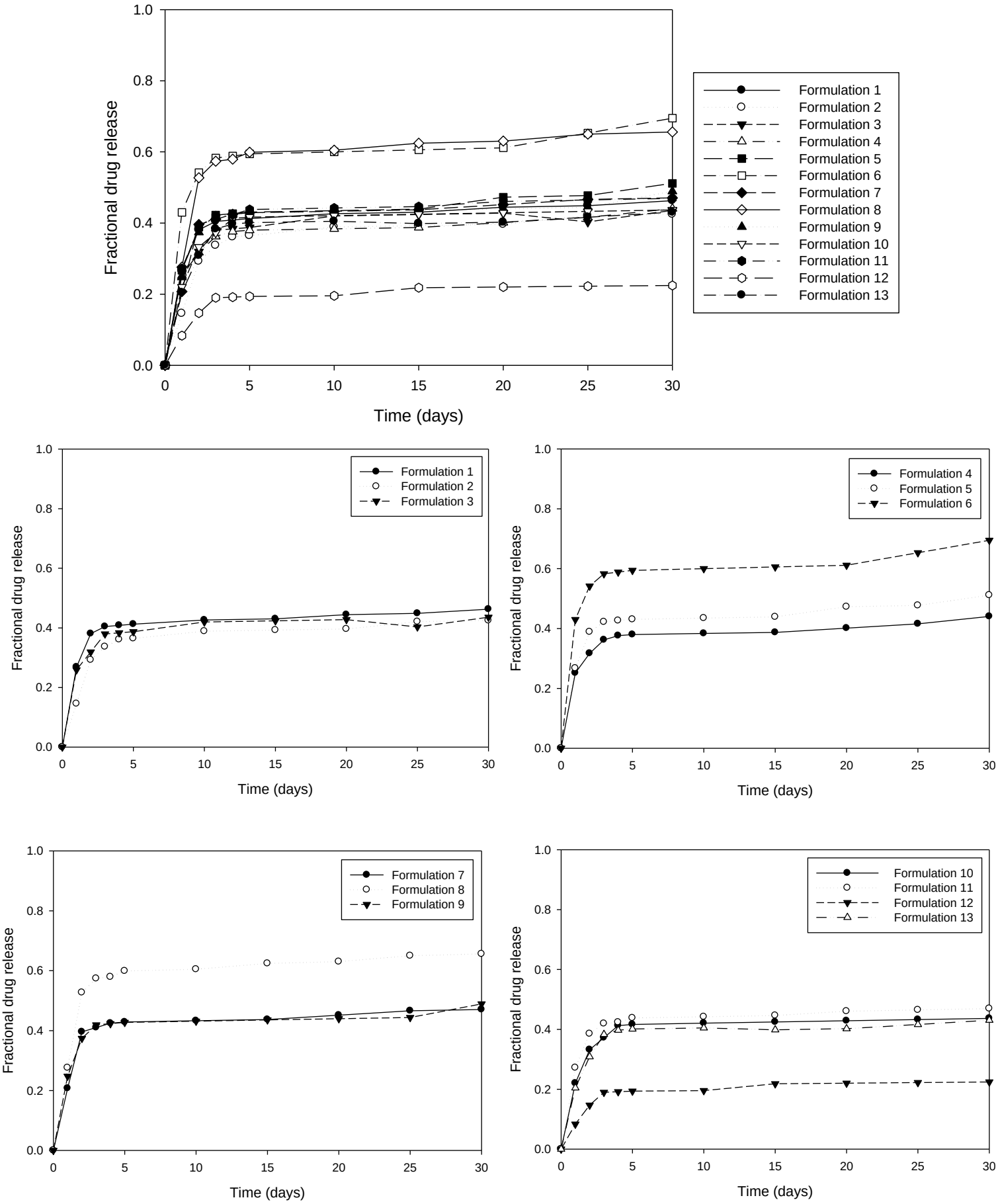

Figure 3.11:*In vitro* CPZ release profiles from PCL based nanoparticles as per experimental design, (SD≤0.04 in all cases, N=3).

Table 3.3: MDT_{30} values achieved for each formulation of the experimental design.

Formulation number	MDT_{30} (Hours)
1	66.23
2	82.46
3	60.79
4	94.13
5	100.81
6	97.87
7	65.12
8	63.73
9	95.93
10	48.94
11	52.23
12	74.66
13	68.59

3.3.8 Analysis of Face-Centered Central Composite Design

Size, zeta potential and CPZ entrapment were incorporated into the experimental design for the determination of the optimal CPZ-loaded, PCL-based nanoparticle formulation. Residual plots for size, zeta potential and CPZ entrapment are depicted in Figure 3.12. Scattering of points on the residual versus fitted plots of were generally good indicating random scatter and no trends however some clustering was observed for zeta potential. The normal probability plots of the residuals for all three responses do not show uniform distribution along the straight line thereby indicating was not normally distributed and could be a result of possible outside influences. Departures and deviations from the line could be as a result of the sample size for each response, being too small. The smaller samples sizes, although associated with large variations, may still be consistent with a normal sample and the deviations from the straight line are not drastic. Histograms for all 3 responses were generally asymmetrical thereby supporting the probability plots of non-uniform distribution. Non-random error was indicated by the residuals versus order of the data plots. A full ANOVA was carried out and is depicted in Table 3.4. A significant effect of any factor is indicated by a $p\text{-}value \leq 0.05$ for any factor.

Table 3.4: Full ANOVA analysis for the measured responses.

	p-values		
Term	**Size**	**Zeta Potential**	**CPZ Entrapment**
[PCL]	0.996	0.344	0.236
[Polysorbate 80]	0.889	0.079	0.131
[PCL*PCL]	0.287	0.121	0.162
[Polysorbate 80*Polysorbate 80]	0.208	0.118	0.083
[PCL*Polysorbate 80]	0.016	0.426	0.554

Where PCL = poly-ε-caprolactone

The complete regression equations generated for size, zeta potential and CPZ entrapment are indicated below:

*Size = 89.6638 + 0.0009[PCL] + 18.8678[Polysorbate 80] + 0.0000[PCL*PCL] + 24.1379[Polysorbate 80*Polysorbate 80] - 0.0682[PCL*Polysorbate 80]*

Equation 3.2

*Zeta Potential = -43.1243 – 0.0112[PCL] + 18.8364[Polysorbate 80] + 0.0000[PCL*PCL] – 1.9433 [Polysorbate 80*Polysorbate80] – 0.0012[PCL*Polysorbate 80]*

Equation 3.3

*CPZ Entrapment = -14922.8 + 7.7[PCL] + 7516.0[Polysorbate 80] - 0.0[PCL*PCL] – 1184.9[Polysorbate 80*Polysorbate 80] + 0.5[PCL*Polysorbate 80]*

Equation 3.4

a)

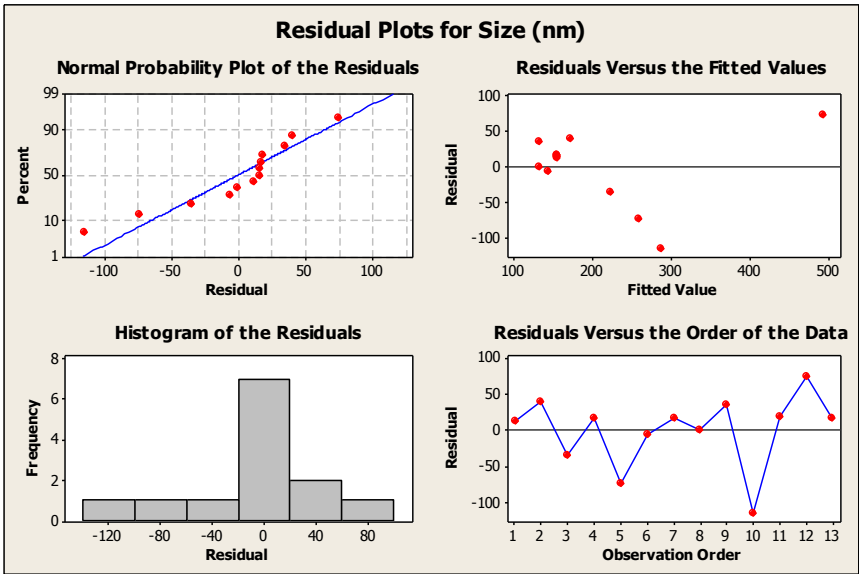

b)

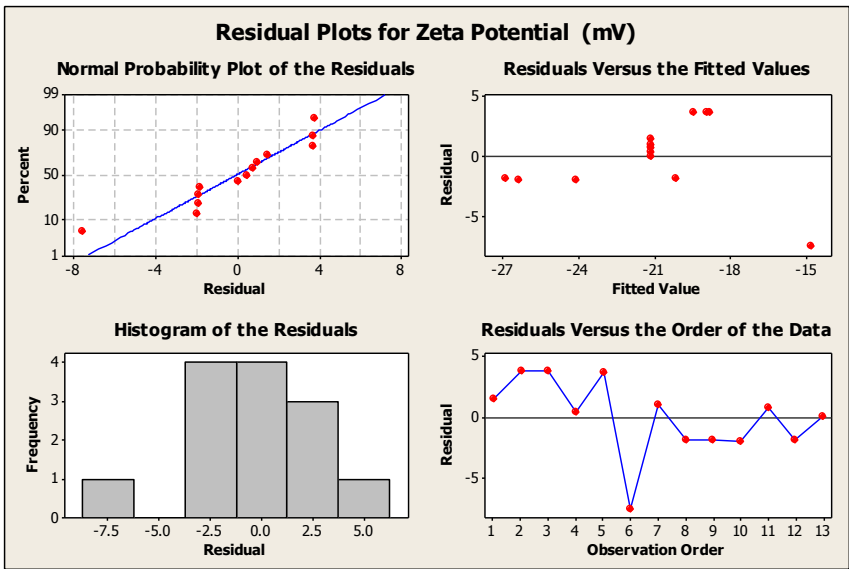

c)

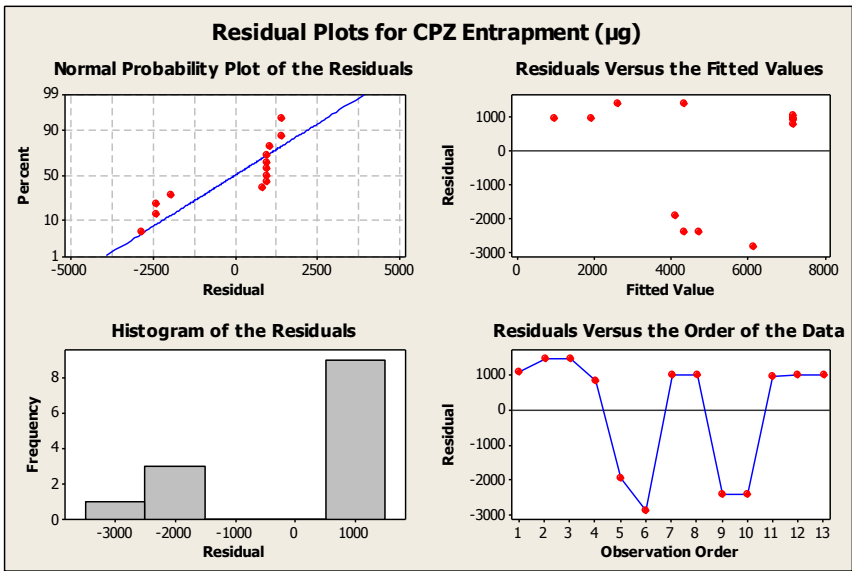

Figure 3.12: Residual plots for the responses a) size, b) zeta potential and c) CPZ entrapment.

3.3.9 Response surface analysis

Response surface and contour plots (Figure 3.13) were derived for the measured responses (size, zeta potential and CPZ entrapment), based on the experimental model. Plots were used to represent the functional relationship between the experimental variables and the responses achieved. The effects of PCL and polysorbate 80 on particle size are depicted in Figure 3.13 a). It can be seen that low levels of PCL results in smaller particles and higher levels of PCL resulted in larger particles. This is typical as greater polymer levels increase the tendency of particles to aggregate and makes shearing and agitation difficult resulting in a larger particle size. Furthermore, increasing the concentration of the polymer results in an increase in the bulk volume of the dispersed phase thereby resulting in increased sizes of nanoparticles produced. It is also demonstrated that increasing levels of polysorbate 80 resulted in moderate decreases in particles size. This is due to the surface-acting capabilities of polysorbate 80. The combination effects of PCL and polysorbate 80 levels demonstrate that at lower levels of PCL and higher levels of polysorbate 80, particle size is significantly larger and as the levels of PCL increase and the levels of polysorbate 80 remain high, particle size is decreased. At low levels of both PCL and polysorbate 80, particle size remains small.

The effects of PCL and polysorbate 80 on zeta potential are demonstrated in Figure 3.13 b). Lower levels of PCL resulted in higher zeta potential absolute values and higher polysorbate 80 values resulted in higher, more desirable zeta potential absolute values. The combined effects of PCL and polysorbate 80 demonstrate that at lower levels of PCL and higher levels of polysorbate 80, zeta potential is most desirable. This is typical as the higher zeta potential absolute values are a result of adsorbed polysorbate 80 imparting the negative charge and the lower levels of PCL used, the more polysorbate 80 can be adsorbed on the PCL thereby increasing the zeta potential absolute value. This adsorbed surfactant decreased the interfacial tension thereby resulting in an increased stability conferred upon the nanoparticles.

The effects of PCL and polysorbate 80 on CPZ entrapment are shown in Figure 3.13 c). It can be seen that lower PCL values resulted in lower CPZ entrapment and as the PCL levels increased to 2000mg, so to, did CPZ entrapment. At the same time, it can also be seen that high PCL values (3000mg) resulted in low CPZ entrapment. A similar trend was observed for the effects of the levels of polysorbate 80 on CPZ entrapment. The combined effects of PCL and polysorbate 80 on the CPZ entrapment illustrate that CPZ entrapment is at a maximum when PCL levels are high and polysorbate 80 levels are low to intermediate. This

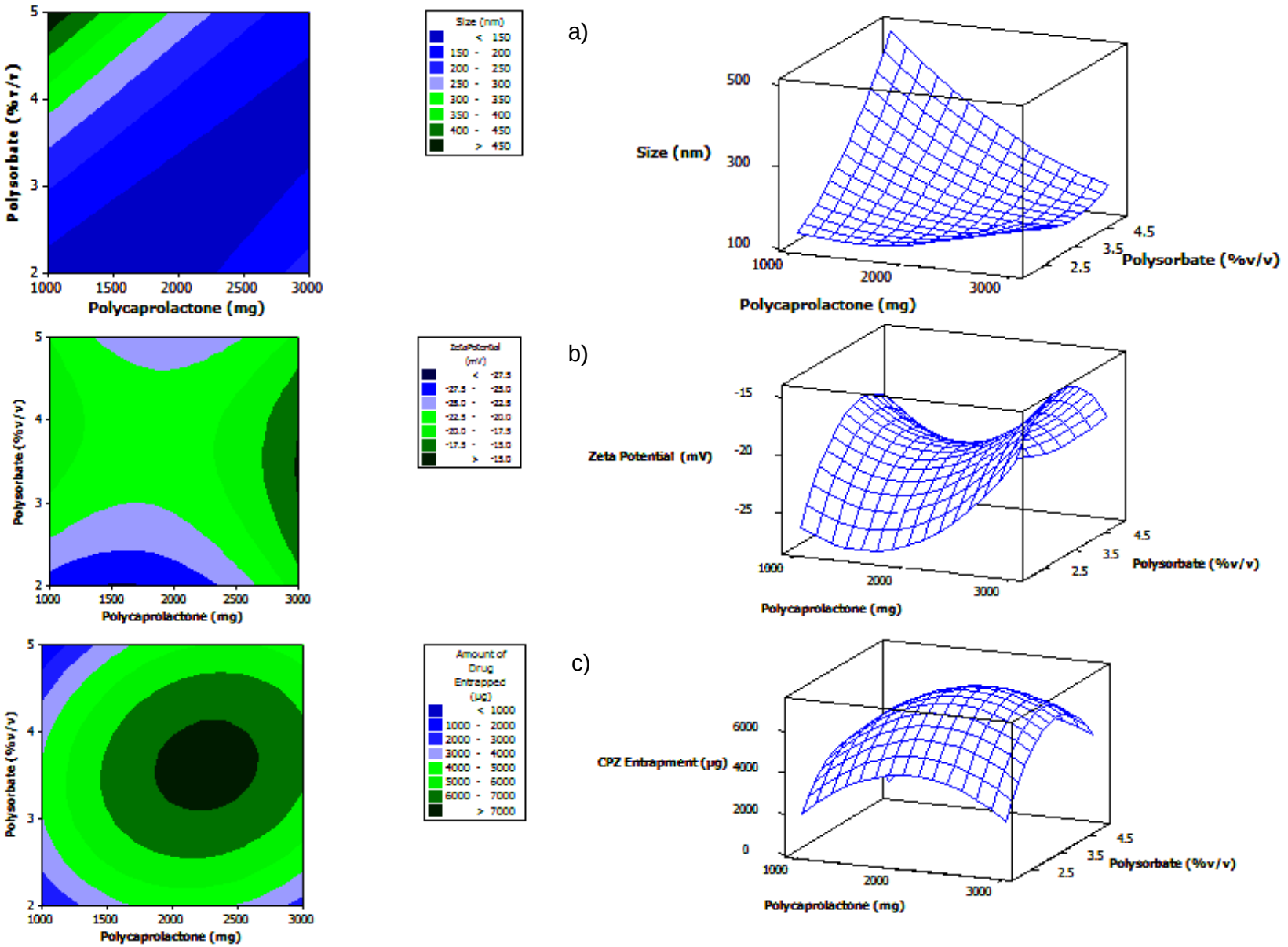

Figure 3.13: Response surface and contour plots depicting the effects of PCL and Polysorbate 80 on a) size, b) zeta potential and c) CPZ entrapment.

is typical as the greater PCL levels effectively result in more polymer available to entrap the drug and the higher polysorbate 80 levels result in greater surface-acting properties, leading to smaller particles and a lower CPZ entrapment. Furthermore, higher surfactant levels result in the drug being amalgamated within surfactant as opposed to entrapped with the nanoparticle. In addition, this can result in higher levels of drug absorbed on the nanoparticle surface and easily removed when the particles are washed post-synthesis. In general CPZ entrapment was significantly low and this is mainly because CPZ is highly hydrophilic and PCL itself is highly hydrophobic and hence do not have an affinity for each other. Furthermore, low CPZ entrapment may also be the result of addition of water to the formed nanoparticle solution post curing. Nanoparticles in general, due to their diminutive sizes and large surface areas allow for very limited amounts of drug to be entrapped.

3.3.10 Response optimization

A single, optimal formulation was developed subsequent to constraint optimization of particle size, zeta potential and CPZ entrapment. Response optimization was carried out utilizing statistical software (Minitab®, V14, Minitab Inc®, PA, USA) to determine the optimum level of each of PCL and polysorbate 80. Figure 3.14 depicts the desirability plots of each constraint for the single optimal formulation. Constraint settings utilized are shown in Table 3.5. The optimal levels of the independent variables that would achieve the desired nanoparticle size, zeta potential and CPZ entrapment are depicted in Table 3.6.

Table 3.5: Formulation constraints utilized for response optimization.

Responses	Limits
Size	Minimize
Zeta Potential	Minimize
CPZ entrapment	Maximize

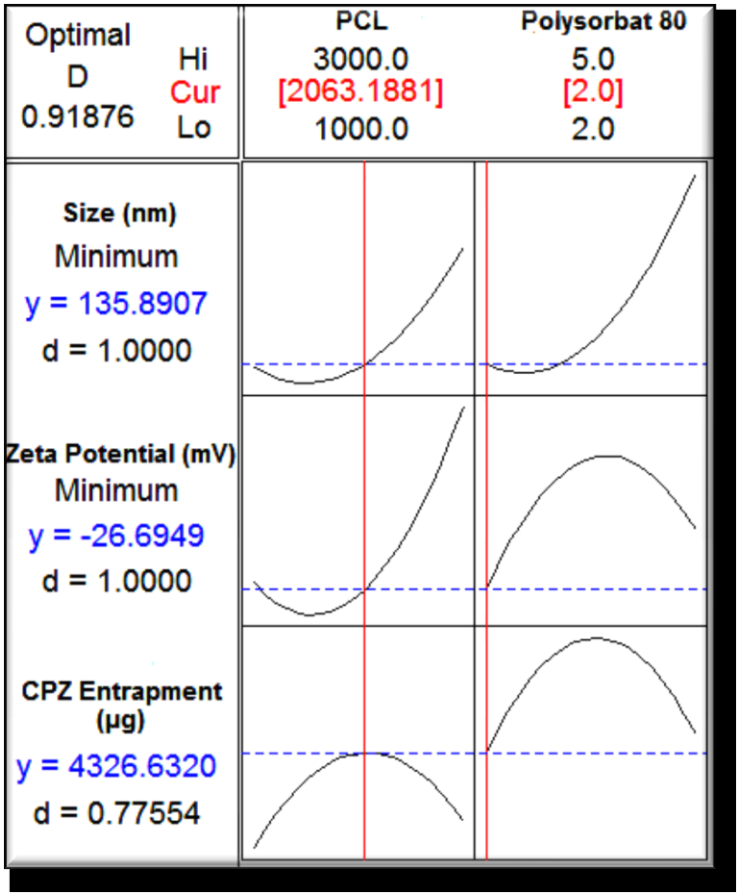

Figure 3.14: Desirability plots representing the levels of PCL and polysorbate 80 required to synthesize the optimized formulation.

Table 3.6: Optimized CPZ-loaded, PCL based nanoparticle formulation derived from the surface response method.

	PCL (mg)	**Polysorbate 80 (%v/v)**
Optimized Formulation	2063.1881	2

Table 3.7 represents the optimized levels of the independent variables, the predicted responses, the desirability score as well as the correlation co-efficient for each response. The experimentally derived values for both size and zeta potential were in close agreement with predicted values of the statistical design with desirability being 96.86 and 98.91% respectively. Figure 3.15 depicts the distribution profiles for a) size and b) zeta potential of the optimized formulation. Once again, the single peaks are representative of the limited distribution in size and zeta potential which are desirable. The experimental value achieved for CPZ entrapment was significantly higher than that of the predicted value and this resulted

in a desirability of 52.96%. Despite the low desirability of CPZ entrapment according to the experimental design, CPZ entrapment was significantly larger than predicted and did not result in larger particle sizes or drastic changes to zeta potential and stability. This therefore makes the CPZ entrapment and the experimental design in general advantageous for practical purposes.

Table 3.7: Predicted, experimental and desirability values of the CPZ-Loaded, PCL based nanoparticle formulation.

Measured response	Predicted value	Actual value	Desirability (%)
Size	135.89	140.30±3.39	96.86
Zeta potential	-26.69	-26.40±2.11	98.91
CPZ entrapment	4326.63	8170.23±173.39	52.96

In addition, the yield and MDT_{30} values of the optimized formulation were calculated to be 98.20% and 62.18 hours respectively and proved to be desirable (Table 3.8). Figure 3.16 is the CPZ release profile of the optimized nanoparticle formulation. A relatively high burst release of 42.0% of the entrapped CPZ is observed. This is justified by the relatively diminutive size (larger surface area) and high CPZ-loading percentage. This is followed by the controlled release of CPZ and 45.6% of the entrapped drug is released after 30 days.

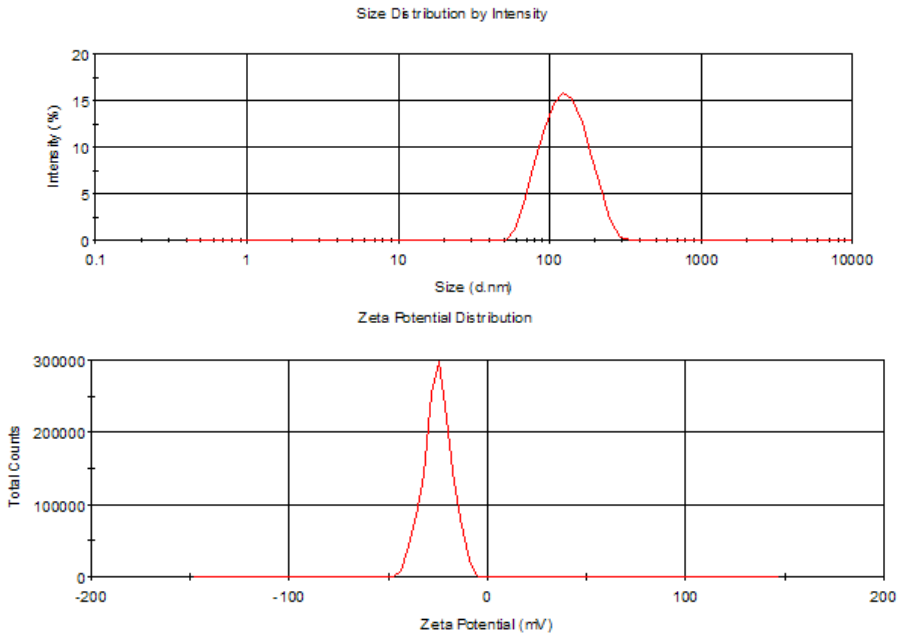

Figure 3.15: Distribution profiles of a) size and b) zeta potential of the optimized CPZ-loaded, PCL based nanoparticle formulation.

Table 3.8: Yield and MDT_{30} achieved for the optimized CPZ-loaded, PCL bases nanoparticle formulation.

	Yield (%)	**MDT_{30}**
Optimized Formulation	98.20±1.25	67.14±9.91

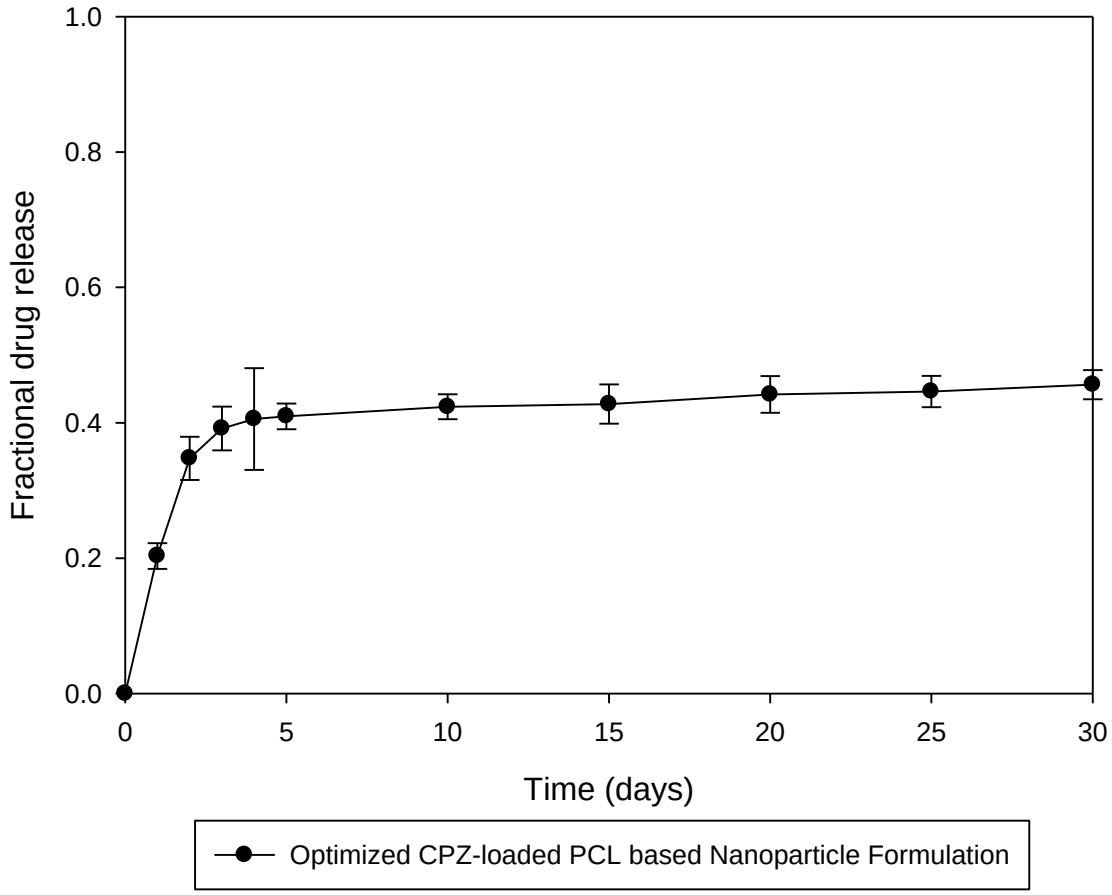

Figure 3.16: CPZ release from the optimized CPZ-loaded, PCL based nanoparticle formulation.

Figure 5.17 is a geometric visualization of conformational profile of the nanoparticle formation performed using the HyperChem^{TM} 8.0.8 Molecular Modeling System (Hypercube Inc., Gainesville, Florida, USA) and ChemBio3D Ultra 11.0 (CambridgeSoft Corporation, Cambridge, UK) on an HP Pavilion dv5 Pentium Dual CPU T3200 workstation.

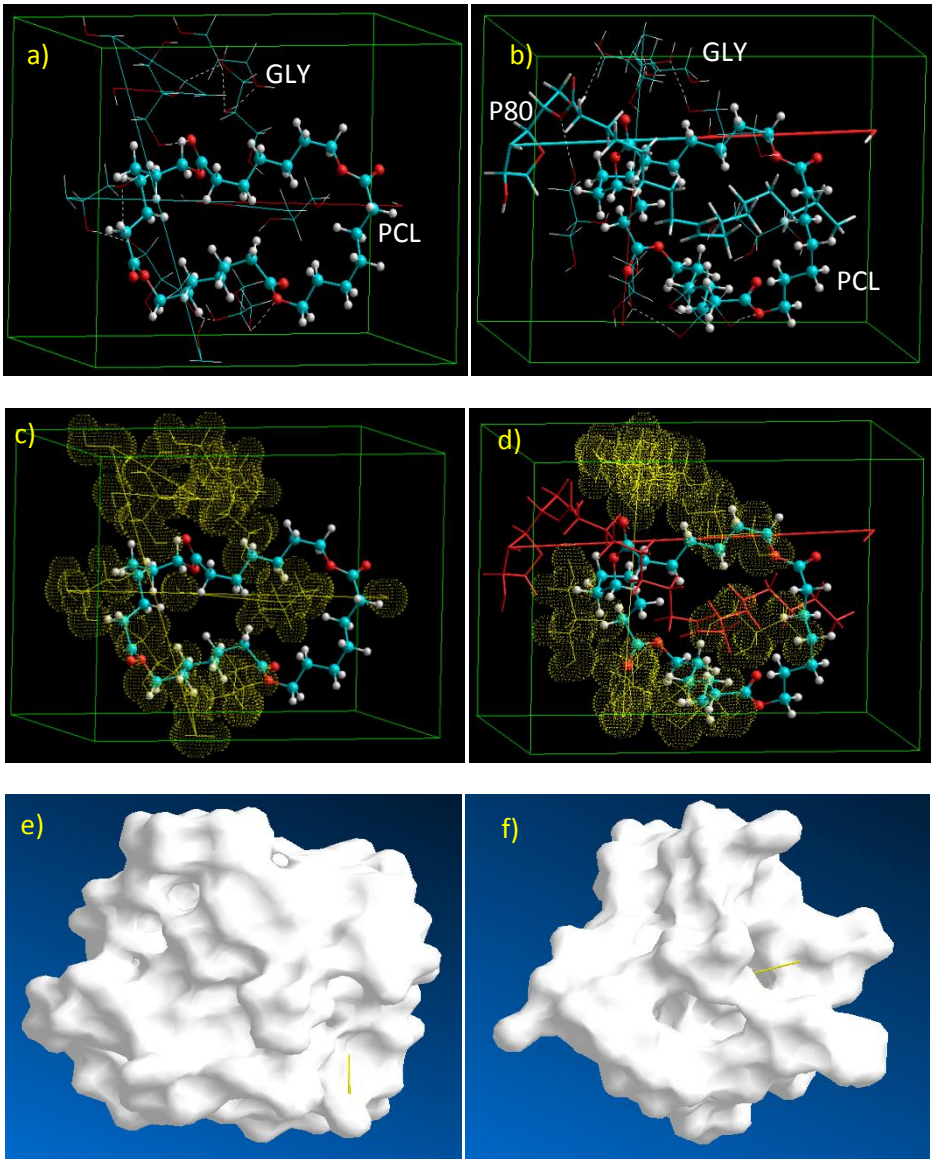

Figure 3.17: Geometric visualization of conformational profile of nanoparticle formation: a) Molecular conformation depicting the reactional and H-bonding profile of the PCL (ball and cylinder rendering)-Glycerol (stick rendering) bi-molecular system; b) Molecular conformation depicting the reactional and H-bonding profile of the PCL (ball and cylinder rendering)-Glycerol (stick rendering)- P80 (tube rendering) tri-molecular system; c) simplistic presentation of the molecular distribution of the PCL (ball and cylinder rendering)-Glycerol (yellow dots) bi-molecular system; d) simplistic presentation of the molecular distribution of the PCL (ball and cylinder rendering)-Glycerol (yellow dots) – P80 (red tubes)tri-molecular system; e) Connolly molecular structure in solid surface representation showcasing the matrix structure of the PCL-Glycerol bi-molecular system; f) Connolly molecular structure in solid surface representation showcasing the matrix structure of the PCL-Glycerol-P80 tri-molecular system showing the hydrated nanoparticle morphology. Color codes for elements: Carbon (cyan); Hydrogen (white); Nitrogen (blue); and Oxygen (red).

3.4 Concluding Remarks

The novel melt-dispersion technique for nanoparticle synthesis proved to be conducted with relative ease and confirmed the success of entrapping the antipsychotic drug, CPZ. Furthermore, the technique did not require the use of physiologically and environmentally toxic organic solvents, was a relatively inexpensive process and was devoid of any major complications. The use of thermoplastic polymers that are not easily melted to a molten state by increased temperatures is a limitation of the melt-dispersion technique as is the use of highly hydrophilic drugs resulting in low drug entrapment. Despite this, extensive *in vitro* testing and optimization supports the application for the use and feasibility of the CPZ-loaded, PCL based nanoparticles for the long-term management of certain psychotropic disorders where the benefits of nanotechnology can be exploited.

CHAPTER 4
COMBINING THE BENEFITS OF CONVENTIONAL AND COMPLEMENTARY MEDICINES: SYNTHESIS OF DUAL-ACTING NANOPARTICLES FOR THE ENHANED NEUROTHERAPY OF CENTRAL NERVOUS SYSTEM DISORDERS

4.1 Introduction

Polyunsaturated Fatty Acids (PUFAs) are long chain fatty acids that are divided into two categories; omega-3 or n-3 and omega-6 or n-6 fatty acids. Omega-3 PUFAs are commonly found in fish and some flora and omega-6 PUFAs are characteristic of vegetable oil. The precursors for both omega-3 and omega-6, Linoleic Acid (LA) and α-Linolenic Acid (ALA), cannot be endogenously synthesized and hence these PUFAs are referred to as essential fatty acids and require dietary supplementation (Mazza et al., 2007). ALA is the precursor for both Docosahexaenoic Acid (DHA) and Eicosapentaenoic Acid (EPA) representing the omega-3 essential fatty acids whereas LA is the precursor for arachidonic acid, which pioneers the omega-6 essential fatty acids (Gadoth et al., 2008). Conventionally, unsaturated fatty acids, in particular, trans-fats are associated with many negative, undesirable health effects (Hu et al. 1997). Unlike these unsaturated fats, PUFAs have been associated with many desirable health benefits.

The omega-3 fatty acids of particular importance in the Central Nervous System (CNS) are DHA and EPA, in particular DHA (and to a lesser extent, EPA). They are key components in growth cones, synaptosomes, astrocytes, myelin, glial and microsomal and mitochondrial membrane phospholipids. Significant amounts of active DHA and EPA are present in fish oil. It has been shown that the dietary supplementation of fish oil directly affects the composition of neuronal cell membrane phospholipids and in turn, affects the biophysical properties of neuronal cell membranes and influences signal transduction and neurotransmission. Furthermore, omega-3 fatty acids are also involved in membrane remodeling and synthesis. An increase in serotonin transport is a result of high membrane fluidity caused by high concentrations of omega-3 concentrations within the neuronal cell membrane (Freeman, 2000, Rapoprt, 2001; Yuen et al., 2005; McNamara and Carlson, 2006).

Apart from serotonergic transmission, DHA may also influence dopaminergic transmission, membrane-bound receptors, NA^+/K^+ dependent ATPase and Blood-Brain Barrier (BBB) functionality (Gadoth, 2008). Recent advances in the area of omega-3 fatty acid research and their neurological benefits, demonstrated that the endogenous DHA-derived mediator, NPD1, is an anti-inflammatory, a potent regulator of an intrinsic neuroprotectant and an anti-apoptotic gene-expression program that promotes survival in stressed human neurons

(Lukiw et al. 2005). Furthermore, omega-3 fatty acids in general may improve cognition, increase neuroplasticity of cell membranes, improve reference memory-related learning and improve physiological functions such as complex cortical processing. It has been demonstrated that deficits of DHA in plasma and blood cell lipids may result in poor neural and visual development in infants as well as cognitive impairment and an increased risk of dementia. Generally, deficits of DHA in the developing brain may lead to a reduction in neurotransmitter metabolism and neurogenesis (Innis, 2008). Pre-clinical and clinical studies have demonstrated that the effects DHA and EPA on neurological conditions such as Parkinson's disease, Alzheimers disease, Attention Deficit Hyperactivity Disorder (ADHD) and mood and peroxisomal disorders, are highly beneficial (McNamara et al., 2006; Ouellet et al., 2009).

In psychoses such as schizophrenia, a low brain DHA accrual may be associated with the underlying pathophysiology of the disorder. This evidence has been supplemented by studies which further prove that; 1) a low sea-food consumption was directly related to an increase in the severity of schizophrenic symptoms; 2) patients with first-episode psychosis or schizophrenia had a diminished DHA concentration in the red blood cells or plasma; 3) DHA levels are significantly low in post-mortem prefrontal cortex of adult schizophrenic patients but not in the post-mortem temporal cortex, caudate nucleus, cingulated gyrus or cerebellum of adult schizophrenic patients. In addition, a significant improvement in schizophrenic patients on conventional medication as well as chronic DHA and EPA or EPA supplementation alone has been demonstrated following interventional trials (McNamara et al., 2006).

Considering the numerous documented neurological benefits of omega-3 fatty acids especially for psychoses such as schizophrenia, the aim of this study was to investigate the possibility of incorporating active DHA and EPA in the form of Cod-Liver Oil (CLO) within a novel chlorpromazine hydrochloride (CPZ)-loaded, polycaprolactone (PCL)-based nanoparticle formulation to optimize the neurotherapy of psychoses such as schizophrenia. The novel 'nano-liposhell' formulation is a dual-acting formulation that combines the benefits of conventional drug therapy with complementary and alternative medicines and further exploits the benefits of nanotechnology in the delivery of the aforementioned. Nano-liposhells prepared this manner, in consequence, are hypothesized to have additional benefits to patients suffering from disorders such as psychoses over and above the targeted delivery of essential drug substances. When the nano-liposhells break down to release the CPZ they will concomitantly bathe the cells in these neuroprotective, anti-inflammatory, synaptogenic, neuronal membrane remodeling complementary agents, thereby enhancing

the neurotherapy of the respective disorders and ultimately leading to an optimal therapeutic outcome.

In addition, this study investigates the effects of incorporating CLO on the physicochemical and physicomechanical properties of conventional CPZ-loaded, PCL based nanoparticles.

4.2 Materials and Methods

4.2.1 Materials

Cod-liver oil (CLO) (*Gadus Morrhua*), poly-ε-caprolactone (PCL), chlorpromazine hydrochloride (CPZ) (*M*w 355.33 g/mol), glycerol B.P. and polysorbate 80 were purchased from Sigma Aldrich (St. Louise, MO, USA). De-ionized water was obtained from a Milli-Q water purification system (Milli-Q, Millipore, Billerica, MA, USA). All other reagents were of analytical grade and used as purchased.

4.2.2 Preparation of nano-liposhells

The fundamentals of nano-liposhell synthesis centered around the synthesis of the CPZ-loaded, PCL-based nanoparticles in Chapter 3 by a novel melt-dispersion technique. Briefly, glycerol (65mL), used as a melting base, was heated to approximately 90°C. This was followed by the addition of PCL (350-2000mg) until completely melted. A separate solution comprising CPZ (50-150mg) and polysorbate 80 (3.5-5%$^{w}/_{v}$) in de-ionized water was simultaneously prepared and heated to approximately 90°C. This was added to the molten PCL and glycerol while stirring under a top stirrer. The solution was allowed to stir at 1500rpm on the top stirrer for 10 minutes to allow moderate cooling. This was followed by the addition of CLO (0.2-0.5mL) and stirring continued for 35 minutes until the dispersion was cooled to room temperature. CPZ and CLO-loaded, PCL-based nano-liposhells were formed upon cooling. Nano-liposhells were allowed to cure for 15 minutes and were collected by centrifuging, removing the supernatant, re-dispersing in de-ionized water, centrifuging again, followed by collection of the nano-liposhell sediment. The sediment was then frozen at -75°C for 48 hours and subjected to lyophilization. Lyophilization generally yielded a free-flowing, golden brown stained powder for nano-liposhells formulated with low CLO levels whereas nano-liposhells formulated with high CLO levels were denser in color, displayed visible adsorption of CLO and lacked the ability to flow freely. Nano-liposhells were synthesized according to a One Variable at a Time (OVAT) approach according to the template generated in Table 4.1

Table 4.1: OVAT template utilized in the preparation of the novel CPZ and CLO-loaded, PCL based nano-liposhells.

Formulation	PCL (mg)	CLO (mL)	CPZ (mg)	De-ionized water (mL)	Polysorbate 80 (%v/v)	Glycerol (mL)	Stirring Speed (rpm)
1	500	0.2	50	2	3.5	65	1500
2	350	0.2	50	2	3.5	65	1500
3	500	0.5	50	2	3.5	65	1500
4	350	0.5	50	2	3.5	65	1500
5	500	0.2	50	2	5	65	1500
6	1000	0.2	50	2	3.5	65	1500
7	750	0.2	50	2	3.5	65	1500
8	750	0.5	50	2	3.5	65	1500
9	1000	0.5	50	2	3.5	65	1500
10	750	0.2	50	2	5	65	1500
11	750	0.2	100	2	3.5	65	1500
12	1000	0.2	150	3	3.5	65	1500
13	1500	0.2	150	3	3.5	65	1500
14	2000	0.2	150	3	3.5	65	1500

4.2.3 Determination of polymeric structural variations incurred during nano-liposhell formation employing infrared spectroscopy

Fourier Transform Infrared Spectroscopy (FTIR) was used to detect the vibration characteristics of chemical functional groups of the novel CPZ and CLO-loaded, PCL-based nano-liposhells and its componential elements, in response to infrared light interactions. FTIR assessed the presence of any structural variations in the nano-liposhells, as a result of any interactions between the CPZ, CLO, and PCL in the formulation. In addition, as discussed in Chapter 3, the novel melt-dispersion technique used does require relatively high temperatures hence FTIR was also carried out to confirm whether thermo-degradation of components such as CLO occurred. Samples were analyzed using a Spectrum 100 FTIR Spectrometer (PerkinElmerLife And Analytical Sciences Inc., Shelton, CT USA).

4.2.4 Determination of CPZ and CLO entrapment within the nano-liposhell formulations

The entrapment of CPZ within the nano-liposhell was determined by dissolving 100mg nano-liposhells in 100mL of PBS, pH 7.4, 37°C. CPZ content (µg) was assessed in triplicate and determined by ultraviolet spectroscopy (Cecil CE 3021, Cecil Instruments Ltd., Milton, Cambridge, UK) at 319nm against standard constructed curves.

CLO entrapment was determined by a simple mass quantification method whereby the mass of the synthesized nano-liposhells were firstly compared to the mass of the corresponding

nanoparticle formulation synthesized with the absence of CLO, and then to the mass of CLO initially utilized in the synthesis process and is outline by Equation 4.1

$$\% \text{ CLO Entrapment} = \frac{(\text{Mass of Nano-liposhells}) - (\text{Mass of nanoparticles without CLO})}{\text{Initial mass of CLO used for synthesis}} \times 100 \quad \textit{Equation 4.1}$$

4.2.5 Determination of size and zeta potential of nano-liposhells

Zeta potential and particle size distribution of the nano-liposhells were determined in de-ionized water using a ZetaSizer Nano ZS (Malvern Instruments Ltd, UK). A $1\%^{w}/_{v}$ solution was appropriately diluted with de-ionized water, filtered using a 0.22µm filter to maintain the number of counts per second in the region of 600 (Millipore Co., Massachusetts, USA) and finally placed into disposal cuvettes (size) or capillary cells (zeta potential) (Malvern Instruments Ltd, Malvern, Worcestershire, UK). The viscosity and refractive index of the continuous phase were set to those specific to de-ionized water.

4.2.6 Morphological analysis of the nano-liposhells utilizing Transmission Electron Microscopy

Surface morphology of the nano-liposhells as well their shape and size were intensively examined using Transmission Electron Microscopy (TEM) (JEOL 1200 EX, Tokyo, Japan, 120keV). Samples were prepared by dispersing the nano-liposhells in ethanol, followed by ultrasonication in an ultrasonic cleaner bath for one minute. Post ultrasonication, the samples were then placed on a copper grid with a perforated carbon film using a dropper and allowed to stand until evaporation of the ethanol occurred. Samples were then viewed at room temperature.

4.2.7 *In vitro* CPZ release from the nano-liposhells

An orbital shaker bath (Labex, Stuart SBS40®, Gauteng, South Africa) set at 25rpm was utilized to perform *in vitro* CPZ release studies on the nano-liposhell formulations. Nano-liposhells were placed in dialysis tubing membranes to prevent any particle loss and for a more accurate drug release elucidation. The dialysis tubing was then immersed in 100mL PBS (pH 7.4, 37°C) contained in 150mL glass ointment jars. At predetermine time intervals 3mL samples of the release media were removed, filtered through a 0.22µm Cameo Acetate membrane filter (Millipore Co., Bedford, MA, USA) and analyzed by UV spectroscopy at a maximum wavelength of 319nm for CPZ content analysis. An equal volume of CPZ-free PBS was replaced into the release media to maintain sink conditions.

4.2.8 *Ex vivo* cytotoxicity analysis

Due to the fact that the componential elements of CLO, namely, the omega-3 fatty acids exhibit a high degree of unsaturation in their chemical backbones, they are very prone to oxidation in particular auto-oxidation. Degradation of CLO occurs when it is exposed to atmospheric oxygen and may be catalyzed by high temperatures and can result in undesirable and potentially toxic byproducts. The primary degradation product of CLO, in particular, lipid oxidation, is HPODE (hydroperoxide). In the presence of initiators such as heat, auto-oxidation results in the formation of free radicals [Figure 4.1 a)]. Initiators act by removing the hydrogen from the unsaturated bonds on the PUFA backbone. The radicals react with the lipids forming HPODE. UV light exposure may also result in CLO oxidation and degradation [Figure 4.1 b)]. This type of reaction occurs more rapidly than auto-oxidation as a lower energy is required. Briefly in the presence of light and an initiator, triplet oxygen ($^3O_2$) is converted to singlet oxygen ($^1O_2$) which then reacts with the PUFA to form HPODE. HPODE may be further broken down to secondary degradation products namely; aldehydes and ketones over time. In addition, it has been demonstrated that 13-HPODE may induce cytotoxicity in rat vascular smooth muscle cells (Heinzelmann and Franke, 1999; Fujioka and Shibamoto, 2004, Turner et al., 2006). It is owing to these facts that the CLO was added at a relatively latter stage in nano-liposhell synthesis as discussed in Section 4.2.2 of this chapter. This was done to eliminate any effects of the increased temperature during the melt-dispersion process. Furthermore, the entrapment of CLO within the PCL nanoparticle would also theoretically, protect the CLO from degradation. Irrespective, adsorption of CLO on the PCL nanoparticle has to be considered. Basic *ex vivo* cytotoxicity studies were thus performed on the nano-liposhells and its componential elements to investigate the possibility of cytotoxic effects on neuronal cells.

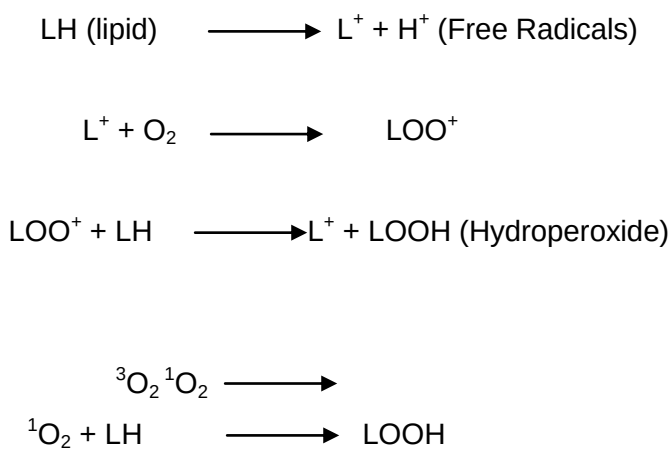

Figure 4.1: Schematic representing a) the auto-oxidation of the PUFAs within CLO and free radical formation as well as b) degradation due to UV light exposure, [Adapted from Turner et al., 2006].

4.3 Results and Discussion

4.3.1 Determination of polymeric structural variations incurred during nano-liposhell formation employing infrared spectroscopy

FTIR was performed on the CLO to assess the possibility of any degradation that may have occurred during nano-liposhell synthesis due to high temperatures. CLO was initially analyzed at room temperature and this was followed by analysis after heating the CLO to 70°C and cooling to room temperature (Figure 4.2). FTIR was also performed on the synthesized nano-liposhells to assess any potential variation in vibrational frequency during nano-liposhell synthesis as well as to assess the possibility of any interactions in the formulation and confirm the entrapment or adsorption of CLO in the PCL nanoparticle. The FTIR spectrum of CLO at room temperature [Figure 4.2 a)], centered around the spectrum of the triglyceride group which is commonly found in most edible oils (Yang et al., 2005). Characteristic peaks of the triglyceride functional group include; asymmetrical C-H stretching (2922.59cm^{-1}), symmetrical C-H stretching (2853.10cm^{-1}), C=O stretching (1743.66 cm^{-1}), scissoring C-H bending (1461.12 cm^{-1}). Furthermore, C-O stretching and C-H bending was observed at 1149.12 cm^{-1} and C-H bending (rocking) at 721.29 cm^{-1}. A weak peak at 3011.84 cm^{-1} is an indication of the stretching vibrations of *cis*-vinylic (Yang et al., 2005; Rohman and Che Man; 2011; Rohman et al., 2012). The FTIR spectra of CLO at room temperature and CLO heated and then cooled to room temperature are super-imposable indicating that all major characteristic peaks of the CLO backbone remain intact after moderate heating and cooling. This confirms that no thermo-degradation occurred during synthesis of the nano-liposhells. The characteristic peaks of the nano-liposhells (Figure 4.2 c), which comprises PCL with either entrapped or adsorbed CLO, depict a strong resemblance of the characteristic peaks of both PCL and the triglycerides of CLO. Asymmetrical C-H stretching (2945.78cm^{-1}), symmetrical C-H stretching (2866.93cm^{-1}) and C=O stretching (1720.76cm^{-1}) are all present on the nano-liposhell backbone and are related to peaks associated with PCL (Elzein et al., 2004; Wu et al., 2004). The FTIR spectra of CLO indicate the same transitions at similar wavelengths. A differentiation can be made at 2945.78cm^{-1} and 2866.93cm^{-1} of the nano-liposhell where the strength of these peaks corresponds with the strength of the peaks associated with the PCL spectra. The C=O stretching at 1720.76cm^{-1} is of similar strength to both PCL and CLO indicating a lack of differentiation. The peaks at 1471.04cm^{-1} (scissoring C-H bending), 1165.57cm^{-1} (C-O stretching and C-H bending) and 731.63cm^{-1} [C-H bend (rocking)] are characteristic of the triglycerides in the CLO. FTIR spectra indicate that the nano-liposhells comprise both functional groups of PCL and CLO thereby confirming the successful assembly of the nano-liposhell.

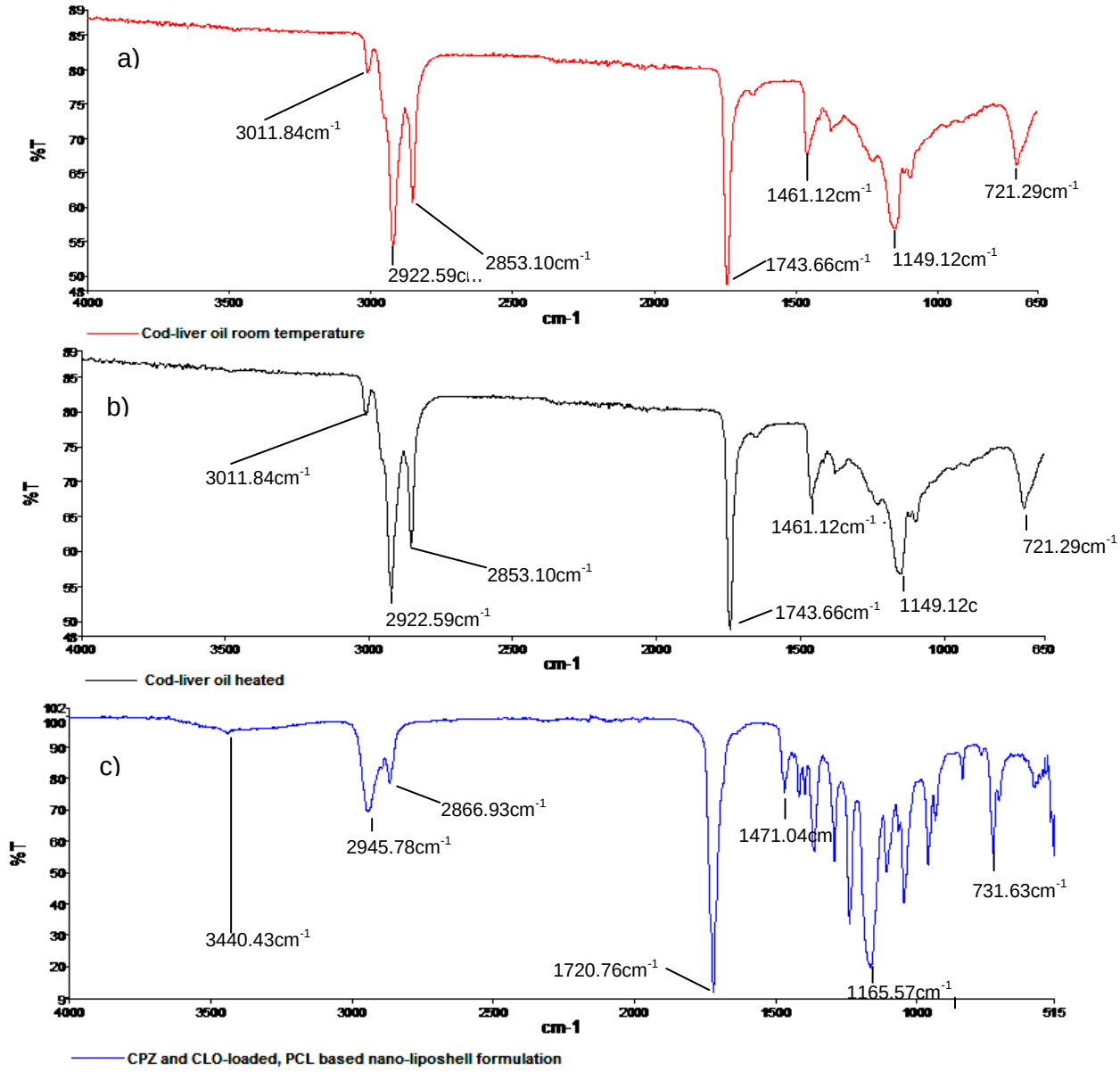

Figure 4.2: FTIR analysis of a) CLO at room temperature, b) CLO heated to 70°C then cooled to room temperature and c) CPZ and CLO-loaded, PCL-based nano-liposhell.

4.3.2 Determination of CPZ and CLO entrapment within the nano-liposhell formulations

CPZ entrapment within the nano-liposhell ranged from 1575.91±37.67-6690.55±207.30µg (Table 4.2). It is revealed once again that CPZ entrapment was very poor. The relatively low CPZ entrapment values are attributed to the fact that CPZ is highly hydrophilic and PCL itself is highly hydrophobic hence their affinity for each other is very low. The hydrophilic CPZ has a great affinity for the aqueous phase hence large amounts of CPZ are lost in the aqueous phase. Furthermore, addition of water to wash out particles and decrease the viscosity of the glycerol could have also resulted in the low CPZ entrapment achieved due to this affinity.

Finally, nanoparticles in general allow for very miniscule amounts of drug to be entrapped, due to their diminutive sizes and large surface areas (Mohanraj and Chen, 2006).

Although CPZ entrapment in general was very poor, the results were comparatively desirable. It is demonstrated that CPZ entrapment values were at their highest when CLO levels were at their lowest. The reason for this could be that the higher hydrophobic CLO levels have a greater attraction for the hydrophobic PCL and hence displaces the CPZ which is highly hydrophilic. Results also revealed that the lowest polysorbate 80 levels resulted in high CPZ entrapment. A possible rationale for this could be the fact that higher polysorbate 80 levels result in greater levels of CPZ being entangled within the polysorbate 80 and removed when the particles were washed. The highest CPZ entrapment was observed when PCL levels were relatively low (500mg). This is atypical as it is expected that higher PCL levels would result in a greater CPZ entrapment as there is more polymer available to entrap the drug. Another atypical finding is that at a lower concentration of CPZ, greater levels of CPZ are entrapped. This could be possibly due to the entanglement of these lower levels of CPZ within the DHA and EPA chemical backbones hence resulting in a greater entrapment of the available CPZ and a greater CPZ entrapment overall. The results are highly desirable as they compare and may supersede the entrapments achieved in chapter 3 of this dissertation, where there was an absence of CLO. They are also desirable considering the relatively low concentrations of CPZ used in this study (2.5%$^{w}/_{v}$ for the majority of the formulations) as compared to the concentration of 5%$^{w}/_{v}$ used in the study in Chapter 3. Furthermore, far lesser levels of PCL were used in this study (350-2000mg) as compared to the study in Chapter 3 of this dissertation (1000-3000mg).

CLO entrapment ranged from 68.19±2.76-98.26±0.13% for all formulations synthesized according to the OVAT template (Table 4.2). Results are typical as the hydrophobic CLO has a great affinity for the hydrophobic PCL hence resulting in large amounts of CLO either entrapped or adsorbed onto the surface of the PCL. It was observed that at lower levels of PCL, CLO entrapment was relatively lower and at higher levels of PCL, CLO entrapment was greater. This is typical as higher levels of PCL present for more polymer and a larger surface area onto or with which the CLO can either be adsorbed or entrapped. Lower levels of CLO resulted in higher CLO entrapment whereas higher levels of CLO resulted in lower CLO entrapment or adsorption. This finding is typical as levels may reach a point of saturation where it can no longer be adsorbed or entrapped and is lost by processing. CPZ and polysorbate 80 had no significant effects on the entrapped or adsorbed CLO.

Table 4.2: CPZ and CLO entrapment of the nano-liposhells achieved for formulations synthesized according to the OVAT template.

Formulation	CPZ Entrapment (µg)	CLO Entrapment (%)
1	6690.55±207.30	91.72±1.19
2	3900.25±30.14	87.44±0.68
3	2625.92±150.23	96.24±2.81
4	2025.17±38.51	68.19±2.76
5	3200.15±342.23	88.96±0.51
6	5920.92±114.93	73.15±2.93
7	2400.06±13.45	90.74±0.52
8	3600.41±31.42	80.38±2.02
9	4700.18±14.47	86.15±0.95
10	1575.91±37.67	94.19±1.58
11	3150.73±71.35	92.86±1.51
12	4275.53±34.92	97.54±0.96
13	4650.25±80.57	96.96±1.92
14	4650.25±72.52	98.26±0.13

4.3.3 Determination of size and zeta potential of nano-liposhells

Table 4.3 represents the z-average size and zeta potential values obtained for each formulation synthesized in accordance with the OVAT template. Nano-liposhell z-average sizes ranged from 16.50±6.79-407.20±5.09nm thus confirming that the particles were of optimal size for nanoneuropharmaceutical applications. It was observed that smaller sizes were obtained when PCL levels were at their lowest and larger nano-liposhell sizes were the result of higher levels of PCL utilized. This is typical as higher levels of PCL generally result in greater aggregation of the particles as well as difficulty in shearing them into smaller particles when melted hence resulting in larger particle sizes. Lower CLO levels resulted in smaller particles whereas higher CLO levels resulted in larger sizes. This is due to the fact that CLO is highly hydrophobic and so is PCL hence the two have a great affinity for one another. This could have resulted in large amounts of CLO either entrapped or adsorbed onto the PCL surface thus resulting in larger particle sizes. Higher CPZ levels resulted in large nano-liposhell sizes whereas lower CPZ levels (2.5%$^{w}/_{v}$) resulted in the formation of particles with sizes below 100nm. This does appear to be typical as higher CPZ levels would invariably result in greater CPZ entrapment thereby resulting in larger particle sizes. However, this is not the case, as the sizes of formulations with the highest CPZ entrapment are smaller than those with lower CPZ entrapment. Polysorbate 80 levels appeared to have no noteworthy effect on the size of the nano-liposhells. When compared to the CPZ-loaded PCL-based nanoparticles synthesized in Chapter 3 of this dissertation, it is markedly evident that the nano-liposhells are of a much smaller size than the nanoparticles. This is probably

due to the very high PCL levels utilized in the nanoparticle formulations as opposed to the nano-liposhell formulations.

The zeta potential values obtained for formulations from the OVAT template ranged from --3.90±1.70-30.25±0.06mV (Table 4.3). All of the formulations, barring Formulation 3, displayed an absolute zeta potential of -20.00mV and above which is an indication of incipient to moderate stability. Increased levels of polysorbate 80 resulted in particles with high absolute zeta potential values whereas lower polysorbate 80 concentrations resulted in relatively lower absolute zeta potentials and unstable particles that tend to aggregate. The stability of the nano-liposhells was maintained by the steric interactions and weak electrostatic repulsive forces of adsorbed polysorbate 80 on the surface of the nano-liposhells (Kato et al., 2009; Ruckmani and Sanket, 2010). It was also noted that higher CLO levels caused a decrease absolute zeta potential when compared to formulations with lower CLO levels. Higher CLO levels tend to cause aggregation of the nano-liposhells and counteract the negative charge enforced by the polysorbate 80. This results in a loss of stability. The stability of the formed nano-liposhells was further enhanced by the high viscosity of the suspension mainly as a result of the glycerol and CLO utilized in the formulations. This increased viscosity resulted in a decreased terminal settling velocity and thus the nano-liposhells were dispersed for longer periods of time and took longer to settle hence high stability was conferred upon them.

Table 4.3: Nano-liposhell size and zeta potential obtained from formulations synthesized according to the OVAT template.

Formulation	Size (nm)	Zeta Potential (mV)
1	16.50±6.79	-24.70±1.27
2	140.30±4.81	-25.60±2.55
3	24.10±2.40	-20.60±2.83
4	100.00±4.95	-10.80±2.69
5	63.50±2.12	-30.25±0.06
6	67.80±2.83	-27.80±2.12
7	214.30±12.18	-26.30±2.55
8	30.00±1.48	-3.90±1.70
9	387.10±13.58	-22.50±2.26
10	100.30±15.84	-29.80±0.57
11	107.00±2.40	-25.60±2.55
12	228.90±1.70	-23.60±1.27
13	186.90±1.84	-28.50±1.70
14	407.20±5.09	-26.40±1.41

The distribution profiles for size and zeta potential of Formulation 3 of the OVAT template are represented in Figure 4.3. A single peak is desirable as it describes a formulation with limited distribution in size or zeta potential.

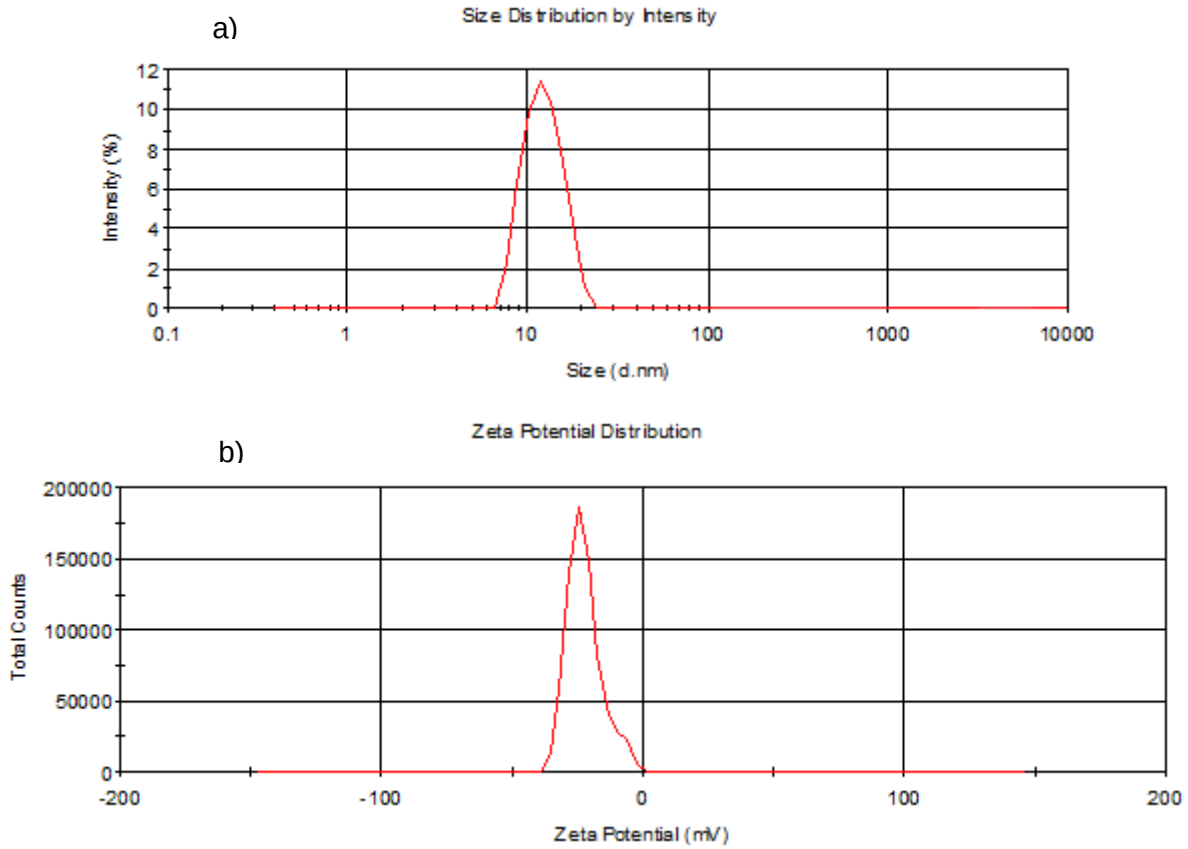

Figure 4.3: Distribution profiles of a) size and b) zeta potential of CPZ and CLO-loaded, PCL based nano-liposhells of Formulation 3 of the OVAT template.

4.3.4 Morphological analysis of the nano-liposhells

Figure 4.4 represents TEM images of the formulated nano-liposhells. Images revealed that nano-liposhells were spherical in shape and were of consistent size. Particles were well-individualized and displayed a high degree of de-flocculation when compared to the nanoparticles devoid of CLO, synthesized in Chapter 3 of this dissertation. This indicated that the formulations were highly stable. TEM images correlated the data achieved for size and zeta potential in Table 4.2. Figure 4.4 a) represents Formulation 4 of the OVAT template. As can be seen, the excess amounts of CLO are interspersed within the nano-liposhells leading to very dense regions and indicating that the nano-liposhells are saturated. Despite this, the nano-liposhells of this formulation are still recognizable and individualized. Figure 4.4 b), c) and d) represent Formulation 6 of the OVAT template. Nano-liposhells of this formulation are not interspersed with CLO and are of consistent shape and size. The surface morphology of nano-liposhells indicate that these formulations are much denser when compared to formulations of CPZ-loaded, PCL-based nanoparticles devoid of CLO

and synthesized in Chapter 3 of this dissertation. This is due to the entrapped and adsorbed CLO in the nano-liposhell formulations. This makes the accurate description of the surface morphology unclear as compared to the nanoparticles where the semi-crystalline nature of the PCL is visible. The nano-liposhells appear to be much smaller in size when compared to the nanoparticles of Chapter 3 and is probably due to the very high levels of PCL utilized in nanoparticle synthesis as opposed to nano-liposhell synthesis. This key variable outweighs the fact that CLO adsorbs onto PCL which theoretically should result in larger particles.

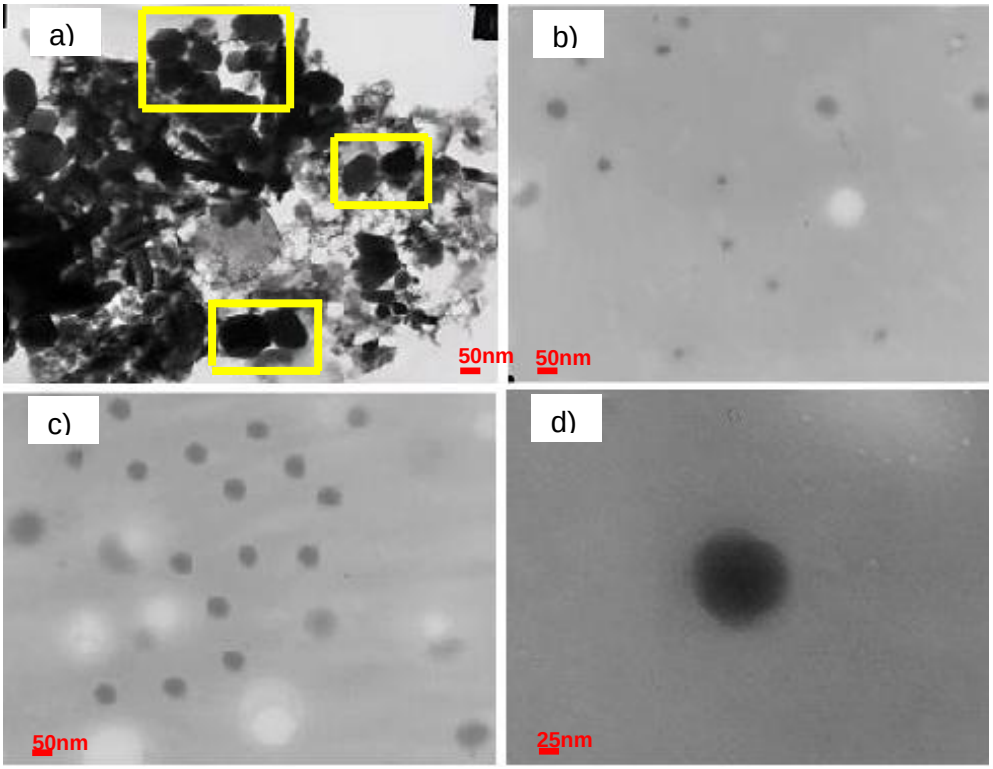

Figure 4.4: TEM of a) CPZ and CLO-loaded, PCL-based nano-liposhell Formulation 4 and c)-d) CPZ and CLO-loaded, PCL based nano-liposhell Formulation 6, [Magnification 25000x (a,b,c), 50000x (d)].

4.3.5 *In vitro* CPZ release from the nano-liposhells

All nano-liposhell formulations exhibited biphasic drug release patterns with an initial burst release followed by controlled release over a period of 32 days. The extent of the burst release varied according to each formulation. The biphasic release pattern is characteristic of nanoparticles based on PCL and may be as a result of various reasons including particle size, drug-loading and the rapid diffusion of adsorbed drug into solution (Hans and Lowman, 2002; Chawla and Amiji, 2002, Midhun et al., 2012). Generally a larger particle size results in a smaller burst release whereas a smaller particle size results in a greater burst release as discussed in Chapter 3 of this dissertation. Results from nano-liposhells are not consistent

with this statement as can been be seen with Formulation 3 which has a z-average particle size of 24.10±2.40nm but only displays a burst release of 25.65% of the entrapped CPZ. Formulation 6, which has a z-average size of 67.80±2.83nm, exhibits a burst release of 51.78% of the entrapped CPZ. The reason for this could be attributed to the effects of the entrapped or adsorbed CLO where Formulation 3 displays a greater CLO entrapment or adsorption when compared to Formulation 6. This higher CLO content may in fact retard the diffusion of CPZ into the PBS thereby resulting in a lower burst release. Formulation 3 exhibits a far lower CPZ entrapment when compared to Formulation 6 and a lower drug entrapment invariably results in a smaller burst release. This coupled with the higher CLO entrapment may solely result in the lower burst release of Formulation 3. Despite this rationale, anomalies in the results still occur. This is confirmed by comparing Formulation 1 which has a z-average size of 16.50±6.79nm and the highest CPZ entrapment of 6690.55±207.30µg but exhibits negligible to no burst release. Formulation 1 does however have a very high CLO entrapment which may result in its atypical release kinetics. Despite the irregularities in the CPZ release kinetics, all formulations displayed highly desirable release kinetics with extended, controlled release of CPZ after the initial burst for the duration of the study.

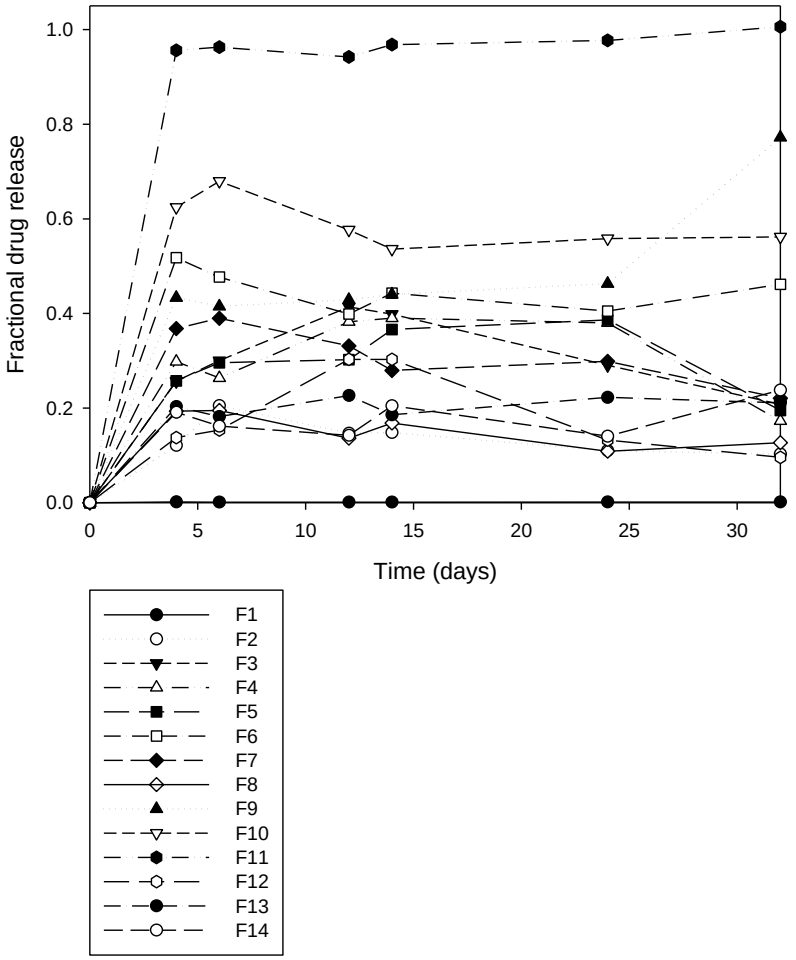

Figure 4.5: *In vitro* CPZ release profiles from CPZ and CLO-loaded, PCL based nanoparticles as per OVAT template, (SD≤0.35 in all cases, N=3).

4.3.6 *Ex vivo* cytotoxicity studies

Please refer to Chapter 6 of this dissertation for a full cytotoxic analysis of the nano-liposhells and its componential elements.

4.4 Concluding Remarks

CPZ and CLO-loaded, PCL-based nano-liposhells were successfully synthesized and display desirable *in vitro* characteristics. Considering the benefits of essential fatty acids in the adjunctive treatment of neurological disorders and the cost-effectiveness of using a source such as CLO to obtain active DHA and EPA, the study proved to be feasible. Despite this, a more extensive statistical design of experiments approach needs to be conducted whereby formulation variables such as CLO levels need to be considered and the relevant

responses such as its effects on drug release, assessed. However, the study does form a platform for expanding the possibility of combining conventional medicines with complementary and alternative medicine to form novel dual-acting drug delivery systems that optimize patient therapy and improve therapeutic outcomes.

CHAPTER 5

FORMULATION OF A NOVEL POLYAMIDE-ETHYLCELLULOSE COMPOSITE MEMBRANE FOR THE DESIGN OF THE IMPLANTABLE NANO-ENABLED POLYMERIC MEMBRANOUS DEVICE

5.1 Introduction

Polymeric membranes may be synthesized by a variety of specialized techniques however the most widespread technique for membrane synthesis involves phase inversion. Controlled phase inversion can be instigated by four major mechanisms; 1) air casting of a polymer solution, 2) Thermally-Induced Phase Separation (TIPS), 3) precipitation from the vapor phase and 4) immersion precipitation. The immersion precipitation is the most favorable due to the absence of interference from a vapor phase and the fact that the reaction is at room temperature. Briefly, a homogenous polymer solution is cast onto molds which are then exposed to a non-solvent in a coagulation bath. This results in the solvent from the polymer solution diffusing into the coagulation bath and the non-solvent from the coagulation bath diffusing into the polymer solution. Subsequently, precipitation of the polymer occurs resulting in the formation of symmetrical or asymmetrical membranes (Zhou, 2006).

Non-solvents play a pivotal role in membrane formation by phase separation. Use of a non-solvent decreases the dissolving power of the solvent subsequently resulting in an increase in polymer-polymer interaction. This in turn, results in polymer chains assuming a more tightly coiled conformation. Non-solvents accelerate the coagulation process from solution to gel by altering the phase separation behavior during the phase separation process. It does so by bringing the initial composition of the casting solution closer to the precipitation point. However, the addition of a non-solvent to the casting solution may also result in rapid polymer solidification at the membrane surface, resulting in uniform membranes with a thinner skin layer (Aroon et al., 2010).

Utilizing the immersion precipitation or wet-phase inversion technique results in the formation of morphologically differing membranes due to the lack of flexibility associated with the procedure. More often than not, alterations to the basic procedure may be required to obtain desired membrane structures (Lai et al., 1996). Due to the structure of the membranes being affected by modest changes in the preparation technique, there is significant incentive for developing mathematical models that will optimize these membranes and reduce the need for extensive trial and error testing (Altinkaya, 2006). An initial mass

transfer model of immersion precipitation was developed by Cohen and co-workers (1979). This was the platform around which many improvements were made (Cohen et al., 1979).

The use of membranes for various applications has been well established. Their use in the Bio-pharmaceutical industry, in particular drug-delivery applications, continues to increase in popularity. A study by Sibeko and co-workers (2008) demonstrated the effects of triethanolamine (TEA) on conjugated methotrexate (MTX)-loaded poly(L-lactic acid) (PLLA) and poly(vinyl alcohol) (PVA) membranes prepared by an immersion precipitation reaction. The study utilized computational molecular modeling and structural rationalization to optimize the design of these novel drug-loaded membranes and concluded that the composite biopolymeric membranes were suitable for the novel delivery of MTX (Sibeko et al., 2008).

Hoare and co-workers (2009) investigated the design and development of a novel magnetically triggered biocompatible, non-toxic membrane, implanted subcutaneously, for 'on-demand' drug delivery. Poly(N-isopropylacrylamide)-based nanogels and magnetite nanoparticles formed the basis of these composite membranes, which were activated by the application of a oscillating magnetic field. Once the magnetic field was applied, the 'on-off' release of sodium fluorescein was successfully achieved. Furthermore, the release of sodium fluorescein was proportional to the duration of device activation. Retention of the desirable switchable flux properties was observed following forty five days of subcutaneous implantation, thus justifying the effectiveness of the membrane as an 'on-demand' drug delivery system (Hoare et al, 2009).

A similar, more recent study by Chen and co-workers (2011) demonstrated the successful preparation of a thermo-responsive polyurethane-based membrane for the rapid, reproducible 'on-off' delivery of incorporated sulfamethoxazole and paclitaxel. The membranes were prepared by phase inversion and activated by an increase in temperature to 44°C. Temperatures below 37°C restricted the diffusion of model drugs through the membrane. In addition, it was established that the fraction of drug released when the membrane was activated was proportional to the duration of heating. Results obtained from the study revealed significant potential for formulating temperature-modulated biomedical implants for the treatment of various pathologies (Chen et al., 2011).

The formulation of a novel biodegradable hybrid polymeric membrane for the sustained ophthalmic delivery of ciprofloxacin epitomizes the wide-spread application of polymeric membranes as drug delivery devices (Jain et al., 2010). The ocular implants were

synthesized by solution casting and comprised PVA and sodium carboxymethylcellulose. Resultant ocular implants were smooth, wettable by simulated lacrimal fluid, non-toxic to the corneal epithelium and exhibited sustained ciprofloxacin release for a period of forty eight hours. This thus confirmed the ocular hybrid membrane as an effective drug delivery device for the management of various topical ocular infections.

The uses of membranes as drug delivery devices for various therapeutic applications are well-established however their use for the site-specific delivery of antipsychotic drugs in the Central Nervous System (CNS) is a facet yet to be thoroughly explored. The purpose of this study was to synthesize, characterize and optimize a novel, nano-enabled composite membrane comprising a novel synthesized polymer, polyamide 6,10 (PA 6,10) and ethylcellulose (EC), employing a modified immersion precipitation (wet-phase inversion) reaction. The Nano-Enabled Polymeric Membranous Device (NPMD) for intracranial implantation will comprise the CPZ-loaded, PCL-based nanoparticles synthesized in Chapter 3, matricized within the optimized membranous composite.

5.2 Materials and Methods

5.2.1 Materials

Hexamethylenediamine (HMD) (*M*w 116.2g/mol), sebacoyl chloride (SC) (*M*w 239.1g/mol), anhydrous *n*-hexane, ethylcellulose (EC), dialysis tubing, anhydrous potassium bromide, and anhydrous sodium hydroxide pellets were purchased from Sigma Chemical Company (St Louis, MO, USA). All other reagents used were of analytical grade and used as purchased.

5.2.2 Construction of a Face-Centered Central Composite Design

The formulation variables in this study were subjected to their higher and lower limits and thereafter Unhydrated Matrix Resilience (UHMR), Hydrated Matrix Resilience (HMR) and the extent of matrix erosion/swelling was determined for each formulation. Table 5.1 indicates the processing variables required for the synthesis of the novel PA 6,10-EC composite membranes and is a summary of the effects reflected in advanced preformulation studies. Based on this, the most influential variables were used to construct a Face-Centered Central Composite Design (FCCCD) comprising 13 statistically derived formulations (Table 5.2). PA 6,10 (150-200mg) and EC (100-200mg) were selected as the independent formulation variables. The dialysis time was kept constant at 7 days. The rationale for this was that a dialysis time below 7 days, indicated that formic acid (FA) was still present in the composite membrane, thereby rendering the device unsuitable for intracranial implantation as the effects of FA when in direct contact with the brain, could be detrimental. Furthermore, any

increase in dialysis time over 7 days, produced no change to the UHMR, HMR and degree of swelling/erosion when compared to dialysis for 7 days. A statistical model incorporating interactive and polynomial terms was utilized to evaluate the responses. Response surface plots were constructed to visually represent the influence of both the independent variables on the UHMR, HMR and erosion/swelling behavior of novel PA 6,10-EC composite membrane.

Table 5.1: Processing variables required for the synthesis of the novel PA 6,10-EC composite membranes and their effects on the membrane formulation based on advanced preformulation studies.

Processing variable	Effect on membrane formulation
PA 6,10 levels	
< 150mg	Considerable decrease in UHMR and HMR (≤45.62%) High degree of swelling
> 200mg	Modest increase in both UHMR and HMR when compared to 150≤PA,10≤200 Decrease in the degree of swelling, matrix erosion observed Loss of plasticity Increased brittleness
EC levels	
< 100mg	Loss of plasticity Increased brittleness Moderate increase in UHMR and HMR when compared to 100≤EC≤200 Low swelling potential, incipient matrix erosion (3.23%)
> 200mg	Increased plasticity Decrease in both UHMR and HMR (≤68.26%) Very high degree of swelling (53.55%)
Dialysis time	
< 7 days	No change to UHMR and HMR Very high degree of matrix erosion and no swelling observed (≥68.32%)
> 7days	No change to UHMR and HMR Swelling observed, no matrix erosion (23.25%)

Table 5.2: FCCCD template with statistically generated formulations for PA 6,10-EC composite membrane synthesis.

StdOrder	RunOrder	PtType	Blocks	Polyamide 6,10 (mg)	Ethylcellulose (mg)
13	1	0	1	175	150
11	2	0	1	175	150
7	3	-1	1	175	100
5	4	-1	1	150	150
3	5	1	1	150	200
2	6	1	1	200	100
12	7	0	1	175	150
10	8	0	1	175	150
6	9	-1	1	200	150
8	10	-1	1	175	200
4	11	1	1	200	200
9	12	0	1	175	150
1	13	1	1	150	100

5.2.3 Preparation of PA 6,10-EC composite membranes

The PA 6,10 utilized in this study is a novel polymer synthesized by Kolowale and co-workers (2007) utilizing a modified interfacial polymerization reaction for use as a rate-modulated monolithic drug delivery system (Kolowale et al., 2007). Prior to synthesis of the PA 6,10-EC composite membranes, PA 6,10 itself had to be synthesized. Briefly, 2 solutions were combined and reacted in the modified interfacial polymerization reaction. These comprised an aqueous (polar) solution of de-ionized water (DW) (10mL) to which, HMD (1.75g) and sodium hydroxide (NaOH) (0.1g) were added and a non-aqueous (non-polar) solution comprising hexane (HEX) (40mL), to which, cyclohexane (C-HXN) (40mL) and SC (0.63g) were added. Under a fume hood, the non-aqueous solution (HEX, C-HXN, SC) was gradually added to the aqueous solution (DW, HMD, NaOH) while stirring with a glass rod. A white gel-like mass formed and stirring continued until this substance could no longer absorb solvent. The excess solvent was then discarded in organic waste disposal unit. The polymer was rinsed with 100mL of de-ionized water 3 consecutive times and then placed on filter paper to remove excess solvent and made to dry on a petri dish for 30 minutes. The polymer was then convection dried in a laboratory oven (Memmert, West Germany) at 50˚C for 72 hours. Subsequent to complete drying, the polymer was blended for 10 minutes using a laboratory blender (CG 100, Kenwood Ltd, Cambridge UK) and then passed through an automatic granulating sieve of 1mm aperture size (Erweka AR 400; Optolabor (Pty) Ltd.) to ensure size uniformity.

Following the successful synthesis of the PA 6,10, PA 6,10-EC composite membranes were prepared by wet-phase inversion reaction according to the FCCCD template in Table 5.2. Briefly, PA 6,10 (150-200mg) was dissolved in 2mL Formic Acid (FA). The solution was heated to 60°C to aid the complete solubilization of the PA 6,10 in the FA. A separate solution was formulated and comprised EC (100-200mg) dissolved in 1mL of acetone (ACN) and this was placed on a magnetic stirrer at 500rpm. Once the PA 6,10 and the EC were completely solubilized in their respective solvents, the PA 6,10-FA solution was the gradually added to the EC-ACN solution and made to stir for 30 minutes on a magnetic stirrer at 500rpm. This led to the formation of a white, murky slurry of consistent texture. The slurry was then removed and added to a dialysis tubing membrane which was then suspended in 5L of de-ionized water. As water permeated through the dialysis tubing and came into contact with the slurry, it led to the formation of a white precipitate (Figure 5.1). The de-ionized water was tested with litmus paper to identify the presence of the FA and changed on a twelve hourly basis until all FA was removed from the precipitate. On average, the removal of FA took approximately 7 days. Once all FA was removed, the precipitate was appropriately molded in molds that were lined and pre-lubricated with liquid paraffin and then air-dried under a fume hood for 24 hours leading to the formation of the composite membranes.

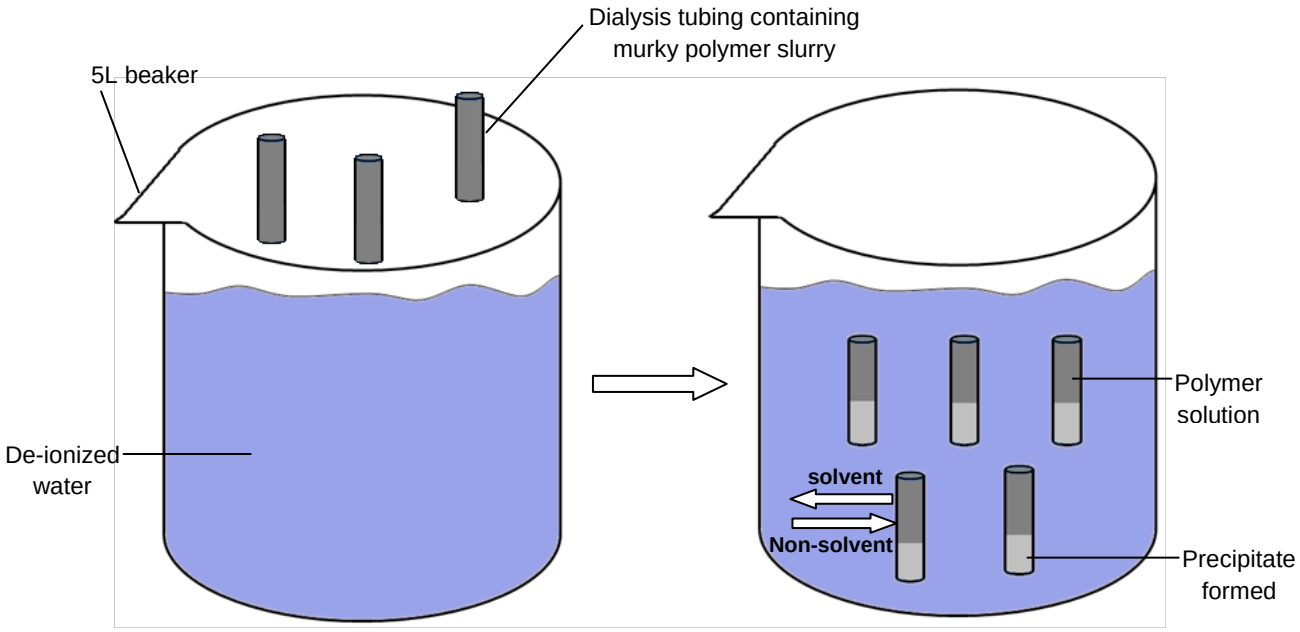

Figure 5.1: Schematic representing the novel wet-phase inversion reaction utilized to prepare the novel PA 6,10-EC composite membrane.

5.2.4 Determination of structural variations of polymers utilized in the PA 6,10-EC membrane synthesis

Fourier Transform Infrared Spectroscopy (FTIR) was undertaken to assess any structural variations in the composite membrane, as a result of any interactions between the polymers in the formulation. Furthermore FTIR was also utilized to determine the extent of blending of both the PA 6,10 and the EC. A Spectrum 100 FTIR Spectrometer (PerkinElmerLife and Analytical Sciences Inc., Shelton, CT USA) was used to detect the vibration characteristics of chemical functional groups in the sample, in response to infrared light interactions.

5.2.5 Determination of swelling/erosion behavior of the PA 6,10-EC composite membrane

Membrane swelling/erosion studies were performed using an orbital shaker bath, LM–530 (MRC Ltd., Holon, Israel). Samples of membranes as per experimental design were placed in beakers containing 100mL PBS at 37^0C and the shaker bath was rotated at 25rpm. After a predetermined period, the membrane samples were removed from the buffer and lightly dried with filter paper to remove any surface hydration. Swelling/erosion behavior was determined gravimetrically on days 3, 7, 14, 21 and 30 by comparing the mass of the samples at the mentioned time intervals to the initial mass of the samples according to Equation 5.1.

$$\% \text{ Mass loss/gain} = \frac{(\text{Initial Mass}) - (\text{Remaining Mass}) \times 100}{\text{Initial Mass}} \qquad \textit{Equation 5.1}$$

5.2.6 Textural profile analysis to determine the physicomechanical behavior of the PA 6,10-EC composite membrane

Textural profile analysis (TA) in terms of matrix resilience was conducted to characterize the 3D salient core regions of the PA 6,10-EC composite membrane using a Texture Analyzer (TA.XT*plus* Stable Microsystems, Surrey, UK). Unhydated (UHMR) as well as hydrated (at day 30 of swelling/erosion study) (HMR) samples of the composite membrane were analyzed. Computations of matrix resilience for both the unhydrated as well as hydrated membranes were performed using serial Force-Time profiles (N=3). UHMR was determined to ensure that the membranes remain robust, intact and durable during handling, storage and sterilization and HMR was determined to ensure that it would retain these properties and be devoid of breakage post-implantation. Table 5.3 outlines the TA settings utilized in the calculation of the matrix resilience values of the formulations of the experimental design.

Table 5.3: Parameters employed in the measurement of the UHMR and HMR of the PA 6,10-EC composite membrane samples employing the texture analyzer.

Parameter	Settings
Test Mode	Compression
Pre-Test Speed	1.0mm/sec
Test Speed	1.5mm/sec
Post-Speed Speed	1.5mm/sec
Target Mode	Strain
Strain	10%
Trigger Type	Force
Trigger Force	0.05N

5.2.7 Morphological characterization of the PA 6,10-EC composite membrane

5.2.7.1 Light microscopy

The surface analysis of the composite membrane was initially evaluated utilizing Light Microscopy (LM). LM, employing visible light, was used to superficially analyze the novel PA 6,10-EC composite membrane for shape, size and consistency. Samples were prepared by placing the membrane on a slide, mounting it to the stage, optimizing the light source and finally adjusting the condenser.

5.2.7.2 Scanning electron microscopy

The surface analysis as well as cross sectional analysis of the novel PA 6,10-EC composite membrane was further analyzed by Scanning Electron Microscopy (SEM) (Phenom™ FEI Company, OR, USA). Samples were prepared by being placed on adhesive carbon paper which was attached to a sample stub and then subjected sputter coating with gold for 90 seconds (SPI Module™ Sputter Coater, SPI Supplies, PA, USA) to make them electrically conductive. The stub was then inserted into the SEM and photomicrographs were taken at various magnifications.

5.2.8 Constraint optimization of formulation responses

A model-independent approach (Minitab® V15, Minitab Inc., Pennsylvania USA) was used to optimize the PA 6,10-EC composite membranes. Statistical optimization was therefore employed to ascertain the ideal polymeric (PA 6,10 and EC) combination with the desired physicochemical properties capable of attaining desirable UHMR, HMR and swelling/erosion characteristics.

5.2.9 Assimilation of the CPZ-loaded, PCL-based nanoparticles into the PA 6,10-EC composite membrane to form the NPMD

The assembly of the NPMD was carried out by incorporating and evenly dispersing the optimized CPZ-loaded, PCL-based nanoparticle formulation described in Chapter 3 into the optimized PA 6,10-EC composite membrane whilst in the process of molding the composite membrane. Briefly, some of the PA 6,10-EC slurry post dialysis was placed in the liquid-paraffin lubricated molds. This was followed by the addition of 500mg of optimized nanoparticles and the further addition of the remainder of the slurry. The molds were then placed under a fume hood and air-dried for 24 hours. This led to the formation of the NPMD (Figure 5.2).

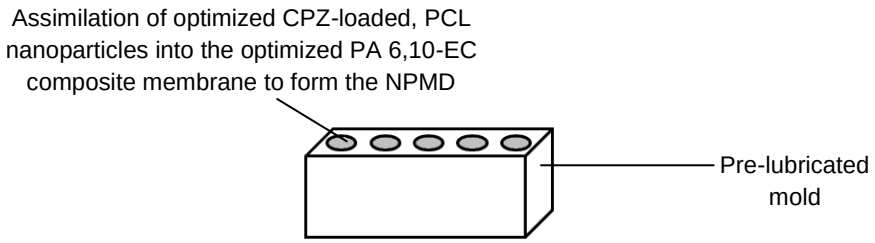

Figure 5.2: Schematic representation of the assembly of the NPMD.

5.2.10 Surface area and porosity analysis of the NPMD

Porosity analysis using a porositometer (ASAP 2020, Micromeritics Instrument Co., Norcross, GA, USA) was used to determine the quantifiable aspects of the NPMD's porous nature, such as pore diameter, total pore volume, surface area, and bulk and absolute densities. Removal of surface moisture and gas particles prior to analysis were necessary hence samples were initially subjected to degassing which included an evacuation phase and a heating phase. The parameters of the evacuation and heating phases are depicted in Table 5.4. NPMD's were weighed and placed in a cylindrical sample tube which was inserted with a glass filler rod to reduce the total free space within the sample tube which allowed for much timely degassing. The samples were covered in a thermal jacket prior to degassing. Degassing time in general was approximately 16 hours. Once the degassing was complete, samples were transferred to the analysis port and immersed in liquid nitrogen just prior to analysis.

Table 5.4: Parameters employed for the evacuation and heating phases during degassing of the NPMD.

Parameter	Rate/Target
Evacuation Phase	
Temperature ramp rate	10°C/min
Target temperature	90°C
Evacuation rate	50.0mmHg/s
Unrestricted evacuation from	5 mmHg
Vacuum set point	500 µmHg
Evacuation time	120 min
Heating Phase	
Temperature ramp rate	10°C/min
Hold temperature	350°C
Hold time	600 min

5.3.11 Drug entrapment efficiency of the NPMD

CPZ entrapment was assessed by crushing the NPMD with a pestle and mortar and then subjecting the crushed composite to high shear grinding using a laboratory blender (CG 100, Kenwood Ltd, Cambridge UK). The resultant powder was dissolved in 100mL PBS (pH 7.4, 37°C) and CPZ content as a percentage of the amount incorporated into the NPMD was assessed in triplicate and determined by ultraviolet (UV) spectroscopy (Cecil CE 3021, Cecil Instruments Ltd., Milton, Cambridge, UK) at 319nm against standard constructed curves.

5.2.12 Construction of calibration curve for spectrophotometric determination of CPZ release from Largactil®

A calibration curve for CPZ was constructed in Simulated Gastric Fluid (SGF) (pH 1.2; 37°C) using a known series of concentrations of CPZ. A linear curve was plotted with the observed absorbance on the y-axis and CPZ concentration (mg/mL) on the x-axis. A statistical representation of the degree at which the function fits the set of values (R^2 value) was computed for the calibration curve.

5.2.13 *In vitro* CPZ release from the optimized NPMD

In vitro release studies were performed on the optimized NPMD in an orbital shaking incubator (Labex, Stuart SBS40®, Gauteng, South Africa) set at 25rpm. The NPMD was once again placed in dialysis tubing membranes to counteract the loss of nanoparticles

during sampling. The NPMD was immersed in 100mL PBS (pH 7.4, 37°C) contained in 150mL glass jars. At predetermine time intervals 3mL samples of each release media were removed and filtered through a 0.22µm Cameo Acetate membrane filter (Millipore Co., Bedford, MA, USA) and analyzed by UV spectroscopy at a maximum wavelength of 319nm for CPZ content. CPZ release was quantified using a linear standard curve (R^2=0.99). An equal volume of CPZ-free PBS was replaced into the release media to maintain sink conditions.

In vitro release studies were also performed on a CPZ-loaded optimized PA 6,10-EC membrane. Free CPZ powder (as opposed to the CPZ-loaded PCL nanoparticles) was loaded into the optimized PA 6,10-EC composite membrane and the release was assessed to determine the release characteristics from the optimized composite itself. In addition, an *in vitro* release study was performed on a commercially available CPZ product (Largactil®) in SGF (pH 1.2, 37°C) utilizing a USP 25 rotating paddle method in a calibrated six-station dissolution apparatus (Caleva Dissolution Apparatus, model 7ST; G.B. Caleva Ltd., Dorset, UK), agitated at 50rpm with 900mL of SGF.

5.2.14 Magnetic Resonance Imaging to evaluate the performance of the NPMD in terms of erosion/swelling

Magnetic Resonance Imaging (MRI) (MARAN™-iP, Oxford Instruments Magnetic Resonance, Abingdon, United Kingdom) was utilized to assess the progression of hydration of the NPMD over a period of time and thus was employed to validate the erosion/swelling behavior of the NPMD. MRI covers a range of widely used techniques for studying the distribution and dynamics of a species within a material based on their nuclear magnetic resonance effects (Richardson et al., 2005; Laity et al., 2010). The NPMD was horizontally placed in a retaining band in the flow-through cell. The flow-through cell, containing the NPMD, operates in a closed loop, and circulated PBS through the loop, traversing the NPMD at a rate of 4mL/min and a temperature of 37°C. MRI images of the NPMD were acquired on days 0, 3, 7, 21 and 30 of the study at the same time of day to ensure accuracy. Between imaging, the NPMD was contained in 100mL of PBS rotating at 25rpm in an orbital shaker bath. The MRI imager acquires images on the basis of detecting mobile hydrogen nuclei associated with water and repeatedly images a slice through the NPMD during its hydration. The contrast difference between the PBS and the NPMD were optimized by manipulating the image acquisition parameters.

5.2.15 Determination of the thermal transition behavior of the NPMD and the constituent polymers utilized in its synthesis

Differential Scanning Calorimetry (DSC) and Temperature-Modulated Differential Scanning Calorimetry (TMDSC) (DSC 1 STAR^e Mettler Toledo system, Uster, Zürich, Switzerland) was performed on the NPMD and its constituent polymers to assess the thermal behavior and interpret their transitions. Furthermore, DSC and TMDSC were also employed to determine the compatibility between the constituents of the NPMD and assess the potential interactions that may have occurred either during the wet-phase inversion reaction or assembly of the NPMD. Sample preparation is described in Chapter 3, Section 3.4.2 of this dissertation.

5.3. Results and Discussion

5.3.1. Preparation of PA 6,10-EC composite membranes

Synthesis of the novel PA 6,10 polymer was conducted with relative ease although the process did prove to be time-consuming. Figure 5.3 illustrates the PA 6,10 polymer post-synthesis and prior to processing.

Figure 5.3: Digital image of the PA 6,10 polymer post-synthesis and prior to granulation.

The wet-phase inversion reaction for the preparation of the PA 6,10-EC composite membranes is depicted in Figure 5.4. The dialysis tubing membranes containing the slurry or PA 6,10-EC polymer solution was suspended in a 5L beaker filled with de-ionized water. De-ionized water acts as the non-solvent and when contact with the solvent inside the dialysis tubing was made, a precipitate was formed. The precipitate was appropriately molded and air-dried under a fume-hood for 24 hours to form the novel PA 6,10-EC composite membranes.

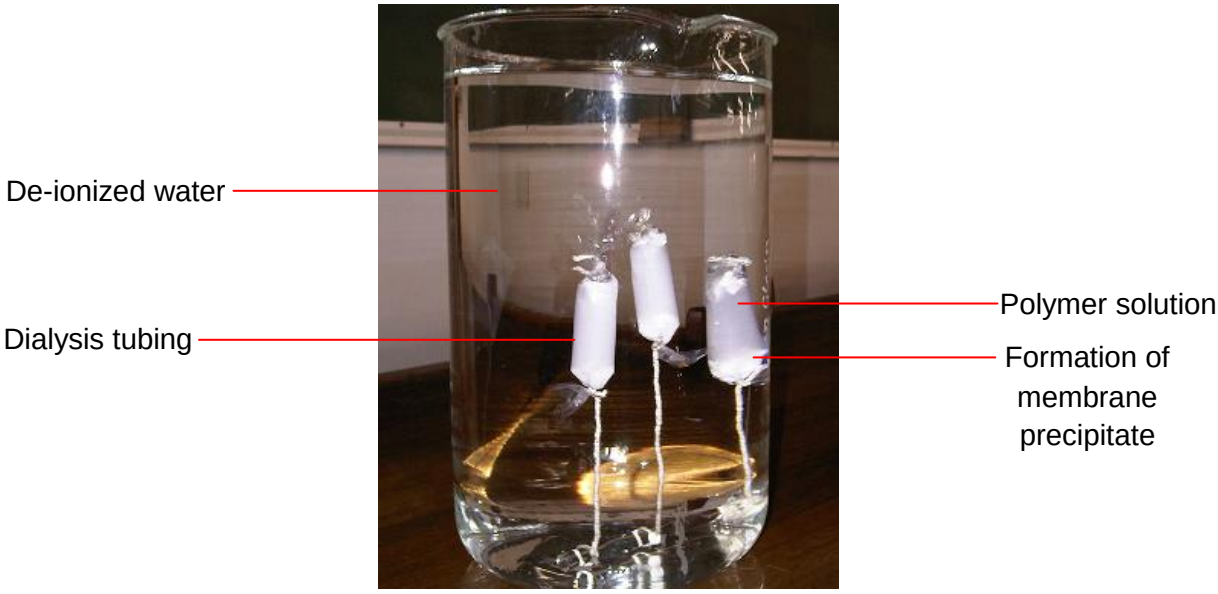

Figure 5.4: Digital image of the wet-phase inversion reaction depicting the formation of the PA 6,10-EC composite membrane.

5.3.2. Determination of structural variations of polymers utilized in the PA 6,10-EC membrane synthesis

FTIR spectra of EC, PA 6,10 and the synthesized PA 6,10-EC composite membrane are shown in Figure 5.5. The spectrum for EC depicts characteristic major absorption

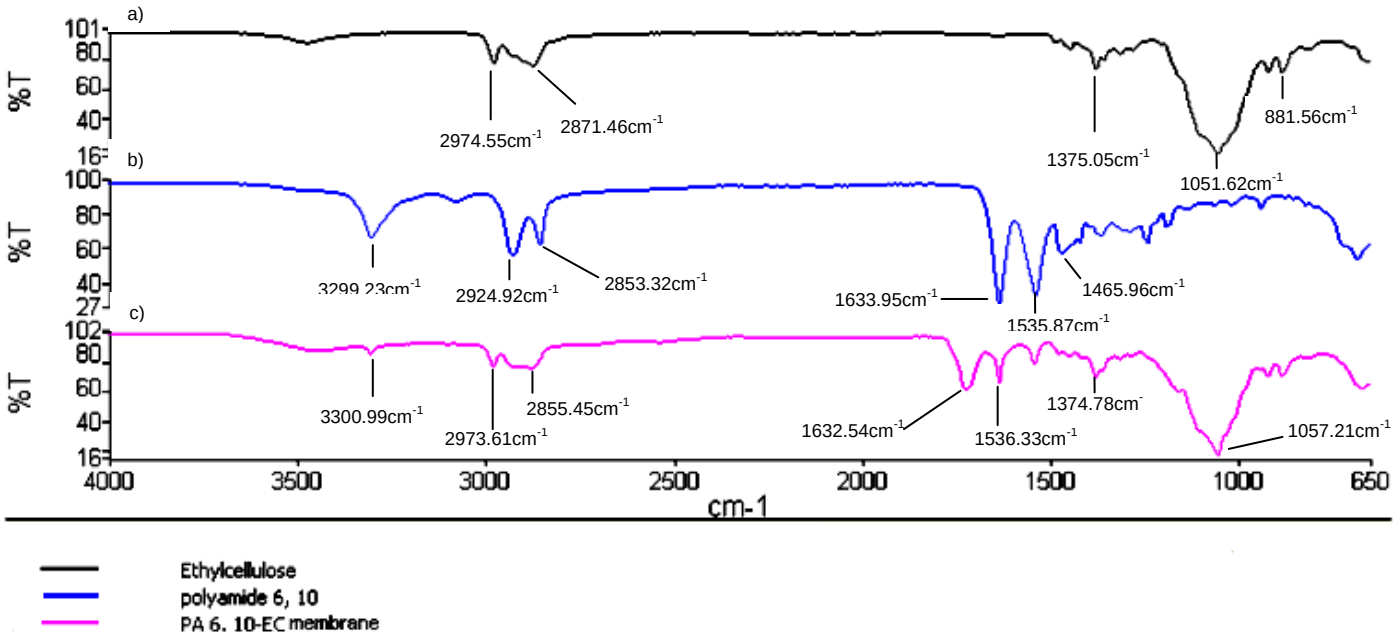

Figure 5.5: FTIR spectra of a) EC, b) PA 6,10 and c) PA 6,10-EC composite membrane.

bands at 2974.55 and 2871.46cm^{-1} which are indicative of C-H stretching, 1375.05cm^{-1} which represents C-H bending and 1051.62 cm^{-1} which is an indication of –C-O-C- stretching

(Suthar et al., 2000). PA 6,10 exhibits transmitting bands of amide (N-H) at 3299.23 cm^{-1}, C-H stretching at 2924.92 and 2853.32cm^{-1}, C=O stretching at 1633.95 cm^{-1}, and a CH_2 wag at 1465.96 cm^{-1} (Kolowale et al., 2007). The novel PA 6,10-EC composite membrane confirmed the presence and integrity of both PA 6,10 and EC functional groups in its chemical backbone. Absorption bands at 3300.99 cm^{-1} confirmed a N-H transmitting band. This is a phenomenon characteristic of the PA 6,10 synthesized. C-H stretching at 2973.61 and 2855.45cm^{-1} of the novel composite membrane were present in both PA 6,10 and EC. C=O stretching in the novel composite at 1632.54cm^{-1} was consistent with C=O stretching of the PA 6,10 and C-H bending at 1057.21cm^{-1} of the novel composite was also present in the EC functional group backbone. Results thus confirmed the success of the wet-phase inversion reaction and were an indication of near-perfect blending of the two polymers in the synthesis of the novel PA 6,10-EC composite membranes.

5.3.3 Determination of swelling/erosion behavior of the PA 6,10-EC composite membrane

The degree of swelling for formulations of the experimental design at day 30 of the study ranged from 14.92±1.75-49.72±5.0% and is depicted in Table 5.5. It is demonstrated that formulations with a greater EC content exhibit a higher degree of swelling. Despite EC being known as a water-insoluble polymer, it does exhibit a certain degree of water uptake resulting in the swelling behavior of the membranes. The water-uptake trait of EC is primarily due to the hydrogen bond capability of EC with water as a result of the polarity difference between the oxygen atom and the ethyl group in the ethoxy group of the polymer. Furthermore, depending on the degree of substitution, the presence of hydroxyl groups can also contribute to the interaction between EC and water resulting in the potential to form weak hydrogen bonds with water molecules (Agrawal et al., 2003, Jackson and Ofoefule, 2011). In addition to this, PA 6,10 itself, is a moderately hydrophilic polymer compared to the rest of the polyamides. This further allows the uptake of hydration media thereby contributing to the swelling properties observed in all formulations of the experimental design (Kolowale et al., 2007). The gravimetric swelling profile of Formulation 1 of the experimental design is represented in Figure 5.6. The initial mass increase due to swelling is relatively large followed by a slower increase in the membrane mass. This is probably due to the initial surface erosion of EC coupled with the moderate hydrophilic nature of PA 6,10 which is followed by PBS uptake and then saturation of the membrane. The swelling ability of the drug delivery system is an integral factor in determining the drug release kinetics. The ability of the membrane to swell, results in retarded, more controlled drug delivery. Despite this, depending on the route of administration of the drug delivery system i.e. implantation, care

must be taken as excessive swelling could result in a pronounced immune response and other major complications.

Table 5.5: Swelling behavior of the novel composite PA 6,10-EC membranes as per experimental design.

Formulation number	% Swelling (Mass increase at day 30)
1	14.92±1.75
2	15.69±1.24
3	20.58±1.78
4	13.78±1.52
5	49.72±5.70
6	32.37±2.91
7	16.86±1.17
8	15.88±1.72
9	20.93±2.13
10	48.49±4.13
11	33.20±2.08
12	16.03±0.83
13	21.55±2.65

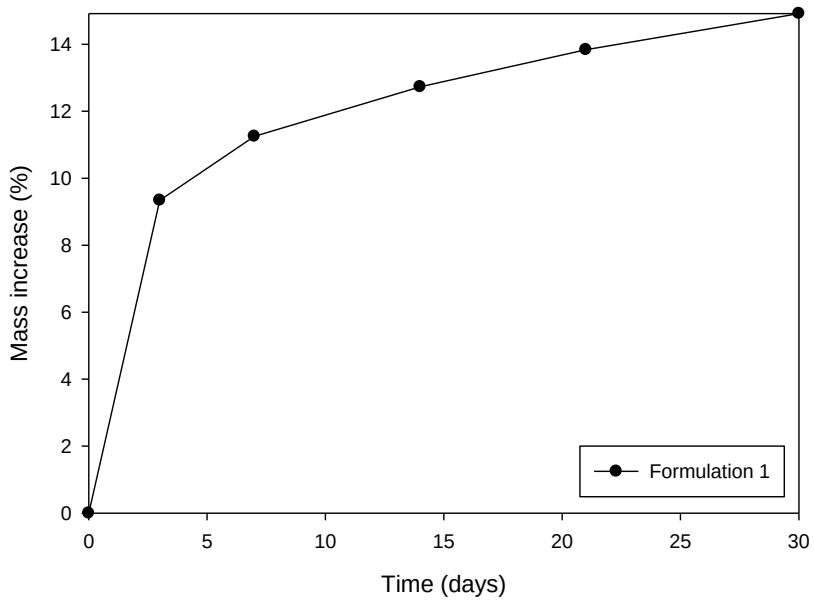

Figure 5.6: Swelling profile of Formulation 1 of the experimental design in PBS (pH 7.4, 37°C) over a period of 30 days.

5.3.4 Textural profile analysis to determine the physicomechanical behavior of the PA 6,10-EC composite membrane

The UHMR values ranged from 69.28±2.45 to 86.05±4.17% whereas the HMR values ranged from 51.11±11.40 to 85.24±2.75% and is depicted in Table 5.6. Results proved that the novel PA 6,10-EC composite membranes were highly resilient in both their unhydrated as well as hydrated states. Samples with a greater EC content and a lower PA 6,10 content generally displayed greater resiliencies than samples with lower EC and greater PA 6,10 content. PA 6,10 is a semi-crystalline polymer that possesses a moderate degree of elastic cohesiveness. Matrices based solely on PA 6,10 may be highly brittle in nature. EC is a polymer that is well-known for enhancing the strength of drug delivery matrices and this is proved by the results obtained. EC alone imparts a large degree of tensile strength, flexibility and plasticizing effects to the composite membrane. Furthermore, EC contributed toward the suppleness of the membranes making them conducive for drug delivery purposes as devices that are highly rigid and brittle may result in a negative immune response from the body. The unhydrated membranes in general showed greater integrity than the hydrated membranes. The lower HMR results are once again probably due to the initial surface erosion of the EC together with the hydrophilicity of the PA6, 10, followed by the uptake of PBS by the membranes, thus resulting in swellable membranes with a loss of rigidness and integrity and hence a lower MR. Despite this, the physicomechanical properties of the novel composite membranes remained to be greatly desirable with MR for all hydrated formulations being above 50% and reaching highs of approximately 85%. High HMR values are thought to be due to the interaction of water molecules with the PA 6,10 which may result in chain entanglement thus resulting in a more resilient membrane (Kolowale et al., 2007).

Table 5.6: MR of unhydrated and hydrated composite membranes as per experimental design.

Formulation number	UHMR (%)	HMR (Day 30) (%)
1	78.13±0.86	70.00±2.19
2	78.72±2.08	71.37±3.50
3	78.24±4.13	51.11±11.40
4	73.10±2.02	76.12±3.67
5	86.05±4.17	76.85±2.58
6	84.19±2.43	78.54±2.34
7	80.84±1.67	76.40±3.17
8	79.91±4.18	73.24±4.34
9	69.28±2.45	67.96±3.18
10	83.52±3.45	73.05±5.58
11	82.04±1.42	85.24±2.75
12	75.99±4.89	65.82±5.95
13	72.34±2.85	52.63±4.57

Figure 5.7 is a typical force-time profile of a) the UHMR of Formulation 1 of the experimental design and b) the HMR of Formulation 1 of the experimental design. Matrix resilience is represented as a percentage of the ratio between the Area Under the Curve (AUC) of anchors 1 and 2 (AUC 1 and 2), and 2 and 3 (AUC 2 and 3).

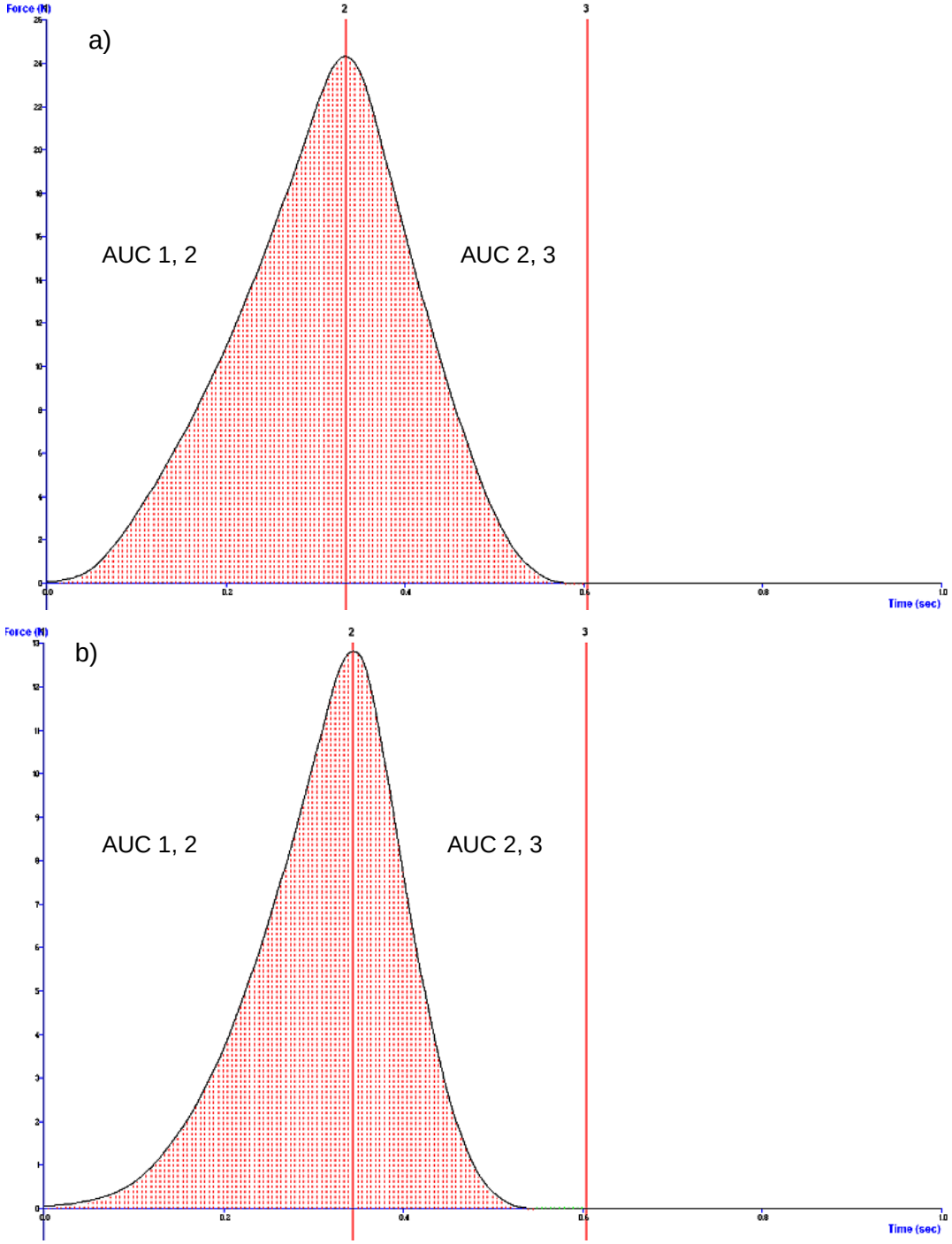

Figure 5.7: Typical force-time profiles of Formulation 1 of the experimental design depicting a) UHMR and b) HMR.

5.3.5 Morphological characterization of the PA 6,10-EC composite membrane

Figure 5.8 depicts LM images of the surface of the novel PA 6,10-EC composite membrane in the a) unhydrated as well as b) hydrated forms at Day 30. Figure 5.8 also depicts SEM images of the surface of the novel PA 6,10-EC composite membrane in b) and c) the unhydrated formed and g) and h) the hydrated forms at Day 30. Furthermore, SEM examines the bulk of the novel PA 6,10-EC composite membrane in its unhydrated state in

Figure 5.8 e) and f). LM images of unhydrated and hydrated membranes revealed dense, irregular matrices with small pores. The surface analysis using SEM confirmed the presence of dense membranes with relatively small pores. The cross sectional analysis of the novel PA 6,10-EC composite membrane a revealed highly porous bulk interspersed with large craters. The porosity and cavernous nature of the bulk region of the membrane was attributed to entrapped air within the formulation during synthesis. Results are indicative of a membrane system with a moderately porous, dense outer structure and a highly porous bulk which is indicative of instantaneous demixing when the membrane is formed (Zhou B, 2006). Upon exposure to PBS, the SEM and LM surface analysis of the hydrated membranes appear to be much more densely packed when compared to the unhydrated membranes and pores were no longer as pronounced as they were in the unhydrated state. As PBS diffused through the unhydrated membrane, it led to an increase in its crystallinity. Furthermore, interactions between water molecules and the PA 6, 10 may have resulted in chain entanglement thus resulting in rigid, densely packed composite membranes.

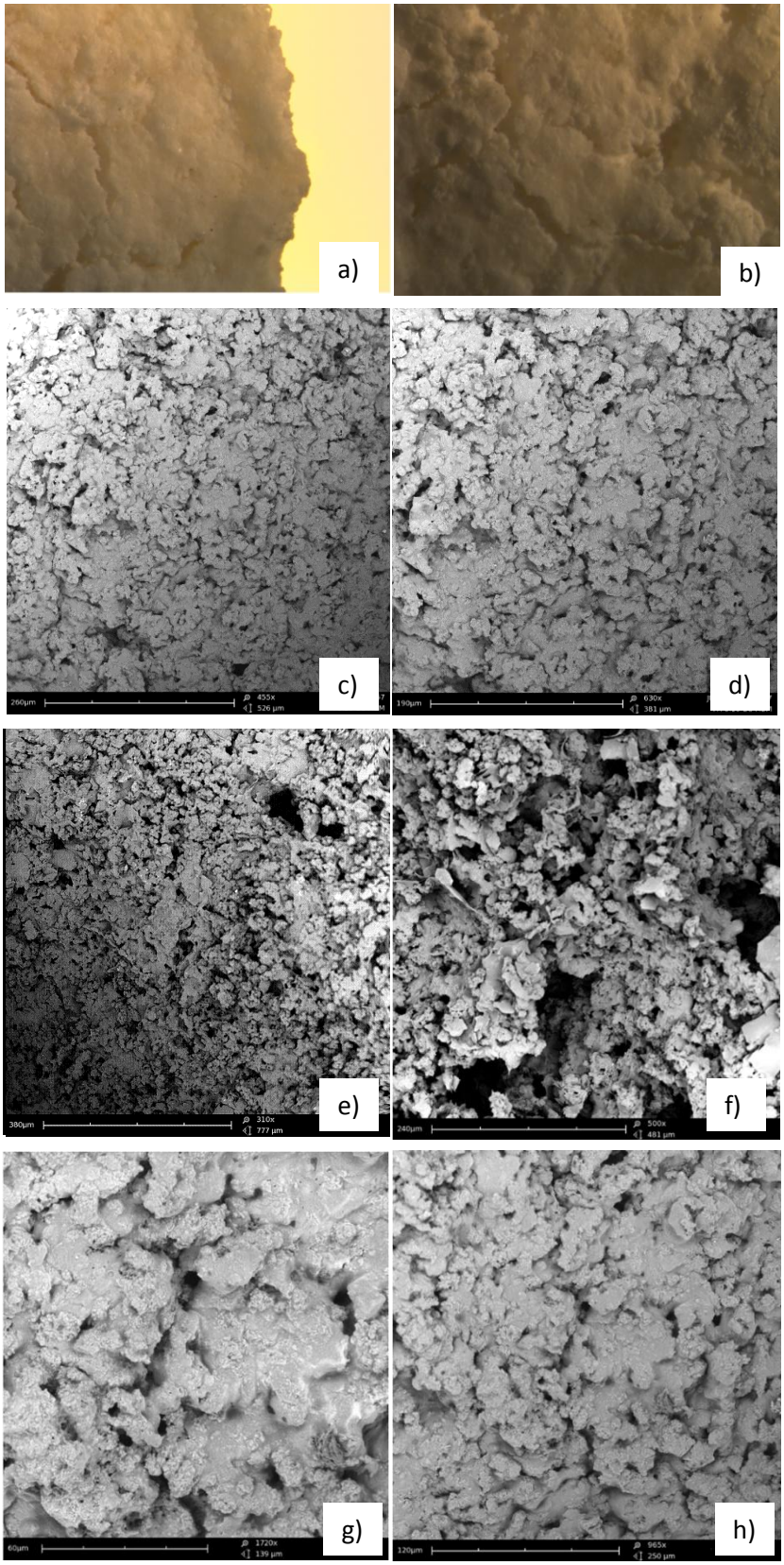

Figure 5.8: Light microscopy of a) unhydrated composite membrane b) hydrate composite membrane and Scanning Electron Microscopy of c)-d) unhydrated surface composite membranes and e)-f) unhydrated bulk of composite membrane and g)-h) hydrated surface of composite membranes.

5.3.6 Analysis of Face-Centered Central Composite Design

In order to optimize the novel PA 6,10-EC composite membrane, UHMR, HMR and the degree of swelling/erosion were incorporated into the experimental design. The residual plots for these respective responses are depicted in Figure 5.9. The normal probability plots of the residuals for all three responses depict a uniform distribution of points along the straight line indicating a normal distribution of data devoid of external influence. Scattering of points on either side of 0 on the residual versus fitted plots were generally good indicating a random scatter with no trends however some clustering was observed for HMR. Histograms further confirmed the normal distribution of the residuals with constant variance and zero mean. Non-random error was indicated by the residuals versus order of the data plots. The residuals bounce randomly on either side of the 0 line indicating that there is no serial correlation. A full ANOVA was carried out and is depicted in Table 5.7. A significant effect of any factor is indicated by a p-value ≤ 0.05 for any factor.

Table 5.7: Full ANOVA analysis for the measured responses (UHMR, HMR and the degree of swelling/erosion).

	p-values		
Term	**UHMR**	**HMR**	**Degree of swelling/erosion**
[PA 6,10]	0.054	0.341	0.713
[EC]	0.771	0.120	0.035
[PA 6,10*PA 6,10]	0.099	0.226	0.794
[EC*EC]	0.02	0.368	0.000
[PA 6,10*EC]	0.047	0.265	0.008

Where PA 6,10 = polyamide 6,10 and EC = ethylcellulose

The complete regression equations generated for UHMR, HMR and degree of swelling/erosion are indicated below:

*UHMR = -149.663 + 2.609[PA 6,10] – 0.100[EC] – 0.006[PA 6,10*PA 6,10] + 0.002 [EC*EC] – 0.003 [PA 6,10*EC]* *Equation 5.2*

*HMR = 166.163 – 2.533[PA 6,10] + 1.292 [EC] + 0.009 [PA 6,10*PA 6,10] – 0.002[EC*EC] – 0.004 {PA 6,10*EC]* *Equation 5.3*

*Degree of Swelling/Erosion = 32.3332 + 0.4893[PA 6,10] – 0.9880[EC] + 0.0010[PA 6,10*PA 6,10] + 0.0071[EC*EC] – 0.0055[PA 6,10*EC]* *Equation 5.4*

a)

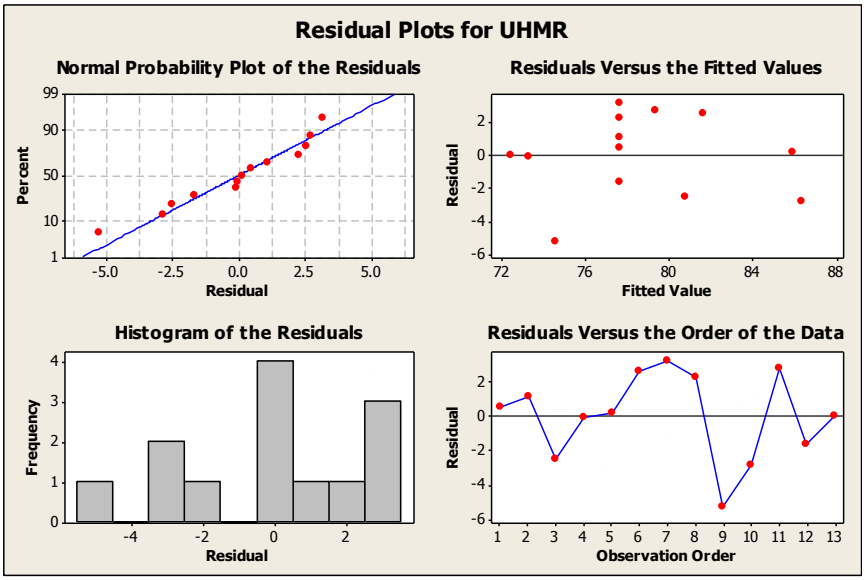

b)

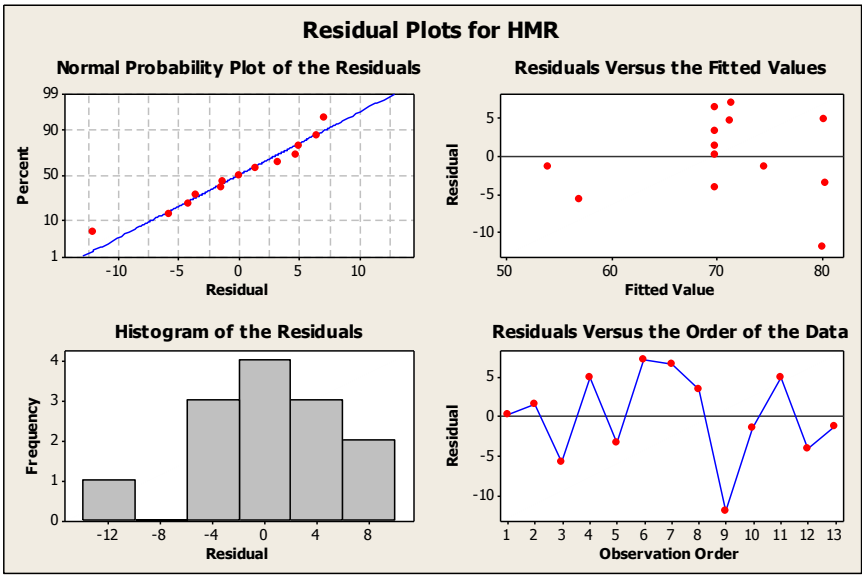

c)

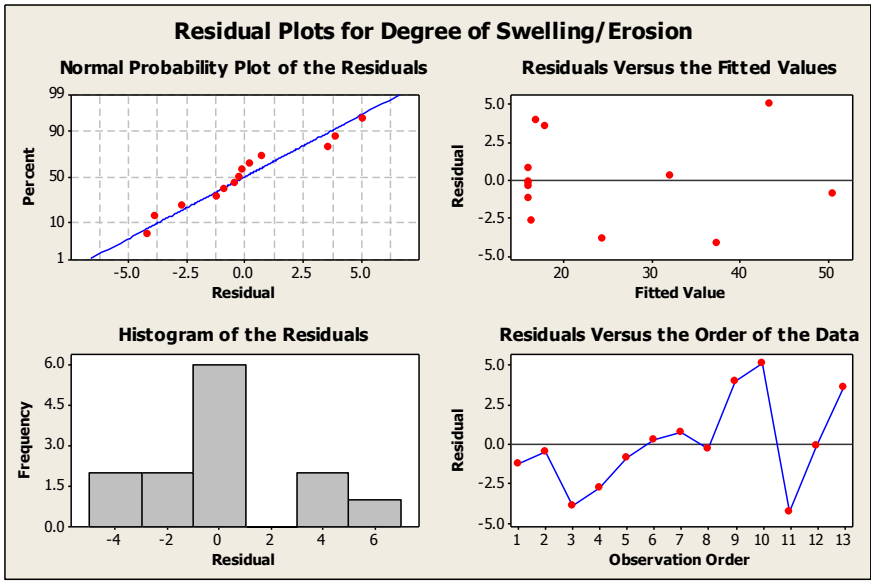

Figure 5.9: Residual plots for the response a) UHMR, b) HMR and c) degree of swelling/erosion.

5.3.7 Response surface analysis

Response surface and contour plots were use to represent the functional relationship between the experimental variables and the responses achieved based on the experimental model and are depicted in Figure 5.10.

The effects of PA 6,10 and EC on UHMR are shown in [Figure 5.10 a)]. It can be seen that at lower EC levels, UHMR is considerably high. As the levels of EC increase, UHMR decrease. This is due to the fact that a greater EC content increases the plasticity and suppleness of the membrane, causing a decrease in its UHMR. It is interesting to note that as EC levels increase from 150-200mg, so too does the UHMR. At lower levels of PA 6,10, UHMR is considerably low. As the levels of PA 6,10 increase, so too does the UHMR. The combined effects of both PA 6,10 and EC display optimum UHMR at increasing levels of EC and decreasing levels of PA 6,10. This is an atypical finding as the PA 6,10 has superior physical and mechanical properties due to their ability to form intra and intermolecular forces between amide (-NH-) and carbonyl (-CO-) within and between the linear chains in the polyamide crystal (Kolowale et al., 2007). Furthermore, EC is known to add a degree of suppleness, elasticity and plasticity to the membranes hence it is expected that higher levels of EC would result in a decreased UHMR. The hydrogen bonding between the hydroxyl groups on the EC polymeric backbone also results in the rigidness and flexibility of EC (Zhang et al., 1997). Furthermore, the highly amorphous nature of EC is hypothesized to be the cause of the increased UHMR (Sakellariou et al., 1985).

The effects of PA 6,10 and EC on HMR are shown in [Figure 5.10 b)]. Results for the effects of PA 6,10 and EC levels on HMR reveal that at lower levels of PA 6,10, the HMR is at a minimum and as the PA 6,10 levels increase so too does the HMR. HMR is at a minimum when EC levels are low. As EC increase so too does HMR however at an EC level of 150mg and above, no additional increase in HMR is observed as the plot plateaus. The combined effects of PA 6,10 and EC on HMR display desirable HMR results when both levels are increased. Effects of EC are limited when hydration occurs, which plateaus out. This is due to the fact that EC only adsorbs minimal water and is primarily hydrophobic.

The effects of PA 6,10 and EC on the degree of swelling/erosion are shown in [Figure 5.10 c)]. The degree of swelling was nominal when PA 6,10 levels were at their lowest and increased minimally as the levels of PA 6,10 increases. This is due to the moderately hydrophilic nature of the PA 6,10. The degree of swelling of the membranes was at its highest when the levels of EC were at its highest. The combined effects of both PA 6,10 and EC on the degree of swelling of the membranes prove that at lower PA 6,10 and higher EC

levels, the degree of swelling is at its highest. Despite EC being known as a water-insoluble polymer, it does exhibit a certain degree of water uptake resulting in the swelling behavior of the membranes. The water-uptake trait of EC is primarily due to the hydrogen bond capability

a)

b)

c)

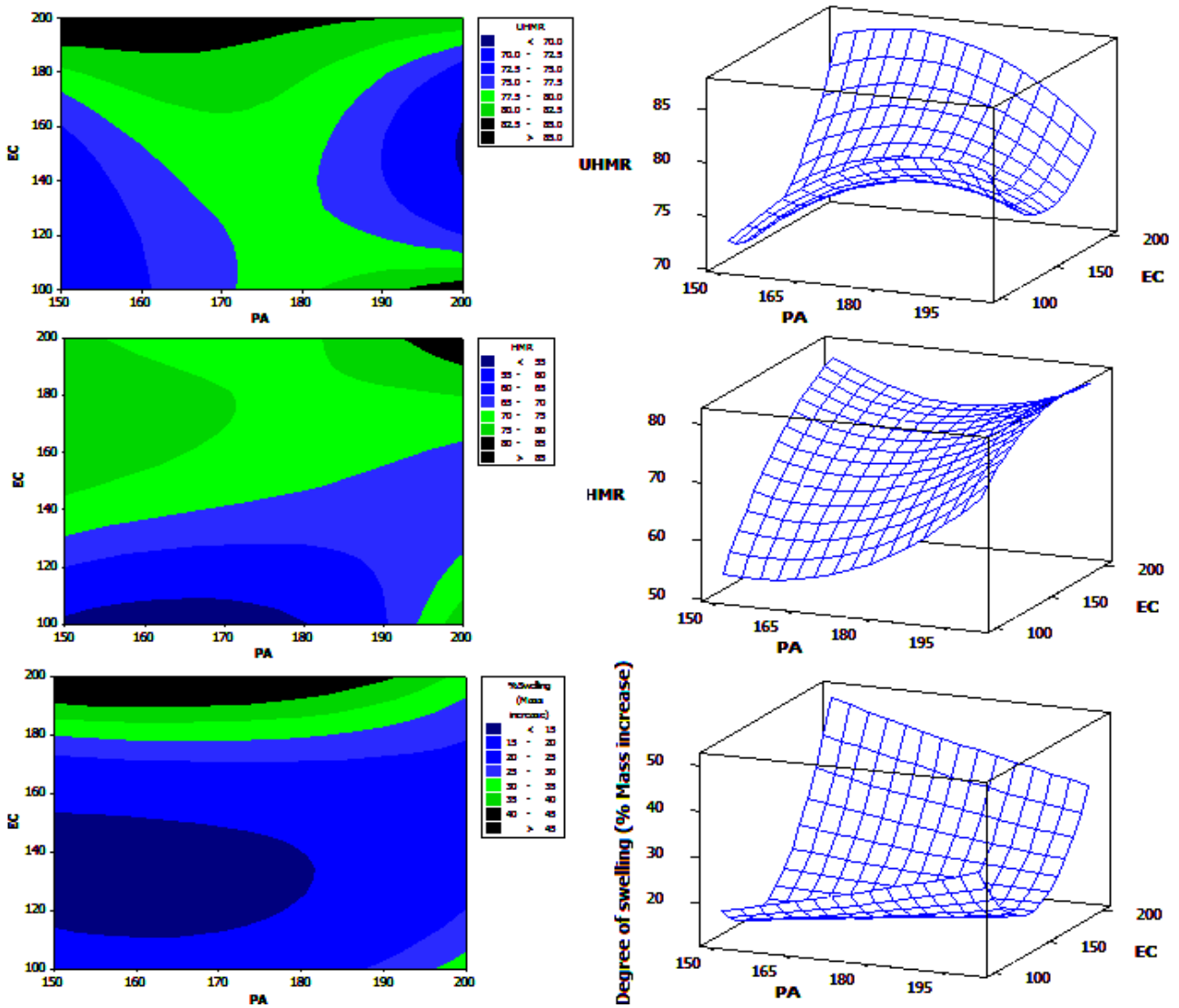

Figure 5.10: Response surface and contour plots depicting the effects of PA 6,10 and EC on a) UHMR, b) HMR and c) degree of swelling/erosion.

of EC with water as a result of the polarity difference between the oxygen atom and the ethyl group in the ethoxy group of the polymer. Furthermore, the presence of hydroxyl groups can also contribute to the interaction between EC and water resulting in the potential to form weak hydrogen bonds with water molecules (Agrawal et al., 2003; Jackson and Ofoefule, 2011).

5.3.8 Constraint optimization of formulation responses

A single, optimal formulation was developed subsequent to constraint optimization of UHMR, HMR and degree of swelling/erosion. Response optimization was carried out utilizing statistical software (Minitab®, V14, Minitab Inc®, PA, USA) to determine the optimum level of each of PA 6,10 and EC. Figure 5.11 depicts the desirability plots of each constraint for the single optimal formulation. Constraint settings utilized are represented in Table 5.8. The optimal levels of the independent variables that would achieve the desired UHMR, HMR and degree of swelling/erosion are depicted in Table 5.9.

Table 5.8: Formulation constraints utilized for response optimization.

Responses	Limits
UHMR	Maximize
HMR	Maximize
Degree of swelling	Minimize

Where UHMR = unhydrated matrix resilience and HMR = hydrated matrix resilience

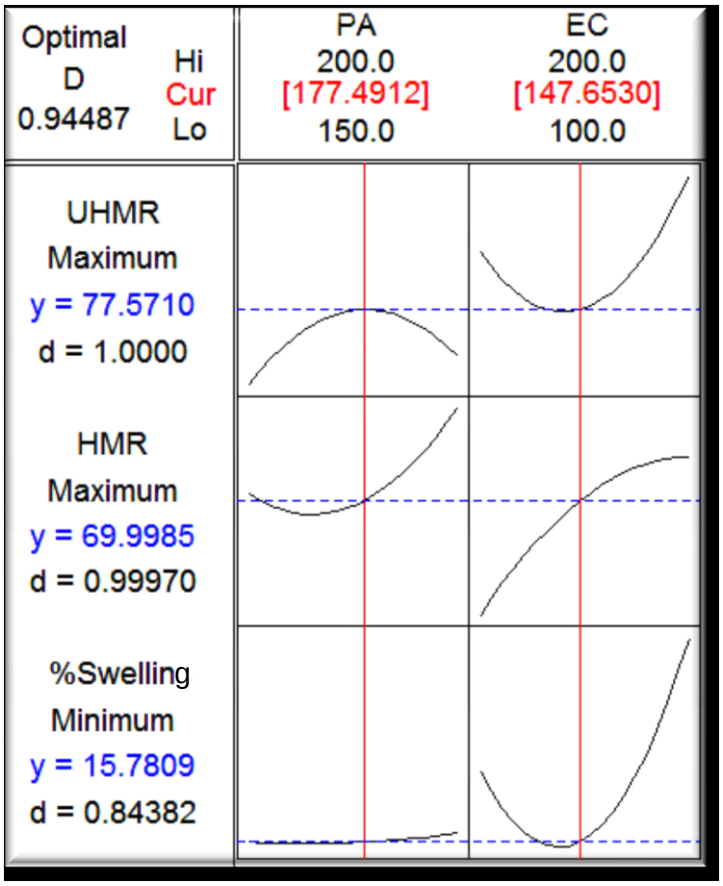

Figure 5.11: Desirability plots representing the levels of PA 6,10 and EC required to synthesize the optimized formulation.

Table 5.9: Optimized PA 6,10-EC composite membrane formulation derived from the surface response method.

	PA 6,10 (mg)	**EC (mg)**
Optimized Formulation	177.4912	147.6530

Table 5.10 represents the optimized levels of the independent variables, the predicted responses, the desirability score as well as the correlation co-efficient for each response. The experimentally derived values for both UHMR and HMR were in close agreement with predicted values of the statistical design with desirability being 95.71 and 82.99% respectively. Figure 5.12 depicts the force-time profiles of both the a) UHMR and b) HMR of the optimized PA 6,10-EC composite membrane. The degree of swelling predicted at day 30 was 15.78% for the optimized PA 6,10-EC composite membrane. The experimental values achieved were rather atypical displaying erosion of the optimized PA 6,10-EC membrane of

3.64±0.08% at day 30. When assessed gravimetrically (Figure 5.13), the optimized PA 6,10-EC composite membrane displayed biphasic hydration phenomena. At Day 7 of the experiment, the optimized membrane exhibited swelling behavior with a gradual increase in mass of 0.97±0.15%. Thereafter the membrane began to erode with decreases in its mass at Days 14, 21 and 30 of 3.31±0.16%, 3.55±0.07% and 3.64±0.08% respectively. A possible cause of this irregularity is the ratio of PA 6,10:EC utilized in the synthesis of the optimized formulation. At the levels utilized, the moderate EC content coupled with the moderate hydrophilicity of PA 6,10 could account for the initial swelling whereas the greater PA 6,10 content in the formulation, which is a semi-crystalline, highly brittle polymer, resulted in the erosion behavior. Despite the major anomaly, the overall performance of the optimized novel PA 6,10-EC composite membrane was highly desirable as this formulation will be utilized in the assembly of the NPMD which is intended for intracranial implantation. An intracranial implant with swelling characteristics may result in an exaggerated immune response as well as an increase in intracranial pressure which can prove to be fatal. Furthermore, the bioerosion behavior of the NPMD will help us understand the clearance of the NPMD from the brain. Figure 5.14 is a geometric visualization of conformational profile of membrane formation performed using the HyperChem^{TM} 8.0.8 Molecular Modeling System (Hypercube Inc., Gainesville, Florida, USA) and ChemBio3D Ultra 11.0 (CambridgeSoft Corporation, Cambridge, UK) on an HP Pavilion dv5 Pentium Dual CPU T3200 workstation.

Table 5.10: Predicted, experimental and desirability values of the optimized PA 6,10-EC composite membrane formulation.

Measured response	Predicted value	Actual value	Desirability (%)
UHMR	77.57	74.24±0.88	95.71
HMR	70.00	84.35±1.22	82.99
Degree of swelling (day 30)	15.78	3.64±0.08 **EROSION**	**+**

Where UHMR = unhydrated matrix resilience and HMR = hydrated matrix resilience

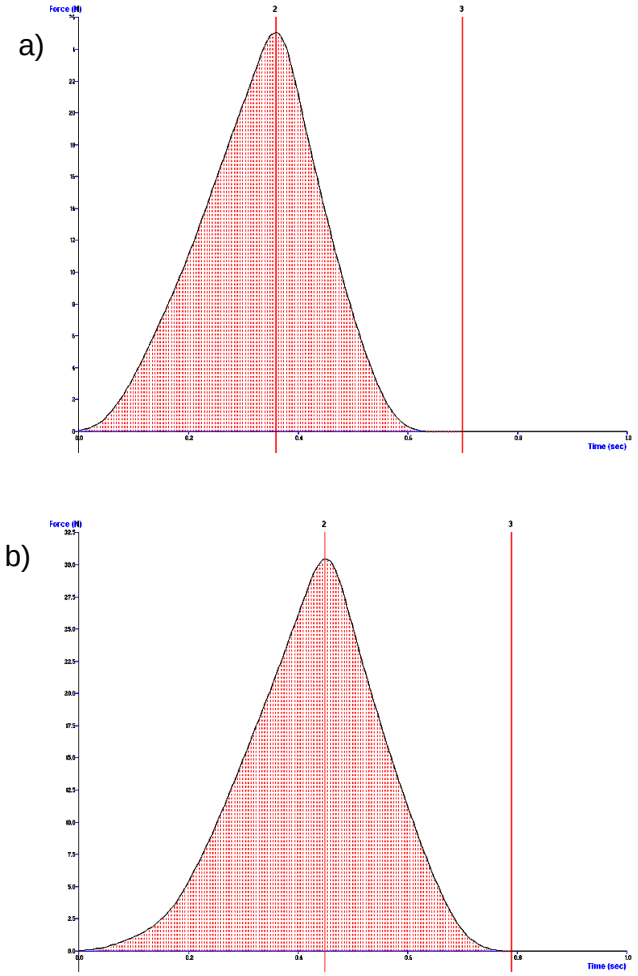

Figure 5.12: Force-time profiles of a) UHMR and b) HMR of the optimized PA 6,10-EC composite membrane.

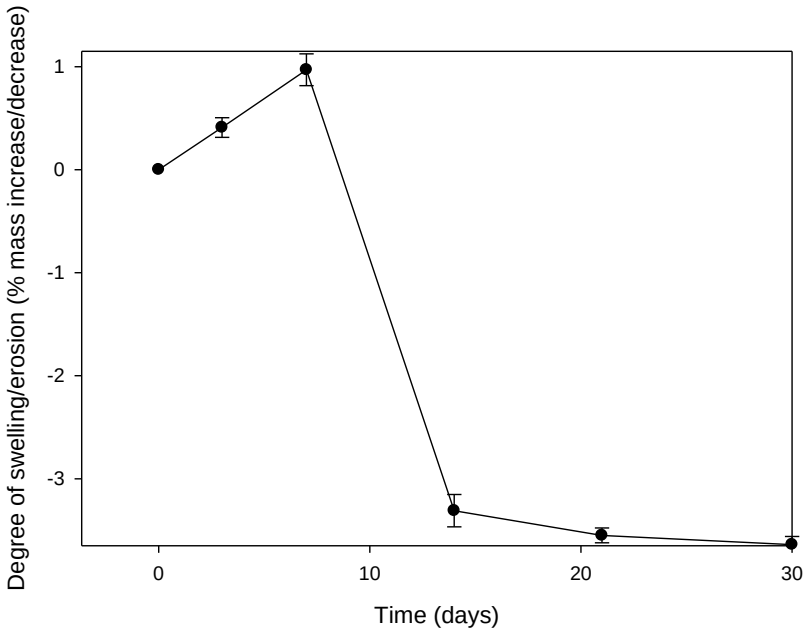

Figure 5.13: Gravimetric analysis of the degree of swelling/erosion displayed by the optimized PA 6,10-EC composite membrane

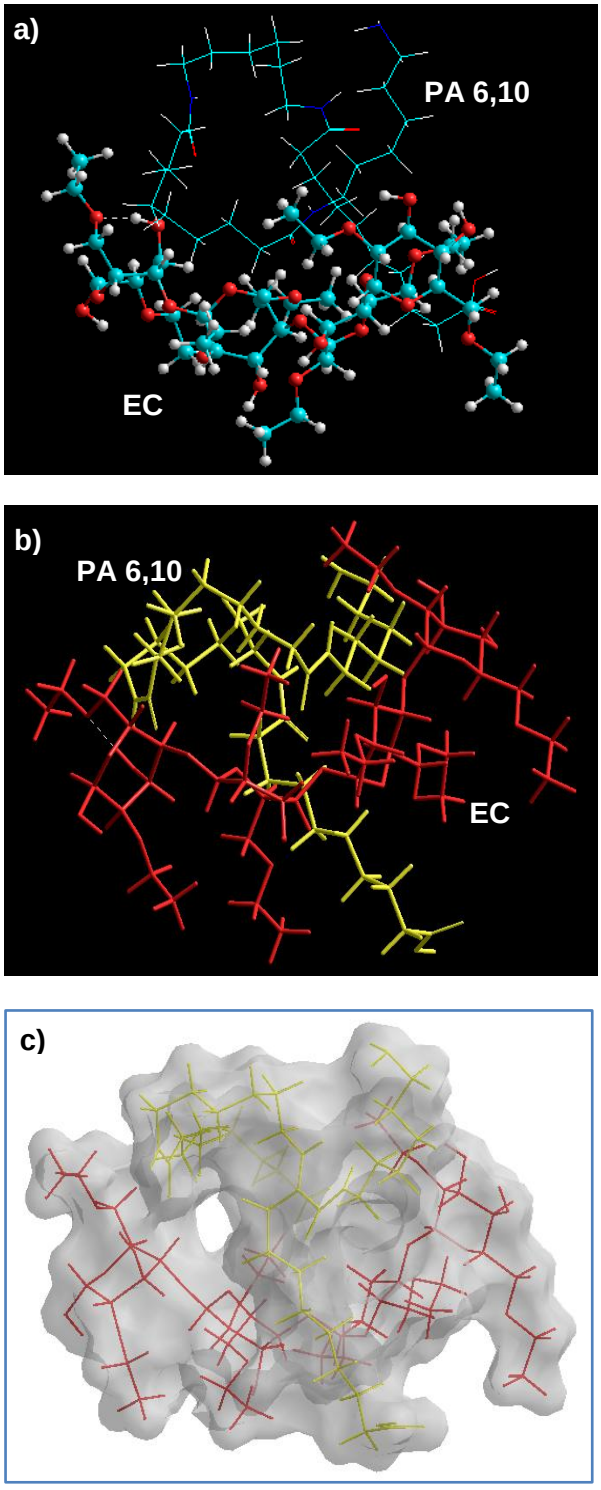

Figure 5.14: Geometric visualization of conformational profile of membrane formation: a) Molecular conformation depicting the reactional and H-bonding profile of the EC (ball and cylinder rendering)-PA6,10 (stick rendering) bi-molecular system; b) simplistic presentation of the molecular distribution of the EC (red tubes)-PA6,10 (yellow TUBES) bi-molecular system; c) Connolly molecular structure in translucent surface representation showcasing the matrix structure of the EC-PA6,10 bi-molecular system. Color codes for elements: Carbon (cyan); Hydrogen (white); Nitrogen (blue); and Oxygen (red).

5.3.9 Assimilation of the CPZ-loaded, PCL based nanoparticles into the PA 6,10-EC composite membrane to form the NPMD

Assembly of the NPMD by incorporation of the CPZ-loaded, PCL-based nanoparticles optimized in Chapter 3 into the optimized PA 6,10-EC composite membrane was carried out by dispersing the nanoparticles within the optimized composite membrane just prior to molding and then allowing the membrane to air-dry under a fume-hood for 24 hours. Resultant nanoparticle-loaded membranes were regular and of consistent size with dimensions of 8mm in diameter and 2mm in height (Figure 5.15).

Figure 5.15: Relative size of the optimized PA 6,10-EC composite membrane when compared to a Great Britain Pound (GBP) post molding and air-drying.

5.3.10 Surface area and porosity analysis of the NPMD

The BET surface area plot and the isotherm log plot for the NPMD are depicted in Figure 5.16 a) and c) respectively. The BET surface area of the NPMD was calculated to be 4.7115m²/g. The average pore width of the NPMD was calculated to be 101.55Å (10.155nm) with the average adsorption and desorption pore diameters being 161.95Å (16.195nm) and 152.08Å (15.208nm) respectively. The modification of membranous structures to form scaffolds by lyophilization generally results in larger pore sizes being achieved (Haugh et al., 2010) compared to this study where the membranes were formed by modified wet-phase inversion reaction and then molded. Molding of the membrane resulted in being highly compact and hence the pore sizes were relatively small. Furthermore, porosity analysis reveal that the novel PA 6,10-EC membrane system was formed as a result of instantaneous demixing during the wet-phase inversion reaction. Hence the membrane system has a moderately porous, dense outer structure and a highly porous bulk. The optimized nanoparticle formulation synthesized in Chapter 3 of this dissertation has a z-average size of 140.3±3.39nm. This is considerably larger than the average pore size of the optimized PA 6,10-EC composite membrane hence diffusion of the nanoparticles from the NPMD would not be efficient. This, however, does prove to be highly beneficial as CPZ release can be controlled over longer periods of time resulting in an extended duration of action, desirable patient compliance, a decreased burden of care and ultimately a positive therapeutic outcome. Furthermore, the burst release effect consistent with nanoparticles and polyamides

is counteracted. This is confirmed by the drug release profile from the NPMD as depicted in Figure 5.18 and is discussed further in Section 5.3.12.

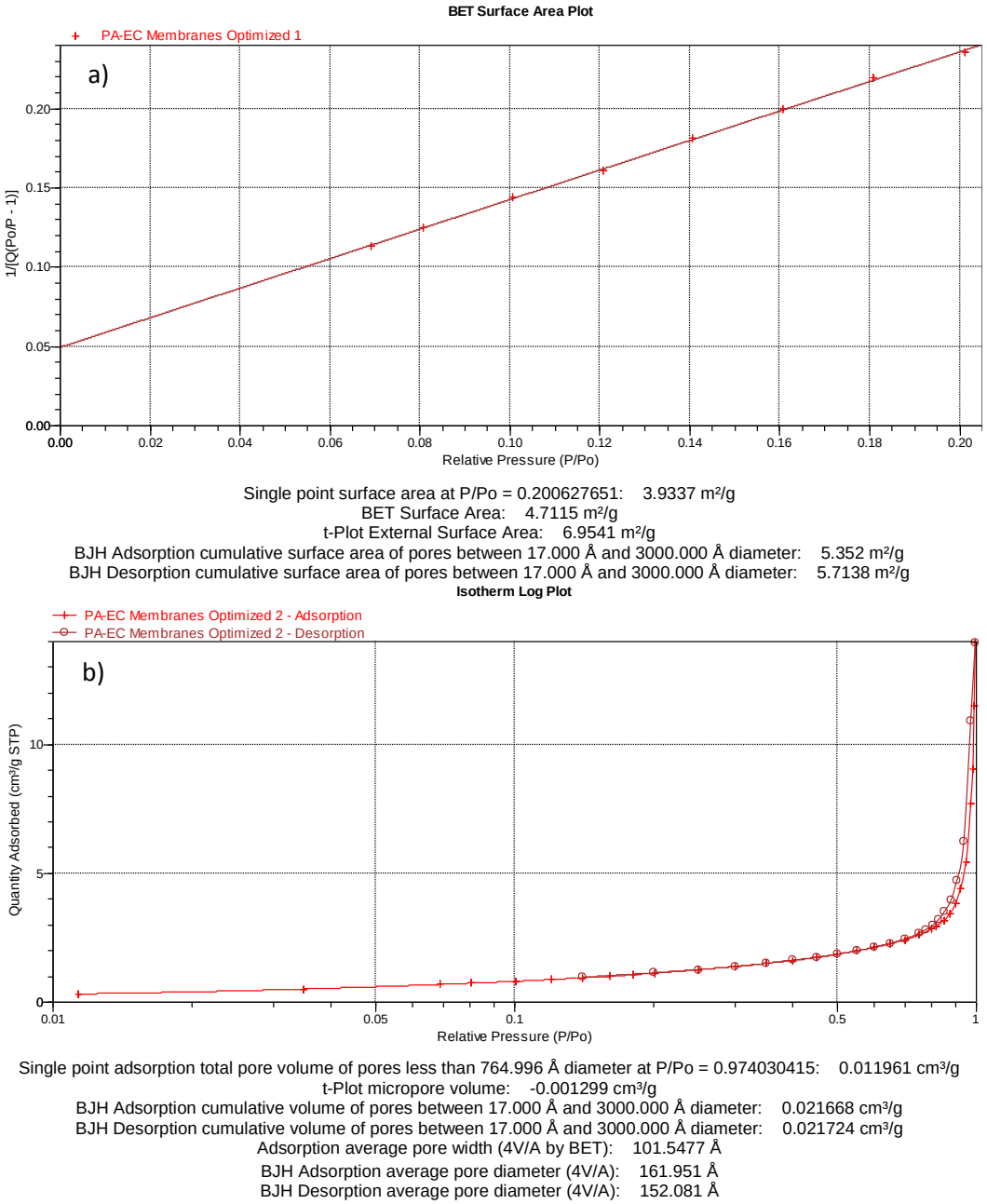

Figure 5.16: BET surface analysis plot (a) and isotherm log plot (b) of the novel PA 6,10-EC composite membrane.

5.3.11 Drug entrapment efficiency of the NPMD

An average drug entrapment of 99.55±0.33% of the dispersed, optimized CPZ-loaded PCL based nanoparticle formulation was computed within the optimized NPMD. This proved that the dispersion and assimilation of the optimized nanoparticle formulation within the optimized

composite membrane formulation to assemble the NPMD was consistent and devoid of any major handling errors.

5.3.12 Construction of calibration curve for spectrophotometric determination of CPZ release from Largactil®

Figure 5.17 represents the calibration curve of CPZ in SGF (pH 1.2, 37ºC) at λ_{254} utilizing UV spectroscopy. The concentration of CPZ ranged from 0-0.0125mg/mL.

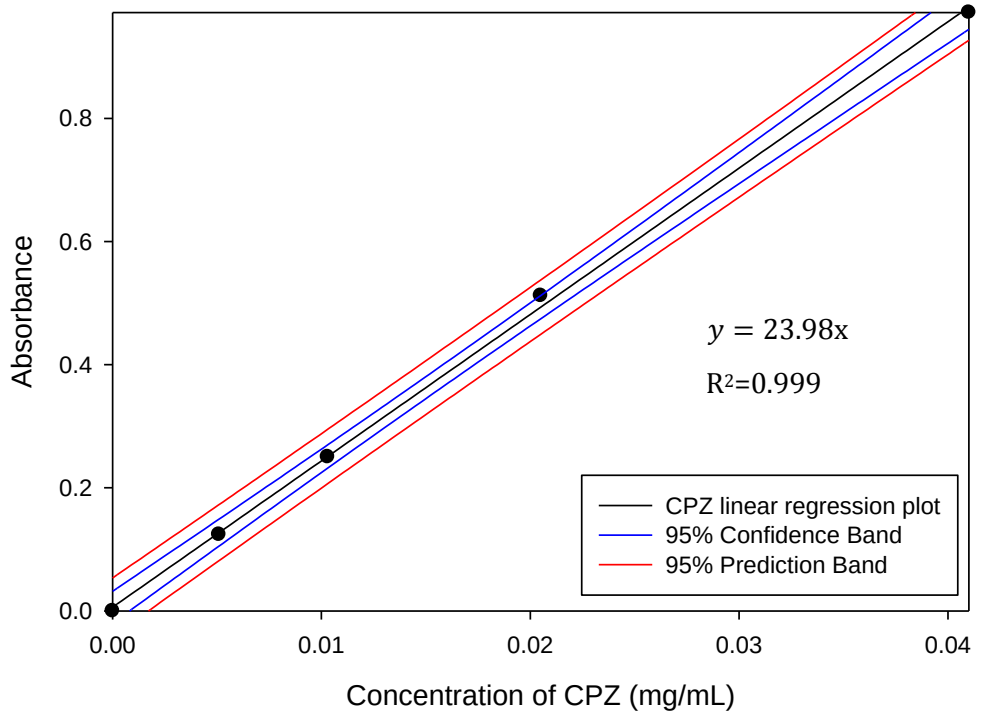

Figure 5.17: Calibration curve of CPZ in SGF (pH 1.2, 37ºC).

5.3.13 *In vitro* CPZ release from the optimized NPMD

In vitro drug release profiles of CPZ from the NPMD, the optimized CPZ-loaded PCL-based nanoparticle formulation and the optimized PA 6,10-EC composite membrane formulation are depicted in Figure 5.18. The optimized CPZ-loaded, PCL based nanoparticle formulation displays a relatively high initial burst release of 42.36% of the entrapped CPZ. This is justified by the diminutive size, larger surface area and relatively high CPZ loading percentage. This is followed by the controlled release of CPZ and 45.63% of the entrapped drug is released after 30 days. Free CPZ release from the membrane itself did exhibit a slight burst release effect of 37.31% over a period of 5 days followed by slow and constant release with 86.85% of the entrapped drug being released over a period of 30 days. The burst release is consistent with the swelling of the optimized PA 6,10-EC composite membrane whereas the controlled pseudo-steady release is consistent with the erosion

behavior of the membrane discussed in Section 5.3.7 of this chapter. CPZ release from the NPMD was controlled, slower than that of the optimized nanoparticle formulation as well as that of free CPZ release from the optimized membrane formulation. Furthermore the NPMD was devoid of any burst release effects. This was due to the matricization of the CPZ-loaded, PCL-based nanoparticles within the optimized PA 6,10-EC composite membrane formulation. CPZ release characteristics were thus dependent on a dual mechanism as depicted in Figure 5.19. Initially, diffusion of the CPZ-loaded nanoparticle from the optimized membrane formulation occurred when the NPMD came in contact with the PBS. This was followed by the diffusion of CPZ from the nanoparticle and into the dissolution media. This dual drug release mechanism and the rate-controlling properties of PCL coupled with PA 6,10 and EC thus counteracted any burst release effects and allowed for controlled pseudo-zero order drug release. The burst release was also further controlled by the porosity of the optimized PA 6,10-EC composite membrane as described in Section 5.3.9 of this chapter. The average pore size was generally smaller than the size of the optimized nanoparticle formulation. This did not allow for the simple diffusion of the nanoparticle through the pores of the NPMD. Hence CPZ release was ultimately further retarded. The mechanism of CPZ thus relied on PBS penetrating through the pores, causing an increase in pressure and swelling followed by the erosion of the NPMD. A total of 27.56% of the entrapped CPZ was released from the NPMD over a period of 30 days. Table 5.11 is a representation of the MDT_{30} values achieved for each of the aforementioned formulations. It can be seen that the NPMD displays the highest MDT_{30} value thus proving its ability to control the release of CPZ over an extended period of time in a pseudo zero order manner.

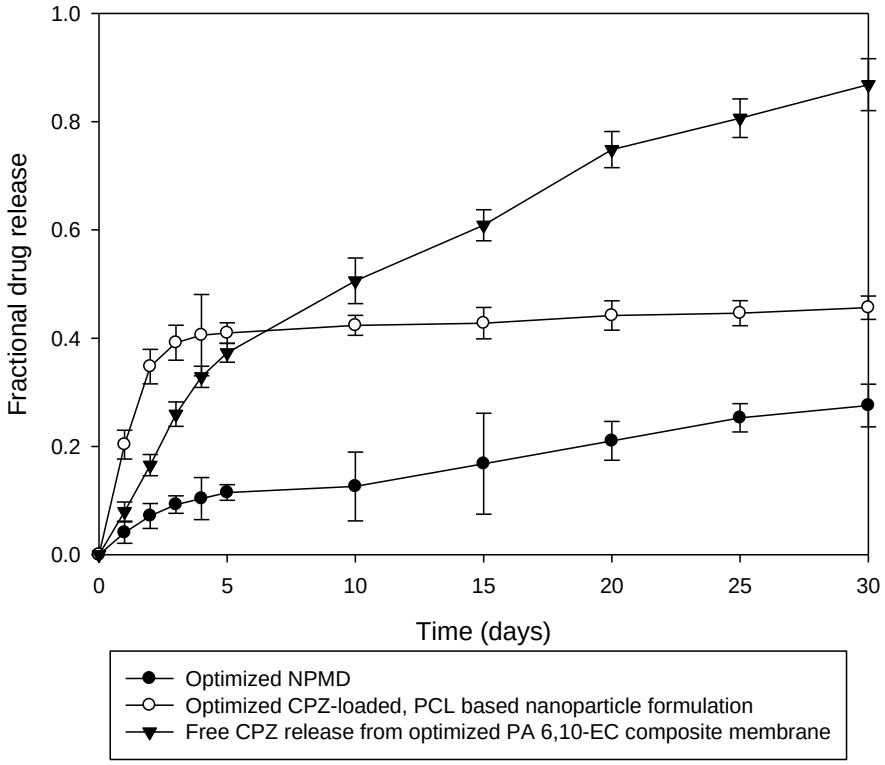

Figure 5.18: Release profiles of the NPMD, the optimized CPZ-loaded, PCL based nanoparticle formulation and free CPZ release from the optimized PA 6,10-EC composite membrane.

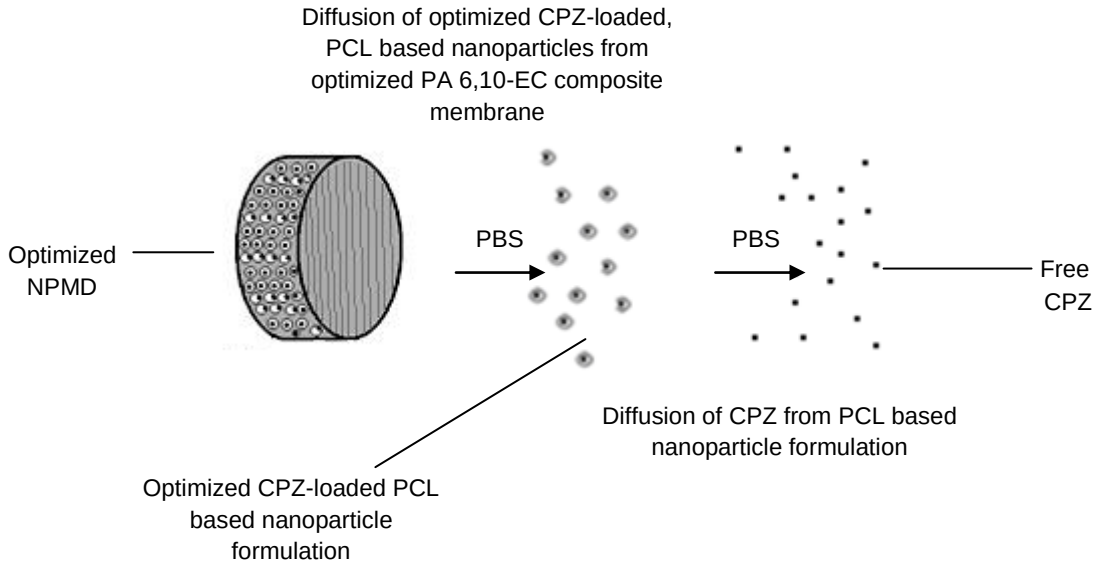

Figure 5.19: Schematic representation of the dual mechanism of CPZ release from the NPMD.

Table 5.11: MDT_{30} values achieved for the optimized CPZ-loaded, PCL based nanoparticle formulation, free CPZ release from the optimized PA 6,10-EC composite membrane and the NPMD.

Formulation	MDT_{30}
Optimized CPZ-loaded PCL based nanoparticle formulation	67.14±9.91
Free CPZ release from the optimized PA 6,10-EC composite membrane	237.2±8.22
NPMD	273.52±3.86

Figure 5.20 is the release profile of a commercially available CPZ product, Largactil®25mg oral tablet. As is evident, more than 80% of the drug was released in the first 30 minutes and the entire drug content of Largactil®25mg oral tablet was release within 90 minutes. The release profile of the commercially available Largactil®25mg displayed rapid dissolution of CPZ into the SGF and is indicative of a dose-dumping effect. This is not desirable as it is an indication that multiple doses will be required to maintain optimum therapeutic levels. This in turn, may result in dose-dependent side-effects. When compared to the release profiles of the optimized CPZ-loaded PCL-based nanoparticle formulation, free CPZ release from the optimized PA 6,10-EC composite membrane and the NPMD itself, it is evident that the aforementioned displayed far more desirable release profiles when compared to the Largactil®25mg oral tablet.

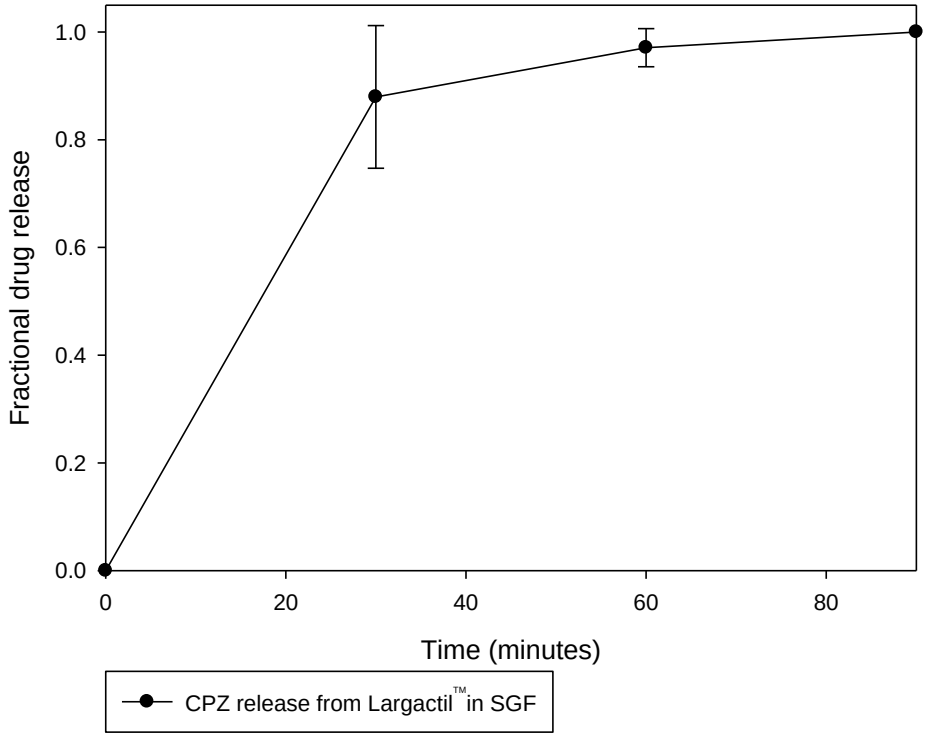

Figure 5.20: Drug release profile of the commercially available oral CPZ product, Largactil®25mg oral tablet in SGF (pH 1.2, 37ºC).

5.3.14 Magnetic Resonance Imaging to evaluate the performance of the NPMD in terms of erosion/swelling

Figure 5.21 depicts the MRI images obtained for the NPMD under continuous PBS flow conditions. The images displayed were obtained on Days 0, 3 7, 14, 21 and 30. The light grey area surrounding the matrix indicates the PBS. The black area within the matrix is an indication of the unhydrated NPMD and is only visible explicitly at day 0. As the NPMD hydrated, it began to swell minimally as indicated by Days 3 and 7 (Figure 5.22). The moderate swelling is depicted by the white area where the surface thickness of the NPMD increased over time. This is correlated with dissolution data of the NPMD which exhibited a modest burst release (Figure 5.23). At Day 14, the white region around the surface appeared to decrease marginally. This is an indication of the moderate erosion elucidated by the NPMD between Days 7 and 14. Similar results are observed at Day 21 and 30 where erosion of the NPMD also occurred but minimal with a total mass loss of 3.55 and 3.64% at Days 21 and 30 respectively. Once again the MRI profiles at these time intervals correspond with the swelling erosion profiles of the NPMD (Figure 5.22). It is also observed that during the duration of the experiment, the MRI profiles of the NPMD did exhibit dense regions of

darkness in the core indicating that full hydration of the NPMD did not occur. This was due to the hydrophobic EC and the partially hydrophilic PA 6,10. This result also bears testament to the minimal total erosion of the NPMD as well as controlled CPZ release over the 30 days (Figure 5.23).

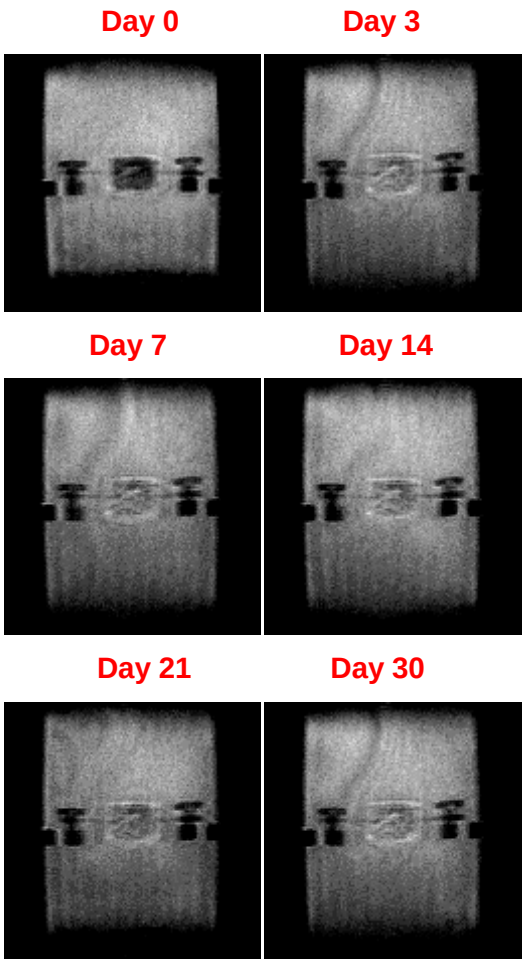

Figure 5.21: MRI profiles of the NPMD at days 0, 3,7, 14, 21 and 30 upon exposure to PBS (pH 7.4, 37°C).

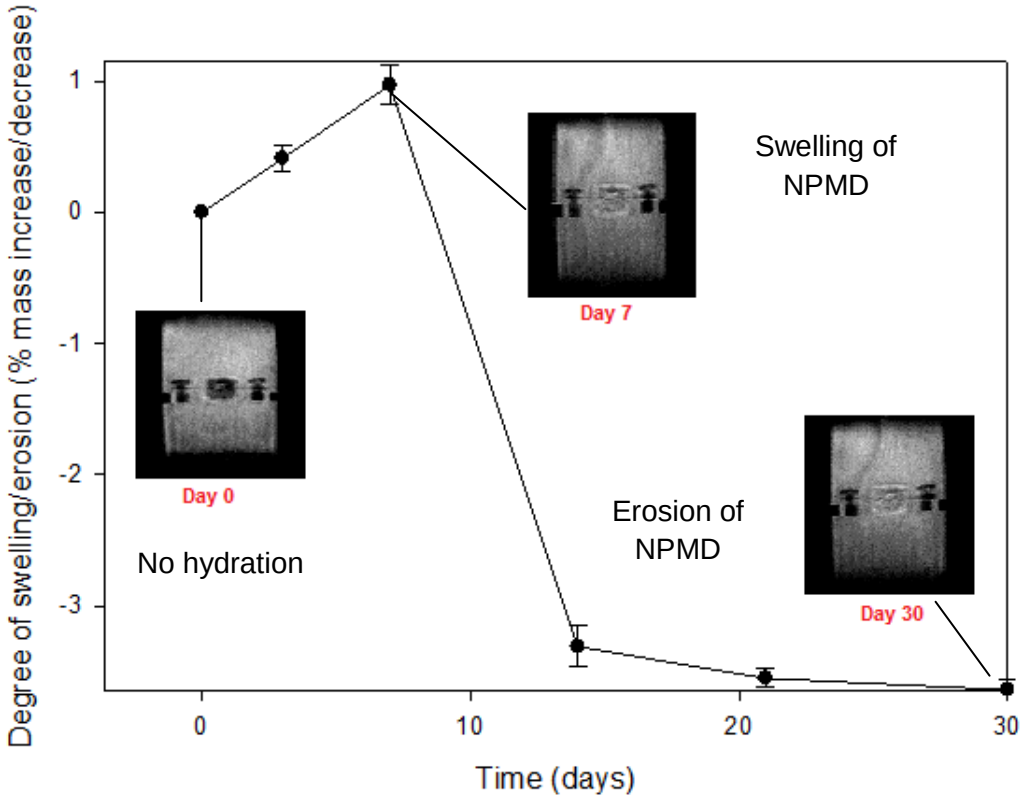

Figure 5.22: Swelling/erosion profile of the NPMD and its relation to the MRI images captured at designated time intervals.

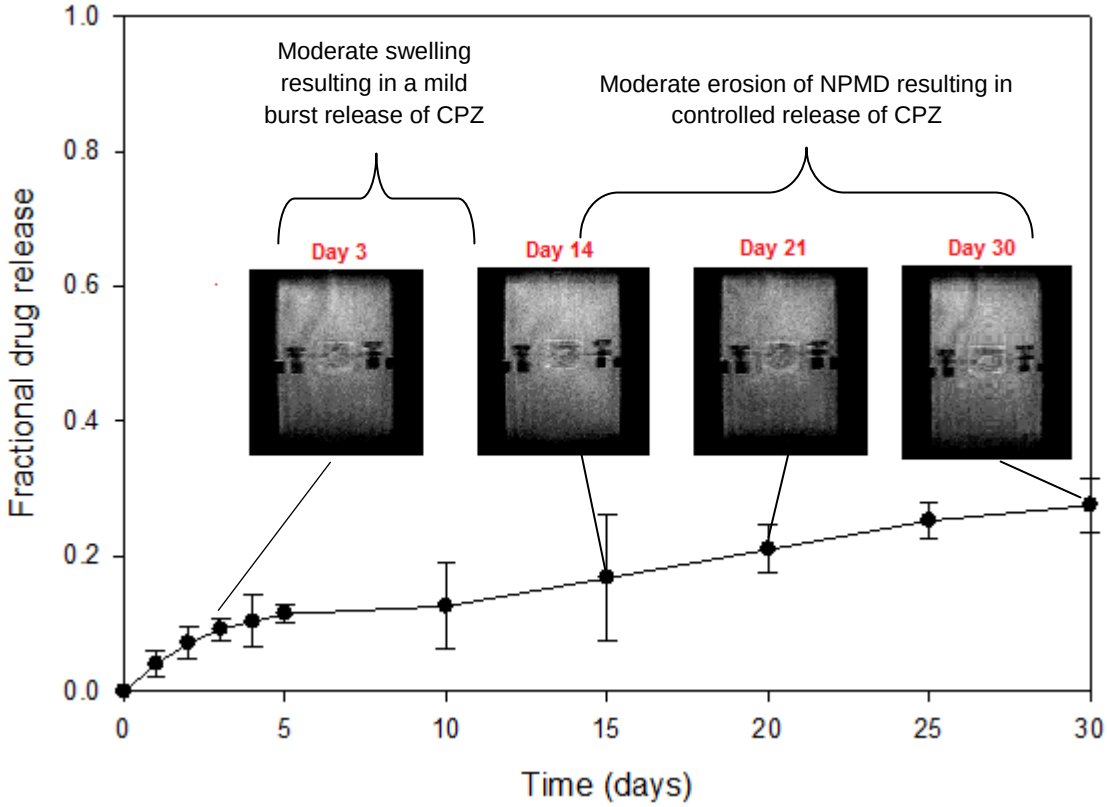

Figure 5.23: Drug release profile of the NPMD and its relation the MRI images captured at designated time intervals.

5.3.15 Determination of the thermal transition behavior of the NPMD and the constituent polymers utilized in its synthesis

The thermal behavior of the componential factors of the NPMD including the NPMD itself is described in Figure 5.24. The DSC thermogram for PA 6,10 [Figure 5.24 a)] displays a well-defined melting endotherm (T_m) at 217.79°C, a shallow, poorly-defined glass transition endotherm (T_g) and a crystallization exotherm (T_c) at 69.35°C and 99.74°C respectively (de Candia et., 1989). The poorly defined endotherms at 137.36°C and 176.16°C [Figure 5.24 b)] on the EC thermogram are indicative of its T_g and T_m respectively (Upadrashta et al., 1994). There is significant baseline drift on either side of the T_g and this is associated with a temperature-dependent heat capacity change. The baseline drift also produces an unknown endothermic peak at 69.90°C. This may be as a result of an increase in molecular mobility of EC from 60-70°C. Furthermore, briefly after the T_m, there is a sharp decline in the DSC curve at approximately 185°C. This is an indication of oxidative degradation of the EC backbone (Lai et al., 2009). The DSC curve of the NPMD [Figure 5.24 c)] comprised thermal transitions from the both the componential elements. Two T_m's are observed at 176.16°C and 221.52°C and correspond to the melting endotherms of EC and PA 6, 10 respectively. The glass T_g is very poorly defined at 127.55°C and has dropped compared to the T_g of EC alone indicating a possible physicochemical reaction probably encountered during the wet-phase inversion reaction. The NPMD, in addition, displays an endotherm transition at 65.58°C. This endotherm could be either the T_m of PCL nanoparticle within the NPMD as it does correspond to the T_m of PCL described in Chapter 3, Section 3.3.2 of this dissertation or the endotherm could be a result of baseline drift due to the increased molecular mobility of EC as discussed earlier. A well-defined overlapping endothermic peak between the two mentioned melting endotherms is observed at 210.24°C. Due to this overlapping endotherm, TMDSC [Figure 5.23 d)] was performed from 190-220°C to further investigate the transition. TMDSC revealed transitions pertaining to the non-reversible heat flow curve and the total heat flow curve occur at 210.24°C. Transitions on these curves are indicative of crystallization or melting. The fact that the transition is endothermic confirms melting had occurred.

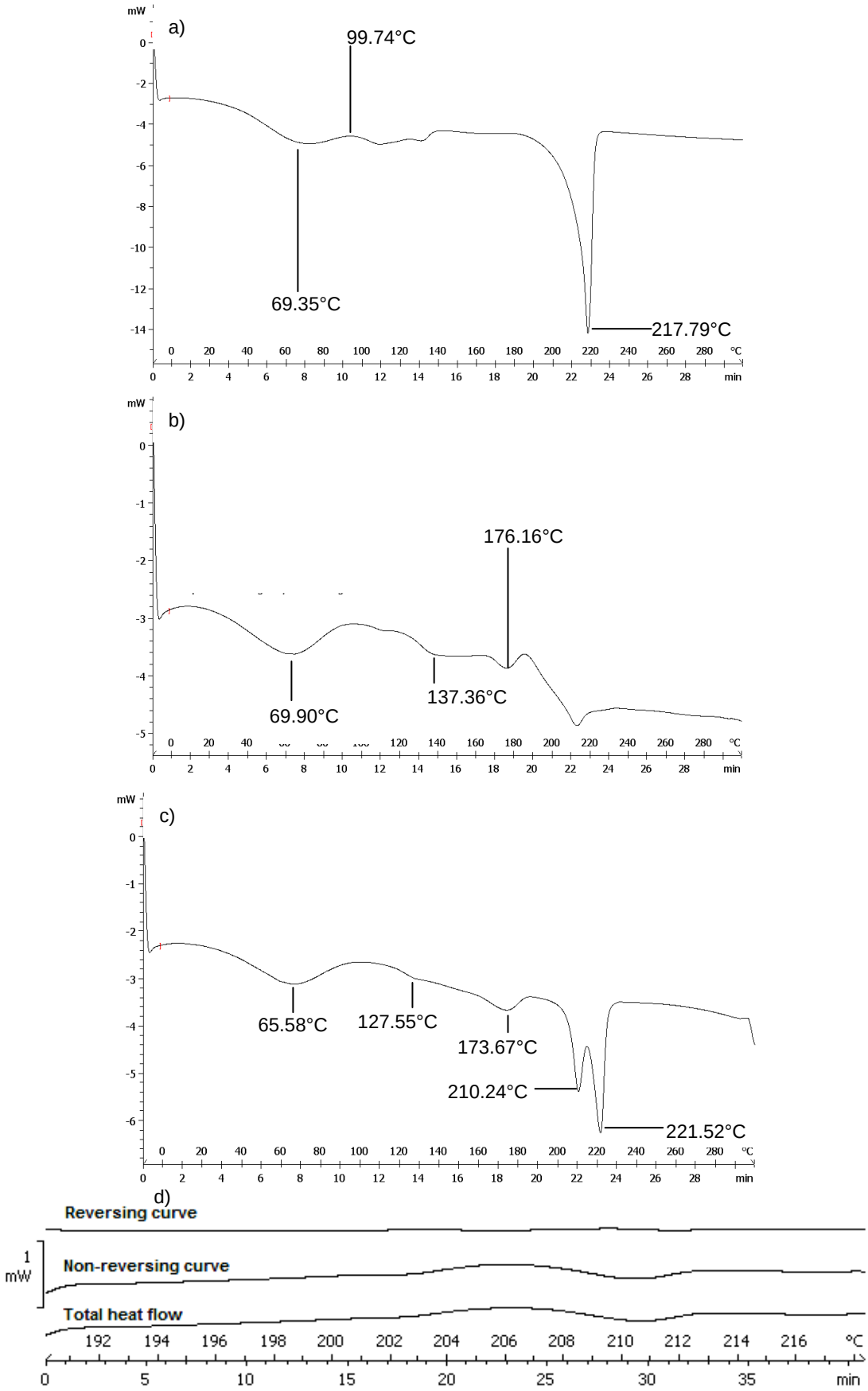

Figure 5.24: DSC profiles of a) PA 6,10, b) EC, c) NPMD elucidating basic thermal transitions and d) TMDSC profile of the NPMD between 190 and 220°C.

5.3.16 Concluding Remarks

The design, development and optimization of a novel PA 6,10-EC composite membrane by a modified wet-phase inversion reaction was successfully carried out. Extensive *in vitro* studies confirmed the optimized membrane as a suitable matrix for the optimized nanoparticle formulation synthesized in Chapter 3 of this dissertation. The assimilation of the CPZ-loaded PCL-based nanoparticles into the optimized PA 6,10-EC composite membrane led to the successful formation of the NPMD. *In vitro* studies confirmed that the NPMD was suitable candidate for intracranial implantation for the treatment of psychoses such as schizophrenia. Drug release profiles of the NPMD proved far superior to that of the commercially available oral CPZ formulation, Largactil®25mg oral tablet and highlighted the potential of the NPMD for controlling the treatment of certain psychoses over extended periods of time.

CHAPTER 6

EX VIVO CYTOTOXICITY STUDIES ON A MAMMALIAN PHEOCHROMOCYTOMA CELL LINE

6.1 Introduction

A cytotoxicity assay is a measure of the biocompatibility of a compound and assesses if the compound is potentially toxic to a specific cell-line by significantly changing its morphology, undesirably affecting cell growth rate, impedes cellular attachment and ultimately leads to death of the respective cells. Cytotoxicity assays are founded on the simple principle that toxic or incompatible compounds will inevitably affect basic basal functions of all cells and toxicity may be measured by evaluating cellular damage attained by exposure to the compound. A cytotoxicity assay has benefits of limiting animal studies, allowing for safer animal studies, rapid toxicological assays of large number of formulations, use of small quantities of test substance and reduction of costs in manufacturing. The death or destruction of a cell can be detected by various mechanisms. Some of these mechanisms include; indirect detection by measuring the metabolic activity of enzymes within cells that are not destroyed, the diffusion of certain dyes such as tryptan blue or eosin through the cell and detection by the release of intracellular substances from the cell (Horvath, 1980; Franke and Posrtmann, 1994; Niles et al., 2008).

A reduction in cellular metabolic activity is an indication of cell damage and is quantified by measuring mitochondrial activity via (3-(4,5-dimethylthiazol-2-yl)-5-(3-carboxymethoxyphenyl)-2-(4-sulfophenyl)-2H-tetrazolium (MTS) metabolism of adenosine triphosphate (ATP) levels within the cell. The use of dyes for cytotoxicity assays relies on the use of fluorescence to detect dyes that have traversed damaged cells. These dyes would not normally enter the healthy cell. A further method for cytotoxic evaluation includes assessing the cell number. Dead cells are normally separated from the culture plate and diffuse into the medium. Cell number can be assessed either by counting of cells or measuring total cell protein (Weyermann et al., 2005).

The release of intracellular substances can be quantified by either initially labeling the cells exogenously or the intracellular substances itself may be physiological cytoplasmic constituents. Lactate dehydrogenase (LDH) is a stable enzyme normally found in the cytosol of biological cells and is utilized in cytotoxicity assays as the quantification of LDH release from within the cell into the extracellular fluid (ECF) is proportional to cell death. A reduction in metabolic activity indicates incipient cell injury whereas LDH detection in the ECF

represents more severe irreversible cell damage and implies death. The LDH assay assesses cell membrane integrity. The cell membrane is responsible for forming a functional barrier around the cell and regulates the exchange of substances via transporters, secretion pathways and receptors. When the membrane is damaged, it becomes highly permeable and large amounts of LDH seep out into the supernatant. The LDH assay is a non-arduous, timely, precise, convenient and sensitive technique that is based on activity determination from culture supernatant and is adapted to the 96 plate microtitration plate format. The LDH assay is an enzymatic test which is illustrated in Figure 6.1. Briefly, LDH catalyzes the conversion of lactate to pyruvate and in doing so, reduces NAD^+ to $NADH/NADH^+$. Subsequently, the enzyme diaphorase, transfers the H/H^+ from $NADH/NADH^+$ to the tetrazolium salt 2-(4-iodophenyl)- 3-(4-nitrophenyl)-5-phenyltetrazolium chloride (INT). This leads to the formation of formazan which is a red, water soluble dye that and can be quantified by ultraviolet spectroscopy at 490nm. An increase in the levels of formazan produced in the supernatant is directly proportional to the number of lysed cells (Decker and Lohmann-Matthes, 1988; Lappalainen et al, 1994; Fotakis and Timbrell, 2005; Weyermann et al., 2005).

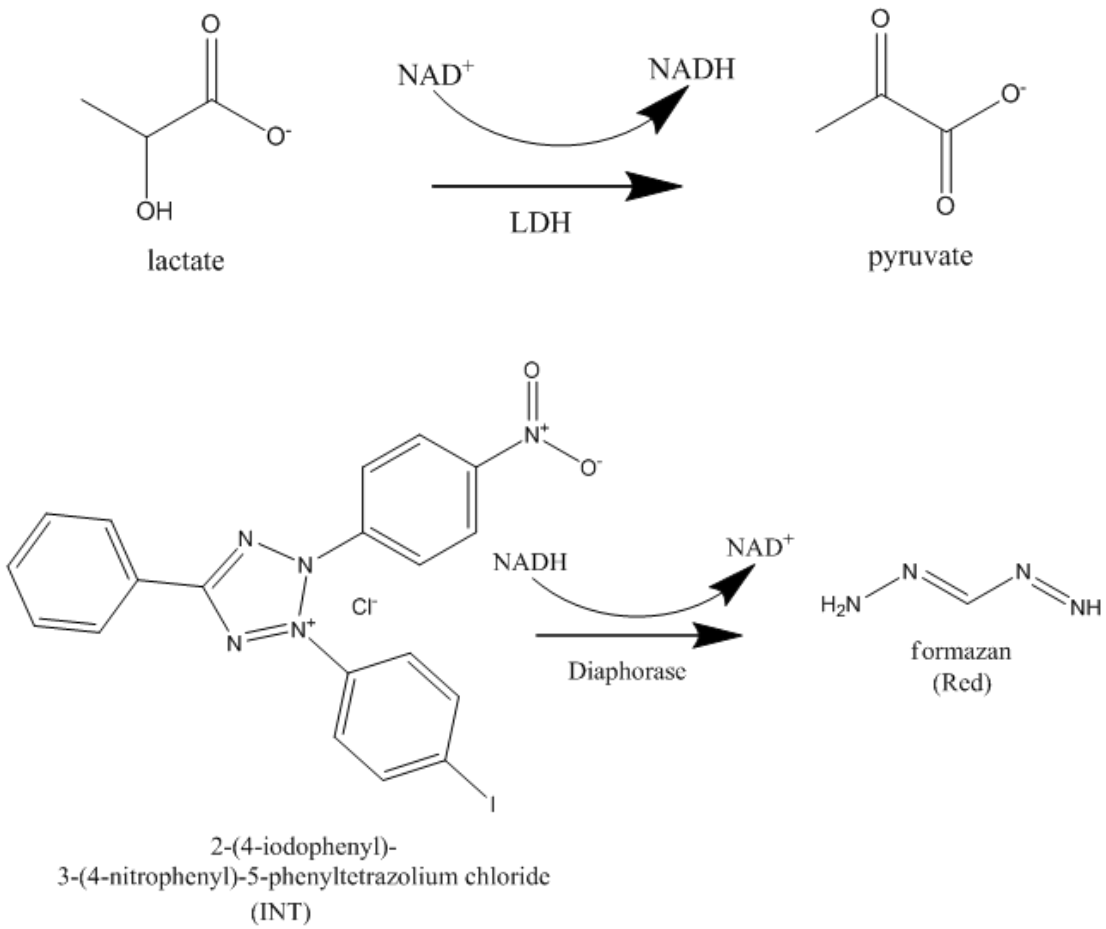

Figure 6.1: General chemical reactions encountered in the LDH cytotoxicity assay (Weyermann et al., 2005, [Drawn using ChemBioDraw Ultra V12.0].

Due to its vast advantages, the LDH assay method was employed in this study utilizing the CytoTox 96® Non-Reactive Cytotoxic Assay. The Nano-Enables Polymeric Membranous Device (NPMD), its componential elements, the chlorpromazine hydrochloride (CPZ) and cod-liver oil (CLO)-loaded nano-liposhells and its componential elements were assayed to assess any cytotoxic effects utilizing the LDH assay method as well as the cell-count method using a hemocytometer. The PA 6,10 utilized in the NPMD was a novel polymer synthesized *in vitro* and hence its cytotoxic potential alone as well as in combination with the other componential elements of the NPMD had to be evaluated. In addition, the concept of combining conventional medicine with complementary and alternative medicines as in the CPZ and CLO-loaded, PCL-based nano-liposhells is a novel concept hence the cytotoxic effects of the nano-liposhells as well as introducing CLO directly to the cells were evaluated. Furthermore, as discussed in Chapter 4, Section 4.2.8 of this dissertation, CLO is prone to auto-oxidation, leading to the formation of potentially toxic free radicals. Similarly, any potential effects of the NPMD and its components needed to be assessed. The cytotoxicity assay was conducted as a basis to eliminate any potential adverse effects in the *in vivo* evaluation.

6.2 Materials and Methods

6.2.1 Materials

The CytoTox96® Non-Reactive Cytotoxic Assay which measures cell viability was purchased from Promega Corporation (Madison, WI, USA). Mammalian Pheochromocytoma (PC12) neuronal cells were purchased from the Health Science Research Resources Bank (HSRRB, Osaka, Japan). The NPMD and its componential elements as well as the CPZ and CLO-loaded, PCL-based nano-liposhells and its componential elements were attained as described in Chapters 3, 4 and 5 of this dissertation. All other chemicals used in the experiments were of analytical grade and were employed as purchased.

6.2.2 Routine cell culture

PC12 neuronal cells were cultured in RPMI-1640 media comprising L-glutamine and sodium bicarbonate. The media was further enhanced with 5% fetal bovine serum (FBS), 10% horse serum (HS) and 1% penicillin/streptomycin (Sigma-Aldrich; St. Louise, MO, USA) (Figure 6.2). The FBS and HS were both heat inactivated. The cells were then maintained in a laboratory incubator (RS Biotech Galaxy, Irvine, UK) with a humidified atmosphere of 5% medical CO_2 at 37°C. Preparation of the media and inoculation of cells were conducted using strict aseptic technique in a laminar flow unit.

Figure 6.2: PC12 neuronal cell growth media constituents.

6.2.3 Exposure of cells to the NPMD and the CPZ and CLO-loaded PCL based nano-liposhells and their componential elements

PC12 neuronal cells were exposed to the following compounds for 48 hours:

a) NPMD (50mg)
b) CPZ-free NPMD (30mg)
c) CPZ-loaded, PCL based nanoparticles (20mg)
d) CPZ-free, PCL based nanoparticles (10mg)
e) Nano-liposhells (20mg)
f) CLO (100µL)
g) EC (10mg)
h) PA 6,10 (10mg)
i) CPZ (5mg)
j) PCL (10mg)

Figure 6.3 is a schematic representation of 96-well microplate containing the respective compounds for analysis

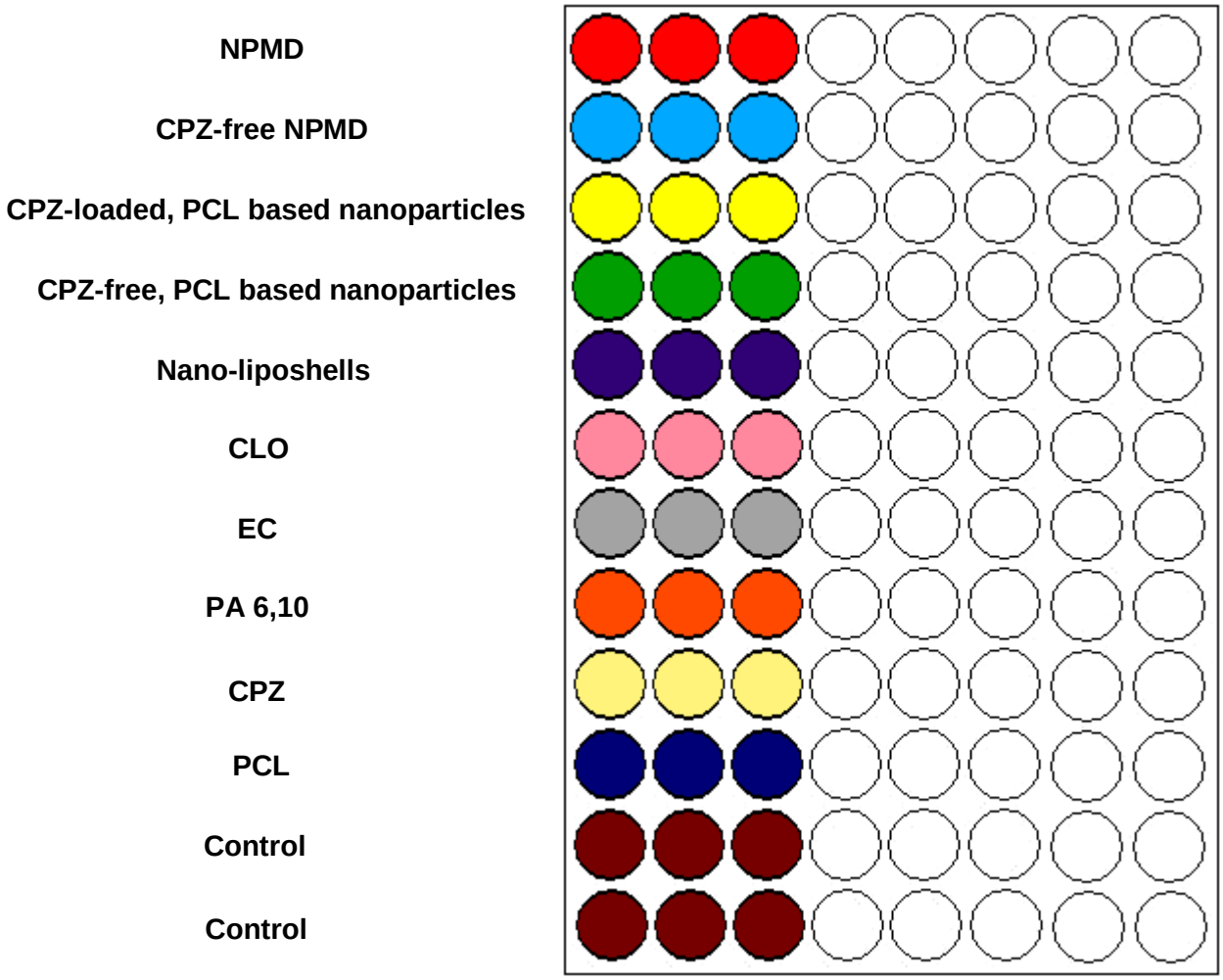

Figure 6.3: Schematic depiction of the 96-well microplate containing the compounds for cytotoxicity analysis.

6.2.4 CytoTox96® Non-Radioactive Cytotoxicity Assay

The released LDH in the culture supernatants were determined using a CytoTox96® Non-Radioactive Cytotoxicity Assay. The released LDH was quantified utilizing a 30 minute enzymatic coupled test ultimately resulting in INT being converted to red formazan and catalyzed by LDH as described in Figure 6.1. Briefly, PC12 neuronal cells were added to the experimental microplate wells. These were treated with the compounds to be tested as described in Figure 6.2. This along with an untreated control was incubated for 48 hr at 37°C. After incubation, a lysis solution (9%$^{v}/_{v}$) Triton® X-100) (10x), was added to all wells. The plate was then incubated at 37°C for 45 minutes. LDH was quantified by firstly transferring 50µL of the supernatant of each well to another 96-well assay plate. The substrate mix was reconstituted using assay buffer and 50µL of this reconstituted substrate was added to each well. The assay plate was covered and incubated at room temperature, stored away from light, for 30 minutes. This was followed by the addition of 50µL of stop

solution to each well of the microplate. This was performed to stop the enzymatic reaction. Absorbance values at 490nm were recorded utilizing a luminometer (Victor™X3, Perkin Elmer Inc., USA). The amount of LDH released and red color formed was directly proportional to the number of dead cells.

In order to relate the number of dead cells formed to the number of living cells and determine the cytotoxicity of the tested compounds, a target cell maximum LDH release control had to be conducted. A known quantity or density of PC12 neuronal cells were added to the culture medium in 3 wells of the microplate so that the final volume and concentration was the same as that utilized in the experimental assay above. In order to determine the known number of PC12 neuronal cells, the number of cells per mL was determined by utilizing a tryptan blue exclusion assay as well as a hemocytometer (Figure 6.4). The counting was based on the fact that viable cells will remain opaque and non-viable cells will stain blue and this would be quantified utilizing a hemocytometer and light microscope.

Briefly, 200µL of the cell suspension was diluted with 300µL PBS and added to 500µL tryptan blue thereby creating a dilution factor of 5. The dilution factor was relatively high so as to easily identify individualized cells. The suspension was mixed thoroughly and allowed to stand for 10 minutes. A pasteur pipette was used to transfer a miniscule quantity of the suspension to the chamber of the hemocytometer. The cells in the 1mm square and four corners were counted. Each square of the hemocytometer is equal to a volume of $0.1mm^3$ $/10^{-4}cm^3$ and since, $1cm^3$=1mL, the cell count per mL could be calculate utilizing Equation 6.1. Only cell suspensions with a viability in excess of 95% were used in the assay.

PC12 neuronal cells/mL = Average count per square x dilution factor x 10^4 *Equation 6.1*

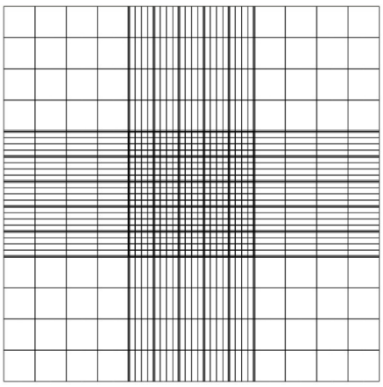

Figure 6.4: Grid layout for the Neubauer Improved hemocytometer, adapted from http://www.microbehunter.com/2010/06/27/the-hemocytometer-counting-chamber, [Accessed July 27th, 2012].

Once the cells were counted and pipetted onto a microplate, 10µL of lysis solution per 100µL of culture medium was added and the cells together with the lysis solution were incubated at 37°C for 45 minutes. This resulted in complete lysis and death of the PC12 neuronal cells. The supernatants were harvested as described above and the ultraviolet reading at 490nm for complete cell destruction was computed. Volume correction as well as culture medium controls was performed to cater for the volume changes by addition of lysis buffer as well as correcting LDH activity contributed by serum in culture medium and the phenol red in the culture medium respectively. Furthermore, a target-cell spontaneous LDH release control was also performed to correct spontaneous LDH release from cells. The cytotoxicity of the compounds towards the PC12 neuronal cells were calculated using Equation 6.2

$$\% \text{ Cytotoxicity} = \frac{\text{Experimental LDH Release}}{\text{Maximum LDH Release}} \times 100 \qquad \textit{Equation 6.2}$$

The statistical significance of the cytotoxic effects of the various compounds was evaluated wherein a probability limit of $p<0.05$ was considered to be significant.

6.3 Results and Discussion

6.3.1 Routine cell culture

Light microscopy, employing visible light, was utilized to assess the growth progression of the PC12 neuronal cells (Figure 6.5). Figures 6.5.a) and b) represents cell growth after 3 days at a magnification of 40x and Figure 6.5 c) represents cell growth progression after 7 days at 25x magnification. Images reveal a highly proliferative cell growth at 7 days. Furthermore, healthy cells were observed microscopically as there was no visible lysis and cells appeared to be intact. This confirmed the success of the culture method.

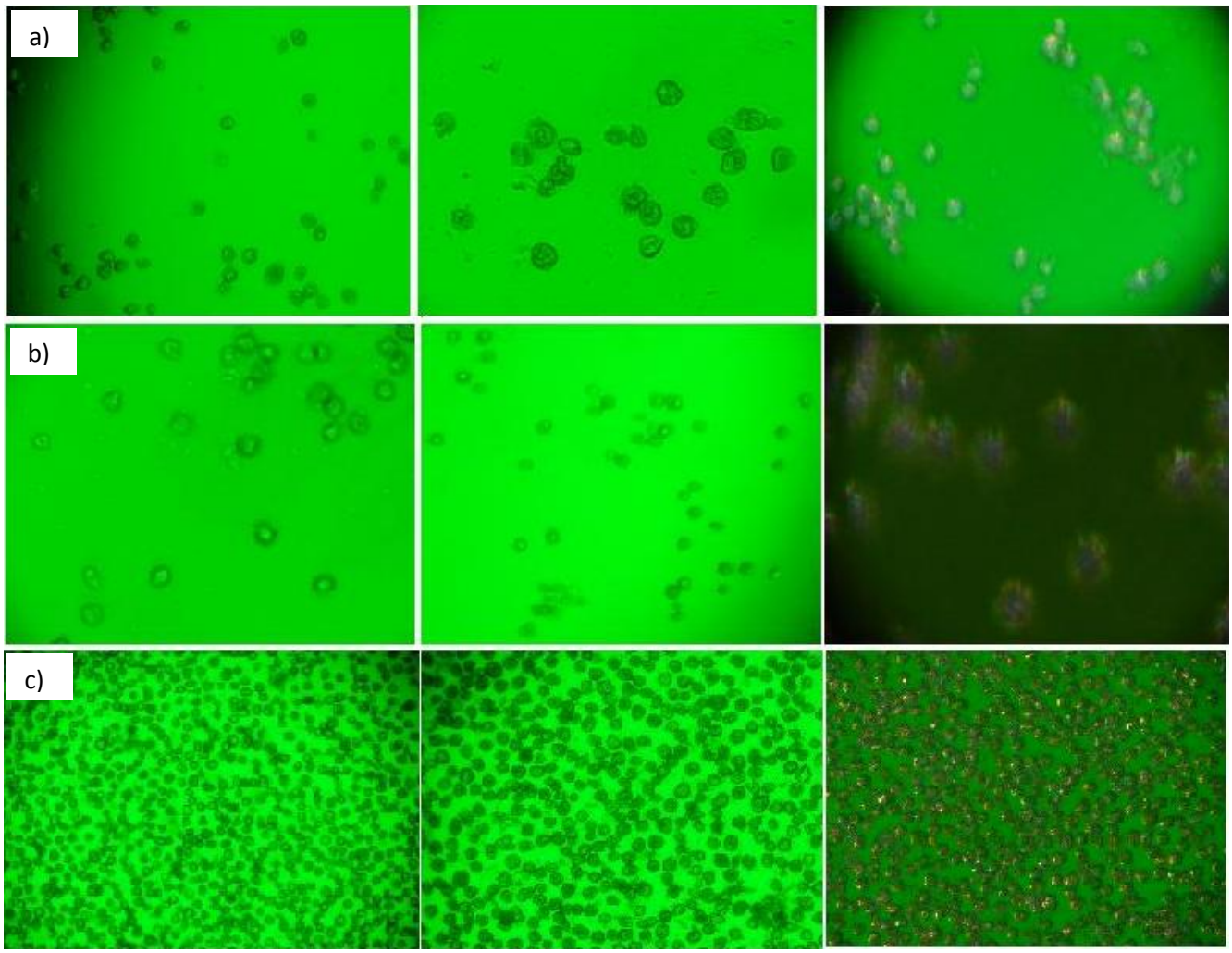

Figure 6.5: Light microscopy images of PC12 neuronal cells at a) and b) 3 days at 40x magnification and c) 7 days at 25x magnification.

6.3.3 CytoTox96® Non-Radioactive Cytotoxicity Assay

After a 48 hour incubation period with the respective compounds, the cell viability in terms of their death relative to the number of cells originally incubated with the respective compounds, was assessed and is depicted in Figure 6.6. It is evident that the CLO significantly decreased cell viability ($p<0.05$) and proved to be the most cytotoxic compound relatively. A reason for this could be because of the auto-oxidation of the CLO resulting in the formation of potentially toxic free radicals. Nano-liposhells reduced cell viability to a lesser extent when compared to free CLO. The reduced viability could be a result of the oxidized surfaced adsorbed CLO. The entrapped CLO is protected from oxidation by the entrapment within the PCL and hence cytotoxicity is not as prominent as with the free CLO. The application of PA 6,10 to the cells caused a moderate decrease in cell viability. This was also noted with the NPMD and the CPZ-free NPMD which comprises the PA 6,10.

It was noted that only the nano-liposhells as well as the free CLO resulted in significant cytotoxic effects comparatively ($p<0.05$). The PCL, EC, CPZ, CPZ-loaded, PCL-based nanoparticles and the CPZ-free, PCL based nanoparticles depicted no cytotoxic effects. This was based on the fact that LDH (formazan) could not be detected by ultraviolet spectroscopy in the supernatant.

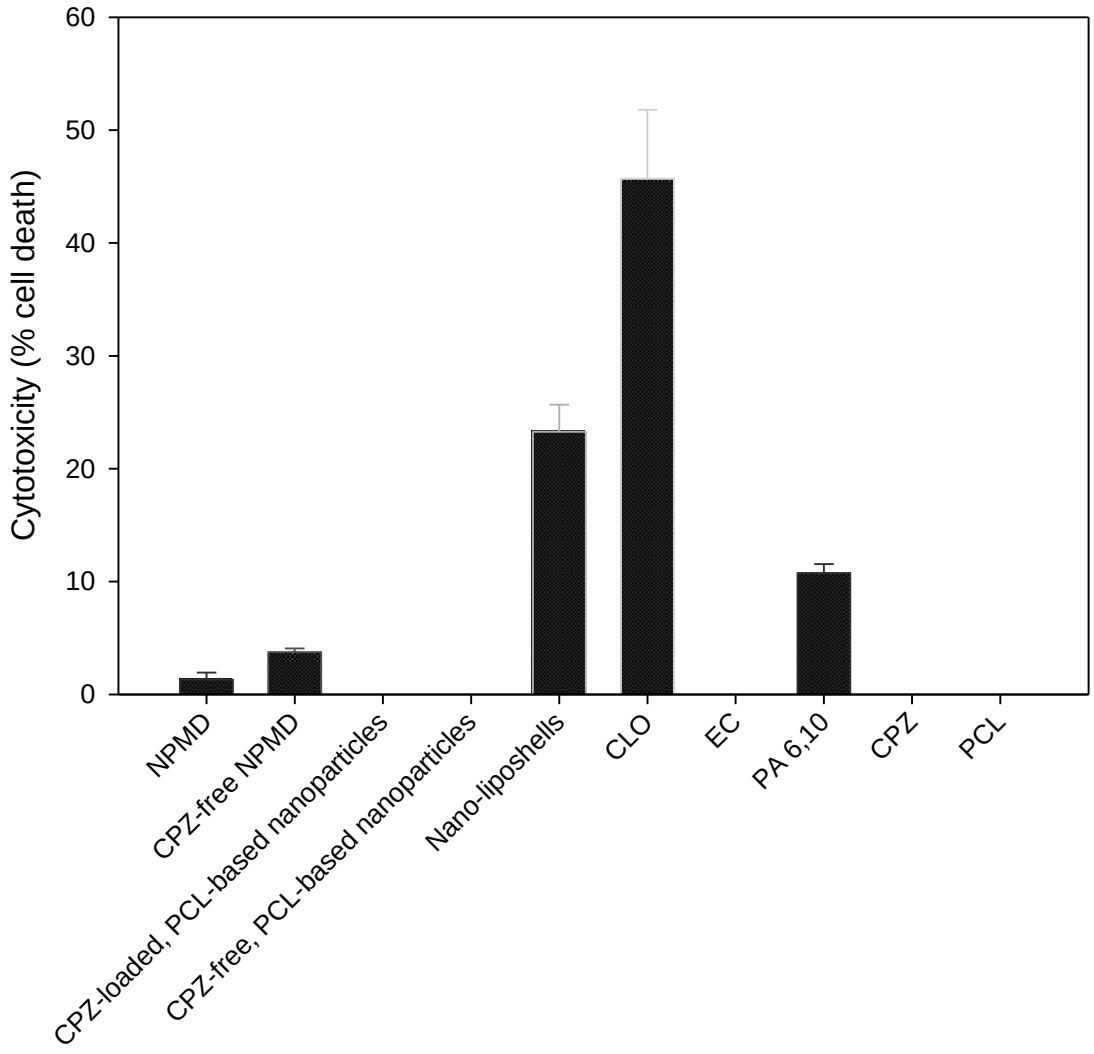

Figure 6.6: Cytotoxic evaluation of PC12 neuronal cells upon exposure to the various compounds utilizing the CytoTox96® Non-Radioactive Cytotoxicity Assay**.**

6.4 Concluding Remarks

Cytotoxicity analysis was conducted to establish the safety of the NPMD prior to the commencement of *in vivo* studies. Results revealed a moderate cytotoxic effect of the NPMD was minimal and did not prove to be significant. This moderate cytotoxic effect could be attributed to the size of the NPMD. Even though the device was scaled down for the purposes of the study, it was still large enough to cause absorption and adsorption of the growth media for the cells. This resulted in a decrease in the media available for cell growth and nutrition and hence stagnation of cell growth was observed. In addition, the study sought to evaluate the cytotoxic potential of the CLO and CPZ-loaded, PCL based nano-liposhells. The fact that the consequences of the direct application of CLO to neuronal cells had not yet been established made the study an effective platform for further research concerning the combined therapeutic benefits of conventional and complementary and alternate medicine. A limitation to this cytotoxic assay was the fact that it only relies on the detection of LDH (formazan). It does not cater for the fact that cell growth and thriving of the PC12 neuronal cells could have occurred upon exposure to the PCL, EC, CPZ, CPZ-loaded, PCL based nanoparticles and the CPZ-free, PCL based nanoparticles. This could have been detected by a hemocytometric cell count. Further cytotoxic assays should focus on at least two methods of evaluation so that results can be corroborated.

CHAPTER 7

IN VIVO EVALUATION OF THE NPMD UPON INTRAPARENCHYMAL IMPLANTATION IN THE REGION OF THE FRONTAL LOBE OF THE NEW ZEALAND WHITE RABBIT BRAIN: A PILOT STUDY

7.1 Introduction

Although *in vitro* evaluations of novel drug delivery systems may provide valid information regarding the drug release characteristics, they cannot completely simulate *in vivo* conditions. Therefore, *in vivo* studies still need to be conducted to obtain salient pharmacokinetic data. The use of an *in vivo* model offers greater pharmacokinetic and pharmacodynamic accuracy as well as a more realistic clinical extrapolation. The use of rabbits for the *in vivo* analysis of drug delivery systems has been extensively studied (Venho and Erikkson, 1986; Kailasam et al., 1994; Ugwoke et al., 1999; Horisawa et al., 2002; Ambrose et al., 2004; Dali et al., 2006; Choonara et al., 2011; Lensing et al., 2012).

Rabbits are widely bred, cost-effective when compared to larger animals, non-aggressive, easy to handle and do not require exclusive, expensive rearing facilities. The animal is classified as a small animal and does not require rigorous, time consuming ethics clearance procedure when compared to larger animals. Furthermore, rabbits have short vital cycles such as puberty and gestation. Collectively, these advantages of the rabbit model make it a popular choice for *in vivo* studies (Mapara et al., 2012). The use of rabbits in neuroscience may be a feasible option for experimental modeling of human brain disorders and provides many advantages. There is significant evidence of polymeric drug delivery devices implanted into the brain of rats, proving that this type of implantation is a highly researched and practiced science (Olivi et al., 1996; Haik et al., 2000; Pillay et al., 2009; Harilall, 2011).

A recent study by Pillay and co-workers (2009) investigated the release of dopamine from a polymeric scaffold device post implantation into the sub-arachnoid space in the region of the frontal lobe of the brain. A similar study was performed by Harilall (2011). A major disadvantage of these studies was the fact that due to the small size of the rat, sampling of Cerebrospinal Fluid (CSF) and blood was only possible after euthanasia of the animal at each time point. Inevitably, this resulted in the use of a greater number of animals (Pillay et al., 2009; Harilall, 2011). Utilizing a larger animal, such as a rabbit for this area of research, combats the problem as the larger animal allows for easier sampling and relatively accurate results when compared to smaller laboratory animals such as rats. In addition, euthanasia of

rabbits to obtain CSF at each time interval may not be necessary due to the larger rabbit model.

The successful intracranial implantation of the polyanhydride PCPP-SA into the frontal lobe of the New Zealand White Male Rabbit brain was carried out by Brem and co-workers (1989). An absorbable gelatin sponge (Gelfoam) was also implanted bilaterally in the frontal lobe, as a control. The study was conducted to assess the biodegradability and biocompatibility of the polymeric device. The study was carried out over a period of 60 days and animals were sacrificed at predetermined intervals for histomorphological examination. No behavioral changes or neurological deficits indicative of toxicity were observed. In addition, histomorphological studies revealed no signs of inflammation thus confirming the success of this study (Brem et al, 1989).

Considering the nature of Central Nervous System (CNS) disorders, their all-round debilitating effects and the renowned shortfalls of current therapeutic approaches as discussed throughout this dissertation, this chapter proposes a novel means of addressing these challenges by corroborating the *in vitro* potential of the NPMD with the *in vivo* intracranial implantation of the NPMD in the rabbit model. Conventionally, when a drug enters the systemic circulation, the uptake into the brain parenchyma depends on the blood flow through the brain, the permeability of the microvascular wall and the amount of drug available for uptake (Misra et al., 2003). Since the CSF can exchange molecules with the interstitial fluid of the brain parenchyma (Misra et al., 2003), administering the drug directly into the CSF and CNS compartment should theoretically result in a greater bioavailability of the drug. Furthermore, the blood-brain and blood-CSF barriers are avoided. This is depicted in Figure 7.1 where the NPMD is proposed to be implanted intraparenchymally in the pia mater of the brain. As can be seen the NPMD comes into contact with the brain extracellular fluid (ECF) causing the release of the nanoparticles and CPZ into the brain ECF which allows for the easier uptake by the ependyma. Furthermore, any nanoparticles that diffused into the CSF of the subarachnoid space could easily pass through the pia mater due to its sheer size.

In this chapter, the therapeutic potential of the synthesized NPMD was evaluated following implantation in the rabbit model. Key parameters such as the *in vivo* CPZ release rate from the NPMD into the CSF and blood, the biocompatibility and the biodegradability of the device were evaluated. Ethics clearance (2011/51/04) from the Animal Ethics Screening Committee (AESC) of the University of the Witwatersrand was obtained for this study (Appendix E).

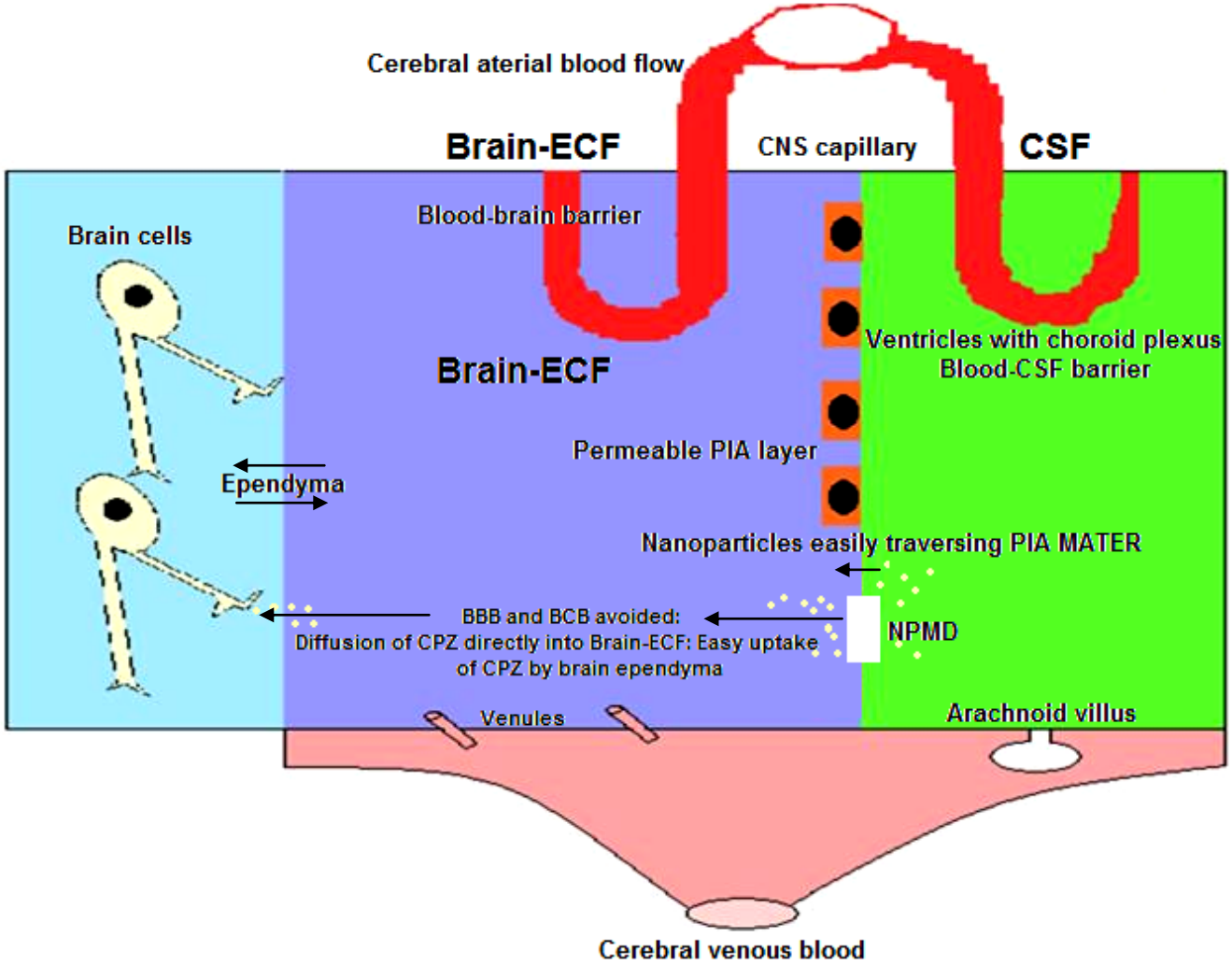

Figure 7.1: Illustration representing the proposed implantation and mechanism of action of the NPMD and its ability to circumvent the BBB and BCB, [Modified from Paulev (1999-2000)].

7.2 Materials and Methods

7.2.1 Materials

New Zealand White Rabbits were utilized in this study and were obtained as per the protocols of the Central Animal Services at the University of the Witwatersrand. Ammonium acetate (*Mw*=77.08g/mol), acetic acid (CH_3COOH) (*Mw*=60.05g/mol), sodium hydroxide (*Mw=40.00*g/mol), chlorpromazine hydrochloride (CPZ) (*Mw=355.33*g/mol) and Isoniazid (INH) (*Mw=137.139*g/mol) were purchased from Sigma Aldrich (St. Louise, MO, USA). Double de-ionized water was obtained from a Milli-Q system, (Milli- Q, Millipore, Johannesburg). All solvents utilized for UPLC-UV detection were of UPLC grade whereas all other reagents were analytical grade.

7.2.2 Animal ethics clearance

Ethics clearance from the Animal Ethics Screening Committee (AESC) of the University of the Witwatersrand was obtained for this study (No. 2011/51/04) (Appendix E).

7.2.3 Animal husbandry

Eight rabbits weighing 4.5-5kg were housed in single cages i.e. one rabbit per cage and were provided with a standard rabbit diet and water *ad libitum* under a controlled temperature (20-24^{o}C) and a 12 hour light/dark cycle. They were weighed weekly so as to ascertain their general state of well being. Housing conditions in general were according to the SOPs of the CAS which follow the South African Standard for the care and use of animals for scientific purposes.

7.2.4 Experimental design

Eight rabbits were utilized in this study which is explicitly explained by Figure 7.2. Preliminary implantation of the NPMD was performed on 2 rabbit cadavers to determine if scaling down of the device will be required. The original NPMD as well as scaled down prototypes of the NPMD were subjected to implantation to determine the appropriate size of the implant. Pre-implantation on cadavers also served to perfect the surgical implantation procedure. This was followed by a once-off pilot study conducted on 6 rabbits. Two rabbits were assigned to 3 sub-groups where the first sub-group was implanted with a drug-loaded NPMD (Group 1), the second with a non drug-loaded NPMD (Group 2) and the third with an intramuscular parenteral dose of commercially available CPZ (Chlorpromazine HCl-Fresenius® 25mg/mL) (Group 3). The dose of the intramuscular CPZ injection was 1mg/kg of body weight. This dose was attained by the veterinary formulary of the University of Minesota. One rabbit from each group was euthanized approximately halfway through the

study (Day 14) and was subjected to histomorphological toxicity studies. The remaining rabbits were euthanized at the end of the study (Day 30) and underwent further histomorphological toxicity studies. A bed letter was kept for each rabbit (Appendix F1) and the following details will be noted:

- A visual assessment of the tolerance of the rabbits towards the drug-loaded and non drug-loaded NPMDs implants as well as the intramuscular injection of CPZ.
- The presence of any undesirable reactions that may occur following implantation as well as the intramuscular injection of CPZ.
- Behavioral and physical changes of the rabbits e.g. mobility, weight change.
- Assessment of vital signs such as Temperature, Respiratory Rate and Pulse.

7.2.5 Sterilization of NPMD prior to surgery and implantation

Due to the invasive nature of the surgery and the fact that it was in the region of the brain, the possibility of infection due to the NPMD had to be ruled out. A contaminated NPMD could have caused complications such as meningitis and other CNS infectious diseases. A sterilization technique suited to the NPMD had to be chosen. Due to the thermoplastic nature of some of the componential elements of the NPMD, sterilization techniques utilizing heat e.g. autoclaving, could not be considered as it may result in deformation. Gamma radiation is widely used for the sterilization of medical devices and implants. A major advantage of gamma irradiation is the fact that it is highly penetrating and does not form any residue. The recommended dose for medical devices is 25kGy which is effective across a wide range of micro-organisms (Burth and Ley, 1963). Despite this studies have proved that effective antimicrobial sterilization can be achieved from doses of 16kGy depending on the conditions. Sterilization at room temperature requires doses ranging from 18-25kGy for the effective destruction of all potential pathogens (Bernkopf, 2007) hence the NPMD underwent sterilization at 20kGy which lies between these values (Appendix F2). Furthermore, this intermediate value was selected as it has been proven that very high energy irradiation may cause structural changes to the polymeric constituents (Bruck and Mueller, 1988).

7.2.6 FTIR analysis of the componential elements of the NPMD post-sterilization

Fourier Transform Infrared Spectroscopy (FTIR) was performed on the componential elements of the NPMD to assess the possibility of any deformation or degradation that may have occurred due to the gamma irradiation process at the dose of 20kGy. A Spectrum 100 FTIR Spectrometer (PerkinElmerLife And Analytical Sciences Inc., Shelton, CT USA) was used to detect the vibration characteristics of chemical functional groups in a sample, in response to infrared light interactions.

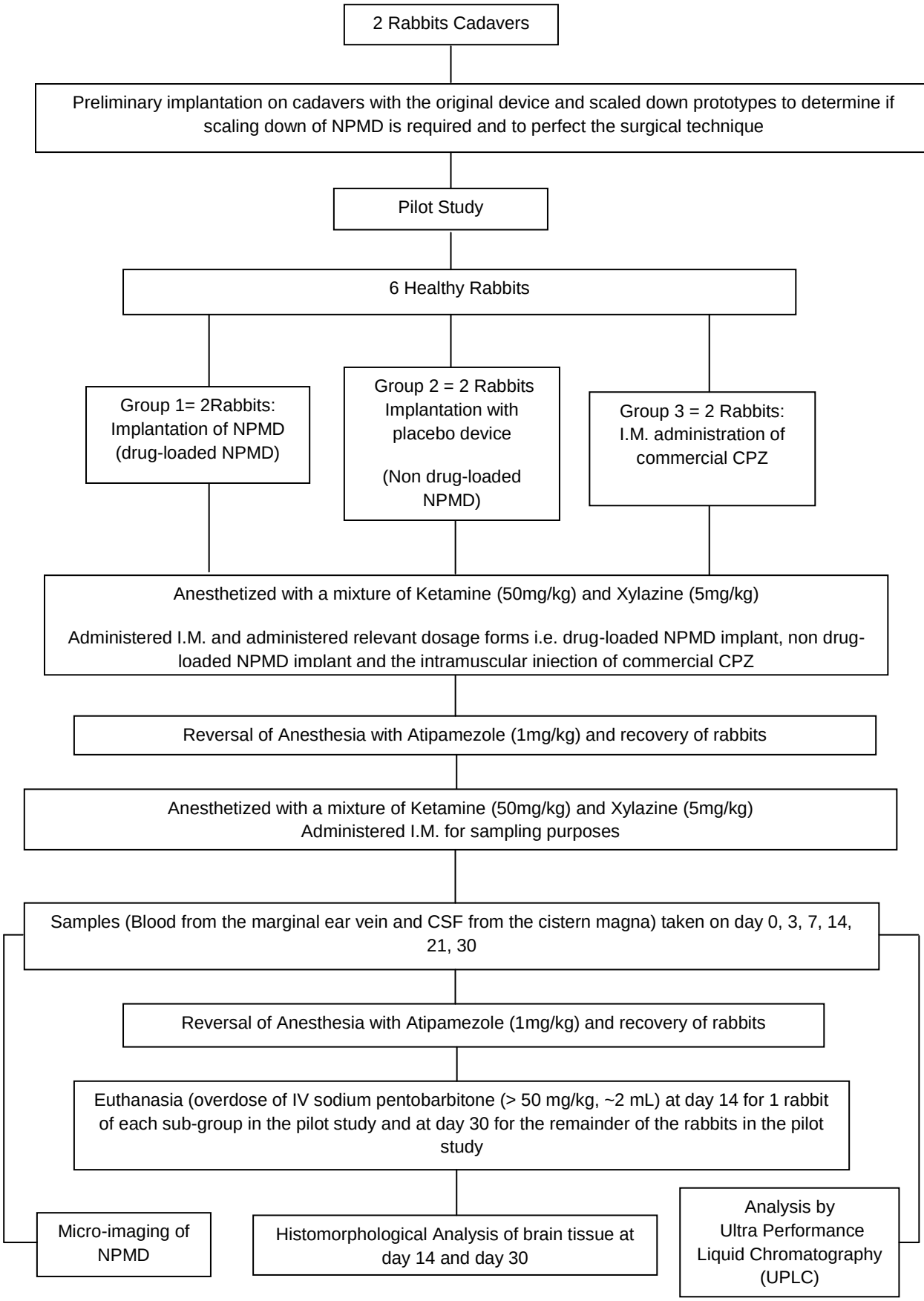

Figure 7.2: Schematic representation of the preliminary implantation and pilot study to be conducted on the rabbit model.

7.2.7 Intraparenchymal implantation of the NPMD in the region of the frontal lobe of the rabbit brain

7.2.7.1 Preliminary implantation on cadavers and implant size determination

Rabbits were humanely euthanized with sodium pentobarbitone (>50mg/kg). NPMD's of various sizes were implanted into the frontal lobe until the appropriate implant was chosen. The bone defect was closed with bone wax and the scalp insertion was appropriately closed with a single layer of non-absorbable suture. Figure 7.3 are digital images which represent a) the different sizes of the NPMDs reviewed for implantation as well as b) the implantation procedure performed on the cadavers

a)

b)

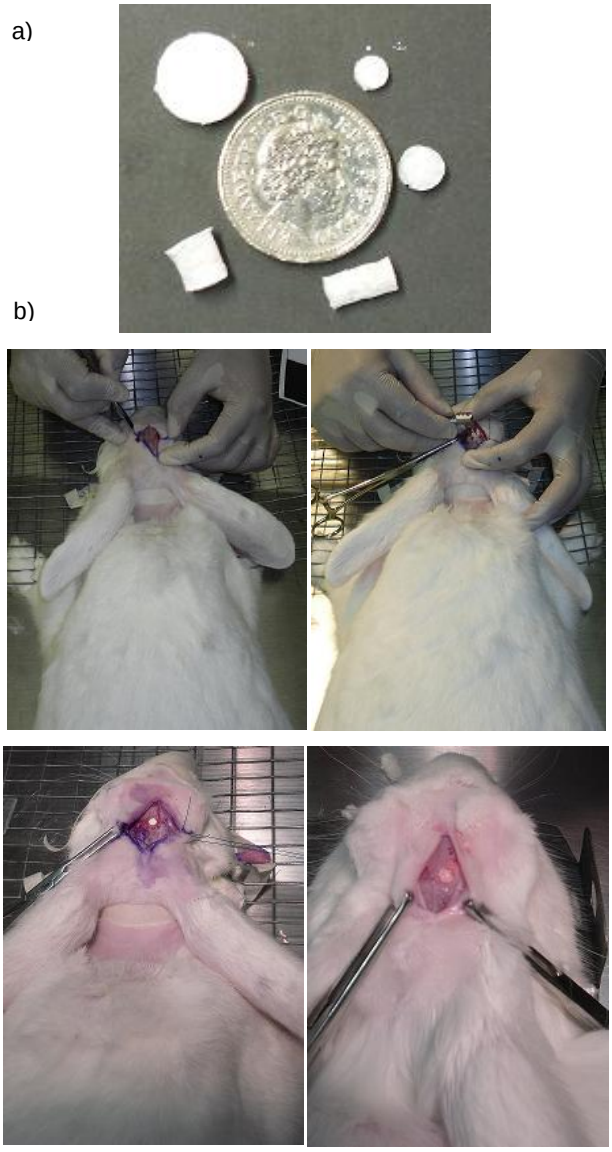

Figure 7.3: Digital images of the various sizes of the NPMD and preliminary implantation procedure performed on rabbit cadavers.

7.2.7.2 Implantation in live, healthy rabbits

Upon completion of the successful intracranial implantation in the cadaver and the determination of an appropriate size, the implantation was conducted on live, healthy, rabbits. Rabbits were initially given half the recommended dose of midazolam to as a sedating agent followed by anesthesia with a mixture of Ketamine (50mg/kg) and Xylazine (5mg/kg). The implantation procedure was adapted from Brem and co-workers (1989) and is briefly outlined; the heads of the animals were shaved and appropriately prepared.

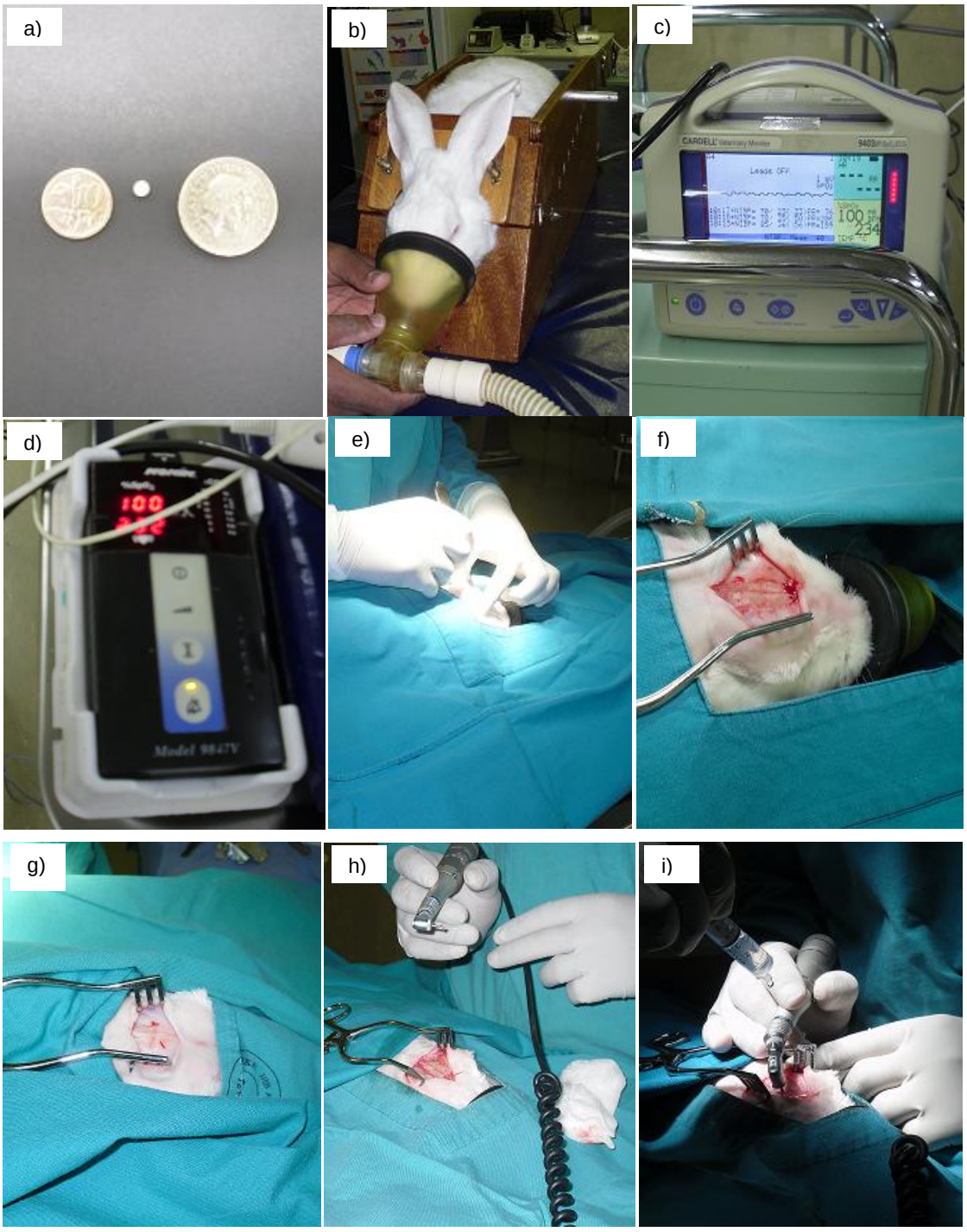

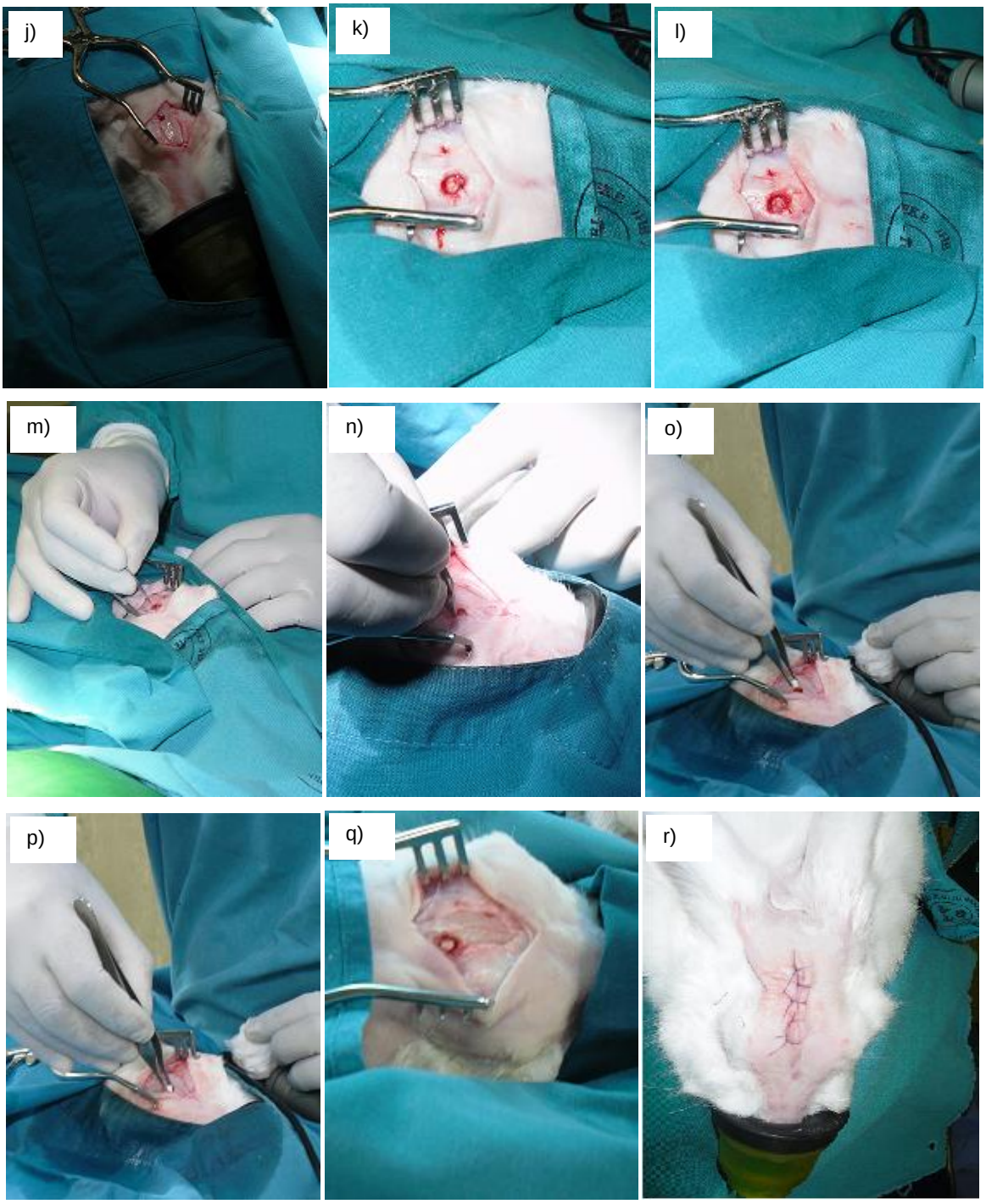

Figure 7.4: Implantation of the NPMD into the frontal lobe of the New Zealand White Rabbit brain (Timeframe = 15 minutes).

A midline incision was made and this was followed by the removal of subcutaneous tissue and periosteum. A unilateral burrhole of approximately 5mm was made using a dental drill. The burrhole was located anterior to the coronal suture and lateral to the sagittal suture. The dura mater and cortex were pierced with minimal resultant bleeding. The burrhole was

flushed with saline and the implant was placed intraparenchymally. The scalp insertion was then appropriately closed with a single layer of non-absorbable suture. Bone wax was not utilized to keep the implant in place as was done with the implantation procedure on the cadavers. The reason for this was the fact that this could affect the NPMDs hydration which inevitably would affect CPZ release. Figure 7.4 outlines the entire implantation procedure and is summarized below:

a) - Relative size of the implanted NPMD when compared to a Great Britain Pound (GBP) and a South African 10 cent coin.

b) - Anesthesia of rabbits with a mixture of Ketamine (50mg/kg) and Xylazine (5mg/kg).

c-d) - Monitoring of vital signs of the rabbit such as heart rate, respiratory rate and temperature during surgery

e) - Midline incision made and the skull is exposed.

f-h) - Skull is exposed and land-marking sutures are clearly visible.

i) - A dental drill is used to drill through the skull and pierce the dura mater with minimal bleeding and the area is flushed with saline.

j-l) - A clearly visible unilateral burrhole (5mm) is made anterior to the coronal suture and lateral to the saggital suture.

m-n) - The cortex and parenchyma of the brain is pierced through the burrhole.

o-q) - The NPMD is placed inside the parenchyma and is clearly visible.

r) - The scalp insertion is closed with non-absorbable suture while the rabbit is maintained on anesthetic.

7.2.8 Cerebrospinal fluid sampling

CSF samples (500µl) were be drawn by cisternal puncture by a method adapted from Chitty (2007) (Figure 7.5). Briefly, the rabbits were anaesthetized and placed in lateral recumbency, with the head flexed at 90° to the neck. The fur was then shaved on the dorsal head and neck and the site was appropriately disinfected. A 23 gauge hypodermic needle was inserted into the dorsal midline between the external occipital protuberance and the craniodorsal tip of the dorsal spine of the C2 vertebra, cranial to the cranial wings of the C1 vertebra. The needle then gently entered the subarachnoid space and CSF was passively

withdrawn into 1mL syringes and stored in eppendorf tubes at -80°C till further analysis. Any contaminated CSF samples were centrifuged at 1300 relative centrifugal force (RCF) and the clear supernatant was collected and stored immediately at -80°C in a laboratory freezer. Blank CSF for base-line data was withdrawn from the rabbit 1 week prior to implantation with the NPMD.

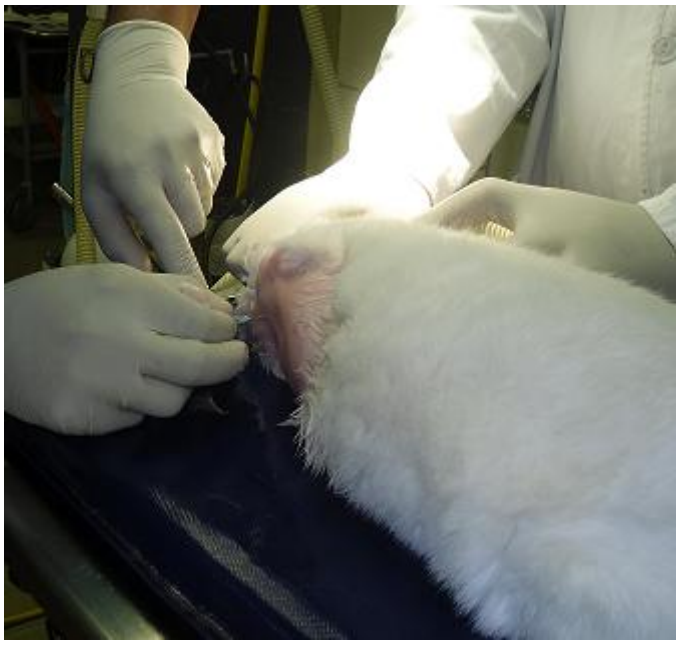

Figure 7.5: CSF withdrawal technique employing a cisternal puncture.

7.2.9 Blood sampling

Due to the fact that the link between CSF and the venous blood flow are the arachnoid granulations, substances within the CSF can enter the blood stream via the arachnoid granulations (Grzybowski et al., 2006). Blood samples were therefore taken to assess the potential levels of CPZ that may have enter the systemic circulation due to the sheer size of the nanoparticles and its potential ability to pass through the arachnoid granulations. Blood samples were withdrawn at specific time intervals through the marginal ear vein of the rabbit on days 0, 3, 7, 14, 21 and 30 (Figure 7.6). An intravenous catheter (22 gauge) was used to draw approximately 1% of the animal's body weight i.e. 3mL of blood from a 3kg rabbit and 4.5mL of blood from a 4.5kg rabbit. These guidelines were attained from "The Guidelines for Collection of Blood from Experimental Animals", Research Animal Resources, University of Minnesota. Blood sampling was conducted on anesthetized rabbits. Blank blood for base-line data was withdrawn from the rabbit 1 week prior to implantation with the NPMD. The blood samples were collected into heparinized vacutainer tubes and gently mixed to prevent clotting. The samples were centrifuged at 1300 RCF soon after. The supernatant, containing the plasma, was carefully aspirated and transferred into a clean appropriate collection tube and frozen at -80°C immediately till further analysis.

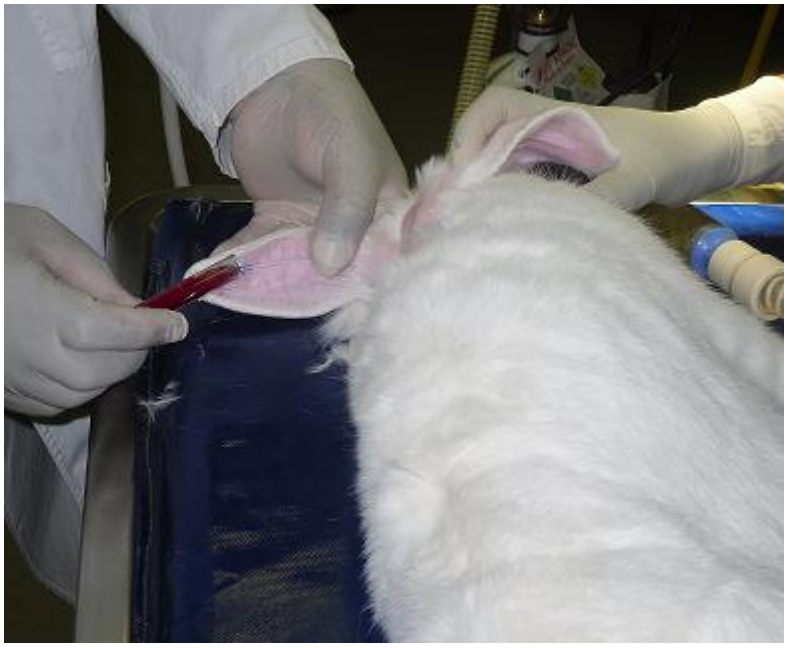

Figure 7.6: Blood withdrawal through the marginal ear vein.

7.2.10 Animal welfare and non-surgical interventions employed

Monitoring of weight, behavior, eating and grooming habits took place periodically (Appendix F1 and F3). Any significant fluctuations in these areas (e.g. a chronic body weight loss of more than 15%) were considered. If the animals developed any inflammatory conditions or infections; they were treated with appropriate analgesia and anti-inflammatories (buprenorphine 0.05-0.1mg/kg and carpofen 4mg/kg, both administered subcutaneously). The inclusion of a placebo group allowed for the comparison against the experimental group in terms of the assessment of the degree of distress experienced by the rabbits.

7.2.11 Endpoints for experiment that may have resulted in potential termination of the study

Any rabbits that developed a severe inflammatory response due to the presence of the implant were treated with appropriate anti-inflammatory agents. However, if the inflammation resulted in severe distress to the rabbits, those animals were removed from the study. Endpoints and termination was also considered if the rabbits experienced severe side effects such as hypotension and extrapyramidal side-effects. Furthermore, a rapid reduction in weight (~ 15%) or animals displaying sickness behavior or showing deteriorating body condition were considered for termination of the study.

7.2.12 High-frequency ultrasound imaging

The Vevo 2100® Micro Imaging Platform enhanced with the Cellvizio® Lab module (VisualSonics (Pty) Ltd, Toronto, Ontario, Canada) was used to evaluate the NPMD post implantation by mico-

imaging. It is a high definition, fluorescence optical imaging system for the observation and quantification of physiological phenomena at the cellular and sub-cellular levels in animals. It provides non-invasive, real time imaging with a high-frequency, high-resolution digital imaging platform. Imaging was performed on euthanized rabbits on Day 14 and Day 30 of the study.

7.2.13 Histomorphological analysis of the rabbit brain post implantation

Histomorphological analysis was conducted to assess the biocompatibility of the NPMD and its immune response in terms of its inflammation response, whether or not it is toxic or causes excessive bleeding. Rabbits were euthanized midway through the study (Day 14) and at the end of the study (Day 30) with sodium pentobarbitone and decapitated. The entire brain was removed and fixed in 10%$^{v}/_{v}$ neutral buffered formalin solution (Figure 7.7). Following the normal fixation period, the brain specimens were cut by cross section in the anterior third region where the NPMD was implanted or where areas of lysis could be identified. Addition sections in the mid-brain and cerebellum were also examined to assess any effects of particles, drug or the NPMD that may have translocated to these areas as a result of biodegradation. These selected blocks were then processed in an automated histological processor overnight. After complete tissue processing, wax blocks were prepared and histological sections of 6µm were cut on a microtome. The slides produced were stained with haematoxylin and eosin (H&E) in an automated stainer prior to mounting for histomorphological evaluation.

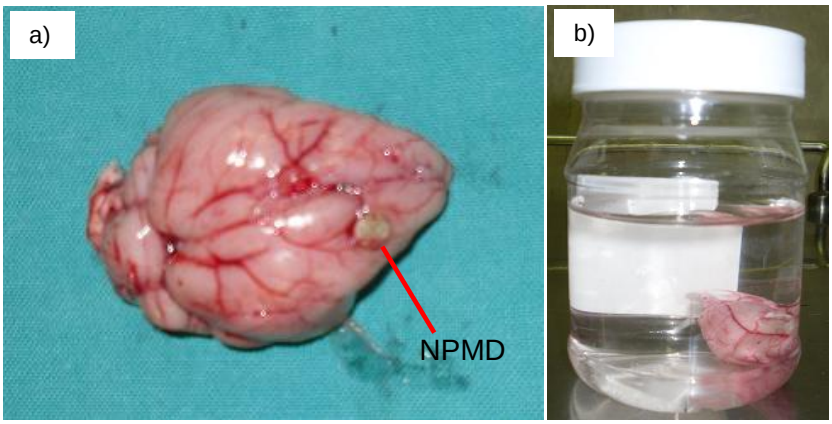

Figure 7.7: Digital images of a) the whole brain removed at Day 30 with the NPMD still intact and b) storage of brain in 10%$^{v}/_{v}$ formalin solution prior to histomorphological analysis.

7.2.14 *In vivo* biodegradation and erosion of the NPMD

The NPMD was removed at the end of the study (Day 30) and the bioerosion of the device was evaluated utilizing visible light of a stand laboratory light microscope (Olympus SZX7, Shinjuku-ku, Tokyo, Japan).

7.2.15 Textural profile analysis to determine the physicomechanical behavior of the NPMD post-implantation

Textural profile analysis (TA) in terms of matrix resilience, was conducted to characterize the 3D salient core regions of the NPMD using a Texture Analyzer (TA.XT*plus* Stable Microsystems, Surrey, UK). Matrix resilience was calculated pre and post-implantation (Day 30) and compared to *in vitro* data.

7.3 Ultra-Performance Liquid Chromatography for the Analysis of CSF and blood samples

7.3.1 Solvents, mobile phases and chromatographic conditions utilized in sample analysis

Strong wash: Acetonitrile (ACN) (90%) and water (10%)
Weak wash: Acetonitrile (10%) and water (90%)
Mobile phase A: Ammonium acetate buffer (AA) (0.1M, pH 5, adjusted with acetic acid)
Mobile phase B: Acetonitrile (100%)

Ultra-performance liquid chromatography (UPLC) was performed utilizing a Waters Acquity® UPLC system (Waters Corp.,Milford, MA, USA). The system contains a binary solvent manager, sample manager and a photoiodide array (PDA) detector, all connected to a Waters Empower 2 data station. An Acquity UPLC BEH C18 column (50 mm×2.1mm, i.d., 1.7µm particle size, Waters) was used at 40°C to achieve separation. The machine was primed with the appropriate solvents mentioned above for 10 cycles each of 5 minutes. The method for separation, identification and quantification was isocratic whereby the mobile phase comprised ammonium acetate buffer and acetonitrile (AA-ACN 65-35%$^{v}/_{v}$), the flow rate through the column was 0.50mL/min, the injection volume was 2µL and the run time was 3 minutes. Between injections, the machine was allowed to equilibrate for 3 minutes so as to attain a constant pressure and more reliable results. Upon completion of analysis, ACN was gradually injected into the system to remove any residue until the entire column was immersed in 100% ACN. The PDA detector was set at 254nm for CPZ and INH detection.

7.3.2 Preparation of standards

Primary stock solutions of CPZ (10µg/mL) and the internal standard (IS), INH (239µg/mL) were prepared separately with ultra-pure double de-ionized water (Milli-Q, Millipore, Johannesburg). The CPZ primary stock solution was diluted to yield working solutions of concentrations ranging between 1.25ng-20ng/mL. The IS, INH, was kept constant at 239µg/mL. In preliminary studies, the CPZ and INH concentrations were kept constant and

subjected to the chromatographic method described in Section 7.3.1 of this chapter, however it was noticed that the peak of the highly active CPZ detection was dwarfing the peak of the IS. All solutions were filtered with a 0.22µm pore size Cameo Acetate membrane filter (Millipore Co., Massachusetts, USA).

7.3.3 Plasma and CSF extraction of CPZ

An uncomplicated and effective liquid-liquid plasma extraction procedure was developed and applied to CPZ in blood samples. Aliquots of plasma (500µL) of sample were transferred into polypropylene tubes followed by the addition of 1mL of ACN in order to precipitate the plasma proteins. The samples were subsequently vortexed for 1 minute followed by the addition of 500µL of ACN. The mixture was vortexed again for 1 minute and was then centrifuged at 1300 RCF (Nison Instrument Limited, Shanghai, China) for 5 minutes. The supernatant was removed and filtered through 0.22µm Cameo Acetate membrane filters. The filtrate was then spiked with a known amount of the IS, INH. The final solution was transferred into Waters® certified UPLC vials for analysis. Due to the fact that CFS does normally contain proteins (Reiber, 2003) and that CPZ is highly protein bound (Okeri et al., 2008), the same extraction procedure was applied to CSF samples.

7.3.4 Validation of extraction procedure

Three CSF and plasma solutions each containing 3 different known concentrations of CPZ were prepared and subjected to the extraction procedure mentioned in Section 7.3.3. The extraction yield percentage was calculated by comparing the peak areas obtained from the extracted CPZ to the peak areas obtained from standard solutions of the same concentration using Equation 7.1

$$\text{Extraction Yield (\%)} = \frac{\text{Peak Area of Extracted CPZ}}{\text{Peak Area of Standard CPZ}} \times 100 \qquad \textit{Equation 7.1}$$

Inter-day variability consisted of multiple injections of samples over 3 consecutive days, (N=3 for each day) and intra-day variability consisted of multiple injections of samples during a 24 hr period N=3. This data provided elucidated the precision and accuracy of the extraction process. The extraction process was further validated by the use of the IS, INH. Since a known quantity is always utilized when spiking CSF or plasma samples, theoretically, the peak area of the INH should always be similar.

7.3.5 Calibration curves of CPZ in CSF and plasma

Blank CSF samples were removed from the freezer (-80°C) and thawed to room temperature. A 200µL aliquot of each CSF sample was transferred to separate centrifuge tubes. Each aliquot was spiked with analyte standard solutions of CPZ at differing concentrations (N=5). The same procedure was applied to 5x500µL of blank plasma. Upon completion, both the spiked CSF and plasma solutions were vortexed for 2 minutes and subjected to the extraction procedure detailed in Section 7.3.3 of this chapter. The CPZ/IS peak area ratios were plotted against the corresponding CPZ concentrations (expressed as ng/mL).

7.4 Results and Discussion

7.4.1 FTIR analysis of the NPMD and its componential elements post-sterilization

FTIR was performed to ensure that there was no deformation of the polymeric backbones of the NPMD and its componential elements subsequent to gamma-irradiation at 20kGy (Figure 7.8).

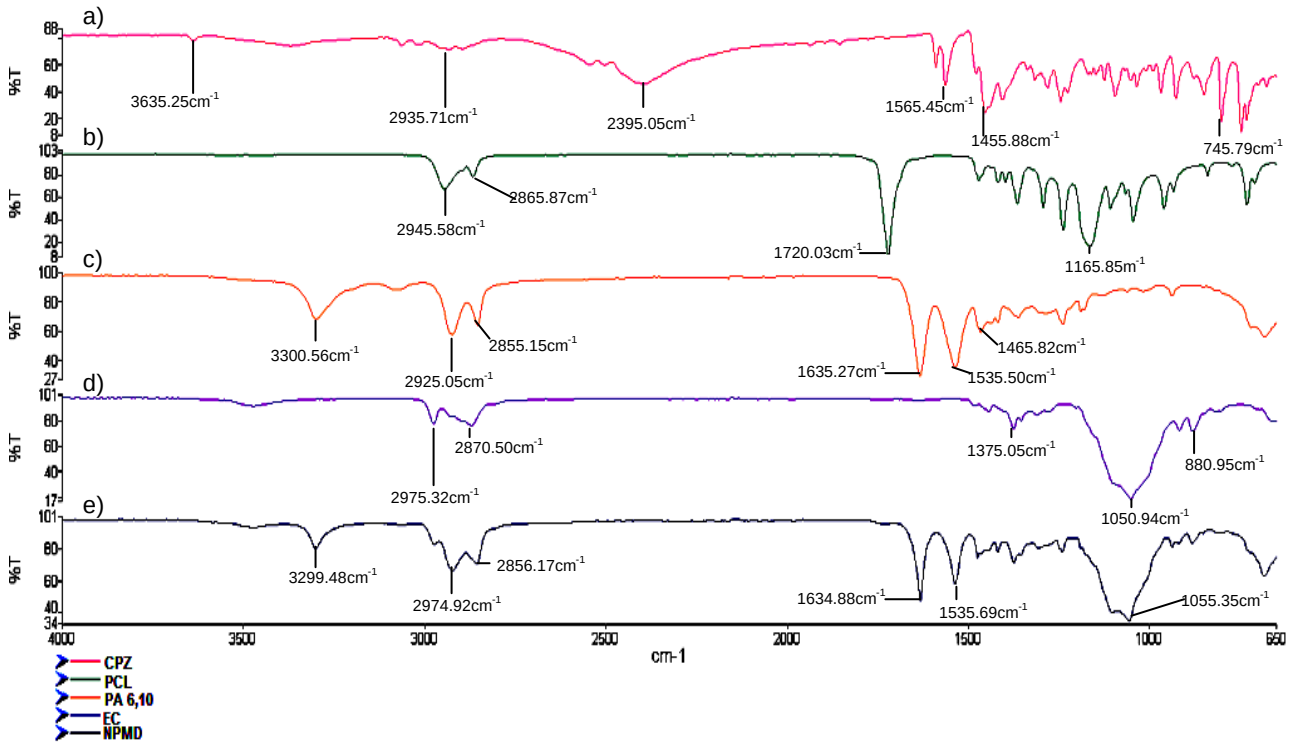

Figure 7.8: FTIR profiles of the NPMD and its componential elements post gamma-irradiation at 20kGy.

The FTIR profile of CPZ [Figure 7.8 a)] depict no deformation and transitions are indicative of aliphatic C-H stretching (2935.71cm^{-1}), H_3C-$^{+}$NH stretching and combination modes

(2395.05cm^{-1}), Phenyl ring vibrational modes (1565.45cm^{-1}), C-H deformational modes (1455.88cm^{-1}) and aromatic C-H bending modes (730-850cm^{-1}) (Abadi et al., 1999). The characteristic peaks of PCL (Figure 7.8 b)) indicate asymmetric CH_2 stretching (2945.58cm^{-1}), symmetrical CH_2 stretching (2865.87cm^{-1}) and carbonyl stretching vibration (1720.03cm^{-1}) indicate that PCL underwent sterilization without any deformation (Elzein et al., 2004, Wu et al., 2004). PA6,10 [Figure 7.8 c)] exhibits transmitting bands of amide (N-H) at 3300.56cm^{-1}, C-H stretching at 2925.05 and 2855.15cm^{-1}, C=O stretching at 1635.27cm^{-1}, and a CH_2 wag at 1465.82cm^{-1} (Kolowale et al., 2007) and displayed no degradation or deformation. EC displayed an intact backbone with absorption bands at 2975.32cm^{-1} and 2870.50cm^{-1} which are indicative of C-H stretching, 1375.05cm^{-1} which represents C-H bending and 1050.94 cm^{-1} which is an indication of –C-O-C- stretching (Suthar et al., 2000). The FTIR profile of the NPMD basically resembled that of its major components (PA 6,10 and EC). A N-H stretching band at 3299.48cm^{-1}, C-H stretching at 2974.92cm^{-1} and 2856.17cm^{-1}, C=O stretching at 1634.88cm^{-1} and C-H bending at 1055.35cm^{-1} were all indicative that the NPMD did not undergo any degradation as these transitions were also visible on the PA 6,10-EC membrane and discussed in Chapter 5, Section 5.32 of this dissertation. FTIR revealed that the gamma-irradiation sterilization of the NPMD did not result in deformation or degradation as the structural backbones of the NPMD and its componential elements remained intact.

7.4.2 Intraparenchymal implantation of the NPMD in the region of the frontal lobe of the rabbit brain

The implantation procedure was non-arduous and timely. Rabbits were awoken post-surgery by a reversal of anesthesia [atipamezole (1mg/kg)] to ensure their quicker recovery. They were then maintained on medical oxygen until fully awake. The rabbits were also administered a subcutaneous stat dose of buprenorphine (0.05mg/kg and carpofen (4mg/kg) as adequate post-operative analgesia. Once fully awake, their vital signs were assessed and were in normal range. Furthermore, key features such as their gait, movement and response to certain stimuli were assessed. The gaits of the rabbits were normal with no signs of abnormal posture or cringing. Furthermore, no abnormal movements were noticed and they were responsive to simple stimuli such as pinching of the skin. This indicated that the surgery was a success and no injury was caused. A pain assessment sheet (Appendix F4) was utilized to monitor any visible signs of discomfort post surgery. Figure 7.9 is a digital image of the rabbits post surgery at a) Day 12 and b) Day 29. It can be seen that the rabbits appear to be in good general health with the skin incision lesion at the site of implantation fully healed after suturing.

a)

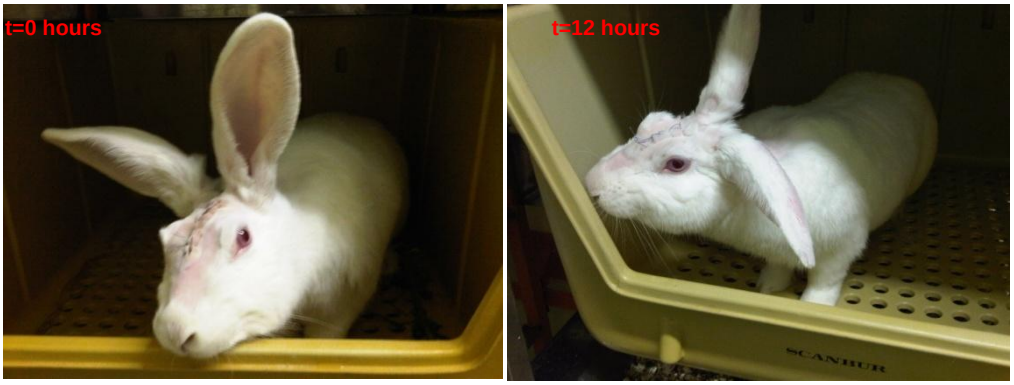

b)

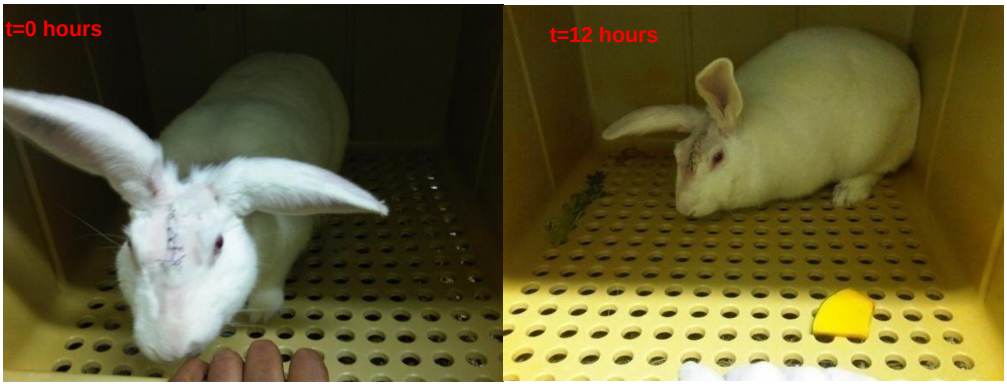

Figure 7.9: Digital images of rabbits post-surgery at a) Day 12 and b) Day 29.

7.4.3 High-frequency ultrasound imaging

High frequency ultrasound imaging utilizes sound waves from the transducer of the machine. As the sound passes through the scalp and brain of the rabbit, they are reflected back and picked up by the transducer where it is translated into a two dimensional image. Since the NPMD is a foreign body, it has different acoustic properties when compared to the brain and surround tissue. This difference in resonance results in the image being formed. Images were taken on euthanized rabbits at Day 14 and Day 30 of this study prior to whole brain removal. The images were used to assess the performance of the NPMD such as the depth of implantation and whether or not the NPMD is intact in the brain parenchyma. Figure 7.10 is an ultrasound image at Day 14 of a) a rabbit given an i.m. dose of CPZ (no NPMD) and b) a rabbit implanted with the NPMD. The rabbit without the NPMD was used as a control. The outer-most layer of the brain, the dura mater as well as the inner layer, the pia mater are clearly visible and are depicted. Between these two layers is the subarachnoid space. Traversing the pia mater, is the NPMD as is explicitly exhibited in Figure 7.10 b). This is not visible in the control as only the two layers of the brain described above are. The NPMD at Day 14 remains intact and no sign of breakage is observed. A similar observation is noted at Day 30 of the study (Figure 7.11). In this case, however, the NPMD is not as defined as it is at Day 14. This could possibly be due to the erosion of the implant. It can be further deduced from both figures that the implant was inserted approximately 4mm intraparenchymally.

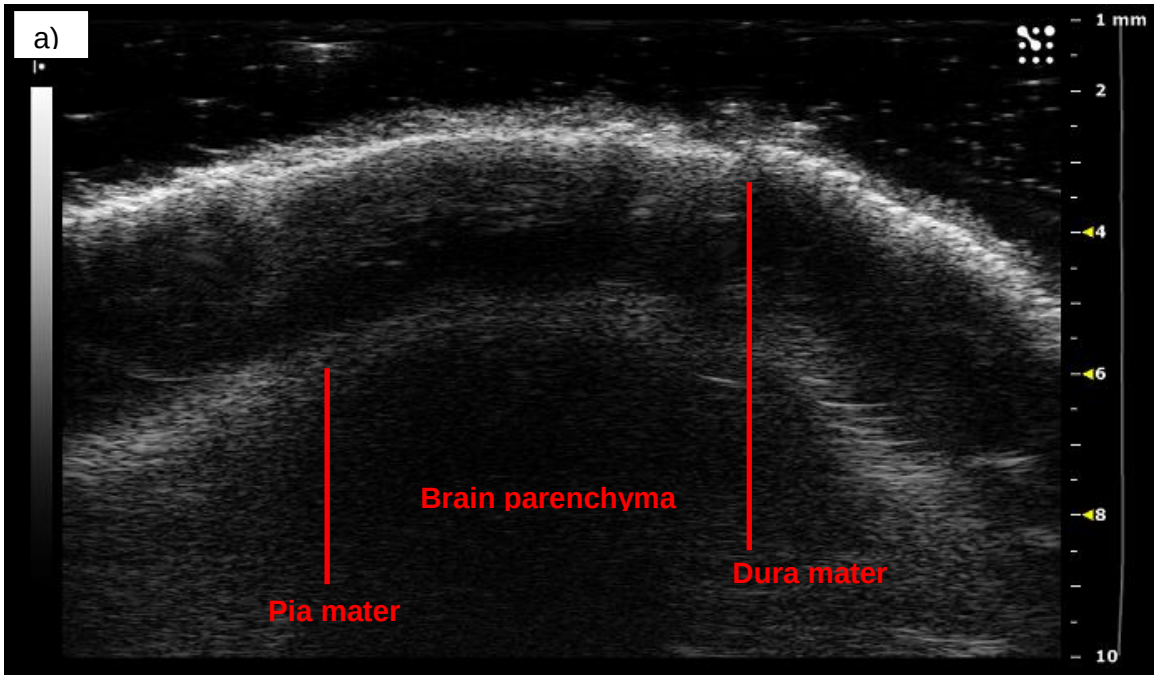

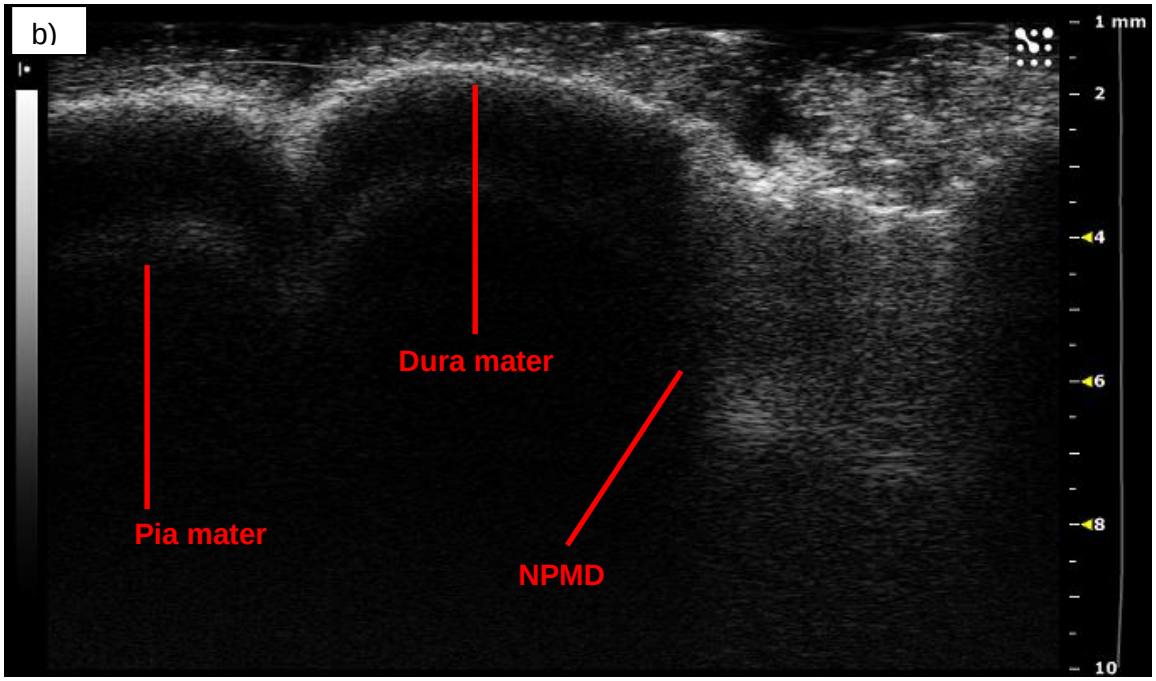

Figure 7.10: Ultrasound images of the brain of a) rabbit devoid of NPMD (control) and a rabbit implanted with the NPMD at Day 14 of the study.

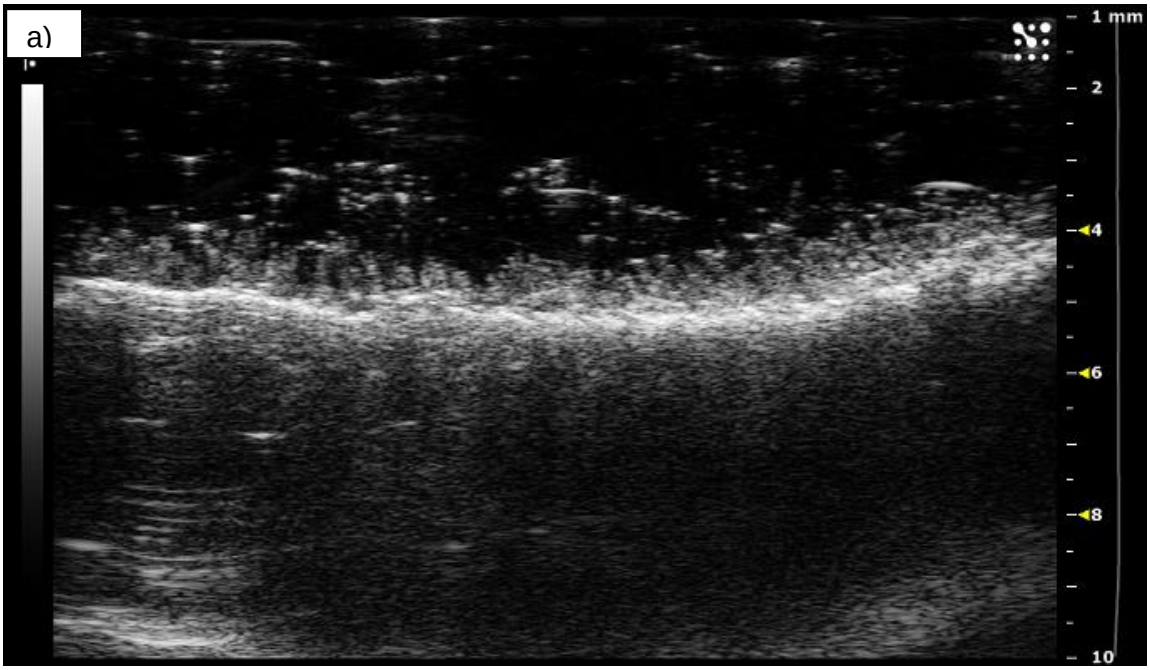

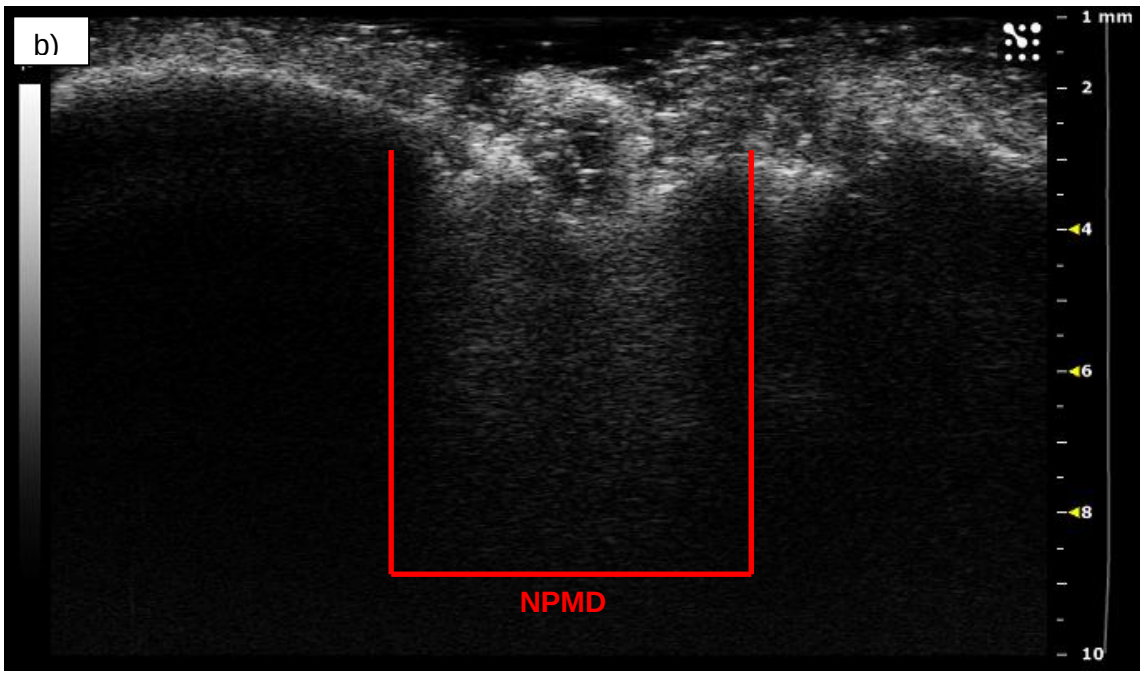

Figure 7.10: Ultrasound images of the brain of a) rabbit devoid of NPMD (control) and a rabbit implanted with the NPMD at Day 30 of the study.

7.4.4 Histomorphological analysis

Macroscopical observations of the brains implanted with the NPMD, the non-drug loaded NPMD and the brains devoid of any implant (the rabbits given an i.m. dose of CPZ) were noted and recorded in Table 7.1

Table 7.1: Macroscopical observations of the brains of rabbits implanted with the NPMD, the non-drug loaded NPMD and the brains of rabbits devoid of an implant.

Group	Macroscopical observations
NPMD	Focal 2mm malacia (softening of brain tissue) on ventral aspect of brain
Non-drug loaded NPMD	Small foci of malacia and adhesions in dorsal brain with implant present
Rabbits administered i.m. Dose of CPZ (No NPMD-Control)	No lesions in several sections of the brain

Where NPMD = nano-enabled polymeric membranous device and CPZ = chlorpromazine hydrochloride

H&E staining and histopathology of the brain implanted with NPMD, the non-drug loaded NPMD and the brains of rabbits devoid of an implant as depicted in Figure 7.11, revealed the following observations;

Drug-loaded NPMD

Day 14

The morphological observation from the anterior cerebrum section confirms a superficial subdural area of liquifactive necrosis [Figure 7.11 a)] where some eosinophilic proteinaceous material with minimal hemorrhage could be confirmed and a peripheral granulomatous process where some large macrophage-type cells of microglial origin as well as few multinucleated cells are present in the periphery [Figure 7.11 b)]. In the surrounding stroma, minimal perivascular cuffing could be confirmed and the implantation site shows only a mild reaction in the wall of the neuroparenchyma. The lesion is very superficial and non-significant.

Day 30

The neuroparenchyma directly surrounding the lytic area displays minimal spongiosis and minimal inflammation [Figure 7.11 c)]. The anterior third of the hippocampus confirms a focal unilateral are of encephalomalacia where some heterophils as well as mononuclear cells are observed in the area of the cortical grey matter necrosis. Inflammation from the leptomeninges into the neuroparenchyma as well as hemorrhage was very minimal. The rest of the sections from the anterior portion of the brain, mid-cerebrum and cerebellum confirmed no morphological neuropathology.

Non-drug loaded NPMD

There were no discrepancies noted between the histomorphological findings of the NPMD and the non-drug loaded NPMD (placebo). This thus confirmed that the CPZ did not cause any adverse effects to the surrounding brain tissue. As with the NPMD, there is a presence of mild inflammation [Figure 7.11 d)]. In both cases, this is probably due to the body's foreign body immune response. In the anterior third of the cerebrum, there is however a superficial subdural focal malacia and slight hemorrhage which could be due to the actual implantation process and piercing of the neuroparenchyma (Figure 7.12). The rest of the sections from the anterior portion of the brain, mid-cerebrum, cerebellum and medulla oblongata appear normal.

Brain of rabbits given i.m. dose of CPZ (no implantation)

No pathological signs are present. The neuroparenchyma appears to be morphologically normal. Other areas of the brain, including the anterior cerebrum, cerebellum and mid-brain appear normal.

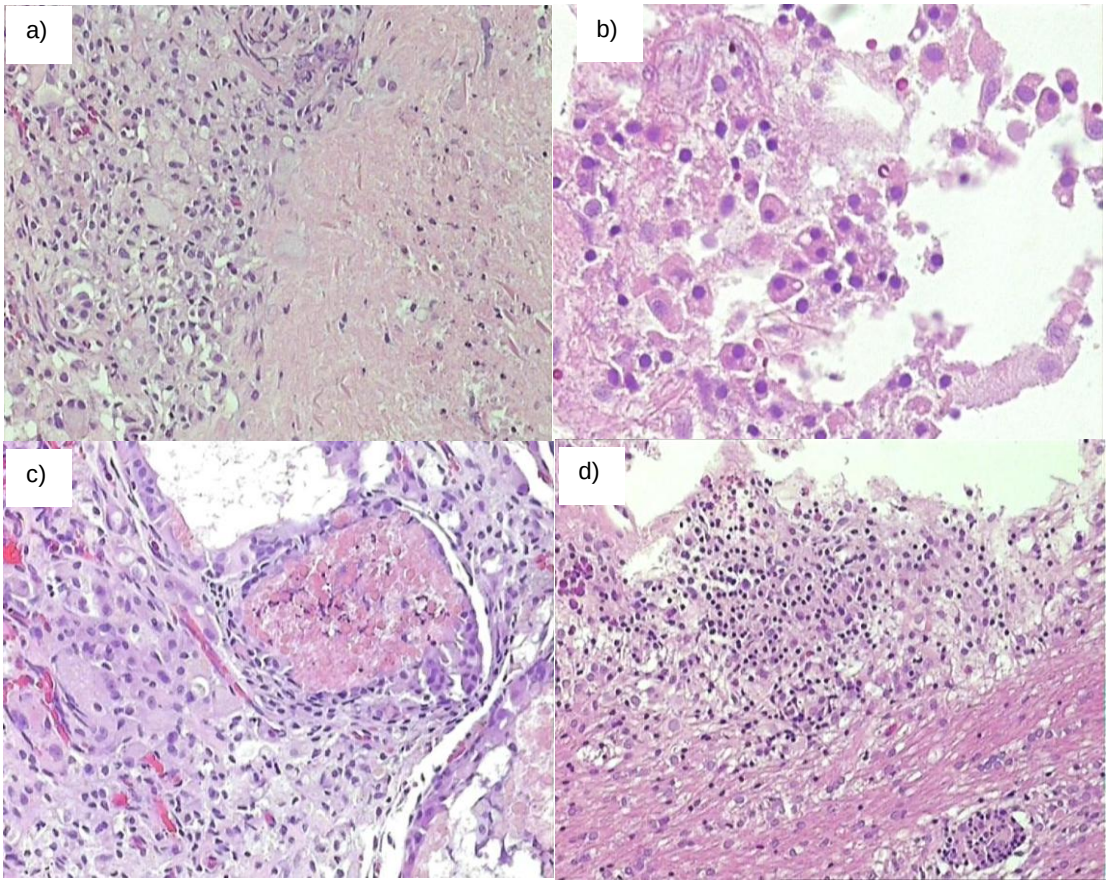

Figure 7.11: Light microscopy images of H%E stained slides of the region of the rabbit brain implanted with the NPMD depicting a) mild inflammation and liquifactive necrosis, b) macrophages/glitter cells due to the foreign body, c) minimal lysis and inflammation and d) mild inflammation from the placebo.

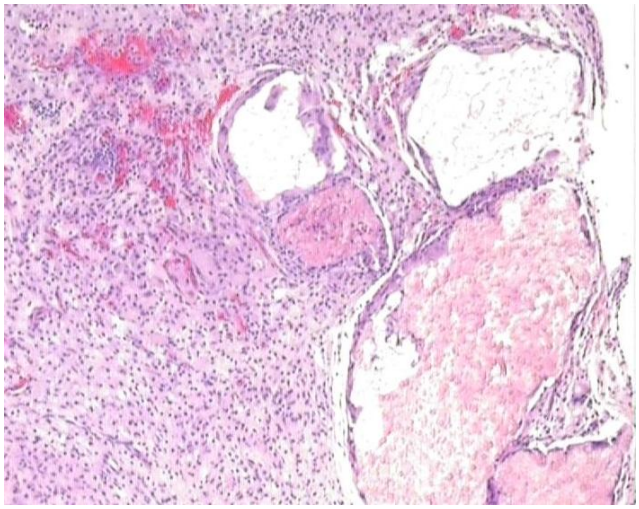

Figure 7.12: Light microscopy histological image displaying slight hemorrhaging possibly caused by the actual implantation process and piercing of the neuroparenchyma.

Generally, the areas of liquifactive necrosis are most like due to the implantation of the NPMD and the placebo device and the subsequent displacement of the neuroparenchyma by the implant with mild inflammation present around the necrotic area. The abundance of macrophages or glitter cells is indicative of healing and phagocytosis of the necrotic brain material. The mild inflammation is only limited to the region of the implant and does not extend widely throughout the brain. Furthermore, minimal hemorrhaging is observed. These results confirm the success of the implantation procedure and elucidates the biocompatibility of the NPMD.

7.4.5 *In vivo* bioerosion of the NPMD

In vivo bioerosion at Day 14 and Day 30 was calculated to be to 7.32% and 14.87% respectively. These erosion dynamics proved that the device remained intact over the duration of the study and that sufficient hydration of the NPMD did in fact occur which could have a bearing on the NPMD's drug release profile. Furthermore this also confirmed that the device would eventually degrade over time. When correlated with the histomorphological observation, results proved that the NPMD was biocompatible as well as biodegradable which ensures that the device would be non-toxic and no additional surgery would be required for its removal. Figure 7.13 represents a) the NPMD prior to implantation, b) the NPMD after 14 days of implantation and c) the NPMD at the end of the *in vivo* study. As can be visibly seen, the erosion at day 14 was substantially less than that at Day 30.

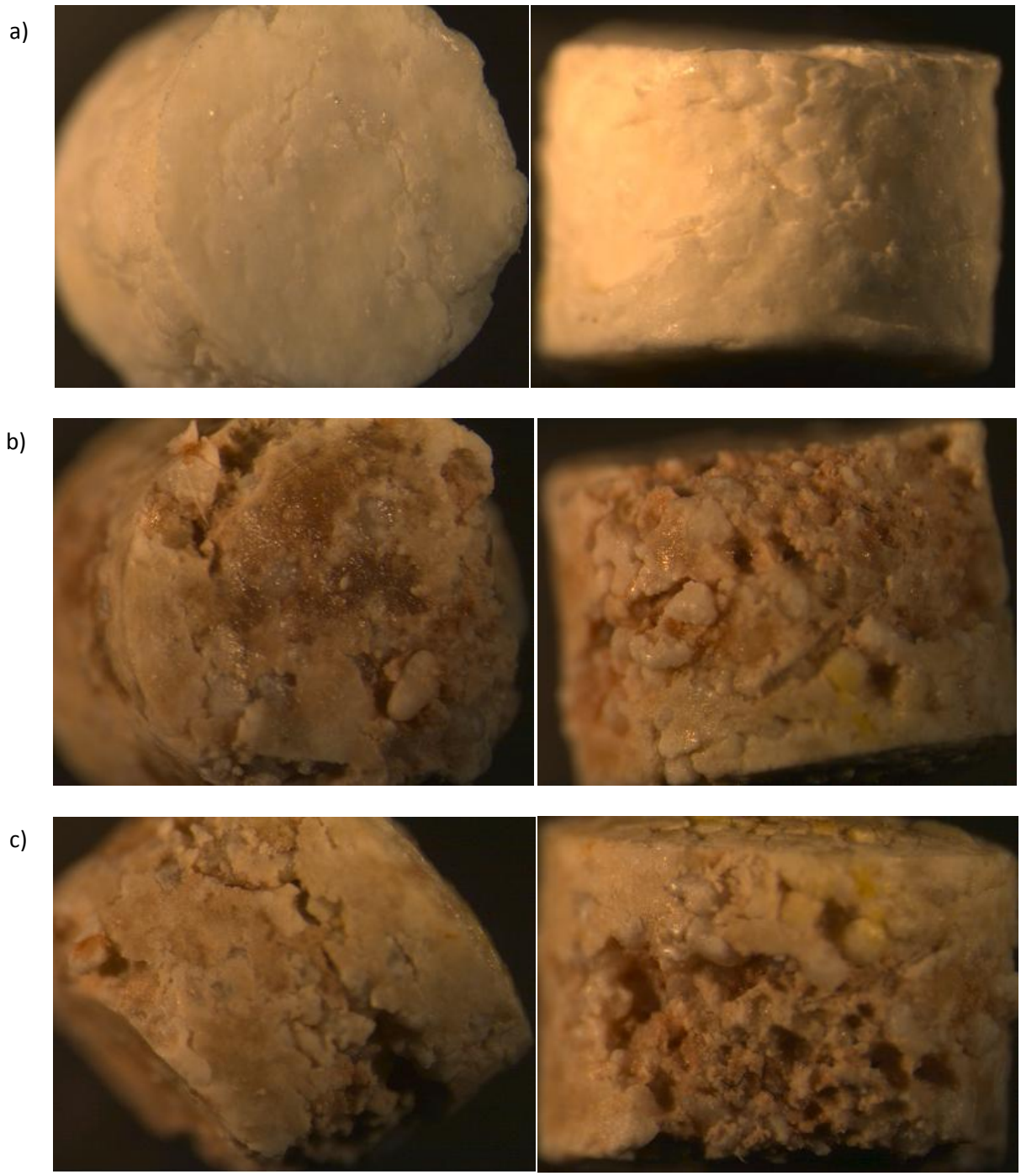

Figure 7.13: Light microscopy images depicting a) the NPMD pre-implantation, b) the NPMD at Day 14 and c) the NPMD at the end of the study (Day30) indicating visible bioerosion and biodegradation of the device.

7.4.6 Textural profile analysis to determine the physicomechanical behavior of the NPMD post-implantation

Textural profile analysis in terms of *in vivo* unhydrated matrix resilience (UHMR) and hydrated matrix resilience (HMR) of the NPMD pre-implantation and the NPMD post-implantation (Day 30) was determined to evaluate the *in vivo* integrity of the NPMD. Figure 7.14 are force-time profiles of a) the unhydrated NPMD and b) the NPMD at Day 30 of the study. UHMR was calculated to be 73.08% which correlates to that of the optimized PA 6,10-EC composite membrane described in Chapter 4 of this dissertation. HMR was calculated to be 59.67%. This is a marked decline in MR and could be a result of the notable erosion of the NPMD as depicted in the light microscopy images [Figure 7.13 c)]. The visible erosion could have caused a decrease in the NPMD's integrity hence resulting in a lower HMR.

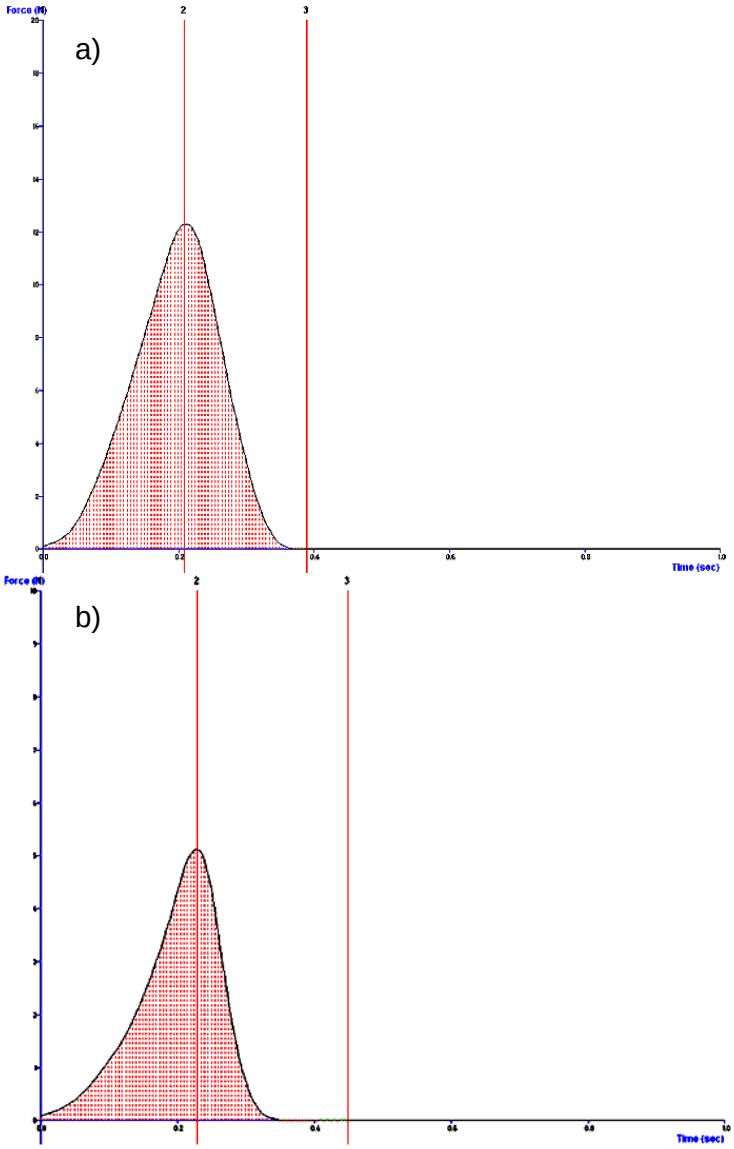

Figure 7.14: Force-time profiles depicting the a) UHMR and b) HMR (Day 30) of the NPMD.

7.4.7 Validation of extraction procedure

Table 7.2 and 7.3 represent the validation of the method utilized for the extraction of CPZ from the CSF and plasma respectively. Extraction from CSF proved to be far more effective when compared to plasma. This is due to the fact that CPZ is highly protein bound and CSF contains far less protein when compared to plasma (Reiber, 2003; Okeri et al., 2008). Nevertheless, the method used was effective in displacing the majority of the CPZ from the proteins. Lower concentrations of drug were harder to remove as there are more proteins for attachment when compared to higher concentrations of CPZ which can cause saturation of the proteins.

Table 7.2: Validation of CPZ extraction method from CSF.

Concentration of CPZ (ng/mL)	Intra-day Extraction (%yield)	Inter-day Extraction (%yield)
200	98.32	97.98
20	99.92	99.85
0.625	99.9	99.67

Table 7.3: Validation of CPZ extraction method from plasma.

Concentration of CPZ (ng/mL)	Intra-day Extraction (%yield)	Inter-day Extraction (%yield)
200	80.32	80.57
20	76.17	77.55
0.625	68.28	68.69

7.4.8 Chromatograms of CPZ and INH in CSF and plasma

Typical chromatograms for CPZ and the IS, INH in CSF are depicted in Figure 7.15 a) and b) and typical chromatograms for CPZ and INH in plasma are represented in Figure 7.15 c) and d). The IS, INH depicts a retention time of 0.175 minutes whereas CPZ displays a retention time of approximately 1.145 minutes. Positive controls were utilized to determine the fact that each of CPZ and INH elutes at these specific times by spiking blank CSF and plasma with CPZ and INH separately and subjecting them to the extraction procedure mentioned in Section 7.3.3 of this chapter and then analyzing the respective solutions. They were then combined and subjected to the extraction procedure and analyzed. This also validated the extraction procedure. The concentration of the IS was kept constant throughout the study. CPZ displayed very minimal AUC values thus confirming the detection of CPZ at very minute concentrations in the CSF and plasma.

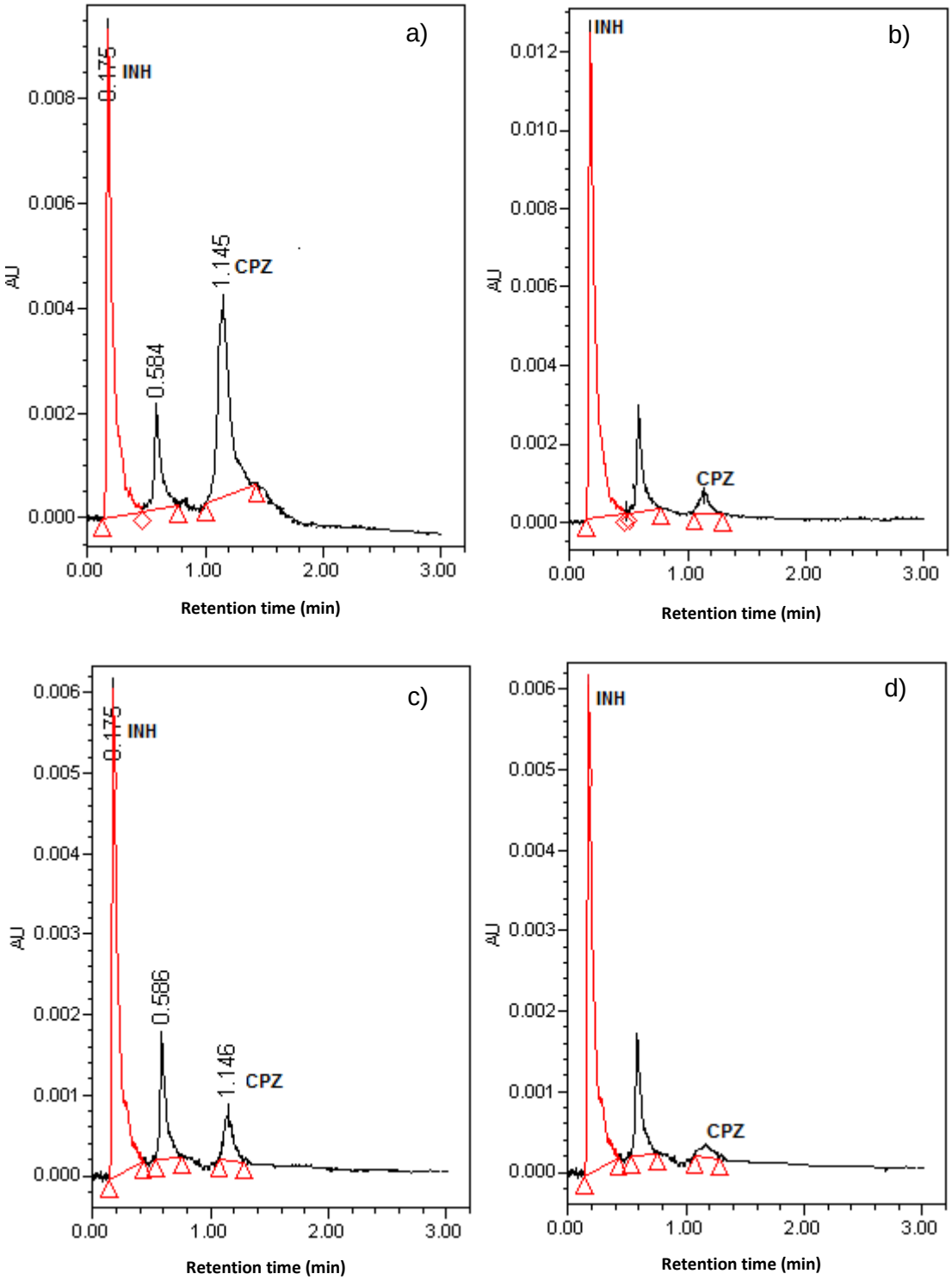

Figure 7.15: Typical chromatograms of CPZ and INH in a)-b) CSF and c)-d) plasma at 254nm.

7.4.9 Construction of calibration curves in CSF and plasma

The calibration curves for CPZ in CSF and plasma are portrayed in Figure 7.16 a) and b) respectively. The concentration of CPZ in CSF ranged from 0-20ng/mL and the concentration of CPZ in plasma ranged from 0-10ng/mL. The use of these curves are validated by their excellent linearity with R^2 of 0.994 and 0.985 for CPZ in CSF and plasma respectively.

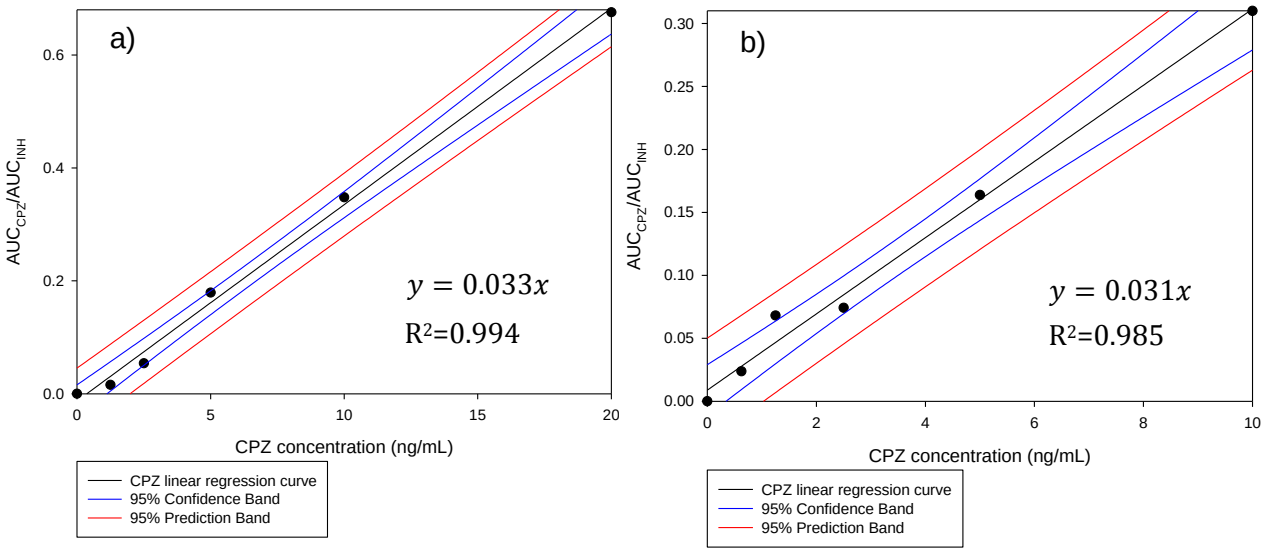

Figure 7.16: Calibration curve of CPZ in a) CSF and b) plasma at 254nm utilizing a UPLC PDA detector.

7.4.10 Determination of i*n vivo* CPZ release

The *in vivo* CPZ release profiles from the NPMD and the stat dose of the commercially available Chlorpromazine HCl-Fresenius®25mg/mL administered intramuscularly are displayed in Figure 7.17. It is noted that the NPMD and the stat dose of the commercially available Chlorpromazine HCl-Fresenius®25mg/mL display contrasting results. The release profiles from the NPMD displayed higher levels of CPZ in the CSF when compared to the commercially available Chlorpromazine HCl-Fresenius®25mg/mL injection which displayed higher CPZ levels in the plasma when compared to the CSF. Furthermore, the CPZ peak levels (C_{max}=2.92ng/mL) from the NPMD are reached after 7 days following implantation and thereafter, CPZ is released in a controlled manner. No irregular fluctuations of CPZ are noted from the NPMD which is highly desirable. A plasma C_{max} value of 0.95ng/mL was detected at Day 3 following implantation with the NPMD. The CPZ detected in the blood could possibly be attributed to the normal CSF flow and turnover, in which substances enter the venous blood flow via the arachnoid granulations (Grzybowski et al., 2006). This theory

is highly substantiated as the size of the nanoparticles which would make them much more susceptible to passing through the arachnoid granulations and into the systemic circulation.

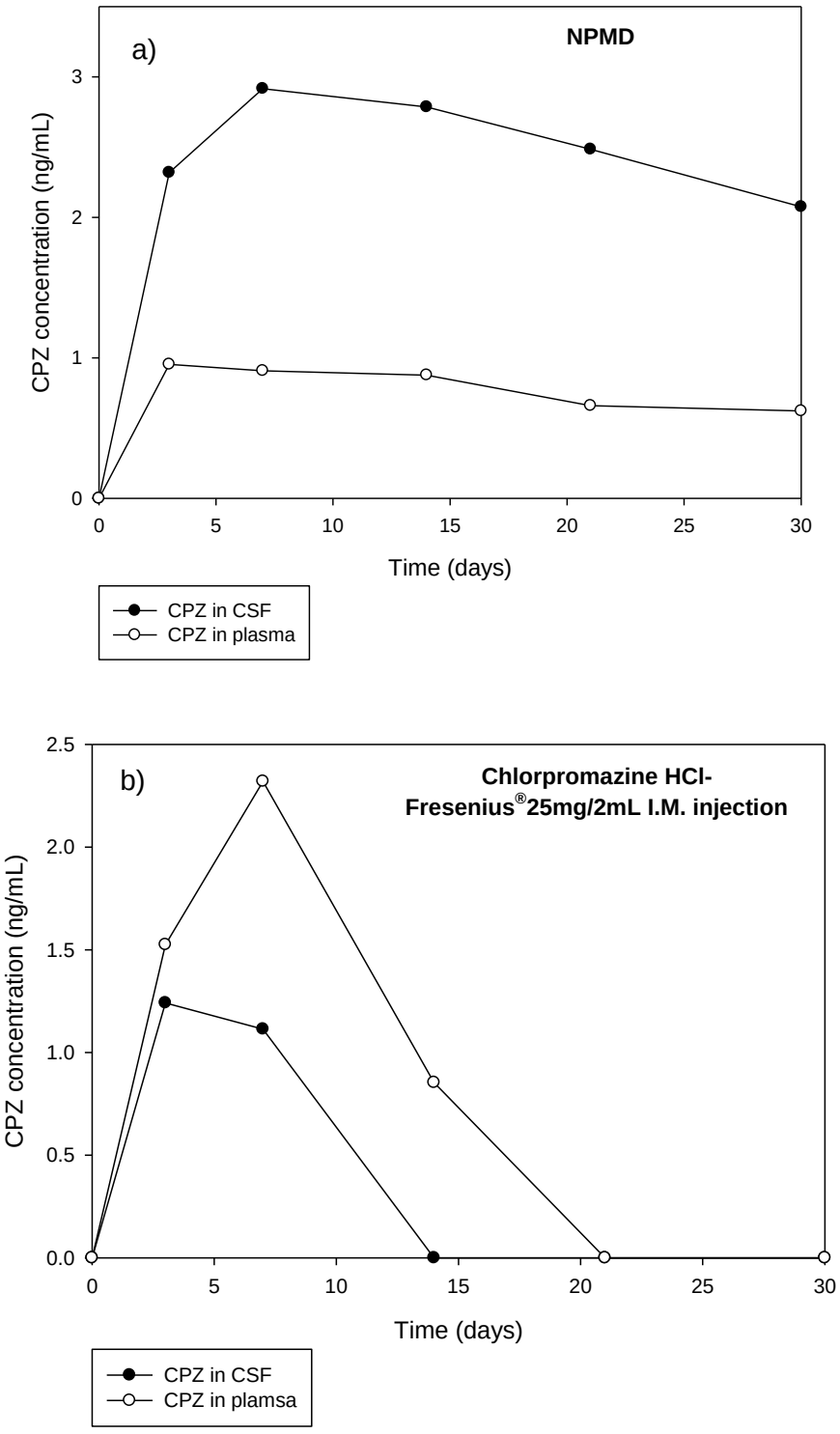

Figure 7.17: *In vivo* CPZ release from a) the NPMD and b) the commercially available Chlorpromazine HCl-Fresenius® 25mg/mL (SD≤0.31 in all cases).

The intramuscular dose of CPZ (Chlorpromazine HCl-Fresenius® 25mg/mL) revealed higher levels of CPZ in the blood plasma when compared to the CSF. This is due to the extremely low bioavailability of CPZ (approximately 20% plasma bioavailability due to high first-pass metabolism). A C_{max} value of 1.24ng/mL was computed in CSF after Day 3 following the intramuscular injection and a C_{max} value of 2.32 ng/mL was determined in plasma at Day 7 following intramuscular administration of the commercially available Chlorpromazine HCl-Fresenius® 25mg/mL injection. CPZ could only be detected in the blood plasma up until Day 14 and the CSF up until Day 7. These results are very atypical and surprising because CPZ in the tablet or injectable forms are dosed up to three times a day. A reason for the CPZ detection in the blood and CSF could possibly be due to the fact that the drug is highly protein bound and may attach itself to the surrounding fatty tissue (Okeri et al., 2008).

The CPZ release from the NPMD was far superior to the commercially available form of the drug. Implantation at the site of action allowed for a drastic increase in the CPZ bioavailability. Furthermore, the drug was released in a pseudo-steady state with CSF levels being maintained between 2.00-3.00ng/mL with no fluctuations observed. CPZ levels in the CSF and plasma attained from the commercially available Chlorpromazine HCl-Fresenius® 25mg/mL injection displayed a high degree of fluctuation in both CSF (1.11-1.24ng/mL) and plasma (0.85-2.32ng/mL). An area of concern is the fact that CPZ is being cleared into the blood. This could result in systemic side-effects. The fact that the visual assessment of the rabbits during the course of the study revealed that the rabbits experienced no visible signs of discomfort or abnormal behavior (including posture, movement) may suggest that the doses entering the systemic circulation are not significant enough to cause any side-effects.

7.5 Concluding Remarks

The *in vivo* pilot study on the New Zealand White Rabbit was highly successful. The study sought to assess the biocompatibility of the NPMD, its biodegradability and its ability to control the release of CPZ in a desirable manner when compared to commercially available products. All three areas of investigation yielded positive responses as the device was proven to degrade without toxicity and control the release of CPZ in the CNS compartment far superiorly than commercially available products. Furthermore, a rapid, non-arduous implantation procedure was perfected without resultant brain damage or motor dysfunction. In addition, a UPLC method for the quantification of CPZ in CSF and plasma was successfully developed. Although the investigation was a pilot study, novelties such as ultrasonic imaging for the NPMD visualization and a more effective means of CSF sampling (as opposed to euthanasia at every time point) were explored. The study served as a

stepping-stone for expanding the NPMD to larger animal models and possibly human trials. Near-future studies should focus on a full experimental study where more animals and data points are available for a more accurate representation of the results attained.

CHAPTER 8
CONCLUSIONS AND RECOMMENDATIONS

8.1 Conclusions

Psychosis continues to have detrimental socio-economic consequences and has been ranked as one of, if not, the most costly disorder to treat (Verma et al., 2012). Furthermore, the unceasing effects of on health, cognition, functionality and general quality of life are detrimental. In addition, the burden of care experienced by the care-givers is further amplified by the cost implications of caring for people with psychosis (Knapp, 1998).

In psychoses such as schizophrenia, ensuring that a patient does not relapse within the first few years has pivotal consequences in terms of life-long outcomes. In addition, long-term maintenance of antipsychotic use is critical for preventing relapse (Caseiro et al., 2012). The use of atypical antipsychotic drugs is common practice due to their better side-effect profile when compared to conventional or typical antipsychotics mainly, their lower occurrences of extrapyramidal side-effects and tardive dyskinesia. In addition, they are thought to improve negative symptoms of psychosis and do not increase prolactin drastically (Knapp, 1998; Glick et al., 2001).

These advantages are however associated with the extremely high cost of the drugs and despite these supposed advantages; studies have demonstrated that they may not be cost-effective when compared to conventional or typical antipsychotics. Davies and co-workers (2007) investigated the value of treatment and relative costs of conventional and atypical antipsychotics in patients suffering with schizophrenia and concluded that conventional antipsychotics were associated with lower costs and a great quality of life adjusted years (QALYs) when compared to newer atypical antipsychotics (Davies et a., 2007). Furthermore, a study by Peuskins and Link (1997) established that chlorpromazine hydrochloride (CPZ) and quetiapine were both effective in the treatment of positive and negative symptoms of schizophrenia, even though the efficacy of the latter was superior (Peuskins and Link, 1997).

This research was undertaken with the aim of developing a nano-enabled polymeric membranous device (NPMD) for intraparenchymal implantation into the frontal lobe of the brain for the long-term management of psychoses such as schizophrenia. The study is novel as it combines the benefits of nanobiotechnology with polymeric membrane technology to form a biodegradable, biocompatible implant that serves to address the key issue of non-

compliance with treatment regimens. Novel CPZ-loaded, polycaprolactone (PCL)-based nanoparticles were synthesized by a melt-dispersion technique and optimized using an experimental design with size, zeta potential and stability as formulation responses. The study exploited the thermoplastic nature of PCL and its relatively low melting point and was basically centered around the fact that once PCL was in its molten state, it was subjected to very high shearing, with CPZ being added to it. The high shearing and cooling to room temperature led to the formation of the nanoparticles.

CPZ was utilized as the model drug owing to a number of reasons. Firstly, the drug has a very low bioavailability (~20%) (Gibbon, 2008). This represents the plasma bioavailability and only a fraction of this will reach the brain. CPZ is considerably cheaper when compared to atypical antipsychotics. Studies suggest that its effectiveness is comparable to atypical antipsychotics and it has the potential to treat both positive and negative symptoms. Furthermore, CPZ is associated with numerous systemic side-effects that are hypothesized to be alleviated by site-specific drug delivery, nanotechnology, controlled release and reducing the dose and this is epitomized with the NPMD.

The actual implantable device matrix was a novel PA 6,10-EC composite membrane. PA 6,10 was synthesized based on previous studies and utilized due to its potential of extremely long drug release characteristics. The study used a modified wet-phase inversion reaction to synthesize the membranes where a solution of PA 6,10-EC was introduced to a non-solvent (water) after being placed in dialysis tubing. The previously optimized nanoparticles were dispersed within the optimized composite membrane to form the NPMD for implantation into the brain.

In the interim, another novel study investigated the possibility of entrapping essential fatty acids in the form of cod-liver oil (CLO) with the CPZ-loaded, PCL based nanoparticles to form dual-acting nano-liposhells. The rationale for incorporating CLO was due to its high levels of omega-3 fatty acids, DHA and EPA, which have been proven to be neuroprotective with proven benefits in conditions such as schizophrenia. The study confirmed the potential of combining conventional medicine with complementary and alternative medicines to optimize patient therapy.

After rigorous *in vitro* evaluation the NPMD and the novel CLO and CPZ-loaded, PCL-based nano-liposhells as well as their componential elements were subjected to an *ex vivo* cytotoxicity assay. PC12 neuronal cells were cultured and incubated with the analytes. The nano-liposhells were relatively toxic due to free radical formation of the CLO. The NPMD and its componential elements, however, were proven to be biocompatible and non-toxic.

The potential of the NPMD after extensive *in vitro* and *ex vivo* analysis was immense and led to its evaluation *in vivo* in the New Zealand White Rabbit model. The device was implanted intraparenchymally in the frontal lobe of the rabbit brain and the CPZ release was determined using UPLC. This was compared to a commercially available CPZ i.m. injection given to rabbits. The histomorphological effects as well as bioerosion of the NPMD were assessed post-implantation and the study confirmed the in vitro and ex vivo potential of the NPMD in the long-term management of psychoses.

Despite the common perception that brain surgery is high risk and low benefit and the skepticism that is associated with it (Prus and Grant, 2010), the implantation of the NPMD was a relatively short procedure (15 minutes) with preparation time being more extensive than the actual surgery itself. Furthermore, rabbits appeared to be in good general health post-surgery and exhibited no signs of motor deficit, brain damage or infection for the duration of the study, thus confirming the success of the procedure. Although CPZ was utilized as the drug of choice in this study, the system is not limited to CPZ and other water-soluble drugs can be utilized. This study creates a platform for expanding polymer-based, nano-enabled brain disease neurotherapy to other compounds.

It is a proof of concept investigation and despite being used for CNS disorders, minor adjustments to the polymeric combinations and drugs of choice can allow it to be used as rate-controlling implantable device for a variety of conditions that require long-term therapeutic management.

8.2 Recommendations

The following recommendations are noted:

A possible animal model for psychoses is recommended to ascertain the psychotropic effectiveness of the device.

Currently, there is no pharmacopoeia-endorsed method for dissolution studies in the brain hence simulation of conditions in the brain is very subjective.

The pilot *in vivo* study on the rabbit model needs to be expanded into a more extensive experimental study with a minimum of 5 animals (N=5) per group. This would result in more accurate data being gained as opposed to the pilot study where there a fewer animals.

The animal model needs to be larger (e.g. pigs or primates) as the larger animal would bear a closer resemblance to humans and allow for more accurate data analysis.

Further studies should involve attaching biomarkers to the drug so as to gain an understanding of the distribution dynamics of the drug within the brain. Alternatively, brain tissue should be broken down an analyzed for CPZ content to assess uptake.

The possibility of combining conventional medicine with complementary and alternative medicine does exhibit promise and needs to be further explored. Future work should focus optimizing these nano-liposhells using an experimental design. Variables such as the levels of CLO need to be considered as high levels of CLO result in saturation of the nanoparticle and adsorption of the CLO on the surface thus making it prone to oxidation and toxicity. Further research should center around inducing injury to the neuronal cells, followed by application of the nano-liposhells to assess the response.

Due to the stigma associated with neurosurgery, the device should also be investigated for alternative delivery modes such as subcutaneous or subdermal implantation. Minor adjustments to the surface characteristics of the nanoparticles can be made to ensure effective Blood-Brain Barrier (BBB) penetration, longer circulation times and the ability to go unnoticed by the body's immune system.

Future work should involve applying the NPMD to a human model. Before this is possible and extensive work is required to model and optimize the device for human application.

REFERENCES

1. Abadi A.H., Rafatullah S. and Al-Badr. Chlorpromazine, Analytical profiles of drug substances and excipients, **26**, (1999), 97-165.
2. Abbot N.J. Physiology of the blood–brain barrier and its consequences for drug transport to the brain, *International Congress Series,* **1277,** (2005), 3-18.
3. Adler L.E., Hoffer L.D., Wiser A. and Freedman R. Normalization of auditory physiology by cigarette smoking in schizophrenic patients, *American Journal of Psychiatry,***150**, (1993), 1856–1861.
4. Agrawal A.M., Manek R.V.,Kolling W.M.and Neau S.H. Studies on the interaction of water with ethylcellulose: effect of polymer particle size, *AAPS PharmSciTech*, **4** (4), 2003.
5. Altinyaka S.A. Modeling of asymmetric membrane formation by a combination of dry/wet phase inversion processes, *Desalination*, **199**, (2006), 459–460.
6. Altman G.H., Diaz F., Jakuba C., Calabro T., Horan RL., Chen J., Lu H., Richmond J., Kaplan D.L. Silk-based biomaterials, *Biomaterials,* **24**, (2003), 401–416.
7. Ambrose C.G., Clyburn T.A., Louden K., Joseph J., Wright J., Gulati P., Gogola G.R. and Mikos A.G. Effective treatment of osteomyelitis with biodegradable microspheres in a rabbit model, *Clinical Orthopaedics and Related Research*, **421**, (2004), 293-299.
8. Amsterdam J.D. A double-blind, placebo-controlled trial of the safety and efficacy of selegiline transdermal system without dietary restrictions in patients with major depressive disorder, *Journal of Clinical Psychiatry*, **64**, (2003), 208-214.
9. Antinori A, Cingolani A, Giancola ML, Forbici F, De Luca A, Perno CF. Clinical implications of HIV-1 drug resistance in the neurological compartment, *Scandinavian Journal of Infectious Diseases. Supplementum,* **106**, (2003), 41–44.
10. Aoi M., Date I., Tomita S. and Ohmoto T. The effect of intrastriatal single injection of GDNF on the nigrostriatal dopaminergic system in hemiparkinsonian rats: Behavioral and histological studies using two different dosages, *Neuroscience Research,* **36** (4), (2000), 319–325.
11. Arnold L.E., Lindsay R.L., Lopez F.A., Jacob S.E., Biederman J., Findling R.L. and Ramadan Y. Treating attention-deficit/hyperactivity disorder with a stimulant transdermal patch: the clinical art, *Pediatrics*, **120** (5), (2007), 1100-1106.
12. Aroon M.A., Ismail A.F., Montazer-Rahmati M.M. and Matsuura T. Morphology and permeation properties of polysulfone membranes for gas separation: Effects of non-

solvent additives and co-solvent, *Separation and Purification Technology*, **72**, (2010), 194–202.

13. Arulmozhi D.K., Dwyer D.S. and Bodhankar S.L. Antipsychotic induced metabolic abnormalities: An interaction study with various PPAR modulators in mice*, Life Sciences*, **79** (19), (2006), 1865-1872.
14. Aulton M.E. Pharmaceutics, The science of dosage form design, 2nd edition, 2002, Churchill Livingstone, Edinburgh.
15. Balfour D.J.K. and Fagerström K.O. Pharmacology of nicotine and its therapeutic use in smoking cessation and neurodegenerative disorders, *Pharmacology & Therapeutics*, **72** (1), (1996), 51-81.
16. Banks W.A. Characteristics of compounds that cross the blood-brain barrier. *BioMedCentral Neurology*, **9** (1), (2009), S3.
17. Begley D.J. Delivery of therapeutic agents to the central nervous system: the problems and the possibilities. *Pharmacology and Therapeutics,* **104**, (2004), 29–45.
18. Benvegnú D.M., Barcelos R.C.S., Boufleur N., Reckziegel P., Pase C.S., Ourique A.F., Beck R.C.R. and Bürger M.E. Haloperidol-loaded polysorbate-coated polymeric nanocapsules increase its efficacy in the antipsychotic treatment in rats, *European Journal of Pharmaceutics and Biopharmaceutics*, **77**, (2011), 332–336.
19. Bernkopf M. Sterilisation of bioresorbable polymer implants, *Medical Device Technology*, **18** (3), (2007).
20. Bodor N. and Buchwald P. Brain-targeted drug delivery: Experiences to date, *American Journal of Drug Delivery*, **1** (1), (2003), 13-26.
21. Boison D. Adenosine Augmentation Therapies (AATs) for epilepsy: prospect of cell and gene therapies. *Epilepsy Research,* **85 (**2-3), (2009), 131–141.
22. Boison D. Cell and gene therapies for refractory epilepsy. *Current Neuropharmacology,* **5,** (2007), 115–125.
23. Boison D., Scheurer L., Tseng J.L., Aebischer P., Mohler H. Seizure suppression in kindled rats by intraventricular grafting of an adenosine releasing synthetic polymer. *Experimental Neurology,* **160,** (1999), 164–174.
24. Brem H., Kader A., Epstein J.I., Tamargo R.J., Domb A., Langer R., Leong K.W. Biocompatibility of a biodegradable controlled-release polymer in the rabbit brain, *Selective Cancer Therapeutics*, **5** (2), (1989), 55-65.
25. Brem H., Piantadosi S., Burger P.C., Walker M., Selker R., Vick N.A., Black K., Sisti M., Brem S., Mohr G., Muller P., Morawetz R. and Schold S.C. Placebo-controlled trial of safety and efficacy of intraoperative controlled delivery by biodegradable polymers of chemotherapy for recurrent gliomas, *Lancet*, **345**, (1995), 1008–1012.

26. Bruck S.D. and Mueller E.P. Radiation sterilization of polymeric implant materials, *Journal of Biomedical Material Research*, **22**, (1988), 133-144.
27. Bryan J. Crossing the blood-brain barrier: Drug delivery to the brain is still elusive, *The Pharmaceutical Journal*, **273**, (2004), 475-476.
28. Burt M.M. and Ley F.J. Studies on the dose requirement for the radiation sterilizationof medical equipment. I. Influence of suspending media, *Journal of Applied Bacteriology*, **26**(3), (1963), 484-489.
29. Caseiro O., Pérez-Iglesias R., Mata I., Martínez-Garcia O., Pelayo-Terán J.M., Tabares-Seisdedos R. , de la Foz V., Vázquez-Barquero J.L. and Crespo-Facorro B. Predicting relapse after a first episode of non-affective psychosis: A three-year follow-up study, *Journal of Psychiatric Research*, **46**, (2012), 1099-1105.
30. Chan Young Park C.Y., Park J.W and Lee J.J. Development of totally implantable pulsatile biventricular assist device. *Artificial Organs,* **27** (1), (2003), 119–123.
31. Chawla J.S. and Amiji M.M. Biodegradable poly(o-caprolactone) nanoparticles for tumortargeted delivery of tamoxifen, *International Journal of Pharmaceutics*, **249**, (2002), 127-138.
32. Chen W., He J., Olson J.J. and Lu D.R. Carboplatin-loaded PLGA microspheres for intracerebral implantation: *In vivo* characterization, *Drug Delivery*, **4** (4), (1997), 301-311.
33. Chen Y., Wang R., Zhou J., Fan H. and Shi B. On-demand drug delivery from temperature-responsive polyurethane membrane, *Reactive and Functional Polymers*, **71** (4), (2011), 525-535.
34. Cheng H., Fraidakis M., Blomback B., Lapchak P., Hoffer B. and Olson L. Characterization of a fibrin glue-GDNF slow-release preparation, *Cell Transplant*, **7** (1), (1998), 53–61.
35. Cheng Y.H., Illum L. and Davis S.S. Schizophrenia and drug delivery systems, *Journal of Drug Targeting*, **8** (2), (2000), pages 1075–117.
36. Choi-Lundberg D.L., Lin Q., Chang Y.N., Chiang Y.L., Hay C., Mohajeri H., Davidson B.L. and Bohn M.C. Dopaminergic neurons protected from degeneration by GDNF gene therapy, *Science*, **275** (5301), (1997), 838–41.
37. Choonara Y.E., Pillay V., Carmichael T.R., Meyer L.C.R., du Toit L.C., Naylor S. and Wanblad C. *In vivo* evaluation of a biodegradable donut-shaped minitablet for prolonged posterior segment drug delivery in the rabbit eye model, *Journal of Pharmaceutical Sciences*, **100**, (2011), 1819–1832.
38. Chopda G. Transdermal drug delivery systems: A review, *Latest Reviews*, **4** (1), (2006).

39. Claas F.H.J. Drug-induced agranulocytosis: review of possible mechanisms and prospects for clozapine studies, *Psychopharmacology*, **99**, (1989), 113-117.
40. Cohen C., Tanny G.B. and Prager S. Diffusion-controlled formation of porous structures in ternary polymer systems, *Journal of Polymer Science*, **17**, (1979), 477.
41. Cole S.L. and Vassar R. The basic biology of BACE1: A key therapeutic target for Alzheimer's disease, *Current Genomics,* **8,**(2007), 509-529.
42. Conners C.K., Levin E.D., Sparrow E., Hinton S.C., Erhardt D., Meck W.H. *et al.* Nicotine and attention in adult ADHD, *Psychopharmacology Bulletin,* **32**, (1996), 67–73.
43. Cudmore S. Elan drug delivery: Delivery across the blood-brain barrier, *The Irish Scientist*, 2002.
44. Cunnane S., Nugent S., Roy M., Courchesne-Loyer A et al. Brain fuel metabolism, aging, and Alzheimer's disease, *Nutrition,* (2010). doi:10.1016/j.nut.2010.07.021.
45. Cysique L.A.J., Maruff P., Darby D. and Brew B.J. The assessment of cognitive function in advanced HIV-1 infection and AIDS Dementia Complex using a new computerised cognitive test battery, *Archives of Clinical Neuropsychology*, **21**, (2006), 185-194.
46. Dali M.M., Moench P.A., Mathias N.R., Stetsko P.I., Heran C.L. and Smith R.L. A rabbit model for sublingual drug delivery: comparison with human pharmacokinetic studies of propranolol, verapamil and captopril, *Journal of Pharmaceutical Sciences,* **95** (1), (2006), 37-44.
47. Davies L.M., Lewis S., Jones P.B., Barnes T.R.E., Gaughran F., Hayhurst K., Markwick A. Lloyd H. Cost-effectiveness of first- *v.* second-generation antipsychotic drugs: results from a randomised controlled trial in schizophrenia responding poorly to previous therapy, *British Journal of Psychiatry*, **191**, (2007), 14-22.
48. de Candia F., Maglio G., Palumbo R. and Sirletti M. Synthesis and physical behaviour of polyamide 6,10-poly(butadiene-co-acrylonitrile) segmented block copolymers, *Journal of Colloid and Polymer Science*, **267**, (1989), 9-15.
49. Decina P., Caracci G., Sandik R., Berman W., Mukherjee S. and Scapicchio P. Cigarette smoking and neuroleptic-induced Parkinsonism, *Biological Psychiatry,* **28**, (1990), 502–508.
50. Decker T. and Lohmann-Matthes, M.L. A quick and simple method for the quantitation of lactate dehydrogenase release in measurements of cellular cytotoxicity and tumor necrosis factor (TNF) activity, *Journal of Immunological Methods*, **115**, (1988), 61–69.
51. Domb A.J. Polymeric carriers for regional drug therapy, *Molecular Medicine Today,* **1**, (1995), 134–139.

52. Domb A.J., Rock M., Perkint C., Yipchuck G., Broxup B. and Villemure J.G. Excretion of a radiolabel led anticancer biodegradable polymeric implant from the rabbit brain, *Biomaterials,* **16**, (1995), 1069-1072.
53. Domb A.J., Rock M., Schwartz J., Perkint C., Yipchuck G., Broxup B. and Villemure J.G. Metabolic disposition and elimination studies of a radiolabel led biodegradable polymeric implant in the rat brain, *Biomaterials*, **15** (9), (1994), 681-688.
54. During M.J., Freese A., Sabel B.A., Saltzman W.M., Deutch A., Roth R.H. and Langer R. Controlled release of dopamine from a polymeric brain implant: *in vivo* characterization, *Annals of Neurology*, **25**, (1989), 351-356.
55. E. Horisawa, T. Hirota, S. Kawazoe et al. Prolonged anti-inflammatory action of DL-lactide/glycolide copolymer nanospheres containing betamethasone sodium phosphate for an intra-articular delivery system in antigen-induced arthritic rabbit, *Pharmaceutical Research*, **19** (4), (2002), 403–410.
56. Ellis P.M. Clozapine: Fatal 'constipation' more common than fatal agranulocytosis, *New Zealand Medicine and Medical Devices Safety Authority*, **28** (1), (2007), 7.
57. Elzein T.,Nasser-Eddine M., Delaite C., Bistac S. and Dumas P. FTIR study of polycaprolactone chain organization at interfaces, *Journal of Colloid and Interface Science*, **273**, (2004), 381–387.
58. Ewing G.W., What is regressive autism and why does it occur? Is it the consequence of multi-systemic dysfunction affecting the elimination of heavy metals and the ability to regulate neural temperature? *North American Journal of Medical Sciences,* **(1)** 2, (2009), 28-47.
59. Fehm H.L., Perras B., Smolnik R., Kern W. and Born J. Manipulating neuropeptidergic pathways in humans: A novel approach to neuropharmacology. *European Journal of Pharmacology*, **405,** (2000), 43–54.
60. Ferber D. Bridging the blood-brain barrier: New methods improve the odds of getting drugs to the brain cells that need them, *PLOS Biology*, **5** (6), (2007).
61. Franke L. and Porstmann T. A highly sensitive non-radioactive cytotoxicity assay for human target cells, *Journal of Immunological Methods*, **171,** (1994) 259-262.
62. Freeman M.P. Omega-3 fatty acids in psychiatry: A review, *Annals of Clinical Psychiatry*, **12** (3), (2000), 159–65.
63. Freese A., Sabel B.A., Saltzman W.M., During M.J. and Langer R. Controlled release of dopamine from a polymeric brain implant: *In vitro* characterization, *Experimental Neurology*, **103**, (1989), 234-238.
64. Frey W.H., Interview, Reuters Health, 16th February (2001).

65. Frith C. Neuropsychology of schizophrenia: What are the implications of intellectual and experimental abnormalities for the neurobiology of schizophrenia? *British Medical Bulletin,* **52**, (1996), 618-626.
66. Frumkin L. Promising Treatments for AIDS Dementia Complex: Highlights of neurological research from the VIII International Conference on AIDS, Amsterdam, July 19-24, 1992, *Seattle Treatment Education Project: STEP Perspective*, **4** (3), (1992).
67. Fujioka K. and Shibamoto T. Formation of genotoxic dicarbonyl compounds in dietary oils upon oxidation, *Lipids*, **39** (5), (2004), 481-486.
68. Gadoth N. On fish oil and omega-3 supplementation in children: The role of such supplementation on attention and cognitive dysfunction. *Brain and Development*, **30**, (2008) 309–312.
69. Gavini E., Manunta L, Giua S., Achenza G., and Giunchedi P. Spray-dried poly(D,L-Lactide) microspheres containing carboplatin for veterinary use: *In vitro* and *in vivo* studies. *AAPS PharmSciTech,* **6** (1), (2005), 108-114.
70. Gelperina S. Nanoparticulate Drug Delivery Systems for the Non-Invasive Chemotherapy of Brain Tumors, *NSTI Nanotechnology Conference and Trade Show*, 2006.
71. Gharabawi G.M., Gearhart N.C., Lasser R.A., Mahmoud R.A., Zhu Y., Mannaert E., Naessens I., Bossie C.A., Kujawa M. and Simpson G.M. Maintenance therapy with once-monthly administration of long-acting injectable risperidone in patients with schizophrenia or schizoaffective disorder: a pilot study of an extended dosing interval, *Annals of General Psychiatry*, **6** (3), (2007).
72. Gibbon C.J. South African Medicines Formulary, 8th edition, 2008, Health and Medical publishing Group of the South African Medical Association, Cape Town.
73. Glick I.D., Murray S.R., Vasudevan P., Marder S.R. and Hu R.J. Treatment with atypical antipsychotics: New indications and new populations, *Journal of Psychiatric Research*, **35** (3), (2001), 187-191.
74. Glycerol material and safety data sheet, Santa Cruz Biotechnology, Inc.,http://datasheets.scbt.com/sc-29095.pdf, [Accessed March 22, 2010].
75. Gorell, J.M., Rybicki, B.A., Johnson, C.C., Peterson, E.L. Smoking and Parkinson's disease: a dose–response relationship. *Neurology*, **52**, (1999), 115–119.
76. Grossman, S.A., Leong, K.W., Lesser, G.J. and Lo, H. Subcutaneous implant. *US Patent 6126956. http://www.patentstorm.us/patents/6126956.html* [Accessed November, 2010].

77. Grzybowski D.M.,Holman D.W., Katz S.E.and Lubow M.*In vitro* model of cerebrospinal fluid outflow through human arachnoid granulations, *Investigative Ophthalmology & Visual Science*, **47** (8), (2006), 3664-3672.
78. Guerin C., Olivi A., Weingart J.D., Lawson H.C. and Brem H. Recent advances in brain tumor therapy: Local intracerebral drug delivery by polymers, *Investigational New Drugs*, **22**, (2004), 27-37.
79. Guo-yu P, Xiao-Dong L, Guo-Quing L. intracarotid infusion of hypertonic mannitol changes permeability of blood-brain barrier to methotrexate in rats, *Acta Pharmacologica Sinica*, **21** (7), (2000), 613-616.
80. Gutwinski S., Müller P. and Koller M. Intervals between hospitalisations in schizophrenia patients under antipsychotics in depot-form versus oral second generation antipsychotics, *Psychiatrische Praxis*, **34** (6), (2007), 289-291.
81. Haik K.L, Shear D.A., Schroeder U, Sabel B.A., Dunbar G.L, Quinolinic acid released from polymeric brain implants causes behavioral and neuroanatomical alterations in a rodent model of Huntington's disease*, Experimental Neurology*, **163**, (2000), 430–439.
82. Harilall S. Formulation and evaluation of an implantable polymeric configuration for application in AIDS Dementia Complex. A dissertation submitted to the Faculty of Health Sciences, University of the Witwatersrand, in fulfillment of the requirements for the degree of Master of Pharmacy, 2011.
83. Haugh M.G., Murphy C.M. and O'Brien F.J. Novel freeze-drying methods to produce a range of collagen-glycosaminoglycan scaffolds with tailored mean pore sizes, *Tissue Engineering*, **16** (5), (2010), 887-894.
84. Heinzelmann K. and Franke K. Using freezing and drying techniques of emulsions for the microencapsulation of fish oil to improve oxidation stability, *Colloids and Surfaces B: Biointerfaces,* **12**, (1999), 223–229.
85. Henningfield J.E., Fant R.V., Buchhalter A.R. and Stitzer M.L. Pharmacotherapy for nicotine dependence, *A Cancer Journal for Clinicians,* **45** (5), (2005), 281-299.
86. Hoane M.R., Gulwadi A.G., Morrison S., Hovanesian G., Lindner M.D. and Tao W. Differential *in vivo* effects of neurturin and glial cell-line-derived neurotrophic factor, *Experimental Neurology*, **160** (1), (1999), 235–43.
87. Hoare T., Santamaria J., Goya G.F., Irusta S., Lin D., Lau S., Padera R., Langer R. and Kohane D.S. A magnetically triggered composite membrane for on-demand drug delivery, *Nanoletters*, **9** (10), (2009), 3651-3657.
88. Hoffman D., Wahlberg L., Aebischer P. NGF released from a polymer matrix prevents loss of ChAT expression in basal forebrain neurons following a fimbria-fornix lesion. *Experimental Neurology,* **110,** (1990), 39–44.

89. Horan R.L, Antle K., Collette A.L., Wang Y., Huang J., Moreau J.E., Volloch V., Kaplan D.L., Altman G.H. *In vitro* degradation of silk fibroin. *Biomaterials,* **26,** (2005), 3385–3393.
90. Horvath S. Cytotoxicity of drugs and diverse chemical agents to cell cultures. *Toxicology*, **16**, (1980), 59 -66
91. Howard M.A., Gross A., Grady M.S., Langer R.S., Mathiowitz E., Winn R. and Mayberg M.R. Intracerebral drug delivery in rats with lesion-induced memory detitits, *Journal of Neurosurgery*, **71**, (1989), 105-112.
92. Hsu D, Chen C, Hsu M, and Beggs JM. An open hypothesis: Is epilepsy learned, and can it be unlearned? *Epilepsy and Behavior,* **13** (3), (2008), 511–522.
93. Hu F.B., Stampfer M.J., Manson J.E., Rimm E., Colditz G.A., Rosner B.A., et al. Dietary fat intake and the risk of coronary heart disease in women, *New England Journal of Medicine*, **337**, (1997), 1491–1499.
94. Hynynen K. Macromolecular delivery across the Blood–Brain Barrier, *Methods in Molecular Biology*. **480**, (2009), 175-185.
95. Illum l. Transport of drugs from the nasal cavity to the central nervous system, *European Journal of Pharmaceutical Sciences*, **11**, (2000), 1–18.
96. Innis S.M. Dietary omega 3 fatty acids and the developing brain, *Brain Research*, **1237**, (2008), 35–43.
97. Iyer S.S., Barr W.H., Dance M.E., Coleman P.R. and Karnes H.T. A 'biorelevant' system to investigate *in vitro* drug released from a naltrexone implant, *International Journal of Pharmaceutics*, **340**, (2007), 104-118.
98. Jackson C. and Ofoefule S. Use of xanthan gum and ethylcellulose in formulation of metronidazole for colon delivery, *Journal of Chemical and Pharmaceutical Research*, **3** (2), (2011), 11-20.
99. Jain D., Carvalho E. and Banerjee R. Biodegradable hybrid polymeric membranes for ocular drug delivery, *Acta Biomaterialia*, **6**, (2010), 1370–1379.
100. Jain J.P., Modi S., Domb A.J. and Kumar N. Role of polyanhydrides as localized drug carriers, *Journal of Controlled Release*, **103**, (2005), 541-563.
101. Jayprakar M., Ramnar J. and Shah S. An overview on brain targeting drug delivery system, *Latest Reviews*, **7** (1), (2009).
102. Jeon Y., Kwak K., Kim S., Kim Y., Lim J and Baek W. Intrathecal implants of microencapsulated xenogenic chromaffin cells provide a long-term source of analgesic substances, *Transplantation Proceedings,* **38** (9), (2006), 3061-3065.
103. Jin H.J., Kaplan D.L. Mechanism of silk processing in insects and spiders. *Nature,* **424,** (2003), 1057–1061.

104. Jollivet C., Aubert-Pouessel A., Clavreul A., Venier-Julienne M., Remy S., Montero-Menei C.N., Benoit J. and Menei P. Striatal implantation of GDNF releasing biodegradable microspheres promotes recovery of motor function in a partial model of Parkinson's disease, *Biomaterials*, **25**, (2004), 933–942.
105. Jones G.M.M., Sahakian B.J., Levy, R., Warburton, D.M. and Gray, J.A. Effects of acute subcutaneous nicotine on attention, information processing and short-term memory in Alzheimer's disease. *Psychopharmacology,* **108**, (1992), 485–494.
106. Kandanearatchi A, Williams B, Everall IP. Assessing the efficacy of highly active antiretroviral therapy in the brain, *Brain Pathology,* **13,** (2003), 104–110.
107. Kane J.M. Schizophrenia, *The New England Journal of Medicine*, **334**, (1996), 34-42.
108. Kane J.M., Aguglia E., Altamura A.C., Gutierrez J.L.A., Brunello N., Fleischhacker W.W., Gaebel W., Gerlach J., Guelfi J.D., Kissling W., Lapierre Y.D., Lindström E., Mendlewicz J., Racagni G., Carulla L.S. and Schooler N.R. Guidelines for depot antipsychotic treatment in schizophrenia, *European Neuropsychopharmacology*, **8** (1), (1998), 55-66.
109. Kato H., Mizuno K., Shimada M., Nakamura A., Takahashi K., Hata K. and Kinugasa S. Observations of bound Tween 80 surfactant molecules on single-walled carbon nanotubes in an aqueous solution, *Carbon*, **47**, (2009), 3434–3440.
110. Khan Y., Durrani S.K.,Mehmooda M., Ahmada J, Khan M.R. and Firdous S. Low temperature synthesis of fluorescent ZnO nanoparticles, *Applied Surface Science*, **257**, (2010), 1756–1761.
111. Kim D.M., Tien R., Byrum C., Krishnan K.R.R. Imaging in Acquired Immunodeficiency Syndrome Dementia Complex (AIDS Dementia Complex): A review, *Progress in Neuro-Psychopharmacology & Biological Psychiatry*, **20**, (1996), 349-370.
112. Knapp M.R.J. Measuring the economic benefit of treatment with atypical antipsychotics, *European Psychiatry*, **13**, (1998), 37-47.
113. Kokaia M., Aebischer P., Elmér E., Bengzon J., Kalèn P., Kokaia Z. and Lindvall O. Seizure suppression in kindling epilepsy by intracerebral implants of GABA-but not by noradrenaline-releasing polymer matrices, *Experimental Brain Research*, **100**, (1994), 385–394.
114. Kolowale O.A., Pillay V. and Choonara Y.E. Novel polyamide 6,10 variants synthesized by modified interfacial polymerization for application as a rate-modulated monolithic drug delivery system, *Journal of Bioactive and Compatible Polymers*, **22**, (2007), 281-313.

115. Koo YL, Reddy GR, Bhojani M, Schneider R, Philbert MA, Rehemtulla A, Ross BD, Kopelman R. Brain cancer diagnosis and therapy with nanoplatforms, *Advanced Drug Delivery Reviews*, **58** (14), (2006), 1556-1577.
116. Koziara JM, Lockman PR, Allen DD, Mumper RJ. The blood-brain barrier and brain drug delivery, *Journal of Nanoscience and Nanotechnology*, **6**, (2006).
117. Krauze M.T., Forsayeth J., Park J.W., Bankiewicz K.S. Real-time imaging and quantification of brain delivery of liposomes, *Pharmaceutical Research*, **23** (11), (2006), 2493-2504.
118. Kubek M.J., Liang D., Byrd K.E. and Domb A.J. Prolonged seizure suppression by a single implantable polymeric-TRH microdisk preparation, *Brain Research*, **809**, (1998), 189 –197.
119. Kumari A., Yadav S.K. and Yadav S.C. Biodegradable polymeric nanoparticles based drug delivery systems, *Colloids and Surfaces B: Biointerfaces*, **75**, (2010), 1–18.
120. Kwan *P. and* Brodie M.J*.* Refractory epilepsy: mechanisms and solutions*, Expert Review of Neurotherapeutics*, **6** (3), (2006), 397-406.
121. Lai H.L., Pitt K. and Craig D.Q. Characterisation of the thermal properties of ethylcellulose using differential scanning and quasi-isothermal calorimetric approaches, *International Journal of Pharmaceutics*, **386** (1-2), (2010), 178-184.
122. Lai J., Lin F., Wang C. and Wang D. Effect of nonsolvent additives on the porosity and morphology of asymmetric TPX membranes, *Journal of Membrane Science*, **118**, (1996) 49-61.
123. Landgraf W., Li N.H., Benson J.R., New polymer enables near zero order release of drugs, *Drug Delivery Technology*, **5** (2), (2005), 48-55.
124. Lappalainen K., Jaaskelainen I., Syrjanen K., Urtti A. and Syrjanen S. Comparison of cell proliferation and toxicity assays using two cationic liposomes. *Pharmaceutical Research*, **11**, (1994) 1127–1131.
125. Lee J.S., An T.K., Chae G.S., Jeong J.K., Cho S.H., Lee H.B. and Khang G. Evaluation of *in vitro* and *in vivo* antitumor activity of BCNU-loaded PLGA wafer against 9L gliosarcoma, *European Journal of Pharmaceutics and Biopharmaceutics*, **59**, (2005), 169-175.
126. Lensing R., Bleich A., Smoczek A., Glage S., Ehlert N., Luessenhop T., Behrens P., Müller P.P., Kietzmann M. and Stieve M. Efficacy of nanoporous silica coatings on middle ear prostheses as a delivery system for antibiotics: An animal study in rabbits, *Acta Biomaterialia,* (2012), [doi:http://dx.doi.org/10.1016/j.actbio.2012.08.016].
127. Levin E.D. and Simon B.B. Nicotinic acetylcholine involvement in cognitive function in animals, *Psychopharmacology,* **138**, (1998), 217–230.

128. Levin, E.D. Nicotine systems and cognitive function. *Psychopharmacology,* **108**, (1992), 418–431.
129. Li C., Vepari C., Jin H.J., Kim H.J., Kaplan D.L. Electrospun silk-BMP-2 scaffolds for bone tissue engineering. *Biomaterials,* **27,** (2006), 3115–3124.
130. Li Y., Owusu A., and Lehnert S. Treatment of intracranial rat glioma model with implant of radiosensitizer and biomodulator drug combined with external beam radiotherapy, *International Journal of Radiation Oncology* Biology* Physics*, **58** (2), (2004), 519-527.
131. Lieberman J.A. Metabolic changes associated with antipsychotic use, *Journal of Clinical Psychiatry*, **6** (2), (2004), 8–13.
132. Lieberman J.A., Stroup T.S., McEvoy J.P., Swartz M.S., Rosenheck R.A., Perkins D.O., Keefe R.S.E., Davis S.M., Davis C.E., Lebowitz B.D., Severe J. and Hsiao J.K. Effectiveness of antipsychotic drugs in patients with chronic schizophrenia, *The New England Journal of Medicine*, **353**, (2005), 1209-1223.
133. Lincoln T.M., Lüllmann E. and Rief W. Correlates and long-term consequences of poor insight in patients with schizophrenia. A systematic review, *Schizophrenia Bulletin*, **33** (6), (2007), 1324-1342.
134. Lindner M.D., Francis J.M. and Saydoff J.A. Intrathecal polymer-encapsulated bovine adrenal chromaffin cells fail to produce analgesic effects in the hotplate and formalin test, *Experimental Neurology*, **165**, (2000), 370–383.
135. Lopez T., Ortiz E., Quintana P. and Gonzalez R.D. A nanostructured titania bioceramic implantable device capable of drug delivery to the temporal lobe of the brain, *Colloids and Surfaces A: Physicochemical and Engineering Aspects,* **300**, (2007), 3–10.
136. Lopez T., Quintana P., Ascencio J. and Gonzalez R.D. The determination of dielectric constants of mixtures used in the treatment of epilepsy and the encapsulation of phenytoin in a titania matrix, *Colloids and Surfaces A: Physicochemical and Engineering Aspects,* **300**, (2007), 99 –105.
137. Loscher W., Gernert M., Heinemann U. Cell and gene therapies in epilepsy - promising avenues or blind alleys? *Trends in Neurosciences,* **31,** (2008), 62–73.
138. Lukiw W.J., Cui J.G., Marcheselli V.L., Bodker M., Botkjaer A. and Gotlinger K. A role for docosahexaenoic acid-derived neuroprotectin D1 in neural cell survival and Alzheimer disease. *Journal of Clinical Investigation*, **115** (10), (2005), 2774–83.
139. Mak M., Fung L., Strasser J.F. and Saltzman W.M. Distribution of drugs following controlled delivery to the brain interstitium, *Journal of Neuro-Oncology*, **26**, (1995), 91-10.

140. Manjunath K. and Venkateswarlu V. Pharmacokinetics, tissue distribution and bioavailability of clozapine solid lipid nanoparticles after intravenous and intraduodenal administration, *Journal of Controlled Release*, **107**, (2005), 215–228.
141. Mapara M., Thomas B.S. and Bhat K.M. Rabbit as an animal model for experimental research, *Journal of Dental Research*, **9** (1), (2012), 111-118.
142. Mayberg M., Langer R., Zervas N. and Moskowitz M. Perivascular meningeal projections from cat trigeminal ganglia: possible pathway for vascular headaches in man, *Science*, **2** (13), (1981), 228-230.
143. Mazza M., Pomponi M., Janiri L., Bria P. and Mazza S. Omega-3 fatty acids and antioxidants in neurological and psychiatric diseases: An overview, *Progress in Neuro-Psychopharmacology and Biological Psychiatry,* **31**, (2007), 12–26.
144. McCauley M. and Connolly G. Evidence for use of depot neuroleptic medication, *Irish Journal of Psychological Medicine*, **21** (3), (2004), 95-99.
145. McNamaraa R.K. and Carlson S.E. Role of omega-3 fatty acids in brain development and function: Potential implications for the pathogenesis and prevention of psychopathology, *Prostaglandins, Leukotrienes and Essential Fatty Acids*, **75**, (2006), 329–349.
146. Menei P., Jadaud E., Faisant N., Boisdron-Celle M., Michalak S., Fournier D., Delhaye M. and Benoit J.P. Stereotaxic implantation of 5-fluorouracil-releasing microspheres in malignant glioma, *Cancer*, **100** (2), (2004), 405-410.
147. Menei P., Pean J.M., Nerrie`re-Daguin V., Jollivet C., Brachet P. and Benoit J.P. Intracerebral implantation of NGF-releasing biodegradable microspheres protects striatum against excitotoxic damage, *Experimental Neurology,* **161**, (2000), 259-272.
148. Menei P., Venier M.C., Gamelin E., Saint-Andr´e J.P., Hayek G., Jadaud E., Fournier D., Mercier P., Guy G. and Benoit J.P. Local and sustained delivery of 5-fluorouracil from biodegradable microspheres for the radiosensitization of glioblastoma, Cancer, **86** (2), (1999), 325-330.
149. Midhun B.T., Shalumon K.T., Manzoor K., Jayakumar R., Nair S.V. and Deepthy M. Preparation of budesonide-loaded polycaprolactone nanobeads by electrospraying for controlled drug release, *Journal of Biomaterials Science*, **22** (18), 2431-2444.
150. Misra A., Ganesh S., Shahiwala A. and Shah S.P. Drug delivery to the central nervous system: A review, *Journal of Pharmacy and Pharmaceutical Sciences*, **6** (2), (2003), 252-273.
151. Mohanraj V.J. and Chen Y. Nanoparticles – A review, *Tropical Journal of Pharmaceutical Research*, **5** (1), (2006), 561-573.
152. Montoya I.D. and Vocci F. Novel medications to treat addictive disorders, *Current Psychiatry Reports,* **10**, (2008), 392– 398.

153. Muthu M.S., Rawat M.K., Mishra A. and Singh S. PLGA nanoparticle formulations of risperidone: preparation and neuropharmacological evaluation, *Nanomedicine: Nanotechnology, Biology, and Medicine*, **5**, (2009), 323–333.
154. Naik A., Kalia Y.N. and Guy R.H. Transdermal drug delivery: Overcoming the skin's barrier function, *Pharmaceutical Science & Technology Today*, **3** (9), (2000), 318-326.
155. Nakao N., Yokote H., Nakai K. and Itakura T. Promotion of survival and regeneration of nigral dopamine neurons in a rat model of Parkinson's disease after implantation of embryonal carcinomaderived neurons genetically engineered to produce glial cell line-derived neurotrophic factor, *Journal of Neurosurgery*, **92** (4), (2000), 659–70.
156. Nelson T.J., Alkon D.L. and Quattrone, A., Artificial low-density lipoprotein carriers for transport of substances across the blood-brain barrier U S Patent 7803400. *http://www.freepatentsonline.com/7803400.html (2010)* [Accessed November 19, 2010].
157. Niles A.L., Moravec R.A. and Riss T.L. Update on *in vitro* cytotoxicity assays for drug development, *Expert Opinion on Drug Discovery*, **3**(6), (2008), 655-669.
158. Okeri H.A., Alonge P.O. and Etareri E. Comparitive determination of chlorpromazine hydrochloride content in multi-sourced chlorpromazine tablets in Nigeria, *International Journal of Health Research*, **1** (1), (2008), 21-26.
159. Olivi A., Ewend M.G, Utsuki T., Tyler B., Domb A.J, Brat D.J, Brem H., Interstitial delivery of carboplatin via biodegradable polymers is effective against experimental glioma in the rat*, Cancer Chemotherapy and Pharmacology*, **39** (1-2), (1996), 90-96.
160. Ouellet M., Emond V., Chen C.T., Julien C., Bourasset F., Oddo S., LaFerla F., Bazinet R.P. and Calon F. Diffusion of docosahexaenoic and eicosapentaenoic acids through the blood–brain barrier: An *in situ* cerebral perfusion study, *Neurochemistry International*, **55**, (2009), 476–482.
161. Pardridge W.M. Drug delivery to the brain, *Journal of Cerebral Blood Flow and Metabolism*, **17**, (1997), 713–731.
162. Pardridge W.M. The Blood-Brain Barrier: Bottleneck in brain drug development, *NeuroRX Research*, **2** (1), (2005), 3-14.
163. Pardridge W.M., Why is the global CNS pharmaceutical market so underpenetrated? *Drug Discovery Today,* **7**, (2002), 5–7.
164. Park C.Y., Park J.W. and Lee J.J. Development of totally implantable pulsatile biventricular assist device. *Artificial Organs,* **27** (1), (2003), 119–123.
165. Park S. and Sinko P.J., P-Glycoprotein and mutlidrug resistance-associated proteins limit the brain uptake of saquinavir in mice, *The Journal of Pharmacology and Experimental Therapeutics,* **312** (3), (2005), 1249-1256.

166. Patel T.B. Recent trends in brain targeted drug delivery systems: An overview, *Latest Reviews*, **5** (2), (2007).
167. Paulev P.E. Textbook in medical physiology and pathophysiology, essentials and clinical problems, 2nd edition, Chapter 3, Copenhagen medical publishers, 1999-2000.
168. Pèan J.M., Menei P., Morel O., Montero-Menei C.M. and Benoit J.P. Intraseptal implantation of NGF-releasing microspheres promote the survival of axotomized cholinergic neurons, *Biomaterials*, **21**, (2000), 2097-2101.
169. Perras B., Marshall L., Kohler G., Born J.and Fehm H.L. Sleep and endocrine changes after intranasal administration of growth hormone-releasing hormone in young and aged humans, *Psychoneuroendocrinology*, **24,** (1999), 743–757.
170. Perras B., Pannenborg H., Marchall L., Pietrowsky R., Born J. and Fehm H.L. Beneficial treatment of age-related sleep disturbances with prolonged intranasal vasopressin. *Journal of Clinical* Psychopharmacology, **19**, (1999), 28–36.
171. Peuskins J. and Link C.G. A comparison of quetiapine and chlorpromazine in the treatment of schizophrenia, *Acta Psychiatric Scandinavica*, **96** (4), (1997), 265-73.
172. Pfeiffer PN, Ganoczy D, Valenstein M. Dosing frequency and adherence to antipsychotic medications, *Psychiatric Services*, **59**, (2008), 1207-1210.
173. Pillay S., Design and development of an implantable drug delivery polymeric scaffold for the treatment of Parkinson's disease. A dissertation submitted to the Faculty of Health Sciences, University of the Witwatersrand, in fulfillment of the requirements for the degree of Master of Pharmacy, 2009.
174. Pillay S., Pillay V., Choonara Y.E., Naidoo D., Khan R.A., du Toit L.C., Ndesendo V.M.K., Modi G., Danckwerts M.P. and Iyuke S.E. Design, biometric simulation and optimization of a nano-enabled scaffold device for enhanced delivery of dopamine to the brain. *International Journal of Pharmaceutics*, **382**, (2009), 277–290.
175. Pillay V. and Fassihi R. *In vitro* release modulation from crosslinked pellets for site-specific drug delivery to the gastrointestinal tract: I. Comparison of pH-responsive drug release and associated kinetics, *Journal of Controlled Release*, **59,** (1999), 229-242.
176. Portegies P., de Gans J., Lange J., Derix M., Speelman H., Bakker M., Danner S. and Goudsmit J. Declining incidence of AIDS dementia complex after introduction of zidovudine treatment, *British Medical Journal*, **299**, (1989), 819-821.
177. Powell E.M., Sobarzo M.R. and Saltzman W.M. Controlled release of nerve growth factor from a polymeric implant, *Brain Research,* **515**, (1990), 309-311.
178. Pranzatelli M.R. Innovations in drug delivery to the central nervous system, Drugs Today, **35** (6), (1999), 435.

179. Prus N. and Grant A.C. Patient beliefs about epilepsy and brain surgery in a multi-cultural urban population, *Epilepsy and Behavior*, **17** (1), (2010), 1-11.
180. Quay S.C. Successful delivery of apomorphine to the brain following intranasal administration demonstrated in clinical study. *PRNewswire*, July 18th (2001).
181. Quik, M. Smoking, nicotine and Parkinson's disease. *Trends in Neurosciences,* **27** (9), (2004), 561–568.
182. RabinC., Liang Y., Ehrlichman R.S., Budhian A., Metzger K.L., Majewski-Tiedeken C., Winey K.I. and Siegel S.J. In vitro and *in vivo* demonstration of risperidone implants in mice, *Schizophrenia Research*, **98** (1-3), (2008), 67-78.
183. Raedt R., Van Dycke A., Vonck K., Boon P. Cell therapy in models for temporal lobe epilepsy, *Seizure-European Journal of Epilepsy,* **16,** (2007), 565–578.
184. Raghavan R., Brady M.L., Rodríguez-Ponce M.I., Hartlep A., Pedain C., Sampson. Convection-enhanced delivery of therapeutics for brain disease, and its optimization, *Neurosurgical Focus*, **20** (4), (2006), E12.
185. Ranganath S.H. and Wang C., Biodegradable microfiber implants delivering paclitaxel for post-surgical chemotherapy against malignant glioma, *Biomaterials*, **29**, (2008), 2996–3003.
186. Ranganath S.H., Fu Y., Arifin D.Y. Kee I.,Zheng L., Lee H., Chow P.K.H., Wang C. The use of submicron/nanoscale PLGA implants to deliver paclitaxel with enhanced pharmacokinetics and therapeutic efficacy in intracranial glioblastoma in mice. *Biomaterials,* **31,** (2010), 5199-5207.
187. Rao M.S, Hattiangady B., Shetty A.K. Fetal hippocampal CA3 cell grafts enriched with FGF-2 and BDNF exhibit robust long-term survival and integration and suppress aberrant mossy fiber sprouting in the injured middle-aged hippocampus, *Neurobiology of Disease,* **21,** (2006), 276–290.
188. Rapoport S.I. and Thompson H.K. Osmotic opening of the blood-brain barrier in the monkey without associated neurological deficits, *Science (New York, N.Y.)*, **180** (89), (1973), 971.
189. Rapoport S.I. *In vivo* fatty acid incorporation into brain phospholipids in relation to plasma availability, signal, transduction and membrane remodelling, *Journal of Molecular Neuroscience*, **16**, (2001), 243–62.
190. Reece A.S. Comparative treatment and mortality correlates and adverse event profile of implant naltrexone and sublingual buprenorphine, *Journal of Substance Abuse Treatment*, (2009).
191. Reiber H. Proteins in cerebrospinal fluid and blood: Barriers, CSF flow rate and source-related dynamics, *Restorative Neurology and Neuroscience*, **21**, (2003), 79-96.

192. Reinhard C.S., Radomsky M.L., Saltzman W.M., Hilton J. and Brem H. Polymeric controlled release of dexamethasone in normal rat brain, *Journal of Controlled Release*, **16**, (1991), 33l-340.
193. Reis C.P., Neufeld R.J., Ribeiro A.J. and Veiga F. Nanoencapsulation I. Methods for preparation of drug-loaded polymeric nanoparticles, *Nanomedicine: Nanotechnology, Biology, and Medicine*, **2**, (2006), 8– 21.
194. Rezvani A.H. and Levin E.D. Nicotine mechanisms in Alzheimer's disease, Cognitive effects of nicotine, *Biological Psychiatry*, **49** (3), (2001), 258-267.
195. Rohman A. and Che Man Y.B. Application of Fourier Transform Infrared (FT-IR) spectroscopy combined with chemometrics for authentication of cod-liver oil, *Vibrational Spectroscopy*, **55**, (2011), 141-145.
196. Rohman A., Sunarminingsih R. and Che Man Y.B. The employment of FTIR spectroscopy and chemometrics for classification and quantification of mutton fat in cod-liver oil, *American Journal of Food Technology*, **7** (3), (2012), 151-159.
197. Rosenblad C., Martinez-Serrano A. and Bjorklund A. Intrastriatal glial cell line-derived neurotrophic factor promotes sprouting of spared nigrostriatal dopaminergic afferents and induces recovery of function in a rat model of Parkinson's disease, *Neuroscience*, **82** (1) , (1998), 129–37.
198. Roullin V.G., Mege M., Lemaire L., Cueyssac J.P., Venier-Julienne M.C., Menei P., Gamelin E. and Benoit J.P. Influence of 5-fluorouracil–loaded microsphere formulation on efficient rat glioma radiosensitization, *Pharmaceutical Research*, **21** (9), (2004), 1558-1563.
199. Ruckmani K. and Sankar V. Formulation and optimization of zidovudine niosomes, *AAPS PharmSciTech*, **11** (3), 2010.
200. Rusted, J.M., Newhouse, P.A., Levin, E.D. Nicotinic treatment for degenerative neuropsychiatric disorders such as Alzheimer's disease and Parkinson's disease, *Behavioural Brain Research*, **113** (1–2), (2000), 121–129.
201. S. Kailasam, D. Daneluzzi, P. R. J. Gangadharam. Maintenance of therapeutically active levels of isoniazid for prolonged periods, *Tubercule and Lung Disease*, **75**, (1994), 361-365.
202. Sahakian B.J. and Jones G.M.M.The effects of nicotine on attention, information processing, and working memory in patients with dementia of the Alzheimer type. In: Adlkofer F, Thruau K, editors, *Effects of Nicotine on Biological Systems.* Basel, Switzerland: Birkhauser Verlag, (1991), 623–230.
203. Sahoo S.K., Jain T.K., Reddy M.K. and Labhasetwar V. Nano-sized carriers for drug delivery, *NanoBioTechnology*, (2008), 329-348.

204. Sakellariou P., Rowe R.C. and White E.F.T. The thermomechanical properties and glass transition temperature of some cellulose derivatives used in film coatings, *International Journal of Pharmaceutics*, **27**, (1985), 267-277.
205. Saltzman W.M., Mak M.W., Mahoney M.J., Duenas E.T., Cleland J.L. Intracranial delivery of recombinant nerve growth factor: release kinetics and protein distribution for three delivery systems. *Pharmaceutical Research,* **16,** (1999), 232–240.
206. Sanberg P.R., Emerich D.F., Aebischer P., Amisetti S.M., Ouellette W., Koutouzis T.K., Cahill D.W., Norman A.B. Substance P containing polymer implants protect against striatal excitotoxicity. *Brain Research,* **628,** (1993), 327–329.
207. Saraon T.S., Gill-Saraon N., Miller A.C. and Sinert, R.H., 2010.Pacemakers and implantable cardioverter defibrillators. http://emedicine.medscape.com/article/780825-overview, [Accessed November 21, 2010].
208. Scherrmann J.M. Drug delivery to brain via the blood–brain barrier, *Vascular Pharmacology*, **38**, (2002), 349-354.
209. Schlegelmilch T. Henke K. and Peri F. Microglia in the developing brain: From immunity to behaviour, *Current Opinion Neurobiology*, **21,** (2010), 1–6.
210. Seju U., Kumar A. and Sawant K.K. Development and evaluation of olanzapine-loaded PLGA nanoparticles for nose-to-brain delivery: *In vitro* and *in vivo* studies, *Acta Biomaterialia*, **7**, (2011), 4169–4176.
211. Shah S. Transdermal drug delivery technology revisited: Recent advances, *Latest Reviews*, **6** (5), (2008).
212. Shahiwala A. and Misra A. Pulmonary absorption of liposomal levonorgestrel, *AAPS PharmSciTech*, (2004).
213. Shetty A.K. and Hattiangady B. Concise review: Prospects of stem cell therapy for temporal lobe epilepsy. *Stem Cells,* **25,** (2007), 2396–2407.
214. Sibeko B., Pillay V., Choonara Y.E., Khan R.A., Modi G., Iyuke S.E., Naidoo D. and Danckwerts M.P. Computational molecular modeling and structural rationalization for the design of a drug-loaded PLLA/PVA biopolymeric membrane, *Biomedical Materials*, **4**, (2009), 1-11.
215. Siegel S.J., Winey K.I., Gur R.E., Lenox R.H., Bilker W.B., Ikeda D., Gandhi N. and Zhang W. Surgically implantable long-term antipsychotic delivery systems for the treatment of schizophrenia, *Neuropsychopharmacology*, **26**, (2002), 817-823.
216. Silva A.C., González-Mirac E., Garcíac M.L., Egeac M.A., Fonsecaa J., Silva R., Santos D., Souto E.B., Ferreira D. Preparation, characterization and biocompatibility studies on risperidone-loaded Solid Lipid Nanoparticles (SLN): High pressure

homogenization versus ultrasound, *Colloids and Surfaces B: Biointerfaces*, **86**, (2011), 158–165.

217. Silva G.A. Nanotechnology approaches for drug and small molecule deliveryacross the blood brain barrier, *Surgical Neurology*, **67**, (2007) 113–116.
218. Singh N., Pillay V. and Choonara Y.E. Advances in the treatment of Parkinson's disease, *Progress in Neurobiology*, **81**, (2007), 29–44.
219. Sinha V.R., Bansal K., Kaushik R., Kumria R. and Trehan A. Poly- ε-caprolactone microspheres and nanospheres: an overview, *International Journal of Pharmaceutics*, **278**, (2004), 1–23.
220. Sittl R., Griessinger N. and Likar R. Analgesic efficacy and tolerability of transdermal buprenorphine in patients with inadequately controlled chronic pain related to cancer and other disorders: A multicenter, randomized, double-blind, placebo-controlled trial, *Clinical Therapeutics*, (2002), 150-168.
221. Soppimath K.S., Aminabhavi T.M., Kulkarni A.R., Rudzinski W.E., Biodegradable polymeric nanoparticles as drug delivery devices , *Journal of Controlled Release*, **70**, 1-20, 2001.
222. Stefanie Wohlfart S., Gelperina S. and Kreuter J. Transport of drugs across the blood–brain barrier by nanoparticles, *Journal of Controlled Release*, (2011) (Article in press).
223. Sugibayashi K. and Morimoto Y. Polymers for transdermal drug delivery systems, *Journal of Controlled Release*, **29** (1-2), (1994), 177-185.
224. Suter D.M. and Krause K.H. Neural commitment of embryonic stem cells: molecules, pathways and potential for cell therapy, *Journal of Pathology,* **215,** (2008), 355–368.
225. Tamargo R.J., Rossell L.A., Kossoff E.H., Tyler B.M., Ewend M.G. and Aryanpur J.J. The intracerebral administration of phenytoin using controlled-release polymers reduces experimental seizures in rats, *Epilepsy Research*, **48**, (2002), 145–155.
226. Tamilvanan S., Venkateshan N and Ludwig A. The potential of lipid- and polymer-based drug delivery carriers for eradicating biofilm consortia on device-related nosocomial infections. *Journal of Controlled Release*, **128,** (2008), 2–22.
227. The British Pain Society 2008. Intrathecal drug delivery for the management of pain and spasticity in adults; recommendations for best clinical practice.
228. The guidelines for collection of blood from experimental animals, *Research Animal Resources, University of Minnesota.* http://www.ahc.umn.edu/rar/blood.html [Accessed October 31, 2011].
229. Tiwari SB, Amiji MM. A review of nanocarrier-based CNS delivery systems, *Current Drug Delivery*, **3** (2), (2006), 219-32.

230. Tomac A., Lindqvist E., Lin L.F., Ogren S.O., Young D., Hoffer B.J. and Olson L. Protection and repair of the nigrostriatal dopaminergic system by GDNF *in vivo*, *Nature*, **373** (6512), (1995), 335–339.
231. Tornqvist N., Bjorklund L., Almqvist P., Wahlberg L. and Stromberg I. Implantation of bioactive growth factor-secreting rods enhances fetal dopaminergic graft survival, outgrowth density, and functional recovery in a rat model of Parkinson's disease, *Experimental Neurology*, **164** (1), (2000), 130–8.
232. Ugwoke M.I., Exaud S., Van Den Mooter G., Verbeke N. and Kinget R. Bioavailability of apomorphine following intranasal administration of mucoadhesive drug delivery systems in rabbits, *European Journal of Pharmaceutical Sciences,* **9**, (1999), 213–219.
233. Unger E.C., Porter T., Culp W., Labell R., Matsunaga T. and Zutshi R. Therapeutic applications of lipid-coated microbubbles, *Advanced Drug Delivery Reviews*, **56** (9), (2004), 1291-1314.
234. Unsicker K. Growth factors in Parkinson's disease, *Progress in Growth Factor Research*, **5** (1), (1994), 73–87.
235. Upadrashta S.M., Katikaneni P.R., Hileman G.A., Neau S.H. and Rowlings C.E. Compressibility and compactibility properties of ethylcellulose, *International Journal of Pharmaceutics,***112**, (1994), 173-179.
236. Venho V.M.K. and Erikkson H. The rabbit: an animal model for comparative bioavailability studies of drugs, *International Journal of Pharmaceutics*, **30**, (1986), 91-94).
237. Verma S., Poon L.Y., Subramaniam M., Abdin E. and Chong S.A. The Singapore Early Psychosis Intervention Programme (EPIP): A programme evaluation, *Asian Journal of Psychiatry*, **5** (1), (2012), 63-67.
238. Veterinary formulary, *Research Animal Resources, University of Minnesota*. http://www.ahc.umn.edu/rar/umnuser/formulary.html#Chlorpromazine, [Accessed October 31, 2011].
239. Wahlberg L.U., Almqvist P.M., Glantz M.J. and Boethius J. Polymeric controlled-release amsacrine chemotherapy in an experimental glioma model, *Acta Neurochirurgica,* **138,** (1996), 1323-1330.
240. Wang P.P., Frazier J. and Brem H. Local drug delivery to the brain, *Advanced Drug Delivery Reviews*, **54**, (2002), 987–1013.
241. Wei X.W., Gong C.Y., Gou M.L., Fu S.Z., Guo Q.F., Shi S., Luo F., Guo G., Qiu L.Y. and Qian Z.Y. Biodegradable poly(ε-caprolactone)–poly(ethylene glycol) copolymers as drug delivery system, *International Journal of Pharmaceutics*, **381,** (2009), 1–18.

242. Weyermanna J., Lochmanna D. and Zimmer A. A practical note on the use of cytotoxicity assays, *International Journal of Pharmaceutics*, **288**, (2005) 369–376.
243. White J., Bell J., Saunders J.B., Williamson P., Makowska M., Farquharson A. and Beebe K.L. Open-label dose-finding trial of buprenorphine implants (Probuphine)® fortreatment of heroin dependence, *Drug and Alcohol Dependence*, **103**, (2009), 37-43.
244. White, H.K. and Levin, E.D. Four week nicotine skin patch treatment effects on cognitive performance in Alzheimer's disease, *Psychopharmacology,* **143**, (1999), 158–165.
245. Wilson, A.L., Langley, L.K., Monley, J., Bauer, T., Rottunda, S., Mcfalls, E. *et al.* Nicotine patches in Alzheimer's disease: Pilot study on learning,memory, and safety, *Pharmacology Biochemistry and Behavior,* **51**, (1995), 509–514.
246. Wilz A., Pritchard E.M., Li T., Lan J.Q., Kaplan D.L., Boison D. Silk polymer-based adenosine release: Therapeutic potential for epilepsy. *Biomaterials,* **29,** (2008), 3609–3616.
247. Wu C. Analysis of Mechanical, thermal, and morphological behavior of polycaprolactone/wood flour blends, *Journal of Applied Polymer Science*, **94**, (2004), 1000–1006.
248. Yamaguchi M, Nagashima T, Kinoshita I, Tsukamoto Y. Opening of blood-brain barrier by infusion of hypertonic mannitol solution did not disturb the active avoidance of learning rats, *Bulletin of Allied Medical Sciences*, **6**, (1990), 177-181.
249. Yang H., Irudayaraj J. and Paradkar M.M. Discriminant analysis of edible oils and fats by FTIR, FT-NIR and FT-Raman spectroscopy, *Food Chemistry*, **93**, (2005), 25-32.
250. Yuen A.W.C., Sander J.W., Fluegel D. and Patsalos P.N. Omega-3 fatty acid supplementation in patients with chronic epilepsy: a randomized trial, *Epilepsy Behaviour*, **7**, (2005), 253–258.
251. Zhang L., Deng X. and Huang Z. Miscibility, thermal behavior and morphological structure of poly(3-hydroxybutyrate) and ethylcellulose binary blends, *Polymers*, **38** (21), (1997), 5379-5387.
252. Zhao Q., Tao J., Yamc R.C.M., Mokc A.C.K., Li R.K.Y. and Song C. Biodegradation behavior of polycaprolactone/rice husk ecocomposites in simulated soil medium, *Polymer Degradation and Stability*, **93**, (2008), 1571–1576.
253. Zhong Y. and Bellamkonda R.V. Biomaterials for the central nervous system, *Journal of the Royal Society Interface*, **5** (26), (2008), 957–975.
254. Zhou B. Simulations of polymeric membrane formation in 2D and 3D. A thesis submitted to the Department of Material Sciences and Engineering in partial

fulfillment of the degree of Doctor of Philosophy, Massachusetts Institute of Technology, 2006.

Appendix A1

In: Advances in Materials Science Research. Volume 10 ISBN 978-1-61324-511-8
Editor: Maryann C. Wythers, pp. 83-120

Chapter 2

POLYMERIC INTRACORPOREAL DEVICES FOR THE MANAGEMENT OF NEUROLOGICAL DISORDERS

Viness Pillay[1,*], Thiresen Govender[1], Yahya E. Choonara[1], Valence M.K. Ndesendo[1], Lisa C. du Toit[1], Girish Modi[2], and Dinesh Naidoo[3]

[1] University of the Witwatersrand, Department of Pharmacy and Pharmacology, 7 York Road, Parktown, 2193, Johannesburg, South Africa
[2] University of the Witwatersrand, School of Neurosciences, Department of Neurology, 7 York Road, Parktown, 2193, Johannesburg, South Africa
[3] University of the Witwatersrand, School of Neurosciences, Department of Neurosurgery, 7 York Road, Parktown, 2193, Johannesburg, South Africa

Abstract

The complexity of the brain and the membranous blood-brain barrier (BBB) has proved to be a significant limitation to the systemic delivery of pharmaceuticals to the brain rendering them sub-therapeutic and ineffective in the treatment of neurological diseases. Apart from this, lack of innovation in product development to counteract the problem is also a major contributing factor to a poor therapeutic outcome. Various innovative strategies show potential in treating some of the neurological disorders; however drug delivery remains the most popular. To attain therapeutic drug levels in the central nervous system (CNS), large, intolerable systemic doses are generally administered. The success of maintenance therapy in many neurological diseases depends on a number of variables, including the constant release of neurotherapeutics, a reduction in the dosing frequency, a greater antipsychotic drug bioavailability and ultimately improved patient compliance, many of which is not achievable by conventional oral or parenteral formulations. This article reviews the therapeutic implantable polymeric and transdermal devices employed in an attempt to effectively achieve therapeutic quantities of drug across the BBB over a prolonged period, to improve patient disease prognosis.

* Email address: viness.pillay@wits.ac.za

centrations (>80% of total loadings) of bacteriophages were rapidly delivered (over 2 hours) across Silescol® *in vitro*.

CONCLUSIONS

In this work, a mechanically robust and phage compatible polymeric microneedle formulation has been developed to deliver a model bacteriophage *in vitro*. We are currently investigating delivery of bacteriophages *in vivo* using this optimised microneedle formulation.

REFERENCES

[1] J.H. Park, M.G. Allen, M. R. Prausnitz, "Polymer Microneedles for Controlled-Release Drug Delivery" *Journal of phatrmaceutical research*, **23** (2006) 1008–1019

[2] A. Sulakvelidze, Z. Alavidze, J. Glenn Morris Jr. "Bacteriophage Therapy" *Antimicrobial agents and chemotherapy*, 45 (2001) 649–659

[3] M.H. Adams. "Bacteriophages" in Bacteriophages: Methods and protocols. Humana Press, New York. publisher, 2009 ch7 pp 69–76

A polyamide-based membranous device for specialised drug delivery

T. Govender[1], V. Pillay[1*], Y.E. Choonara[1], L.C. du Toit[1], G. Modi[2], D. Naidoo[3]

[1]University of the Witwatersrand, Dept. of Pharmacy and Pharmacology, 7 York Road, Parktown, Johannesburg, 2193
[2]University of the Witwatersrand, Dept. of Neurosciences, Division of Neurology, 7 York Road, Parktown, Johannesburg, 2193
[3]University of the Witwatersrand, Dept. of Neurosciences, Division of Neurosurgery, 7 York Road, Parktown, Johannesburg, 2193
*Correspondence: viness.pillay@wits.ac.za

INTRODUCTION

This study is aimed at investigating the design and development of a novel polyamide-based polymeric membrane for implantable drug delivery.

MATERIALS AND METHODS

1) *Preparation of polymeric membranes:* Polymeric membranes were prepared by a precipitation reaction. Novel polyamide 6,10 (PA 6,10) synthesised by modified interfacial polymerisation reaction [1], was firstly dissolved in formic acid. The solution was placed under magnetic stirring at 3000rpm and the temperature was raised to 65°C until all PA 6,10 dissolved. Another solution comprising ethylcellulose (EC) dissolved in acetone was prepared. The PA 6,10-formic acid solution was then added to the EC-acetone solution while under magnetic stirring. Stirring continued until the formation of a homogenous solution. The solution was left to stir for approximately an hour and upon completion of stirring, double de-ionised water was added to the solution. This resulted in the formation of a white gel-like precipitate at the interface. The precipitate was collected by filtration with a Buchner apparatus with the continuous addition of double de-ionised water. Following filtration, the precipitate was collected, appropriately moulded and left to dry under a fume hood for 24 hours. Resultant membranes were round, regular and exhibited surface porosity.
2) *FTIR Spectrophotometric Analysis:* Fourier transform infrared (FTIR) spectroscopy was undertaken on the resultant membranes to assess any structural variations in the polymeric membranous device, as a result of any interactions in the formulation.
3) *Morphological characterisation of polymeric membrane:* Surface morphology was characterised by Scanning Electron Microscopy (SEM). Photomicrographs were taken at different magnifications and samples were prepared after sputter-coating with gold. Morphological characterisation of the membranes revealed the shape, surface morphology and structure of the device.
4) *Textural profile analysis:* Textural analysis was used to determine the physicomechanical properties of the membranes in terms of their Brinell Hardness and deformation energy. This was compared to Brinell Hardness values obtained from a PA 6,10-EC disc, compressed with a Carver Hydraulic Press.

RESULTS AND DISCUSSION

Structural characterisation was performed on the PA 6,10, EC and the PA 6,10-EC membrane synthesised by precipitation reaction. Results confirmed the presence and integrity of a combination of both PA 6,10 and EC functional groups in the membranes produced by precipitation reaction. This thus confirmed the formation of a novel PA 6,10-EC membranous device. SEM images of the novel polymeric membrane at varying magnifications confirmed that membranes were irregular and highly porous. Textural profiling confirmed the integrity of the synthesised membranous matrices with BHN values ranging from 2.42–2.54 N/mm^2. BHN values of the compressed PA 6,10-EC discs ranged from 3.09–4.01 N/mm^2. The lower BHN values of the PA 6,10-EC membranes are indicative of a device that is non-crystalline and potentially more favourable for implantation.

Appendix A3

Novel Approaches to Antipsychotic Drug Delivery: Design, Development and Optimization of Chlorpromazine Containing Polycaprolactone Nanoparticles by a Novel Melt Dispersion Technique

Thiresen Govender[1], Viness Pillay*[1], Yahya E. Choonara[1], Lisa C. du Toit[1], Girish Modi[2] and Dinesh Naidoo[3]

1. *University of the Witwatersrand, Department of Pharmacy and Pharmacology, 7 York Road, Parktown, 2193, Johannesburg, South Africa*
2. *University of the Witwatersrand, School of Neurosciences, Department of Neurology, 7 York Road, Parktown, 2193, Johannesburg, South Africa*
3. *University of the Witwatersrand, School of Neurosciences, Department of Neurosurgery, 7 York Road, Parktown, 2193, Johannesburg, South Africa*

*Corresponding author:
Email: viness.pillay@wits.ac.za
Tel: +27-11-717-2274
Fax: +27-11-642-4355
Fax2Email: +27-86-553-4733

Abstract

The systemic delivery of antipsychotic drugs generally results in minimal transport of these agents across the highly restrictive blood-brain barrier (BBB) and subsequently results in therapeutic failure. Nanotechnology provides many promising solutions to impediments arising from conventional neurotherapy. Popular methods for the design and development of nanoparticles include; the solvent evaporation method, spontaneous emulsification/solvent diffusion method, salting out/emulsification-diffusion method, supercritical fluid technology, ionic gelation and polymerization of monomers. Most of these methods have proved unsatisfactory and are related to a variety of shortcomings. The aim of this study was to design, synthesize and optimize Chlorpromazine hydrochloride (CPZ)-loaded, Poly-ε-caprolactone (PCL) based nanoparticles using a melt-dispersion technique that is non-arduous, inexpensive and devoid of any hazardous organic solvents. A central composite design was used to determine the direct additive effects of the study variables on the physicochemical and physicomechanical properties and interactive effects on PCL nanoparticle formulation. Experimental trials were performed on 13 statistically derived formulations of various combinations of polymers and stabilizers. PCL (1000-3000mg) and Polysorbate 80 (2-5%v/v) were selected as the independent formulation variables. Differential scanning calorimetry (DSC), Temperature modulated differential scanning calorimetry (TMDSC) and Fourier transform infrared spectroscopy (FTIR) revealed that there was no thermodegardation of the constituents utilized in the melt dispersion technique. Nanoparticle yields achieved were very high however entrapment of CPZ proved to be relatively low due to the highly hydrophilic nature of CPZ and the processing of the nanoparticles post synthesis. Particle sizes were in the nanotherapeutic range and varied from 132.7±6.8nm-566.6±5.5nm. Zeta potential ranged from -15.1±0.65mV-28.8±0.84mV revealing particles that were of incipient to moderate stability. Transmission electron microscopy revealed nanoparticles that were spherical shape, well individualized with a moderate degree of flocculation. *In vitro* CPZ release was biphasic for all formulations with an initial burst release followed by pseudo-steady controlled release over 30 days. Response optimization was performed using statistical software (Minitab ®, V14, Minitab Inc®, PA, USA) and an optimized CPZ-loaded, PCL based nanoparticle formulation was synthesized. Extensive *in vitro* testing and optimization supports the application for the use and feasibility of the CPZ-loaded, PCL based nanoparticles for the long-term management of certain psychotropic disorders where the benefits of nanotechnology can be exploited.

Keywords: antipsychotic, blood-brain barrier, therapeutic failure, nanotechnology, neurotherapy, chlorpromazine hydrochloride, poly-ε-caprolactone, polysorbate 80, melt-dispersion technique, central composite design

Appendix A4

An Intracranial Nano-Enabled Polymeric Membranous Device for the Site-Specific Delivery of Chlorpromazine Hydrochloride

Thiresen Govender[1], Yahya E. Choonara[1], Lisa C. du Toit[1], Girish Modi[2], Dinesh Naidoo[3] and Viness Pillay*[1]

1. *University of the Witwatersrand, Department of Pharmacy and Pharmacology, 7 York Road, Parktown, 2193, Johannesburg, South Africa*
2. *University of the Witwatersrand, School of Neurosciences, Department of Neurology, 7 York Road, Parktown, 2193, Johannesburg, South Africa*
3. *University of the Witwatersrand, School of Neurosciences, Department of Neurosurgery, 7 York Road, Parktown, 2193, Johannesburg, South Africa*

*Corresponding author:
Email: viness.pillay@wits.ac.za
Tel: +27-11-717-2274
Fax: +27-11-642-4355
Fax2Email: +27-86-553-4733

Abstract

The study focused on the design, development and optimization of a novel Nano-Enabled Polymeric Membranous Device (NPMD) for the site-specific delivery of chlorpromazine hydrochloride (CPZ) to counteract the challenges of conventional antipsychotic drug delivery. The NPMD comprised an optimized CPZ-loaded, polycaprolactone (PCL)-based nanoparticle formulation synthesized by a novel melt-dispersion technique, matricized within an optimized polyamide-ethylcellulose (PA 6,10-EC) composite membrane synthesized by a modified wet-phase inversion reaction. The optimized nanoparticle formulation displayed a desirable size (140.30±3.39nm), stability in terms of its zeta potential (-26.40±2.11mV) and CPZ entrapment (8170.23±173.39µg) (~16%). Furthermore, no thermo-degradation of the drug and constituent polymers were observed with the novel melt-dispersion technique. The optimized PA 6,10-EC composite membrane were highly resilient with an unhydrated and hydrated matrix resilience of 74.24±0.88 and 84.35±1.22% respectively. Furthermore, minimal erosion was observed over a period of 30 days (3.64±0.08%). *Ex vivo* cytotoxicity studies using mammalian Pheochromocytoma (PC12) neuronal cells were carried out on the NPMD and its componential elements and proved that the NPMD and its componential elements were biocompatible and displayed no significant cytotoxicity ($p>0.05$). An *in vivo* pilot study involved the surgical intraparenchymal implantation of the NPMD into the brain of the New Zealand White Rabbit model. Results revealed higher levels of CPZ in the CSF (2.08-2.92ng/mL) from the NPMD when compared to a commercially available CPZ injection (0.85-2.32ng/mL). Furthermore, miniscule quantities of CPZ from the NPMD were detected in the blood (≤0.95ng/mL) The CPZ release from the NPMD was far superior to the commercially available form of the drug. Implantation at the site of action allowed for a drastic increase in the CPZ bioavailability. Furthermore, the drug was released in a pseudo-steady state with CSF levels being maintained between 2.00-3.00ng/mL with no fluctuations observed. Ultrasonic imaging was utilized to view the NPMD post-implantation. Rabbits displayed no evidence of motor dysfunction or general brain damage post-implantation for the duration of the study. Histomorphological analysis revealed that the NPMD was biocompatible as no evidences of bleeding, ischemia or major chronic inflammation was observed. Minimal erosion of the NPMD at the termination of the study was noted (14.87%). The NPMD release CPZ in a controlled manner over of period of 30 days and degraded without toxicity. The success of the study creates a platform for expanding polymer-based, nano-enabled brain disease neurotherapy to other compounds.

Keywords: Nano-Enabled Polymeric Membranous Device, chlorpromazine hydrochloride, polycaprolactone, polyamide, ethylcellulose, melt-dispersion technique, wet-phase inversion reaction, cytotoxicity, Pheochromocytoma (PC12 cells), intraparenchymal implantation, New Zealand White Rabbit, ultrasonic imaging, histomorphological analysis

Appendix B1

Evaluation of Chlorpromazine Release from a Polyamide-Ethylcellulose Implantable Mini-Disc

Thiresen Govender[1], Viness Pillay[1*], Girish Modi[2], Dinesh Naidoo[3], Yahya E. Choonara[1] and Lisa C. du Toit[1]

[1]Department of Pharmacy and Pharmacology, University of the Witwatersrand, 7 York Road, Parktown, Johannesburg, 2193

[2]Department of Neurosciences, Division of Neurology, University of the Witwatersrand, 7 York Road, Parktown, Johannesburg, 2193

[3]Department of Neurosciences, Division of Neurosurgery, University of the Witwatersrand, 7 York Road, Parktown, Johannesburg, 2193

*Corresponding Author: viness.pillay@wits.ac.za

Purpose

The purpose of this study was to investigate the possibility of developing a biodegradable polyamide-based intracranial implantable device capable of chlorpromazine hydrochloride (CPZ) release over a prolonged period of time.

Methods

Preparation of mini-discs: Polyamide 6,10 (PA 6,10) membranes were prepared by an immersion precipitation reaction. The PA 6,10 was firstly dissolved in formic acid (3mg/mL), cast in appropriate molds and immersed in de-ionized water (F1), a $5\%^{w}/_{v}$ $CaCl_2$ solution (F2), a $1.15\%^{w}/_{v}$ NaCl solution (F3) and a $5\%^{w}/_{v}$ NaOH solution (F4). Resultant membranes were dried, ground, sieved and granulated with ethylcellulose (EC) and CPZ. Mini-discs with dimensions of 8×2mm were compressed using a Carver Hydraulic Press. In addition, a fifth disc (F5), comprising the PA 6,10 powder, EC and CPZ, was compressed. *FTIR spectrophotometric Analysis:* FTIR was performed on resultant membranes and the PA 6,10 powder to assess major structural variations that may have occurred during the immersion precipitation reaction. *In vitro drug release and matrix erosion studies:* Drug release studies were performed in 100mL PBS (pH 7.4, 37˚C) at 25rpm using an orbital shaker bath. Samples were taken at predetermined intervals and analyzed at 254nm using UV spectroscopy. Matrix erosion was determined at 168 hours.

Results

All formulations barring F4 exhibited negligible structural changes thereby confirming the integrity of major functional groups on the polyamide backbone. F4 displayed a lack of minor peaks characteristic of the polyamide backbone indicating the formation of a structurally distinct compound with purportedly novel properties. F2 and F4 exhibited total drug release within a period of 27 and 15 hours, respectively. In addition, these two formulations demonstrated an average mass loss of ~91% after 168 hours. F1, F3 and F5 demonstrated desirable drug release behavior with drug release ranging from 5.8-19.8% over 168 hours. Furthermore, these longer-acting formulations revealed an average mass loss of ~17%.

Conclusions

In vitro assays highlighted the potential of the fabricated systems for controlling drug release over extended periods of time. This could prove beneficial for the management of psychotic patients over prolonged periods, overcoming patient non-compliance and relapse.

Appendix B2

A polyamide-based membranous device for specialized drug delivery

T. Govender[1], V. Pillay[1*], Y. E. Choonara[1], L. C. du Toit[1], G. Modi[2], D. Naidoo[3]
[1]University of the Witwatersrand, Department of Pharmacy and Pharmacology, 7 York Road, Parktown, Johannesburg, 2193
[2]University of the Witwatersrand, Department of Neurosciences, Division of Neurology, 7 York Road, Parktown, Johannesburg, 2193
[3]University of the Witwatersrand, Department of Neurosciences, Division of Neurosurgery, 7 York Road, Parktown, Johannesburg, 2193
*Correspondence: viness.pillay@wits.ac.za

INTRODUCTION

This study is aimed at investigating the design and development of a novel polyamide-based polymeric membrane for implantable drug delivery.

MATERIALS AND METHODS

1) *Preparation of polymeric membranes:* Polymeric membranes were prepared by a precipitation reaction. Novel polyamide 6,10 (PA 6,10) synthesized by modified interfacial polymerization reaction [1], was firstly dissolved in formic acid. The solution was placed under magnetic stirring at 3000rpm and the temperature was raised to 65°C until all PA 6,10 dissolved. Another solution comprising ethylcellulose (EC) dissolved in acetone was prepared. The PA 6,10-formic acid solution was then added to the EC-acetone solution while under magnetic stirring. Stirring continued until the formation of a homogenous solution. The solution was left to stir for approximately an hour and upon completion of stirring, double de-ionized water was added to the solution. This resulted in the formation of a white gel-like precipitate at the interface. The precipitate was collected by filtration with a Buchner apparatus with the continuous addition of double de-ionized water. Following filtration, the precipitate was collected, appropriately molded and left to dry under a fume hood for 24 hours. Resultant membranes were round, regular and exhibited surface porosity.

2) *FTIR Spectrophotometric Analysis:* Fourier transform infrared (FTIR) spectroscopy was undertaken on the resultant membranes to assess any structural variations in the polymeric membranous device, as a result of any interactions in the formulation.

3) *Morphological characterization of polymeric membrane:* Surface morphology was characterized by Scanning Electron Microscopy (SEM). Photomicrographs were taken at different magnifications and samples were prepared after sputter-coating with gold. Morphological characterization of the membranes revealed the shape, surface morphology and structure of the device.

4) *Textural profile analysis:* Textural analysis was used to determine the physicomechanical properties of the membranes in terms of their Brinell Hardness and deformation energy. This was compared to Brinell Hardness values obtained from a PA 6,10-EC disc, compressed with a Carver Hydraulic Press.

RESULTS AND DISCUSSION

Structural characterization was performed on the PA 6,10, EC and the PA 6,10-EC membrane synthesized by precipitation reaction. Results confirmed the presence and integrity of a combination of both PA 6,10 and EC functional groups in the membranes produced by precipitation reaction. This thus confirmed the formation of a novel PA 6,10-EC membranous device. SEM images of the novel polymeric membrane at varying magnifications confirmed that membranes were irregular and highly porous. Textural profiling confirmed the integrity of the synthesized membranous matrices with BHN values ranging from 2.42-2.54 N/mm^2. BHN values of the compressed PA 6,10-EC discs ranged from 3.09-4.01N/mm^2. The lower BHN values of the PA 6,10-EC membranes are indicative of a device that is non-crystalline and potentially more favorable for implantation.

CONCLUSIONS

The PA 6,10-EC membranes were successfully synthesized. Furthermore, resultant membranes were regular and of consistent size, rigid and displayed no evidence of easy breakage.

ACKNOWLEDGMENTS

National Research Foundation of South Africa (NRF)
Gauteng Department of Agriculture and Rural Development (GDARD)
University of the Witwatersrand

REFERENCES

[1] O.A. Kolawole, V. Pillay and Y.E. Choonara, "Novel Polyamide 6,10 Variants Synthesized by Modified Interfacial Polymerization for Application as a Rate-Modulated Monolithic Drug Delivery System" *Journal of Bioactive and Compatible Polymers,* **22** (2007) 281-313.

Appendix B3

Design, Development and Optimisation of a Novel Neurotherapeutic Intracranial Implantable Composite Device

Thiresen Govender[1], Viness Pillay[1*], Yahya E. Choonara[1], Lisa Claire du Toit[1], Dinesh Naidoo[2] and Girish Modi[3]

1. *University of the Witwatersrand, Department of Pharmacy and Pharmacology, 7 York Road, Parktown, Johannesburg, South Africa 2193*
2. *University of the Witwatersrand, Department of Neurosciences, Division of Neurosurgery, 7 York Road, Parktown, Johannesburg, South Africa, 2193*
3. *University of the Witwatersrand, Department of Neurosciences, Division of Neurology, 7 York Road, Parktown, Johannesburg, South Africa, 2193*

Correspondence: viness.pillay@wits.ac.za

Introduction

Therapeutic failure of the majority of neurotherapeutic drugs relies on the fact that these drugs are only transported minimally across the BBB. Apart from this, the lack of innovation in product development to counteract these challenges is also a major contributing factor to a poor therapeutic outcome [1]. The aim of this study was to undertake the design, development and optimisation of a novel, biocompatible neurotherapeutic polymeric matrix for implantable intracranial drug delivery. Chlorpromazine hydrochloride (CPZ) was used as the model neurotherapeutic in this study.

Methods

Preparation of membranes: Membranes were prepared by modified wet phase inversion reaction according to a face-centred composite design. Briefly, novel polyamide 6,10 (PA 6,10) [2], was firstly dissolved in formic acid. The solution was subjected to magnetic stirring at 450rpm until all the PA 6,10 dissolved. Another solution comprising ethylcellulose (EC) dissolved in acetone was prepared. The PA 6,10-formic acid solution was then added to the EC-acetone solution while under magnetic stirring. Stirring was continued until the formation of a homogenous solution. The homogenous solution was placed in a dialysis membrane and submerged in de-ionized water, leading to the formation of the membranes which were then appropriately moulded.

FTIR Spectrophotometric Analysis: Fourier transform infrared (FTIR) spectroscopy was undertaken on the resultant membranes to assess the presence of any structural variations that may have been introduced during the reaction and thus determine if there were any pertinent interactions in the formulation.

Textural Profile Analysis: Textural analysis was used to determine the physicomechanical properties of the membranes in terms of their unhydrated and hydrated (post 30 days) Matrix Resilience (MR).

Swelling studies: The swelling behaviour of the membranes was determined in 100mL Phosphate Buffered Saline (PBS) (pH 7.4, 37°C) at 25rpm using an orbital shaker bath. Samples were removed at predetermined intervals, convection dried and weighed to determine the extent of swelling.

Drug-loading and Drug Entrapment Efficiency Testing: CPZ was incorporated into the membranes prior to moulding. DEE was determined by dissolving the membranes in PBS over a period of time and analysing the solution using ultraviolet spectroscopy against standard curves.

Drug Release Studies: *In vitro* drug release studies were performed on the optimised membrane in 100mL PBS (pH 7.4, 37°C) at 25rpm using an orbital shaker bath. Samples were taken at predetermined intervals over a period of 30 days and analyzed at using UV spectroscopy.

Morphological Analysis and Porosity: Scanning Electron Microscopy (SEM) and porosity analysis was used to determine the surface morphology of the membranes.

Results

FTIR confirmed the presence of both PA 6,10 and EC functional groups in the synthesised membranes indicating very desirable blending and the formation of a novel matrix. Texture analysis demonstrated desirable Unhydrated MR results ranging from approximately 69% for membranes with a greater PA concentration to 86% for membranes with a higher EC concentration. Hydrated MR values were also desirable ranging from 51 to 85%. Swelling studies at 30 days demonstrated mass increases ranging from approximately 16 to 50% with trends which indicate that increases in EC resulted in greater swelling. MR values are indicative of a highly resilient and robust matrix favourable for implantation. The swelling behaviour of the device could possibly present problems such as stimulating the inflammatory response post implantation and increased intracranial pressure; however the swelling does not appear to be dramatically high. Morphological and porosity analysis revealed regular and highly porous membranes thereby allowing for the efficient diffusion of drug into the Central Nervous System. A highest DEE value of 96% was computed for the optimised formulation. Furthermore, controlled drug release over an extended period was observed from the optimised membrane over a period of 30 days indicating that the device is capable for effective, long-term management of responsive neurological conditions.

Conclusion

Novel PA 6,10-EC composites, which show highly desirable *in vitro* characteristics, were successfully synthesised and may be used as implantable intracranial neurotherapeutic drug carriers that offer numerous benefits in the long-term treatment and positive therapeutic outcome of a variety of chronic neurological conditions.

References

[1]. Pardridge W.M. The Blood-Brain Barrier: Bottleneck in Brain Drug Development, *NeuroRX*, **2**(1), (2005), 3-14.

[2]. O.A. Kolawole, V. Pillay and Y.E. Choonara, Novel Polyamide 6,10 Variants Synthesized by Modified Interfacial Polymerization for Application as a Rate-Modulated Monolithic Drug Delivery System, *Journal of Bioactive and Compatible Polymers*, **22** (2007), 281-313.

Appendix B4

Novel Approaches to Personality Disorder Treatment: Design of Dual-Acting Nanoparticles for the Enhanced Neurotherapy of Borderline Personality Disorder

Thiresen Govender[1], Nabeela Bhabha[1], Viness Pillay[1*], Yahya E. Choonara[1], Lisa Claire du Toit[1], Dinesh Naidoo[2] and Girish Modi[3]

1. *University of the Witwatersrand, Department of Pharmacy and Pharmacology, 7 York Road, Parktown, Johannesburg, South Africa 2193*
2. *University of the Witwatersrand, Department of Neurosciences, Division of Neurosurgery, 7 York Road, Parktown, Johannesburg, South Africa, 2193*
3. *University of the Witwatersrand, Department of Neurosciences, Division of Neurology, 7 York Road, Parktown, Johannesburg, South Africa, 2193*

Correspondence: viness.pillay@wits.ac.za

Introduction

Cod Liver Oil (CLO) is a complementary medicine, rich in Omega-3 fatty acids. Omega-3 fatty acids, in particular, Ethyl-Eicosapentaenoic Acid, has been shown to be effective in the treatment of Borderline Personality Disorder (BPD) [1]. Furthermore, the use of antipsychotic drugs may be modestly beneficial when psychotic symptoms of BPD occurs [2]. The aim of this study was to investigate the development of Chlorpromazine Hydrochloride (CPZ) and CLO-loaded, Polycaprolactone (PCL)-based, dual acting nanoparticles using a specialised melt-emulsion technique.

Methods

Preparation of Nanoparticles: Nanoparticles were prepared by a specialised melt-emulsion technique according to a one variable at a time (OVAT) approach. Briefly, glycerol, used as a melting base, was heated to approximately 70°C. This was followed by the addition of PCL until complete melting was achieved. Once melted, Cod Liver Oil and Polysorbate 80 were added. A separate solution comprising CPZ in de-ionized water was simultaneously prepared and heated to approximately 65°C. This was added to the molten PCL, CLO, Polysorbate 80 and glycerol while stirring under a top stirrer. The resultant emulsion was stirred at 1800rpm until cooled to room temperature. CPZ-loaded, PCL-based nanoparticles formed upon cooling.

Fourier Transform Infrared Spectroscopy (FTIR) and Differential Scanning Calorimetry (DSC): Thermal analysis of nanoparticles were performed to determine the presence of degradation due to the melt dispersion technique.

Drug entrapment efficiency (DEE): Drug-loading percentages of nanoparticles were determined to assess the extent of drug entrapment during nanoparticle formation.

Determination of Particle Size and Zeta Potential of Nanoparticles: The average size, size distribution and physical stability of the nanoparticles were determined by Dynamic Light Scattering employing a Zetasizer NanoZS instrument.

Transmission Electron Microscopy (TEM): TEM was used to asses the morphology of the nanoparticles in greater detail in terms of their, shape, size and surface characteristics.

Drug Release Studies: In vitro drug release studies were performed in Phosphate Buffered Saline (pH 7.4, 37°C) at 25rpm using an orbital shaker bath and samples analyzed using ultraviolet spectroscopy.

Results

Thermal analysis confirmed no indication of degradation to nanoparticles and constituents. DEE values ranged from 3.1-13.38% which is expected due to the high hydrophilicity of CPZ and the hydrophobic nature of the PCL. The hydrophobic nature of PCL and the lipophilic nature of the CLO ensured that CLO would be entrapped and adsorbed on the nanoparticles however this was not quantified. The presence of entrapped or adsorbed CLO was confirmed by FTIR and the noticeable buoyancy of the particles when suspended in water. Particle size ranged from 16.5-387.1nm which is optimum for neuronanopharmaceutics. Zeta potential ranged from -0.04 to -29.8mV indicating the formation stable particles. Drug release studies were desirable as all formulations exhibited controlled and extended release over 32 days.

Conclusion

The novelty of both the method of preparation of the nanoparticles and the concept of combining conventional medicine and complementary medicine to achieve positive therapeutic outcomes has the potential for revolutionizing the treatment of BPD.

References

[1]. Zanarini M.C.and Frankenburg F.R., Omega-3 Fatty Acid Treatment of Women Omega-3 Fatty Acid Treatment of Women A Double-Blind, Placebo-Controlled Pilot Study, *Am J Psychiatry,* **160**(2003), 167–169.

[2]. Tyrer P. and Newton-Howes G., Rational drug treatment for personality disorders, *Psychiatry*, **4**, 11-14.

Appendix B5

Advances in Neurotherapeutics: Intracranial Implantation of a Novel Optimised Polymeric Composite in the New Zealand White Rabbit Cadaver

Thiresen Govender[1], Viness Pillay[1*], Yahya E. Choonara[1], Lisa Claire du Toit[1], Dinesh Naidoo[2], Girish Modi [3]and Leith Meyer[4]

1. *University of the Witwatersrand, Department of Pharmacy and Pharmacology, 7 York Road, Parktown, Johannesburg, South Africa 2193*
2. *University of the Witwatersrand, Department of Neurosciences, Division of Neurosurgery, 7 York Road, Parktown, Johannesburg, South Africa, 2193*
3. *University of the Witwatersrand, Department of Neurosciences, Division of Neurology, 7 York Road, Parktown, Johannesburg, South Africa, 2193*
4. *University of the Witwatersrand, Central Animal Services, 7 York Road, Parktown, Johannesburg, South Africa, 2193*

Correspondence: viness.pillay@wits.ac.za

Introduction

Brain implantation is a technique that has been utilized in the past, however, the majority of these procedures are extremely invasive, may result in infection and inflammation and require removal of the non-biodegradable implant. The aim of this study was to perfect the surgical implantation procedure of a novel biodegradable, biocompatible neurotherapeutic intrancranial implant in the New Zealand White Rabbit Cadaver.

Methods

Two New Zealand White Rabbits were humanely euthanized with sodium pentobarbitone. The implantation procedure was adapted from Brem and co-workers (1989) [1] and is briefly outlined; the heads of the animals were shaved and appropriately prepared. A midline incision was made and this was followed by the removal of subcutaneous tissue and periosteum. A unilateral burrhole of approximately 6mm was made in the region anterior to the coronal suture and lateral to the sagittal suture using a hand-held dental drill. The dura mater and cortex were then pierced with minimal resultant bleeding. The burrhole was flushed with saline and the implant was placed intraparenchymally. The bone defect was closed with bone wax and the scalp insertion was appropriately closed with a single layer of non-absorbable suture. Implants were optimised novel neurotherapeutic carrier composite matrices with approximate dimensions of 5mm in diameter by 3mm in height.

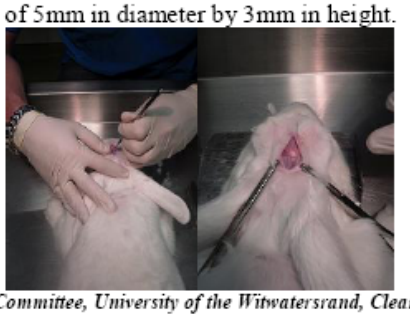

Animal Ethics Screening Committee, University of the Witwatersrand, Clearance number 2011/51/04

Results

The implantation procedure in general was not arduous nor was it time consuming. Minimal amounts of superficial damage or contusion were observed, however, its clinical significance could not be established as the study was performed on cadavers as opposed to live, healthy rabbits. Utilizing live rabbits allows for a visual assessment of the tolerance of the rabbits towards the implants and the presence of any undesirable reactions that may occur following implantation. Furthermore, a battery of tests of behavioural asymmetry tests may be performed on the rabbits to indicate the degree of motor dysfunction present.

Conclusion

The study creates a platform for expanding polymer-based neurotherapy to a variety of neurological conditions including personality disorders. Future work will focus on performing the surgery on live, healthy, anaesthetised rabbits, reversing the anaesthesia, awakening the animals and conducting a variety of tests to assess the tolerability, as well as ascertaining the pharmacokinetics and pharmacodynamics of the implant *in vivo*.

References

[1]. Brem H., Kader A., Epstein J.I., Tamargo R.J., Domb A., Langer R., Leong K.W. Biocompatibility of a Biodegradable Controlled-Release Polymer in the Rabbit Brain, *Selective cancer therapeutics*, **5** (2), (1989), 55-65.

Appendix C1

Govender Thiresen
Pillay Viness, Choonara Yahya, du Toit Lisa, Modi Girish, Naidoo Dinesh
School of Therapeutic Sciences

First preference: Oral
Second preference: Free standing poster

A membrane-fixated nano-liposhell device for specialized central nervous system drug delivery

The limitations of central nervous system drug delivery have proved to be significant impediments to the long-term management of psychiatric conditions such as psychosis. Furthermore, lack of innovation in product development to counteract these challenges is also a major contributing factor to a poor therapeutic outcome. The aim of this study was to develop a novel implantable nano-enabled polymeric membranous device for the chronic treatment of psychosis. Composite, biodegradable polyamide 6,10-ethylcellulose (PA6,10-EC) membranes were prepared by a modified immersion precipitation reaction followed by desiccation. Fourier transform infrared (FTIR) spectroscopy confirmed the presence and integrity of polyamide and ethylcellulose functional groups in the membranes. This proved the formation of a novel co-blended PA6,10-EC membrane for nano-liposhell fixation. Surface morphology was characterized by scanning electron microscopy and revealed asymmetrical, highly porous matrices. Chlorpromazine-loaded, polycaprolactone-based nano-liposhells were prepared by a specialized melt-dispersion technique and comprised encapsulated essential fatty acids in the form of cod-liver oil. FTIR and differential scanning calorimetry revealed no evidence of thermal degradation of the drug and polymers during melt-dispersion. A mean drug entrapment efficiency (DEE) value of 66% was computed for chlorpromazine-loaded nano-liposhells with a 14:1 polymer:drug ratio. The nano-liposhells displayed a mean size of 106.5±10.44nm and a zeta potential of -22.7±1.84mV. *In vitro* dissolution was desirable with drug release ranging from 7.71-17.31% over 18 days highlighting the potential of the devices to control release kinetics over an extended period of time. This could prove beneficial for the prolonged management of psychotic patients, overcoming non-compliance and relapse.

Appendix C2

Development of Chlorpromazine-Loaded, Polycaprolactone Based Nanoparticles Utilizing a Novel Melt-Dispersion Technique

Thiresen Govender[1], Viness Pillay[1]*, Yahya E. Choonara[1], Lisa C. du Toit[1], Girish Modi[2] and Dinesh Naidoo[3]

[1]University of the Witwatersrand, Department of Pharmacy and Pharmacology, 7 York Road, Parktown, Johannesburg, 2193

[2] University of the Witwatersrand, Department of Neurology, 7 York Road, Parktown, Johannesburg, 2193

[3] University of the Witwatersrand, Department of Neurosurgery, 7 York Road, Parktown, Johannesburg, 2193

*Correspondence: viness.pillay@wits.ac.za

Purpose:

Polymeric nanoencapsulation of highly hydrophilic drugs by conventional nanoparticle formation techniques is a fairly arduous task. Furthermore, conventional techniques are time-consuming and require the use of potentially toxic organic solvents. Consequently, there is a great need for novel and more effective methods of nanoparticle formation. The aim of this study was to synthesize polycaprolactone (PCL)-based nanoparticles for specialized drug delivery, employing a novel melt-dispersion process. Chlorpromazine hydrochloride (CPZ) was selected as the model drug due to its high hydrophilicity.

Methods:

Preparation of nanoparticles: Briefly, glycerol was heated to 70°C and formed the base for PCL melting. PCL was added to the glycerol and melting occurred. Polysorbate 80 was added to the molten PCL solution. The solution was then transferred to a top stirrer at 1000rpm. A second solution comprising CPZ dissolved in water was heated to 70°C and gradually added to the molten PCL solution. The solution was left to stir for 45 minutes at room temperature. Nanoparticles were formed upon cooling of the solution. The particles were centrifuged at 3000rpm for 15 minutes. This was followed by freezing and lyophilization to obtain a free-flowing powder.

Drug Entrapment Efficiency Testing: Polymeric nanoparticles were dissolved in 80mL of phosphate buffered solution (PBS) (pH 7.4, 37°C) and thereafter agitated at room temperature over a period of 7 days. The solution was subsequently analyzed for drug content using UV Spectroscopy.

Determination of Particle Size and Zeta Potential of Nanoparticles: The average size, size distribution and physical stability of the nanoparticles were determined by Dynamic Light Scattering employing a Zetasizer NanoZS instrument.

Thermal and Molecular Structure Characterization: FTIR and DSC were performed to determine the possibility of thermal degradation of CPZ and PCL during the melt-dispersion technique.

Morphological Analysis: TEM was performed to assess particle shape and size at greater resolution and higher definition.

Drug Release Studies: In vitro drug release studies were performed in 100mL PBS (pH 7.4, 37°C) at 25rpm using an orbital shaker bath. Samples were taken at predetermined intervals and analyzed at 255nm using UV spectroscopy.

Results:

The highest drug entrapment efficiency value of 53% was computed for CPZ-loaded nanoparticles with a 10:1 polymer:drug ratio. An average size of 102.5±15.55nm and a zeta potential of -25.7±2.32.44mV was recorded. FTIR and DSC revealed no evidence of thermal degradation of the CPZ and PCL during melt-dispersion. TEM depicted the presence of highly efficient nanoparticles which were spherical and of consistent size. *In vitro* drug release studies were desirable with drug release ranging from 9.44-15.56% over 30 days highlighting the potential of the nanoparticles to control release kinetics over an extended period of time. A successful novel method for PCL-based nanoparticle synthesis was developed.

Appendix D

1. (WO2012070034) A DRUG DELIVERY DEVICE

Pub. No.: WO/2012/070034 **International Application No.:** PCT/IB2011/055345
Publication Date: 31.05.2012 **International Filing Date:** 28.11.2011

IPC: ***A61K 9/26*** (2006.01), ***A61K 31/5415*** (2006.01), ***A61K 38/08*** (2006.01), ***A61K 9/51*** (2006.01), ***A61P 25/18*** (2006.01), ***A61P 25/28*** (2006.01), ***B82Y 5/00*** (2011.01)

Applicants: **UNIVERSITY OF THE WITWATERSRAND, JOHANNESBURG** [ZA/ZA]; 1 Jan Smuts Avenue Braamfontein 2050 Johannesburg, Gauteng (ZA) *(For All Designated States Except US)*.
GOVENDER, Thiresen [ZA/ZA]; (ZA) *(For US Only)*.
PILLAY, Viness [ZA/ZA]; (ZA) *(For US Only)*.
CHOONARA, Yahya, Essop [ZA/ZA]; (ZA) *(For US Only)*.
DU TOIT, Lisa, Claire [ZA/ZA]; (ZA) *(For US Only)*.
MODI, Girish [ZA/ZA]; (ZA) *(For US Only)*.
NAIDOO, Dinesh [ZA/ZA]; (ZA) *(For US Only)*.
MUFAMADI, Maluta, Steven [ZA/ZA]; (ZA) *(For US Only)*

Inventors: **GOVENDER, Thiresen**; (ZA).
PILLAY, Viness; (ZA).
CHOONARA, Yahya, Essop; (ZA).
DU TOIT, Lisa, Claire; (ZA).
MODI, Girish; (ZA).
NAIDOO, Dinesh; (ZA).
MUFAMADI, Maluta, Steven; (ZA)

Agent: **ADAMS & ADAMS**; PO Box 1014 Pretoria 0001 (ZA)

Priority Data: 2010/03743 26.11.2010 ZA
2010/07276 26.11.2010 ZA

Title **(EN)** A DRUG DELIVERY DEVICE
(FR) DISPOSITIF D'ADMINISTRATION DE MÉDICAMENT

Abstract: **(EN)**The invention provides an implantable intracranial device for the site-specific delivery of a pharmaceutically active agent to a human or animal for treating a mental or neurological disorder, such as Alzheimer's disease, schizophrenia or other psychoses. The biodegradable device includes a pharmaceutically active agent for treating the disorder, polymeric nano-lipoparticles into or onto which the pharmaceutically active agent is embedded; and a polymeric matrix or scaffold incorporating the nano-lipoparticles. The nano-lipoparticles can be in the form of nano-liposhells or nano-lipobubbles. The nano-liposhells or nano-lipobubbles can include an essential fatty acid or can be conjugated to a peptide ligand which targets the device to a specific cell into which the therapeutic agent can be delivered. The device can be implanted in the sub-arachnoid space in the region of the frontal lobe of the brain.
(FR)L'invention porte sur un dispositif intracrânien implantable pour l'administration spécifique à un site d'un agent pharmaceutiquement actif à un être humain ou à un animal pour le traitement d'un trouble mental ou neurologique, tel que la maladie d'Alzheimer, la schizophrénie ou autres psychoses. Le dispositif biodégradable comprend un agent pharmaceutiquement actif pour le traitement du trouble, des nano-lipoparticules polymères dans ou sur lesquelles l'agent pharmaceutiquement actif est incorporé ; et une matrice polymère ou un échafaudage polymère comprenant les nano-lipoparticules. Les nano-lipoparticules peuvent se présenter sous la forme de nano-lipo-enveloppes ou de nano-lipo-bulles. Les nano-lipo-enveloppes ou les nano-lipo-bulles peuvent comprendre un acide gras essentiel ou peuvent être conjuguées à un ligand peptidique qui cible le dispositif sur une cellule spécifique dans laquelle l'agent thérapeutique peut être administrée. Le dispositif peut être implanté dans l'espace sous-arachnoïdien dans la région du lobe frontal du cerveau.

Designated States: AE, AG, AL, AM, AO, AT, AU, AZ, BA, BB, BG, BH, BR, BW, BY, BZ, CA, CH, CL, CN, CO, CR, CU, CZ, DE, DK, DM, DO, DZ, EC, EE, EG, ES, FI, GB, GD, GE, GH, GM, GT, HN, HR, HU, ID, IL, IN, IS, JP, KE, KG, KM, KN, KP, KR, KZ, LA, LC, LK, LR, LS, LT, LU, LY, MA, MD, ME, MG, MK, MN, MW, MX, MY, MZ, NA, NG, NI, NO, NZ, OM, PE, PG, PH, PL, PT, QA, RO, RS, RU, RW, SC, SD, SE, SG, SK, SL, SM, ST, SV, SY, TH, TJ, TM, TN, TR, TT, TZ, UA, UG, US, UZ, VC, VN, ZA, ZM, ZW.
African Regional Intellectual Property Org. (ARIPO) (BW, GH, GM, KE, LR, LS, MW, MZ, NA, RW, SD, SL, SZ, TZ, UG, ZM, ZW)
Eurasian Patent Organization (EAPO) (AM, AZ, BY, KG, KZ, MD, RU, TJ, TM)
European Patent Office (EPO) (AL, AT, BE, BG, CH, CY, CZ, DE, DK, EE, ES, FI, FR, GB, GR, HR, HU, IE, IS, IT, LT, LU, LV, MC, MK, MT, NL, NO, PL, PT, RO, RS, SE, SI, SK, SM, TR)
African Intellectual Property Organization (OAPI) (BF, BJ, CF, CG, CI, CM, GA, GN, GQ, GW, ML, MR, NE, SN, TD, TG).

Publication Language: English (EN)
Filing Language: English (EN)

Appendix E

AESC3

STRICTLY CONFIDENTIAL

ANIMAL ETHICS SCREENING COMMITTEE (AESC)

CLEARANCE CERTIFICATE NO. 2011/51/04

APPLICANT: **Mr T Govender**

DEPARTMENT: **School of Pharmacy and Pharmacology**

PROJECT TITLE: ***In vivo* evaluation of an implantable nano-enabled polymeric membranous device containing chlorpromazine hydrochloride in the rabbit model**

Number and Species

23 rabbits
Approved unconditionally

Approval was given for to the use of animals for the project described above at an AESC meeting held on **29 November 2011**. This approval remains valid until **30 November 2013**.

The use of these animals is subject to AESC guidelines for the use and care of animals, is limited to the procedures described in the application form.

Signed: _____ (Chairperson, AESC) Date: 13/12/2011

I am satisfied that the persons listed in this application are competent to perform the procedures therein, in terms of Section 23 (1) (c) of the Veterinary and Para-Veterinary Professions Act (19 of 1982)

Signed: _____ (Registered Veterinarian) Date: 13/12/2011

cc: Supervisor:
Director: CAS

BEDLET.XLS

RECORD SHEET (MPU)

INVESTIGATOR : _____ AESC No: _____ PAGE:

DEPARTMENT : _____ SPECIES: _____

DATE	TIME	HEALTH STATUS	CAGE No./ ANIMAL ID	NOTES / OBSERVATIONS / INVESTIGATIONS / TREATMENTS.	SIGN

Appendix F1

Appendix F2

Synergy Sterilisation
SOUTH AFRICA (PTY) LTD
(Reg. No. 1998/024219/07)
5 Waterpas Street
Isando Extension 3
P.O. Box 3219
Kempton Park 1620
Tel: (011)974-8851
Fax: (011)974-8986

synergyhealth
our work protects your world

Gamma Radiation Processing

Certificate Of Gamma Irradiation

This is to certify that

SYNERGY STERILISATION SA (PTY) LTD

Has given an irradiation treatment in accordance with :

. The national and international quality assurance system standards: ISO 9001:2008

. The precision and accuracy of the dosimetry system used is traceable to International Standar

to the following goods (as described by the Manufacturer):

Customer	THIRESEN GOVENDER (C0D)	Customer Order No.	GRN date
Isotron Internal order number (Certificate No)	36781 \1	18/05/2012	2012/05/18
Isotron Stock Code	000 020 TR01	Conforms to the Specified Irradiation Dose of :	
Product description	TRIAL/SAMPLE FOR 20kGy	Minimum :	20 kGy
Quantity of Containers	Mass Of Containers Kg	Maximum :	0 kGy
1	1.00	Routine Dose Reading :	22.4 kGy
		Ref. Dose Mapping :	

Irradiation Completion Date 22/05/2012 Product Released By Quality Department

ISO-9 REV 12

Appendix F3

ANIMAL WEIGHT CHART

INVESTIGATOR: ____________

DEPARTMENT: ____________

AESC No. ____________

ANIMAL NO.																COMMENTS
DATE	SPECIES:							STRAIN:								

Appendix F4

PAIN ASSESSMENT SHEET (Rabbit post surgery)

DATE OF SURGERY					**ANMAL ID:**			
MASS (g)								
DATE								
STUDY DAY	0							
TIME								
MASS (g) once a day								
UNDISTURBED OBSERVATION								
Not eating (food weight)								
Not drinking (H_2O Volume)								
Lack of grooming								
Abnormal movement - circling								
Pained posture (hunching/ guarding)								
Vocalisation								
Depressed/ Lethargy/ Facing back of cage								
ON HANDLING								
Not inquisitive & alert								
Vocalisation on gentle palpation								
Dehydration (Tented skin)								
Type of breathing*								
Not approachable/Moribund								
SPECIFIC CLINICAL SIGNS								
Pale / Cyanotic								
Tremors								
Eyes recessed/3rd eyelid protrude								
Soft Distended Abdomen								
Firm Distended Abdomen								
Diarrhoea/ bleeding								
Nothing abnormal detected (NAD)								
OTHER COMMENTS / Treatment								
SIGNATURE								

Animals to be observed 4 hourly during day & 6 hourly at night

Scoring details:

* Breathing: R = rapid; S = Shallow; L = Laboured; N = Normal

Scoring:

- = No effect; + = Moderate; ++ = Severe; +++ = Extreme